Synthesis and evaluation of receptors for phosphatidylinositol phosphates

GILLIAN F. WHYTE

A thesis submitted for the degree of Doctor of Philosophy of Imperial College

Supervisors: Prof. Ramon Vilar, Dr. Rudiger Woscholski
Imperial College London,
Department of Chemistry
July 2013

Declaration of Authorship

I certify that all the work described in this thesis is all my own, except where clearly stated, and a list of references is provided in the bibliography.

Gillian F. Whyte

Dedicated to my parents, Joy and Glenn Whyte,

and my husband Adrian Lovell.

Acknowledgements

Contents

Abstract

Phosphatidylinositol phosphates (PIPs) are signalling phospholipids with a diverse set of cellular functions. The most important of these PIPs are phosphatidylinositol (4,5) bisphosphate (PI(4,5)P_2) and phosphatidylinositol (3,4,5) trisphosphate (PI(3,4,5)P_3). These two are responsible for a number of cellular events which regulate cell growth, proliferation and apoptosis. Deregulation of PIP levels disrupts these pathways and can therefore lead to uncontrolled cell growth and which can lead to tumourigenesis. Control of PIP levels has been identified as a potential target for diagnosis and intervention in diseases including Alzheimer's disease, cancer, and the genetic disorder Lowe Syndrome.

The use of small molecules that bind PIPs has been shown by our group to interfere with protein-PIP interactions. By preventing proteins from binding to PIPs, the effective concentration of the target PIP is reduced, proteins are not recruited to the membrane for activation and downstream signalling pathways are attenuated. Therefore, in this project a series of small artificial receptors were synthesised and were shown to bind PI(4,5)P_2 and PI(3,4,5)P_3. The aim of this was to control their effective levels and manipulate their downstream signalling pathways.

PI(4,5)P_2-binding receptors were developed based on existing lead compounds established within our group. Comparison of a receptor with only one binding motif with the established two motif receptor showed differences in affinity as well as specificity for the phospholipid target PI(4,5)P_2 over the headgroup IP_3. In cells, the effect of the receptors on the downstream signalling pathways was examined using phosphorylated Akt as an indicator of this pathway's activation. Two fluorescent receptors were designed and one of these was used as a novel PI(4,5)P_2 detection tool on immobilised phospholipid. Preliminary results show that this receptor may also be used to directly image PI(4,5)P_2 in fixed cells.

Novel PI(3,4,5)P_3 receptors were designed with phosphate-binding motifs and a range of spacers. The specificity of each receptor was identified and binding affinities towards PI(3,4,5)P_3 were established. Inhibition of protein-lipid interaction and inhibition of PIP-metabolising enzymes were also studied. The effect of these new receptors in attenuating the Akt pathway in cancer cells was also investigated, and they were found to lack the efficacy of PI(4,5)P_2-binding receptors.

The ability of some of these artificial receptors to bind phospholipids in the cell and affect subsequent signalling pathways indicates that phospholipids are a viable additional drug targets for many diseases.

Abbreviations

A.M.U.	*Atomic mass units*
ACN	*Acetonitrile*
ADP	*Adenosine diphosphate*
AEBSF	*4-(2-Aminoethyl) benzenesulfonyl fluoride hydrochloride*
AMP	*Adenosine monophosphate*
ANTH	*AP180 N-terminal homology*
ATP	*Adenosine triphosphate*
ATPase	*Adenosine triphosphate phosphatase*
BATS	*Barkor autophagosome targeting sequence*
BOC	*tertiary-butoxycarbonyl*
BSA	*Bovine serum albumin*
C2	*Conserved region-2 of protein kinase C*
CBP	*Cyclohexane 1,2-diphosphate*
CDI	*Carbonyl diimidazole*
CTP	*Cyclohexane triphosphate*
Cyclen	*1,4,7,10-tetraazacyclododecane*
DABCO	*Diazabicyclo[2.2.2]octane*
DAG	*Diacylglycerol*
DCM	*Dichloromethane*
DEPT	*Distortionless enhancement by polarisation transfer*
DHR-1	*Dock homology region 1*
DIPEA	*Diisopropylethylamine*
DMEM	*Dulbecco's Modified Eagle's Medium*
DMF	*Dimethylformamide*
DMSO	*Dimethylsulfoxide*
DNA	*Deoxyribonucleic acid*
DPA	*Dipicolylamine*
DTT	*Dithiothreitol*
ECL	*Enhanced chemiluminescence*
EDTA	*Ethylenediamine tetraacetic acid*
ELISA	*Enzyme-linked immunosorbent assay*
ENTH	*Epsin N-terminal homology*
ESI-MS	*Electrospray ionisation mass spectrometry*

FYVE	*Fab1, YOTB, Vac1 and EEA1*
GOLPH3	*Golgi phosphoprotein 3*
GRP1	*General Receptor for Phosphoinositides isoform 1*
GST	*Glutathione-S-Transferase*
HCA	*Human Carbonic Anhydrase*
HEPES	*N-(2-Hydroxyethyl)piperazine-N'-(2-ethanesulfonic acid)*
HPLC	*High performance liquid chromatography*
HRMS	*High Resolution mass spectrometry*
HRP	*Horseradish peroxidase*
IC_{50}	*Inhibitor concentration at 50% response*
IDA	*Indicator displacement assay*
IGFR	*Insulin growth factor receptor*
IP_3	*Inositol (1,4,5) triphosphate*
IP_4	*Inositol (1,3,4,5) tetraphosphate*
IPTG	*Isopropyl β-D-1-thiogalactopyranoside*
IR	*Infrared*
IRS	*Insulin receptor substrate*
kDa	*kiloDaltons*
LB	*Lysogeny broth*
MHz	*Megahertz*
mTOR	*Mammalian target of rapamycin*
mTORC2	*Mammalian target of rapamycin complex-2*
NMR	*Nuclear magnetic resonance*
OCRL	*Oculocerebrorenal Syndrome of Lowe*
OMF	*Ortho-methyl fluorescein*
OMFP	*Ortho-methyl fluorescein phosphate*
P4M	*PI(4)P bindingof SidM/DrrA*
PBS	*Phosphate buffered saline*
PC	*Phosphatidylcholine*
PDK1	*Phosphoinositide dependent kinase 1*
PDZ	*Postsynaptic density 95, disk large ,zonula occludens*
PFA	*Paraformaldehyde*
PHDM	*Pleckstrin Homology Domain mimetic*
PI(3)P	*Phosphatidylinositol 3-phosphate*

PI(3,4)P$_2$	*Phosphatidylinositol (3,4) bisphosphate*
PI(3,4,5)P$_3$	*Phosphatidylinositol (3,4,5) trisphosphate*
PI(3,5)P$_2$	*Phosphatidylinositol (3,5) bisphosphate*
PI(4)P	*Phosphatidylinositol 4-phosphate*
PI(4,5)P$_2$	*Phosphatidylinositol (4,5)bisphosphate*
PI(5)P	*Phosphatidylinositol 5-phosphate*
PIP	*Phosphatidylinositol phosphate*
PLC	*Phosphoinositide phospholipase C*
PLCδ1-PH	*Phosphoinositide phospholipase C (delta-1 isoform) Pleckstrin Homology domain*
PPM	*Parts per million*
PROPPINs	*β-propellers that bind PIs*
PS	*Phosphatidylserine*
pSer 473	*Akt phosphorylated on serine residue 473*
PTB	*Phosphotyrosine binding*
PTEN	*Phosphatase and Tensin Homolog*
PTP-1B	*Protein Tyrosine Phosphatase-1B*
p-TsOH	*para toluenesulfonic acid*
PV	*Pyrocatechol violet*
PX	*Phox Homology*
RCF	*Relative centrifugal force*
RPM	*Revolutions per minute*
RTK	*Receptor Tyrosine Kinase*
SDS-PAGE	*Sodium dodecylsulfate- polyacrylamide gel electrophoresis*
SHIP	*Src-homology 2-containing phosphatase*
SopB	*A bacterial phosphoinositide phosphatase*
SYLF	*SH3YL1, Ysc84p/Lsb4p, Lsb3p and plant FYVE protein*
Synj1	*Synaptojanin 1*
TBST	*Tris-buffered saline with 0.1 % Tween-20*
TFA	*Trifluoroacetic acid*
TLC	*Thin layer chromatography*
Tm	*Melting point*
Tris	*2-Amino-2-hydroxymethyl-propane-1,3-diol*
UV-Vis	*Ultraviolet-visible spectroscopy*

List of Figures

Figures in Chapter 1

Figures in Chapter 2

Figures in Chapter 3

Figures in Chapter 4

Figures in Chapter 5

Figures in Chapter 6

Figures in Chapter 9

List of Schemes

Schemes in Chapter 2

Scheme 2.19: Addition of zinc acetate to ligand **13** forms complex **14**.

List of Tables

Tables in Chapter 1

Tables in Chapter 2

Tables in Chapter 3

Tables in Chapter 4

List of compounds

Synthesis and characterisation of these compounds is detailed in Chapter 7.

Compound **1**

Compound **2**

Compound **3**

Compound **4**

Compound **5**

Compound **6**
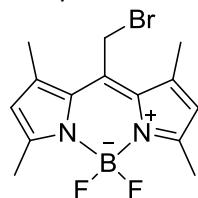
Compound **7**
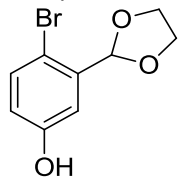
Compound **8**
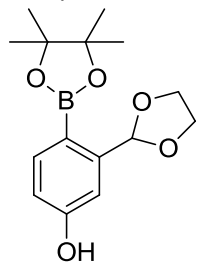
Compound **9**
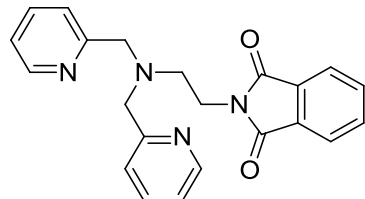
Compound **10**
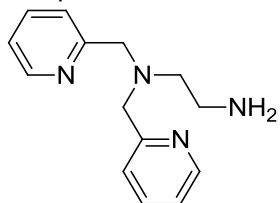
Compound **11**
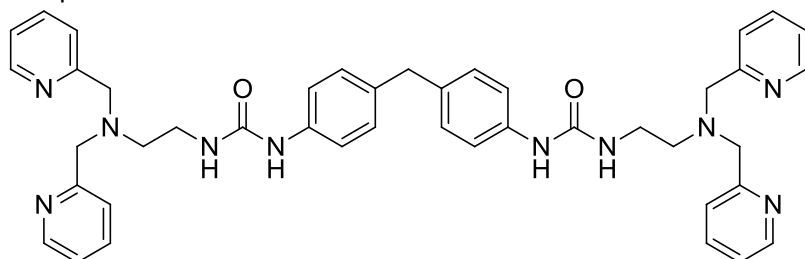
Compound **12**
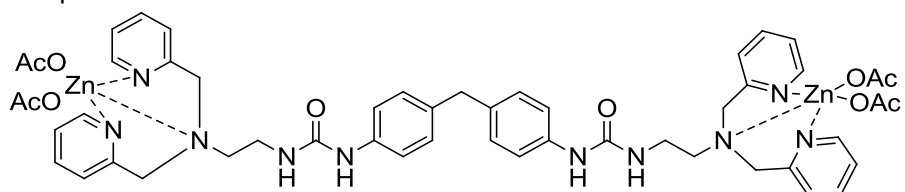
Compound **13**
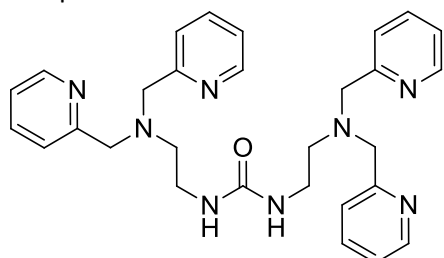
Compound **14**
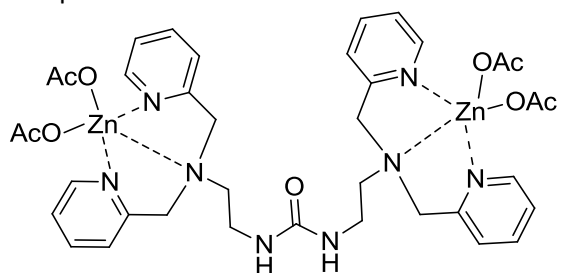
Compound **15**
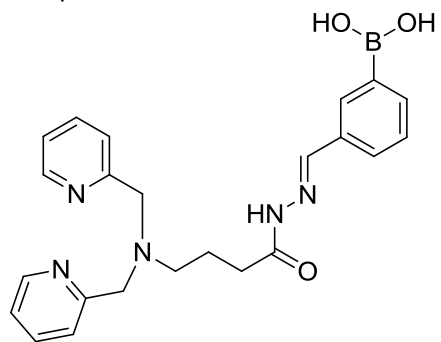
Compound **16**
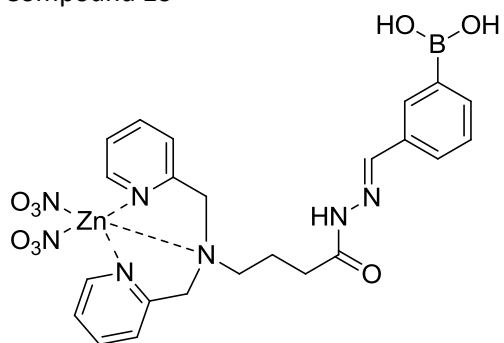
Chapter 1: Introduction

1.1 Phosphatidylinositolphosphates

Phosphatidylinositol phosphates (PIPs) are signalling molecules that consist of a long fatty acid tail (two hydrocarbon chains, one of which is saturated and the other polyunsaturated) which enables them to associate to cell membranes, and an inositol headgroup (a six-membered carbon ring) which resides in the cytosol. The headgroup is phosphorylated on the 3-, 4-, and 5-positions in seven different combinations (see Figure 1.1). These seven anionic phospholipids are a minor component of cell membranes, making up less than 1% of total lipids (*1*),(*2*); however they are vitally important in signal transduction and the regulation of membrane traffic (*3*).
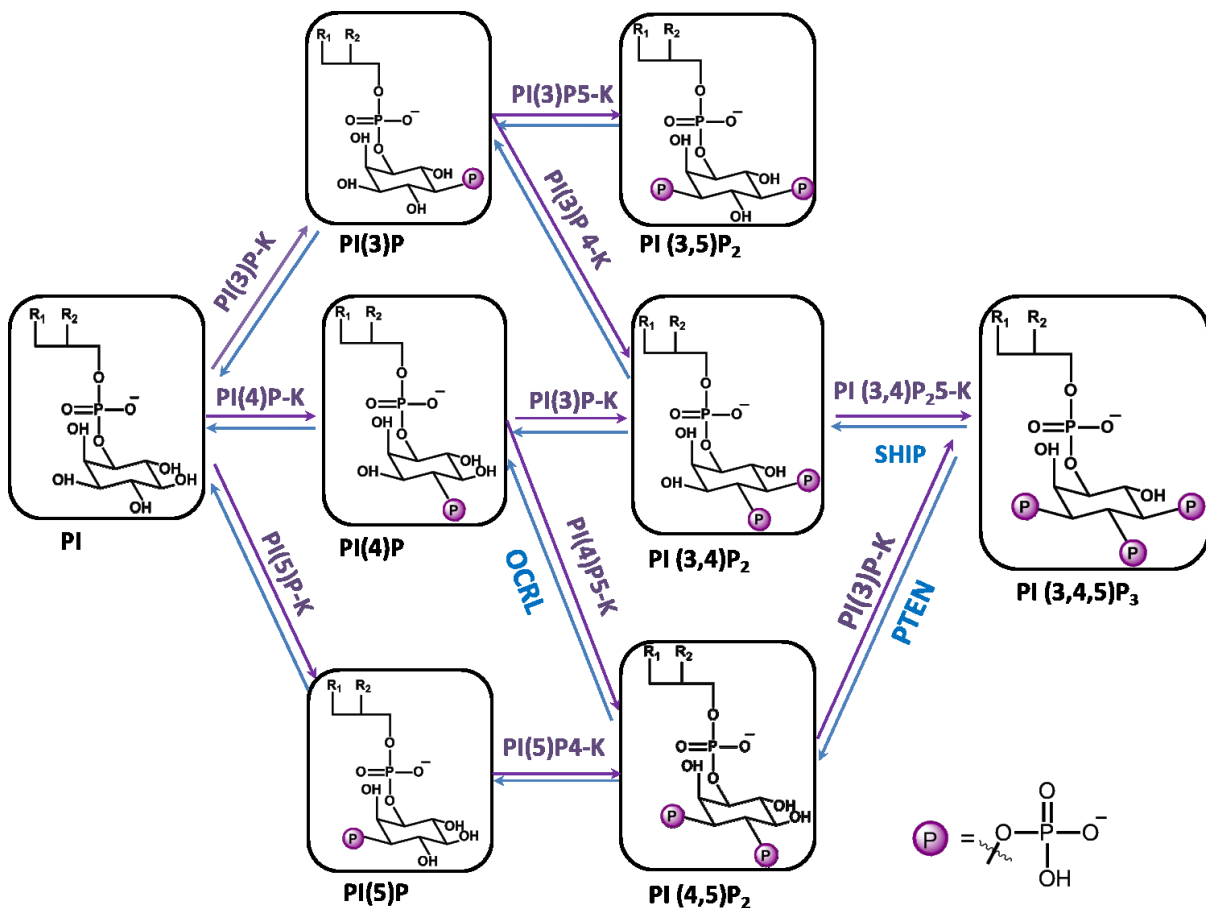
Figure 1.1: Seven phosphatidylinositol phosphates and the enzymes that interconvert them. PIP-Ks (Phosphoinositide kinases) are indicated in purple and phosphatases are shown in blue (OCRL = Oculocerebrorenal Syndrome of Lowe, a 5-phosphatase; PTEN = Phosphatase and Tensin Homolog, a 3-phosphatase; SHIP= SH2-domain containing Inositol 5-phosphatase). R_1 = 1-octadecanoyl; R_2 = 2 (5Z-, 8Z-, 11Z-, 14Z- eicosatetraenoyl).

Each PIP is mainly localised in a specific organelle- the main constitutive phosphoinositide pools are PI(4)P, which is present mostly in the Golgi, and PI(4,5)P_2 which is predominantly localised at the

plasma membrane (*3*),(*4*). As well as being heterogeneously positioned throughout the cell PIPs have a diverse set of functions; each PIP has a different repertoire of interacting proteins and therefore their influence in the cell is widespread.

1.1.1 PI(4,5)P$_2$ and PI(3,4,5)P$_3$

The headgroup of PI(4,5)P$_2$ is phosphorylated at the 4 and 5 positions as shown in Figure 1.2, with hydroxyl groups on the remaining carbons, while PI(3,4,5)P$_3$ has an additional phosphate group at the 3-position. The inositol rings are attached to diacylglycerol via a phosphodiester link. Both of these phospholipids interact with proteins that possess PH (Pleckstrin Homology) domains.
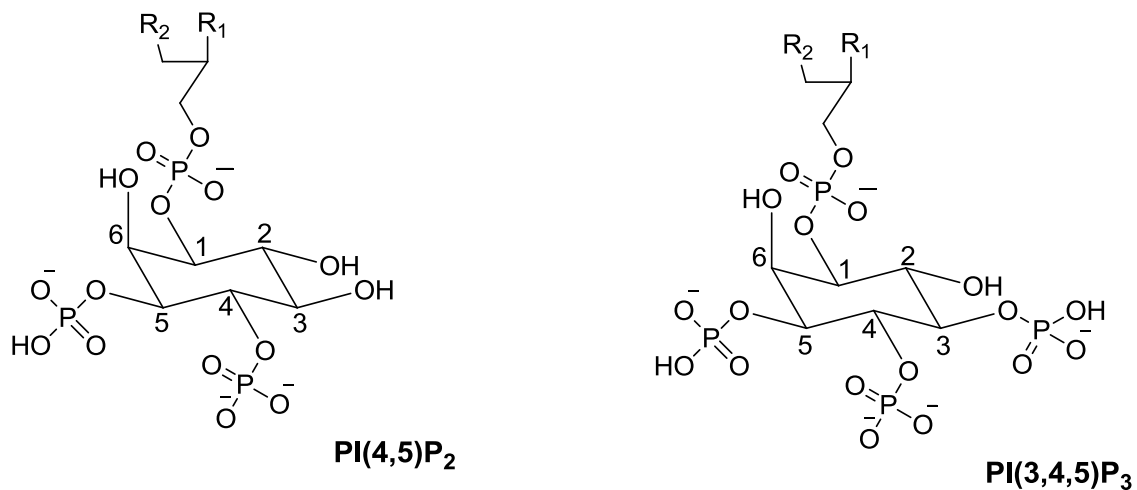
Figure 1.2: The structures of PI(4,5)P$_2$ and PI(3,4,5)P$_3$. R$_1$ = 1-octadecanoyl; R$_2$ = 2 (5Z-, 8Z-, 11Z-, 14Z-eicosatetraenoyl).

PI(4,5)P$_2$ is one of the most abundant phosphoinositides in the cell, existing at the inner leaflet of the plasma membrane. It is known to have roles in diverse cellular functions such as motility, endocytosis, actin regulation, calcium release and survival signalling (*5*). PI(4,5)P$_2$ is mainly generated by the 5-phosphorylation of PI(4)P which is the other major phospholipid component of cells (*6*). The 4-phosphorylation of PI(5)P can also form PI(4,5)P$_2$, although this is a minor contribution due to the low levels of PI(5)P in the cell. PI(4,5)P$_2$ levels can be depleted by 3-phosphorylation to generate PI(3,4,5)P$_3$, a process which is generally reversed by the 3-phosphatase PTEN (Phosphatase and Tensin Homolog), regenerating PI(4,5)P$_2$ (Figure 1.3) (*7*). Levels of PI(3,4,5)P$_3$ are very low in resting cells, and increase only for a short amount of time in response to stimulus (*3*).
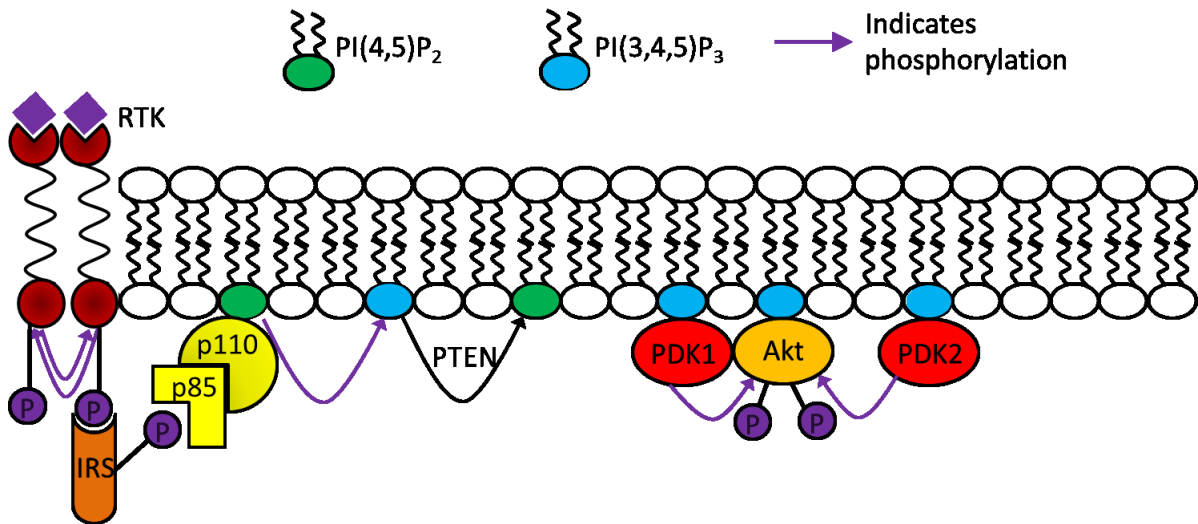
Figure 1.3: A signalling cascade is initiated by ligand binding to the extracellular domain of IGFR (insulin growth factor receptor). After transphosphorylation of intracellular components the receptor recruits PI3K (phosphoinositide 3-kinase) to the membrane via IRS (adaptor protein Insulin Receptor Substrate). PI3K converts PI(4,5)P$_2$ to PI(3,4,5)P$_3$ which recruits a number of proteins to the membrane, including PDK1 and PDK2 (Phosphoinositide dependent kinases 1 and 2). These kinases phosphorylate Akt at the Threonine 308 and Serine 473 positions respectively. Image reproduced from reference (8).

The binding of ligands (including insulin) to the extracellular components of IGFR (insulin growth factor receptor, a type of receptor tyrosine kinase, RTK) initiates dimerisation of the receptors (9). This process allows the cytosolic components of the receptor to come into close proximity to each other, and trans-phosphorylation of several tyrosine residues occurs (10). IRS-1 (insulin receptor substrate 1) interacts with these phosphorylated tyrosine residues via a PTB (phosphotyrosine binding) domain and is then phosphorylated by the cytosolic receptor component (11). The p85 (regulatory) subunit of PI3K (phosphoinositide 3-kinase) binds the phosphorylated tyrosine of IRS-1 via its Src Homology 2 (SH2) domain (which specifically recognises pTyr residues in certain peptide sequences (12)). When the p85 subunit binds IRS-1, PI3K is translocated to the membrane and there can phosphorylate PI(4,5)P$_2$ to PI(3,4,5)P$_3$ (13), (14).

The PI(3,4,5)P$_3$ thus generated recruits a number of proteins to the plasma membrane including Akt which is phosphorylated by PDK 1 and 2. While PDK1 (phosphoinositide-dependent kinase 1) has been shown to phosphorylate Akt at the threonine 308 residue, mTORC2 (mammalian target of rapamycin complex 2, identified as PDK2 (13)) phosphorylates Akt at the serine 473 residue (15).

1.1.2 PI(4,5)P$_2$- and PI(3,4,5)P$_3$-interacting proteins

Proteins interact with PIPs using specific PIP-binding domains; these bind via the inositol headgroup which is accessible at the membrane-cytosol interface. Many different protein domains have so far been identified (see Figure 1.4), and these have two general binding mechanisms (*16*).
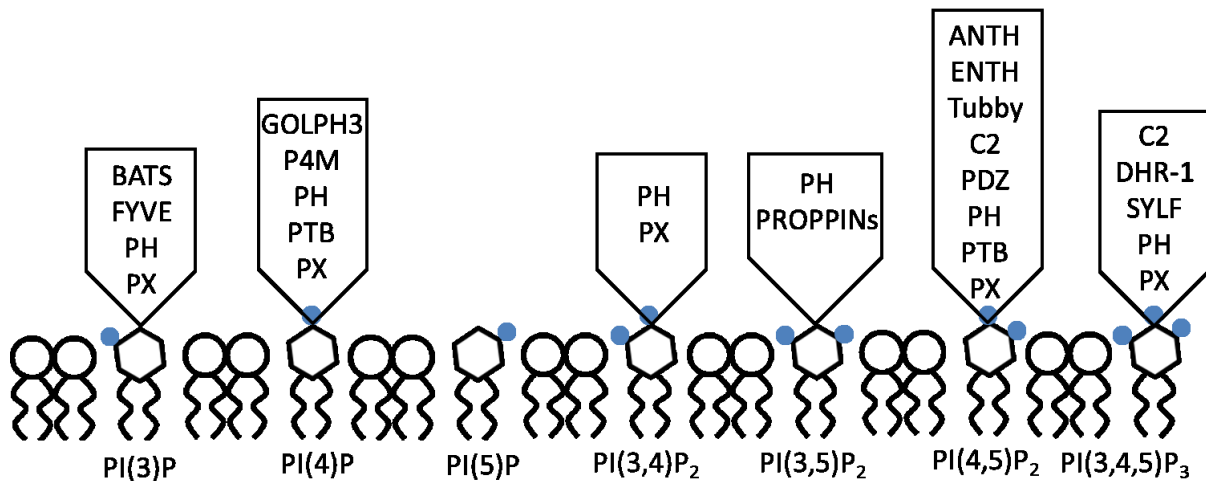
Figure 1.4: Several protein domains which directly interact with certain PIPs have been identified. PIP-metabolising enzymes and downstream effectors of PIP signalling use these domains to bind their targets. PH (Pleckstrin Homology) and PX (Phox homology) domains are used to bind a number of PIPs, while other domains have more specific interactions. BATS (Barkor autophagosome targeting sequence); FYVE (Fab1, YOTB, Vac1 and EEA1); GOLPH3 (Golgi phosphoprotein 3); P4M (PI(4)P binding of SidM/DrrA); PTB (Phosphotyrosine binding); PROPPINs (β-propellers that bind PIs); ANTH (AP180 N-terminal homology); ENTH (epsin N-terminal homology); C2 (conserved region-2 of protein kinase C); PDZ (postsynaptic density 95, disk large ,zonula occludens) DHR-1 (dock homology region 1), SYLF (SH3YL1, Ysc84p/Lsb4p, Lsb3p and plant FYVE protein) . Figure reproduced from reference (16).

Although phosphoinositides have low abundance, they are highly charged (*17*) and can attract a diverse range of proteins to the plasma membrane. They recruit proteins that have clusters of basic residues, which are protonated at physiological pH and therefore positively charged (*18*). Other proteins possess complex folded domains which form three dimensional structures in which residues are aligned for maximum interaction with the phosphate groups of the target phospholipid (*3*),(*19*). As indicated in Figure 1.4, the PH (Pleckstrin Homology) domain is used to bind to various PIPs, and is present in a number of proteins.

PLC (Phospholipase C) makes use of the PH domain to bind PI(4,5)P$_2$. PLC breaks the phosphodiester bond linking the headgroup to the fatty acid tails, generating inositol (1,4,5) trisphosphate (IP$_3$) and diacylglycerol. By co-crystallising the PH domain of PLC (PLCδ1-PH) with IP$_3$ Essen *et. al.* (*20*) and Lemmon *et. al.* (*21*) both showed that the protein binds IP$_3$ using a combination of electrostatic

interactions (via positively charged lysine residues) and multiple hydrogen bonds (between glutamine residues and hydroxyl groups; histidine and asparagine residues and phosphate groups). In addition, Lemmon *et. al.* determined the dissociation constant between isolated PLCδ1-PH domain and vesicles containing PI(4,5)P$_2$ to be 1.66 ± 0.80 µM (*21*) by means of isothermal titration calorimetry (ITC).

The PH domain of GRP1 (General Receptor for Phosphoinositides) is known to bind with high affinity and selectivity to PI(3,4,5)P$_3$. Amino acid residues interact with PI(3,4,5)P$_3$ via hydrogen bonding (in the case of tyrosine) and electrostatic interactions with protonated lysine residues. In contrast to the PLCδ1-PH domain, the GRP1-PH domain possesses two lysine residues which are positioned to bind to the 3'-phosphate. The binding affinity of GRP1-PH domain for IP$_4$ was determined to be 0.027 µM by means of ITC (*22*).

The GRP1-PH domain has a much higher affinity (approximately 60 times higher) for IP$_4$ than PLCδ1-PH domain for PIP$_2$ (*22*). GRP1-PH domain has 11 total interactions with IP$_4$ (*22*) while PLCδ1-PH domain has 9 interactions with IP$_3$ (as well as a number of indirect interactions via hydrogen bonding with water molecules) (*23*). IP$_4$ is more negatively charged than IP$_3$; in addition the GRP1-PH domain interacts via seven basic residues while PLCδ1-PH domain interacts via four basic residues. The electrostatic attraction between IP$_4$ and GRP1-PH domain should therefore be much stronger than that of IP$_3$ and PLCδ1-PH domain (*22*),(*23*).

These protein domains are commonly used as tools to probe and quantify their binding targets in *in vitro* assays (protein-lipid overlay assay (*24*), ELISA (enzyme-linked immunosorbent assay) (*25*)) and in microscopy techniques (*26*).

1.1.3 Phosphoinositides and disease

The lipids PI(4,5)P_2 and PI(3,4,5)P_3 are upstream of several complex signalling networks, and their levels determine the activation of these pathways. The lifecycle of the cell is controlled in this way and therefore it is no surprise that PI(4,5)P_2 and PI(3,4,5)P_3, and the proteins that act on them, have been implicated in a number of diseases including cardiac failure (*27*), Alzheimer's disease (*28*), bipolar disorder (*29*) and several types of cancer (*30*), (*31*) (Table 1.5).

*Table 1.5: Enzymes that metabolise PI(4,5)P_2 and PI(3,4,5)P_3 have been linked to human diseases. Reproduced from reference (*3*).*

Enzyme	Predominant Substrate	Product	Disease
Class I PI(3)Kinase	PI(4,5)P_2	PI(3,4,5)P_3	Cancer (*15*)
3-Phosphatase PTEN	PI(3,4,5)P_3	PI(4,5)P_2	Cancer (*32*),(*33*)
5-Phosphatase SHIP2	PI(3,4,5)P_3	PI(3,4)P_2	Type 2 diabetes
5-Phosphatase OCRL	PI(4,5)P_2	PI(4)P	Oculocerebrorenal Syndrome of Lowe (*34*)
Polyphosphoinositide phosphatase Synaptojanin 1	PI(4,5)P_2 and other phosphoinositides	PI(4)P	Bipolar disorder (*5*)

PI(4,5)P_2 is the substrate of several enzymes, among the most important are PLC; the 5-phosphatase OCRL1 (Oculocerebrorenal Syndrome of Lowe); and the previously mentioned PI3K(*35*),(*36*),(*23*). PI3K phosphorylates PI(4,5)P_2 on the 3'-position to generate PI(3,4,5)P_3. In response to PI(3,4,5)P_3, several proteins are recruited to the plasma membrane, including the kinases Akt and PDK1 (see Figure 1.2). Akt is activated by phosphorylation at the serine 273 and threonine 308 positions, and by attracting effector proteins, initiates a large number of signalling cascades which control cell growth and proliferation (*35*). PI(3,4,5)P_3 is rapidly dephosphorylated by phosphatases including PTEN, and the 5-phosphatase SHIP (Src-homology 2-containing phosphatase). PTEN effectively opposes the action of PI3K and negatively regulates downstream activation of the Akt pathway, regenerating PI(4,5)P_2. SHIP generates PI(3,4)P_2 which also interacts with Akt (*35*),(*37*) and has a unique set of effectors and functions (*38*).
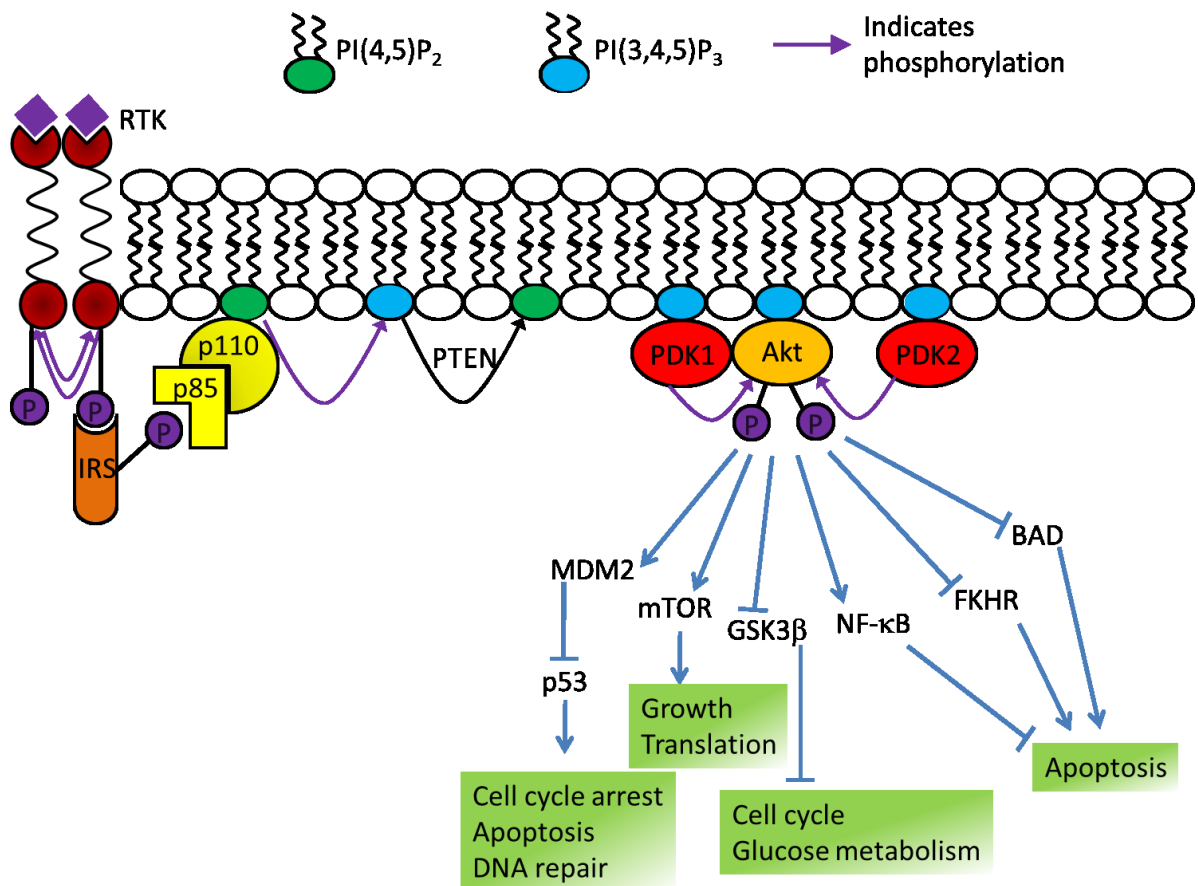
Figure 1.6: The PI3K-Akt signalling pathway. PI(4,5)P$_2$ is phosphorylated to PI(3,4,5)P$_3$, which recruits PDK1 and Akt to the plasma membrane. PI3K is represented as heterodimeric subunits p85 and p110 and regulates Akt-independent effectors SGK (serum and glucocorticoid-inducible kinase), RAC1 (Ras-related C3 botulinum toxin substrate 1) and CDC42 (cell division control protein 42), and PKC (protein kinase C). Akt phosphorylates a number of downstream proteins: MDM2 (Mouse double minute 2 homologue), mTOR (mammalian target of Rapamycin), GSK3β (glycogen synthase kinase 3 β), NF-$\kappa\beta$ (nuclear factor $\kappa\beta$), FKHR (Forkhead in human rhabdomyosarcoma; also known as FOXO1, forkhead box protein 01), BAD (Bcl-2-associated death promoter). These proteins control several aspects of the cell cycle, growth, translation, metabolism, DNA repair and apoptosis. Figure redrawn from reference (8).

These enzymes carefully maintain the balance of phosphoinositides in the cell. When the enzymes are downregulated or function improperly, the ratio of phosphoinositides changes. This imbalance can cause over- or underactivation of the subsequent signalling pathways, leading to disease states.

Overactivation of the PI3K-Akt pathway leads to uncontrolled cell survival and proliferation and is linked to many types of cancer (35),(31), (39),(8). One of the most prevalent causes of PI3K overactivation is the mutation of the gene encoding PTEN resulting in loss of its function. PTEN is a known tumour suppressor, and mutations are indicated in 80 % of patients with Cowden syndrome- a genetic disorder that predisposes individuals to multiple carcinoma and lesions (40). Somatic mutations of PTEN are also known to occur and are found in many instances of skin, brain and

prostate cancers (*30*),(*8*). PI3K is activated when insulin binds to insulin receptors. Levels of PI(3,4,5)P$_3$ increase and downstream effectors which control glucose transport and metabolism are activated (*41*). Akt is recruited to the plasma membrane by PI(3,4,5)P$_3$ and activated by phosphorylation, and subsequently returns to the cytosol and nucleus. Akt phosphorylates a number of downstream effectors, and one of these pathways promotes the uptake of glucose and synthesis of glycogen (*42*). In type II diabetes, tissues are insensitive to this pathway so that glucose uptake and glycogen synthesis are inhibited. It has been proposed that a drug mimicking PI(3,4,5)P$_3$ could promote these processes and therefore be a novel method of treating diabetes (*42*). Excess PI(3,4,5)P$_3$ in cells has also been linked to mood disorders and epilepsy, since drugs which treat these disorders inhibit PI(3,4,5)P$_3$ synthesis and downstream effectors are not recruited to the plasma membrane (*43*),(*44*). These disorders have been noted in individuals with PTEN mutations (*45*). An excess of cellular PI(3,4,5)P$_3$ can cause cancer and a range of neurological disorders, however a lack of PI(3,4,5)P$_3$ could have an effect similar to type II diabetes. Controlling PI(3,4,5)P$_3$ and its activation of Akt is therefore vital for treatment of a large number of diseases (*5*),(*36*).

The action of PLC removes the inositol headgroup from the associated lipid, generating inositol (1,4,5) triphosphate (IP$_3$) and DAG (diacylglycerol). IP$_3$ releases stores of intracellular calcium by interacting with IP$_3$ receptors (*46*) therefore activating calcium signalling pathways. Aberrant IP$_3$ signalling has been linked to diseases including bipolar disorder and epilepsy. Studies of the mechanism of action of three drugs commonly used in the treatment of both bipolar disorder and epilepsy indicate these diseases may be caused by abnormally high levels of IP$_3$ signalling (*47*). Although all three of the drugs tested have different uses and side effects, they all reduce levels of inositol and subsequently IP$_3$ in cells. One of these drugs (valproic acid) is also known to decrease cellular PI(3,4,5)P$_3$ levels and is being tested for treatment of colon and breast cancer (*43*).

The phosphatase OCRL1 removes the 5-phosphate from PI(4,5)P$_2$, generating PI(4)P. The gene for this enzyme is deleted in individuals with Lowe Syndrome, causing loss of function of the enzyme and elevated PI(4,5)P$_2$(*36*). Patients with this genetic disorder experience abnormalities in the eyes, brain and kidneys with symptoms including renal failure, mental retardation, cataracts, and behavioural problems; life span is shortened to less than 40 years (*48*). Deregulation of PI(4,5)P$_2$ affects endocytosis, the polymerisation of actin cytoskeleton and protein trafficking pathways; all of which are detected in Lowe syndrome sufferers.

Until recently, attention has mainly been focused on manipulation of PIP levels by attempting to selectively activate or inhibit the interacting proteins and enzymes (*39*),(*49*),(*50*),(*51*). However the significance of PIPs themselves has led to these signalling molecules being identified as potential

druggable targets towards potential treatment of the wide range of diseases mentioned in Table 1.2 (*52*),(*36*).

1.2 Control of PIP-protein interactions

$PI(4,5)P_2$ and $PI(3,4,5)P_3$ lie upstream of key signalling pathways. They activate these pathways by recruiting effectors to the membrane, which then interact with kinases and other proteins which propagate signals to other parts of the cell (*53*). Control of activation of these pathways is often achieved by inhibition of the downstream effectors, many of which are kinases. However the Akt pathway activates a diverse set of signalling cascades, and development of inhibitors for every effector is time-consuming. In addition, the signalling cascades are complex with activation occurring via several routes (*54*).

The ability to regulate PIP-controlled signalling by inhibition of protein-lipid interactions would be extremely beneficial in the examination of the mechanisms of many diseases, and $PI(4,5)P_2$ and $PI(3,4,5)P_3$ themselves have been identified as potential targets for therapeutic intervention (*36*),(*5*),(*55*),(*56*). In order to reduce the activation of downstream pathways, binding of effector proteins to PIPs must be prevented or reduced. This can be achieved by using small molecules to compete for binding to either the protein or the lipid.

Prevention of protein-PIP interactions has been shown to decrease the phosphorylation of Akt (which is often used as a measure of activation of this pathway). Inositol (1,3,4,5,6) pentakisphosphate (IP_5) was used to bind to the PH domain of Akt and thus stopped the recruitment of Akt to the plasma membrane- preventing its activation, which occurs only at the membrane (*55*). An inhibitor based on the structure of IP_5 also effectively competed with PH domains and in addition directly inhibited PDK1 (*57*). Recently it has been demonstrated that a small molecule inhibitor can be used to inhibit the interaction between $PI(3,4,5)P_3$ and $PI(3,4,5)P_3$-binding PH domains (*56*). This family of inhibitors prevented the recruitment of Akt to the plasma membrane and induced apoptosis in cancer cells.

Work carried out in our group has demonstrated that targeting the lipid $PI(4,5)P_2$ instead of its interaction proteins is another successful method of blocking protein-lipid interactions. By using a small molecule receptor with high affinity and selectivity for $PI(4,5)P_2$, protein-lipid interactions were inhibited and Akt was not recruited to the plasma membrane. A number of $PI(4,5)P_2$-dependent processes were also inhibited, including transferrin endocytosis and formation of actin stress fibres (*58*).

1.3 Artificial and Biological receptors

Small molecule artificial 'receptors' are often used to bind to biological species. Although many means already exist for molecular recognition of biological molecules (for example, an antibody which recognises a specific protein; a protein which recognises a specific phosphoinositide), the use of synthetic receptors has many advantages. They can be much more resistant to changes in temperature and pH than proteins, with a longer shelf life and higher stability. Their structure is often more easily modified than that of proteins so that reporter groups such as fluorophores can be readily incorporated. Many other properties can be tuned including lipophilicity which often enhances cell uptake. Once inside the cell, artificial receptors can act on its native state without the need to overexpress any proteins.

Synthetic receptors can use any of a large number of functional groups to bind their target. By arranging several binding motifs around a molecular scaffold, these receptors can be designed and synthesised to achieve even stronger binding than protein domains, and selectivity can often be tuned to the target molecule. Artificial receptors can be used to mimic their biological counterparts for the purpose of detection of their target molecule, as well as inhibiting protein-substrate interactions.

Table 1.7 summarises a number of current artificial receptors for biological molecules. Their applications vary from enzyme inhibition, to inhibition of protein-lipid interactions, to recognition of biomarkers of disease.

Table 1.7: Substrates and their biological and chemical receptors

Substrate	Biological receptor	Chemical receptor
Phosphorylated tyrosine residue of peptides. R_1 and R_2= polypeptides.	Src Homology 2 (SH2) domains	SH2 Domain Mimetic (*59*)
Saccharides including TF antigen disaccharide (*60*). R = protein anchor.	Lectins: carbohydrate-binding proteins	Boronolectins: Small peptides with boroxole side chains. R= any amino acid. (*60*)
Insulin (*61*)	Transmembrane insulin receptor	Cucurbit[7]uril (*62*)
ATP (as part of tRNA complex) (*63*) (*64*)	tRNA synthetases	AN2690 (*63*) (*64*)

1.4 Phosphate and polyhydroxy recognition by artificial receptors

The recognition of anions such as phosphate in aqueous media is a challenging area (*65*). It is extremely relevant to biological systems since over 70% of vital substrates and cofactors *in vivo* are negatively charged and many are phosphorylated (*66*). Hence artificial receptors that interact with anionic species are potentially useful as tools to probe chemical species in the cell.

There are several reasons why the recognition of anions in aqueous conditions remains a challenge. Firstly, in aqueous solution ions are surrounded by an organised layer of water molecules, arranged to minimise the effective charge. In order to bind to anions, these solvation layers need to be disrupted. Any receptor binding to an anion in water will therefore increase the overall entropy of the system as the ordered solvation layer is decreased. Secondly, anions are generally larger than their isoelectronic cations. The charge is diffused over a greater area; hence the charge density is lower, so electrostatic interactions are generally weaker. While inorganic cations are generally small and spherical in shape, anions possess several different geometries. It is therefore necessary to design different receptors based on the shape of the target anion, which can be beneficial for creating a receptor with selectivity for one anion over another. Thirdly, many oxyanions are protonated at low pH. This affects both the net charge and the hydrogen-bonding properties of the anion, so the pKa of the anion and the pH of the surrounding environment must be taken into account when anion receptors are designed.

Receptors for anions can be separated into three broad classes: neutral, which depend mostly on hydrogen-bonding, dipole and π-π interactions; charged, which bind via electrostatic interactions; and metal-based, which make use of metal-anion coordination. In other receptors, metal ions are coordinated but have roles other than binding, including structural or reporter functions. Boronic acids are also increasingly being used as anion-binding motifs, since they are Lewis acids and can therefore accept pairs of electrons from Lewis bases.

1.4.1 Neutral anion receptors

Most neutral anion receptors use multiple hydrogen bonds and other weak interactions to bind to their targets. Functional groups such as amides (*67*), thioureas (*68*) and ureas (*69*) are often employed as hydrogen bond donors and acceptors, and can be arranged around a scaffold to complement the structure of the target anion.
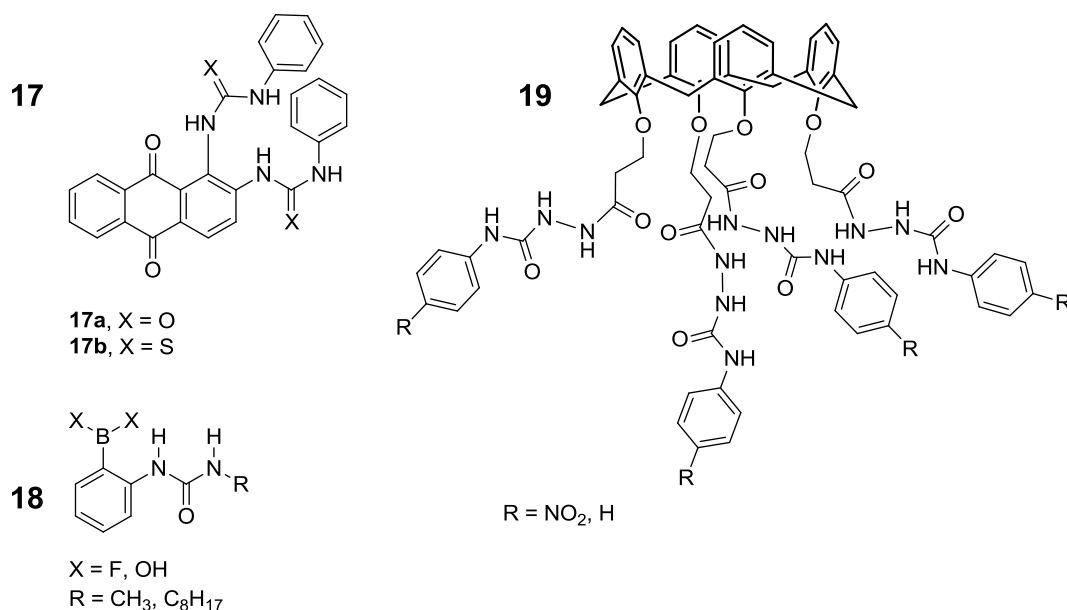
Figure 1.8: Selected examples of neutral receptors for anions (70), (71), (72) .

Figure 1.8 shows three examples of anion-binding receptors which interact with anion targets including phosphate via hydrogen bonding. Hydrogen bond donor groups include thiourea and urea (Receptors **17** and **18**) and amidourea (Receptor **18**). These receptors were shown to interact strongly with oxyanions including acetate and phosphate, however the binding studies in each case were not carried out in an aqueous environment. Dimethylsulfoxide (DMSO) was used as solvent which is aprotic and therefore possesses no hydrogen bonding groups which would compete with the anions. When carried out in protic or aqueous environments, receptors which make use of hydrogen bonding to interact with their target often have very low binding affinities.

1.4.2 Charged anion receptors

Polyamine compounds are often used in anion receptors. They can act as hydrogen bond donors and since they are often protonated at physiological pH, possess a positive charge which can attract anions. Ammonium (*73*),(*74*) and guanidinium (*75*),(*76*) functional groups are often used in this way to successfully bind anions. Electrostatic interactions are less affected by the presence of polar water molecules and therefore these receptor-anion interactions often have a higher binding affinity than neutral receptors. While hydrogen bonding interactions are linear and directional, electrostatic interactions are not, hence those receptors utilising charges are often even more pre-organised than their hydrogen-bonding counterparts. The use of protonated amines and guanidiniums is advantageous because of the presence of hydrogen bond donors and positive charge, both properties which attract anions.
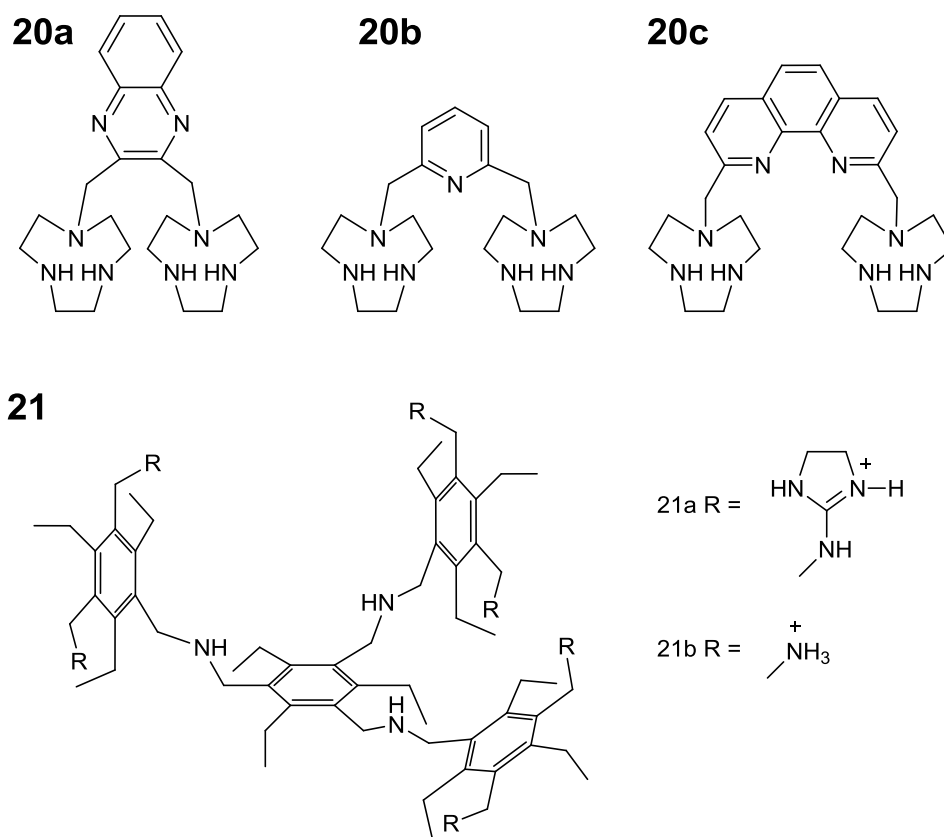
*Figure 1.9: Polyamine receptors **20**a-c bind phosphate anions and can differentiate between ATP, ADP and AMP (74). Tripodal receptors **21**a and **21**b also bind phosphate anions via guanidinium groups (**21**a) and ammonium groups (**21**b) (76). Neutral forms of amines shown.*

Receptors **20a** - **20c** (Figure 1.9) were designed by Bencini *et. al.* in order to probe the effect of cavity size (i.e. distance between binding units) on selectivity of the receptors for polyphosphorylated targets (*74*). Receptors **20a**, **20b** and **20c** formed 1:1 complexes with monophosphate, diphosphate and triphosphate respectively, in aqueous conditions. Interestingly, **20c** which possesses the largest spacer length showed no binding interaction with the smallest anion, monophosphate. This indicates that the anions need interactions from both binding units are necessary to overcome interference from competing water molecules.

Trends observed in this work show that receptors with more protonated amines (and therefore more positively charged) bind their targets more strongly. In addition, protonation of the anion (less negatively charged) decreases the binding affinity. These protonation states, and therefore the binding constants between receptor and anion, are pH-dependent.

Receptors **21a** and **21b** (Figure 1.9) were designed by Anslyn *et. al.* to bind selectively the second messenger IP_3 (*76*). By creating a cavity which complements the size of IP_3 and using two guanidinium (**21a**) or ammonium groups (**21b**) to bind each phosphate, these receptors can bind IP_3 with high affinity. The shape of the receptor confers selectivity; each pair of guanidinium or

ammonium groups are preorganised for maximum interaction with their target. Both receptors bind IP$_3$ with a higher affinity than other polyphosphates including ATP.

The binding constants of **21a** and **21b** for IP$_3$ were similar: K$_a$ = 4.7 x 10^5 M^{-1} and 5.0 x 10^5 M^{-1} respectively. However upon addition of sodium chloride to the aqueous receptor, the binding affinity of **21b** for IP$_3$ decreased almost 10-fold, whereas that of **21a** remained unaffected. This outcome suggests that polyammonium-based receptors experience stronger nonspecific interactions (which can be overcome by the addition of counterions). The positive charge on guanidinium groups is more delocalised and the addition of counterions has little effect on the binding of IP$_3$ by **21a**.

1.4.3 Metal-based anion receptors

A third class of anion receptors are those that contain metal ions. The metal ions in these receptors can have a number of different functions:

- they may coordinate to the target anion (*77*);
- act as electrochemical reporters (e.g. in the case of ferrocenyl-containing receptors), as emissive or fluorescence quenching metal ions(*78*);
- and they may be used as structural scaffolds, arranging the accompanying ligand around the preferred geometry of the metal ion (*79*).

Such versatility means metal ions are commonly used in the design of anion receptors.

Polyamine motifs are often used as ligands to chelate metal ions such as copper (II), zinc (II), cadmium (II) or nickel (II) (*77*), among others. These d-block metal (II) ions are Lewis bases and therefore can accept a lone pair of electrons and form a dative bond with a Lewis acid such as an anion. This makes them very useful components of anion receptors. Figure 1.10 shows two ligands which are commonly used to chelate metal ions as part of anion receptors.
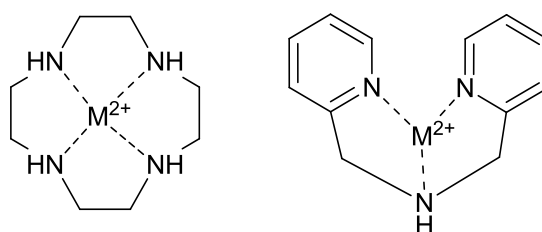
Figure 1.10: Ligands commonly used to chelate metal ions which are often incorporated into anion receptors. Left =1,4,7,10-tetraazacyclododecane (cyclen); right = 2,2'-dipicolylamine (DPA)

Van Eldik *et. al.* used receptor **22** (Figure 1.11) to bind to carbonate anions (*80*). The negatively charged oxygen in the anion bound to the Lewis acid zinc, forming a 5-coordinate metal species. The

zinc complex was found to catalyse the equilibrium between CO_2 and HCO_3^-, acting as a mimic for the enzyme human carbonic anhydrase (HCA).
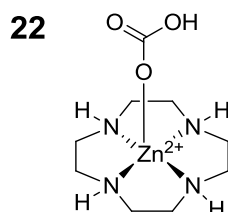
Figure 1.11: Receptor **22**, *a zinc (II) complex of cyclen, binds to the HCO_3^- anion, mimicking the active site of the HCA enzyme.*

One of the first receptors that made use of the M^{2+}-DPA motif was designed by Hamachi *et. al.* to bind phosphate anions in aqueous conditions (Figure 1.12)(*81*). By appending two Zn^{2+}-DPA moieties to anthracene, fluorescent receptors **23a** and **23b** were formed. Both experienced fluorescence enhancement in the presence of a phosphorylated peptide, while the presence of other anions (sulfate, nitrate, acetate, chloride, and carbonate) elicited little or no response indicating selectivity towards phosphorylated species.
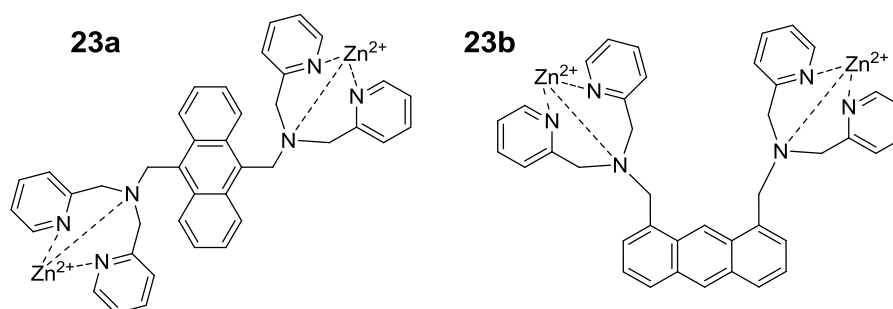
Figure 1.12: The first fluorescence turn-on receptors designed by Hamachi et. al. to bind to phosphorylated peptides.

Receptors **23a** and **23b** were later applied to a biological assay (Figure 1.13). Both receptors experienced fluorescence enhancement upon binding to a phosphorylated peptide which is a substrate for the Protein Tyrosine Phosphatase-1B (PTP1B) - but they do not bind to the dephosphorylated peptide, and the fluorescence intensity is low (see Figure 1.13). By monitoring the decrease in fluorescence intensity as the enzyme acts on the peptide, the enzyme activity can be monitored. In this case the metal ion is part of the anion-binding motifs and the fluorescent reporter group is the linker between these.
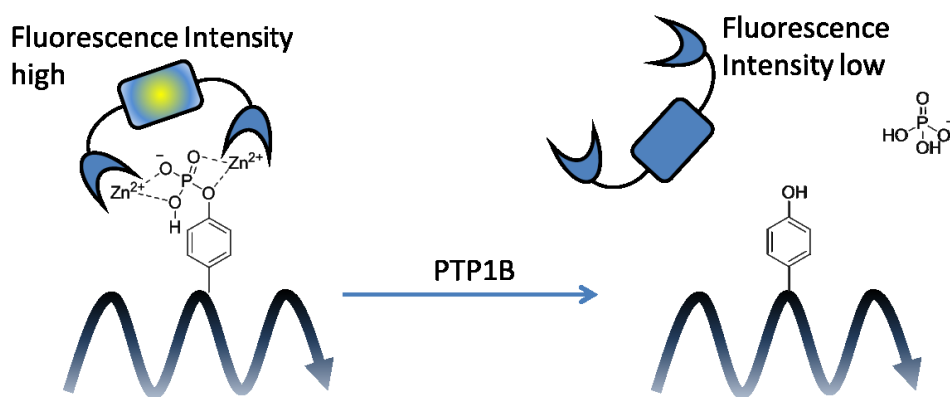
*Figure 1.13: Receptor **23** binds to a phosphorylated peptide with high fluorescence intensity. Upon dephosphorylation the receptor no longer binds and fluorescence intensity is low. This effect has been used by Hamachi et. al. to monitor the activity of this enzyme (82).*

The ability of these receptors to bind to phosphorylated peptides in water was an important step which allowed the receptors to be applied in a biological context. It is important to note that although **23a** and **23b** are water-soluble, the receptors were not present in the reaction solution. At each time-point, an aliquot of the reaction solution was taken and added to the receptor, and the fluorescence intensity was measured. Further work was carried out with these dizinc-DPA complexes including sensing of polyphosphorylated compounds (pyrophosphate, ATP and ADP) and disruption of protein-protein interactions (*83*).

In another application of zinc-DPA complexes, Hamachi *et. al.* appended four zinc-DPA groups to a pyrene-labelled dipeptide, with the aim of forming a cell-permeable complex with phosphorylated substrates. They found that the resulting zinc-DPA-phosphopeptide complexes showed enhanced uptake into HeLa cells relative to the uptake of the phosphopeptides alone (*84*). The uptake was inhibited in the presence of pyrophosphate ($H_2P_2O_7{}^{2-}$) which bound with high affinity to the zinc-DPA motifs, preventing formation of the zinc-DPA-phosphopeptide complex.

More recently the zinc-DPA motif has been used by Gunning *et. al.* to develop a series of synthetic receptors that mimic the Src Homology 2 (SH2) protein domain (*59*). SH2 domains are present in many kinases and signal transduction proteins, and bind specifically to phosphorylated tyrosine (pY). A library of small molecules was created with the aim of binding to the pY-containing peptide target, and thus inhibiting the protein-peptide interaction (the general structure of the library of compounds is shown in Figure 1.14). Each of the receptors possessed two zinc-DPA motifs which bind strongly to phosphate esters, as well as a second binding motif which was varied. The structure of the second binding site was based on amino acids which were capable of forming complementary hydrogen bonds and electrostatic interactions with the target peptide. Firstly the receptors were

shown to bind to fluorescently labelled peptides containing pY residues, and high affinity interactions were demonstrated. Six peptide SH2 domain targets were tested, and some receptors in the library (those which formed stronger electrostatic interactions with their targets) showed specificity for one peptide over the others. Cytotoxicity testing showed the library of receptors to have a range of toxicities against various cancer cell lines, and the authors attribute this to activity of the receptors in the cells: the receptors bind to their peptide targets and inhibit pY peptide-SH2 domain interactions.
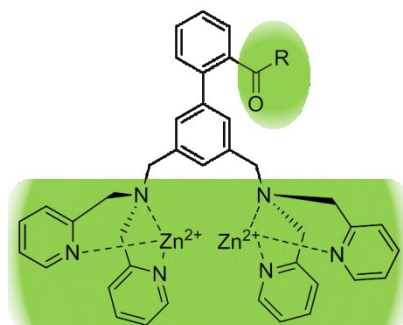
Figure 1.14: General structure of the receptors generated in the library by Gunning et. al.. Zinc dipicolylamine (zinc-DPA) motifs target the phosphate of phosphotyrosine. The R- group was optimised by the library with groups interacting with amino acids via electrostatic and hydrogen bonding interactions.

Metal complexes of DPA continue to be popular for anion binding, and phosphate binding in particular. They have been used as chemosensors (*81*),(*85*), as protein domain mimetics (*59*), for disruption of protein-protein interactions (*86*), and as fluorescent sensors to monitor the progress of a biological reaction (*87*); and their use in these and other applications has been thoroughly reviewed (*85*),(*87*),(*88*).

1.4.4 Boronic acid-based artificial receptors

Increasingly, boronic acids are also being used as anion recognition motifs. As Lewis acids they can accept lone pairs of electrons from anions such as fluoride, forming a tetrahedral boronate (Figure 1.15).
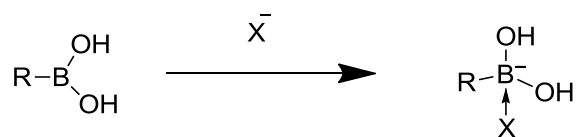
Figure 1.15: Anions donate pairs of electrons to Lewis acid boron. The neutral trigonal boronic acid becomes a tetrahedral boronate anion.

This interaction has formed the basis of several anion sensors (two of which are shown in Figure 1.16).
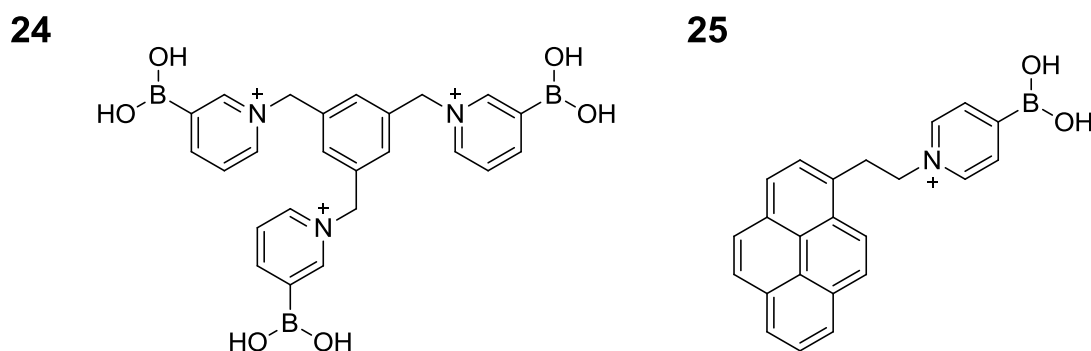
Figure 1.16: Left, Receptor 24 recognises cyanide anions in aqueous solution (89); Right, receptor 25 has been used as a fluoride detection sensor (90).

Receptor **24** was used in a sensing ensemble for the detection of cyanide anions. When **24** binds to the anionic fluorescent indicator 8-hydroxypyrene-1,3,6-trisulfonic acid trisodium salt (HPTS) the receptor quenches the fluorescence of the indicator. When cyanide anions (CN^-) are added they coordinate to the boronic acid of **24**, creating a negative charge. The indicator HPTS is released and the fluorescence is recovered. This sensing ensemble is selective for cyanide over other anions tested (Cl^-, Br^-, F^-, NO_2^-, CH_3COO^-, NO_3^-, I^-), none of which induced fluorescence recovery (*89*).

Receptor **25** underwent fluorescence enhancement in the presence of fluoride anions. When fluoride (F^-) was added, B-F-B bridges were formed which brought together two receptor molecules-enhancing π-π stacking and increasing the fluorescence. In this way the authors were able to reliably detect F^- concentrations as low as 0.1 ppm (*90*).

The most common use of boronic acids as recognition motifs is in the recognition of 1,2- and 1,3-diols. Carbohydrates are ubiquitous in biological systems and typically contain at least one diol motif; therefore artificial receptors for carbohydrates are of great interest. Boronic acids are extremely useful in this aspect as they form stable cyclic esters with diols in a reaction that is highly specific.
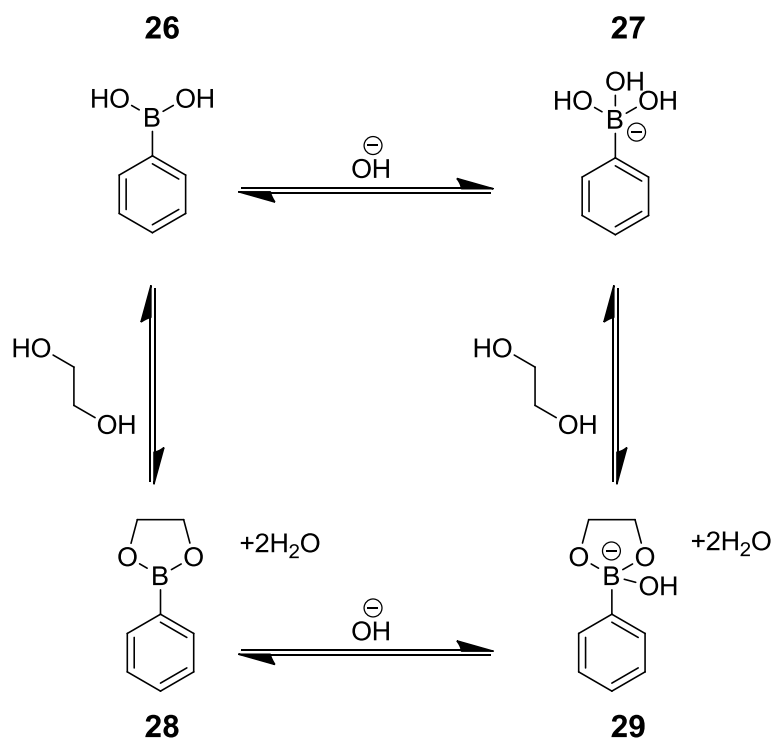
*Figure 1.17: Reaction of phenylboronic acid **26** with ethylene glycol forms trigonal cyclic ester **28**. The reaction of boronate **27** with ethylene glycol forms boronate ester **29**. The latter reaction is favoured at physiological pH.*

When boronic acids interact with 1,2-diols (aliphatic, aromatic or catechols) a 5-membered cyclic ester is formed (compounds **28** and **29** in Figure 1.17). This strong, reversible interaction is favoured when the pH is above the pKa of the boronic acid. The pKa of compound **26** is 8.8, while that of **27** is 6.8. Therefore at physiological pH compound **27** will undergo cyclisation in the presence of a diol, while compound **26** is less likely to do so.

A common method of forming tetrahedral boron compounds similar to **27** is to incorporate an amine group adjacent to the boronic acid as shown in Figure 1.18. The nitrogen can donate a lone pair of electrons to the boron, causing it to become tetrahedral sp^3 hybridised. These intramolecular dative bonds are a popular method of maintaining the tetrahedral boron to ensure the boronic acid is reactive at physiological pH (*91*).
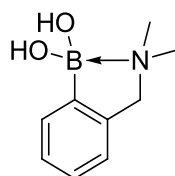
Figure 1.18: "Wulff-type" boronic acids incorporate a methylamino group adjacent to the boronic acid. By forming a dative bond from the nitrogen to the boron, the pKa of the boronic acid is lower and therefore interactions with diols are favoured at physiological pH.

Anslyn *et. al.* have reported a number of boronic acid-based receptors for carbohydrates and oligosaccharides such as heparin. Two of these are shown in Figure 1.19.
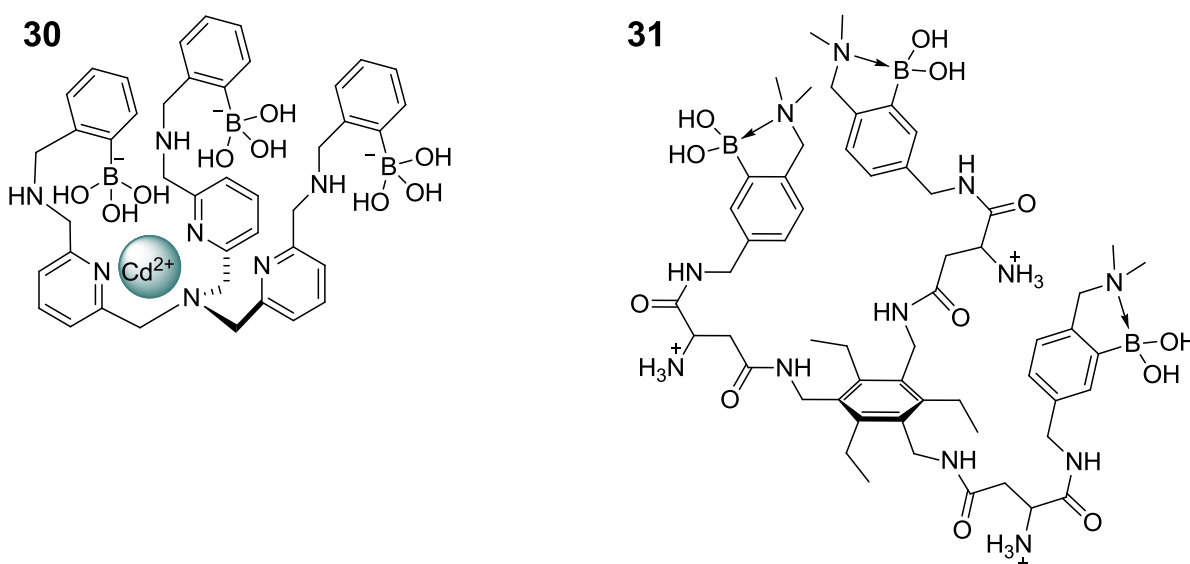
*Figure 1.19: Receptors **30** and **31** designed by Anslyn et. al. to bind carbohydrates(92),(93).*

Receptor **30** was used to bind various carbohydrates (*92*). The boronic acid groups interacted with the diols present on many carbohydrates, forming cyclic esters. The cadmium centre was present in order to coordinate to the nitrogen of the pyridine, which pulled the binding arms of the molecule together, creating a cavity that would fit the target molecules. The receptor was shown to bind with good affinity to several carbohydrate substrates.

Receptor **31** was designed to bind to heparin (*93*). This target oligosaccharide is comprised of repeating units of sulfated monosaccharides (iduronic acid and glucosamine). Receptor **31** possesses positively charged ammonium groups which interact with sulfate, and boronic acids which form cyclic esters with diols commonly present in carbohydrates. Using these two methods of interaction the receptor was shown to bind to heparin with good affinity. More importantly

receptor **31** displayed good selectivity for heparin over other oligosaccharides which lacked the negative charge of heparin. Using two modes of interaction enabled the authors to create a receptor with good affinity and selectivity, generating a chemical receptor that has potentially useful applications in molecular recognition of biomolecules (*93*).

Due to their Lewis acid nature boronic acids and their cyclic counterparts- boroxoles- have also been shown to interact with the nucleophilic side chains of amino acids, including lysine, serine and histidine (*94*),(*95*),(*96*). These side chains donate electrons to the boron and a dative bond is formed. This binding property has been used in the synthesis of enzyme inhibitors. Artificial enzyme substrates have been formed by incorporating boronic acid or boroxole moieties onto the natural substrate molecule. When the substrate entered the enzyme active site, the boronic acid formed a strong bond to the amino acid residues (see Figure 1.20) (*97*). This prevented the inhibitor from leaving the active site and in some cases disrupted the catalytic triad; the enzymes could no longer function (*96*).
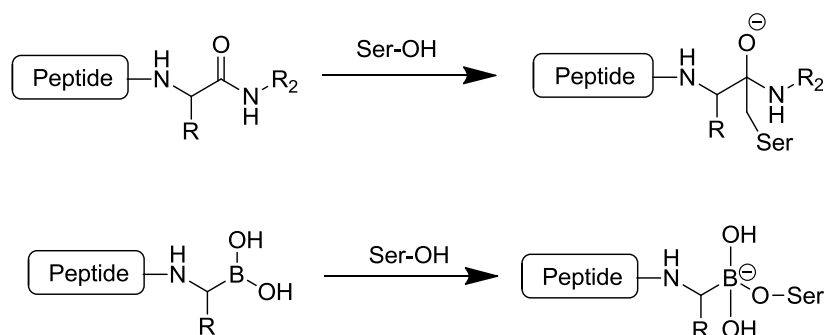
Figure 1.20: Boronic acids can inhibit enzymes which rely on a serine residue in the active site. Top: the first step in the mechanism of action of serine proteases. Bottom: a boronic acid is appended to the peptide substrate and on entering the enzyme active site, the boronic acid forms a dative bond with the OH of the catalytic serine residue, inhibiting the enzyme (98).

The most successful example of a boronic acid-based enzyme inhibitor is the proteasome inhibitor PS-341, now approved by the FDA and marketed as the anti-tumour drug Velcade (structure shown in Figure 1.21) (*99*). This small molecule is based on a dipeptide motif and specifically inhibits the ubiquitin-proteasome pathway, leading to a buildup of intracellular proteins which promote cell death (*100*).
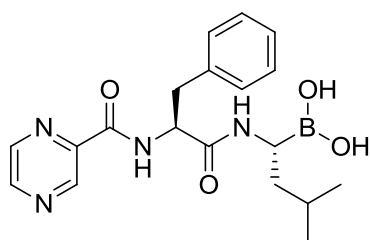
Figure 1.21: The proteasome inhibitor Velcade.

Velcade functions by binding to a threonine residue in the active site of the 26S proteasome, forming a tetrahedral adduct with the side chain hydroxyl group (*101*). Based on a dipeptide scaffold, it is selective for the 26S proteasome over serine proteases which favour tripeptide substrates.

1.5 Binding to Phosphoinositides and Inositol Phosphates using artificial receptors

1.5.1 Binding to IP$_3$

There are very few examples of synthetic receptors for IP$_3$, the headgroup of PI(4,5)P$_2$. Most of these use a tripodal 1,3,5-substituted phenyl scaffold (see Figure 1.22), creating a binding cavity which complements the size and shape of the inositol phosphate target. These receptors are usually selective for inositol phosphates over other biological phosphates; however in many cases the selectivity between various inositol phosphates has not been examined. Changing the binding motif can have large effects on the affinity of the receptors for IP$_3$, while changing the scaffold can alter the selectivity.
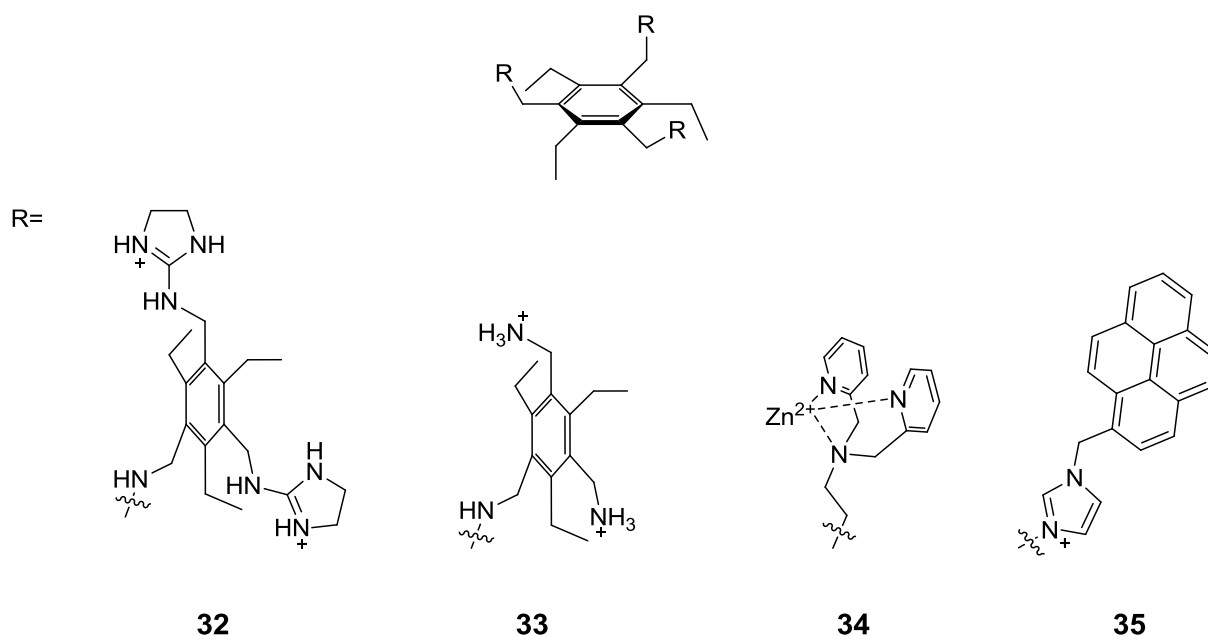
*Figure 1.22: Four tripodal receptors for IP$_3$ using various binding motifs. Guanidinium and ammonium receptors **32** and **33** synthesised by Anslyn et. al. (76); zinc-DPA receptor **34** by Anh et. al. (102), (103), and imidazolium receptor **35** by Yoon et. al. (104).*

The receptors designed by Anslyn *et. al.* used the same type of interactions as the PLCδ1-PH domain to interact with IP$_3$, namely charged primary amines similar to the protein's lysine side chains, and guanidinium groups to mimic the arginine side chains (*76*). Arranging these around a central benzene unit creates a cavity which complements the size of IP$_3$, and the cationic binding motifs are placed such that they interact strongly with the anionic phosphate groups of IP$_3$.

By using indicator displacement assays (IDAs) to assess binding affinity these receptors were shown to bind strongly to IP$_3$ (K$_a$ = 4.7 x 10^5 M^{-1} for **32**; K$_a$ = 5.0 x 10^5 M^{-1} for **33**) and the

hexaphosphorylated IP_6. Although other inositol phosphates were not tested, the receptors showed good selectivity for IP_3 (**32** and **33**) and IP_6 (**32** only) over other anionic biological analytes including ATP and fructose diphosphate.

 Ahn *et. al.* developed a receptor for IP_3 and IP_6 which comprised three metal-chelating dipicolylamine motifs (*102*), (*103*). Using this metal-based phosphate binding motif produced receptors with a much higher affinity for inositol phosphates in aqueous solutions (K_a (IP_3) = 4.6 x 10^8 M^{-1} for **34**).

More recently Yoon *et. al.* designed two fluorescent IP_3 receptors using imidazolium groups as the recognition motif (**35** and **36**); these receptors were thoroughly examined for selectivity between inositol phosphates. The tripodal receptor **35** was shown to bind weakly to various inositol phosphates (IP_4, IP_5 > IP_3, *scyllo*-IP_3, IP_6 > IP_2, IP) with little selectivity observed. However by changing the scaffold, receptor **36** (Figure 1.23) showed much stronger binding to IP_3 than to any of the other inositol phosphates (*104*).
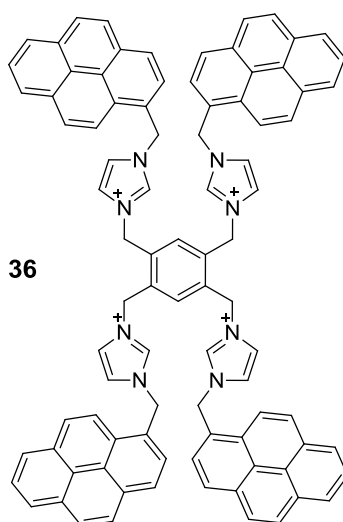
*Figure 1.23: Yoon et. al.'s fluorescent IP_3-selective receptor (104). K_a (IP_3) **35**= not reported; K_a (IP_3) **36**= 1.6 x 10^5 M^{-1}.*

The careful arrangement of binding motifs around the central phenyl led to the development of a receptor with remarkable selectivity for IP_3 over other inositol phosphates, which its tripodal counterpart lacks.

Another early receptor that was designed to bind IP_3 made use of a central ruthenium, around which cylen-appended N,N'-bipyridyl (bipy) ligands were assembled (*105*). When zinc(II) was coordinated to the cyclen motifs, a receptor with six phosphate-binding motifs was generated. By examination of the crystal structure of receptor **37** (see Figure 1.24) with the IP_3 analogue *cis,cis*-1,3,5-

cyclohexanetriphosphate (CTP$_3$) the authors showed that the receptor was capable of binding to two CTP$_3$ molecules simultaneously via the three phosphate groups.
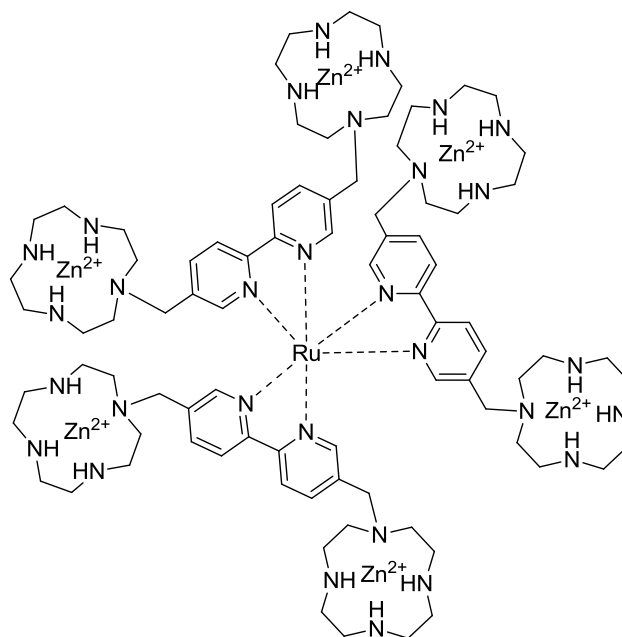
*Figure 1.24: Receptor **37** designed by Kimura et. al. to bind IP$_3$ (105).*

Due to the central ruthenium(bipy)$_3$, this receptor showed emissive properties which were enhanced upon binding to CTP$_3$ and IP$_3$. This enhancement was not observed on addition of mono- and di-phosphates, showing that **37** is selective for triphosphorylated species. Interestingly, chiral guest molecule IP$_3$ was shown to bind less strongly than achiral guest CTP$_3$ due to the supramolecular orientation of the binding arms.

Although few synthetic receptors for IP$_3$ have been developed, many exist for carbohydrates such as glucose which are structurally similar to inositol (*93*),(*92*),(*106*). It is well established that boronic acids are useful motifs for binding carbohydrates, since boronic acids form cyclic esters with 1,2-diols. It is therefore surprising that none of the synthetic IP$_3$ receptors designed thus far make use of this interaction since IP$_3$ possesses two adjacent hydroxy groups at the 2- and 3-positions.

1.5.2 Previous work towards IP$_3$ receptors from our group

Previously in our group work was carried out towards the design of a small artificial receptor which would bind to IP$_3$ (*107*). A series of molecules were designed which incorporated functional groups which would interact with the groups present on IP$_3$ (Figure 1.25). Neutral urea groups were chosen to interact with phosphate via hydrogen bonding. Although neutral receptors which interact via hydrogen bonds often have poor affinity for anions in an aqueous environment, the binding affinity is often improved with the use of multiple urea motifs, especially when combined with other functional groups (*69*), (*108*). A boronic acid motif was chosen to recognise the vicinal alcohol groups, due to the strong and specific nature of the boronic acid-diol interaction. In addition, boronic acids are not naturally occurring functional groups and therefore have no competing counterpart in cells.

These functional groups were connected via a range of spacers with varied length and flexibility, with some aromatic and some aliphatic.
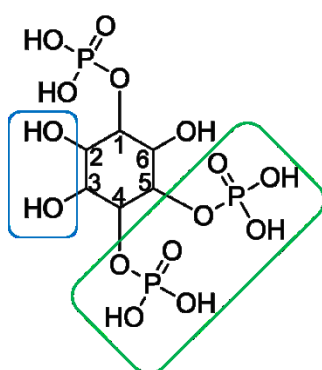
Figure 1.25: The structure of IP$_3$. Phosphate groups are present on the 1, 4 and 5 positions of the ring, with a hydroxy group on the other positions. The phosphates of 4 and 5 (highlighted in green) were targeted using urea groups and the diol present on the 2,3 positions was targeted by boronic acid motifs.

By synthesising the central bisurea compounds without the boronic acid groups present, the ability of the urea groups to bind vicinal phosphates (using the target molecule cyclohexane 1,2-bisphosphate, CBP, as a model for IP$_3$) was measured. This was achieved using ^{1}H NMR titrations in 2:3 D$_2$O,DMSO, following the changing chemical shift of the urea protons as the concentration of target molecule CBP was increased. Bisurea compounds with aromatic groups directly adjacent to

the urea showed higher binding affinities than those directly attached to aliphatic linkers, with the 4,4'-methylene biphenyl bisurea compound **47** (highlighted in red, Figure 1.26) possessing the highest binding affinity towards CBP (K_a around 10-fold higher than the compound with the second-strongest binding affinity).

Module	Association constant K_a with CBP (M^{-1})
38	101 ± 12
39	184 ± 14
41	283 ± 19
42	319 ± 23
43	3090 ± 41
44	1010 ± 38
45	5790 ± 36
46	6340 ± 43
47	11600 ± 81
48	191 ± 12
49	1110 ± 35

Figure 1.26: The structures of the bisurea modules synthesised previously in our group. The binding affinities of these compounds towards cyclohexane 1,2-bisphosphate were determined by ^1H NMR titrations in 2:3 D_2O, DMSO.

The receptors were then synthesised with added diboronic acid components, to bind to the diol of IP_3 (Figure 1.27). Their ability to bind IP_3 was indirectly analysed by means of a phosphatase assay. The 5-phosphatase OCRL dephosphorylates IP_3, and the release of phosphate can be measured. By binding to IP_3 and sequestering it, the receptors reduce the enzyme turnover and the amount of phosphate release is reduced. Receptor **54** possessed the lowest EC_{50}, which suggests that it has the highest affinity towards IP_3 (i.e. it requires less of receptor **54** to induce 50 % inhibition, than the other receptors).
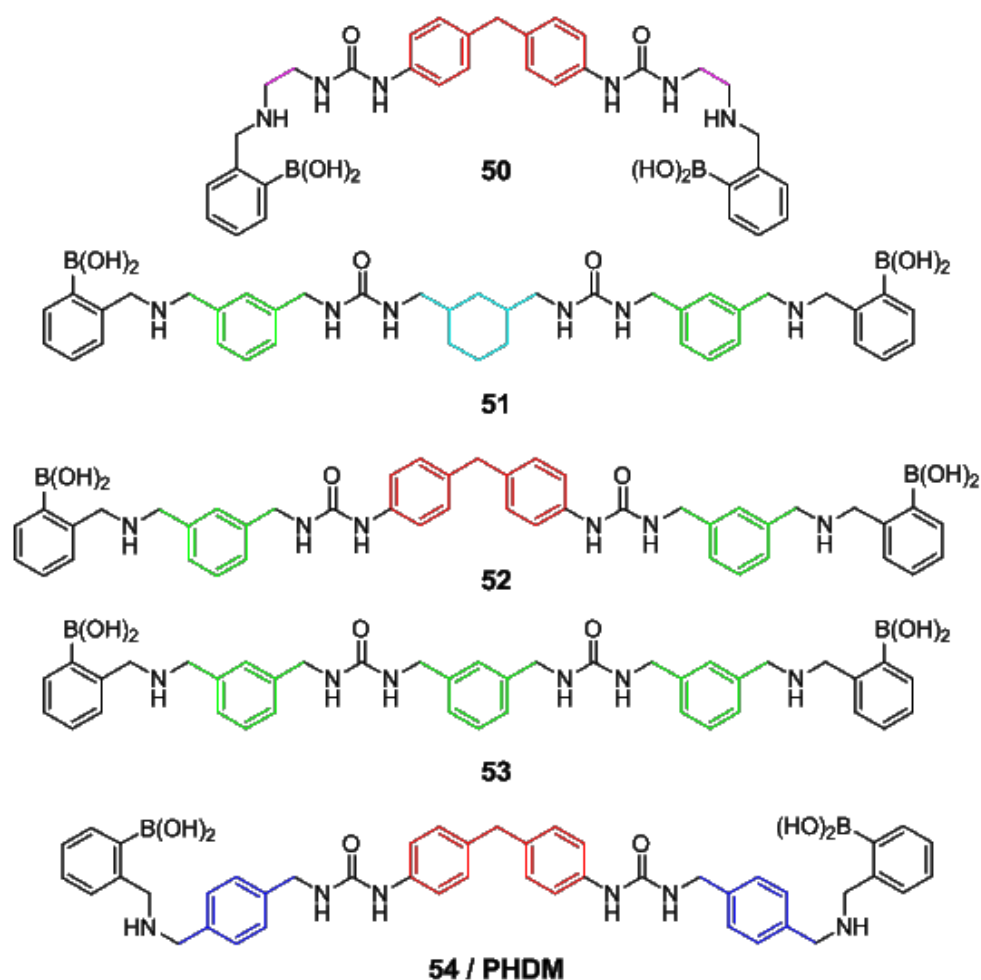
*Figure 1.27: Diboronic acid compounds **50**-**54** synthesised in our group as IP$_3$ receptors. Receptors were tested for ability to bind IP$_3$ using a phosphatase assay; EC$_{50}$ values indicated that compound **54** had the highest binding affinity towards IP$_3$, the substrate of 5-phosphatase OCRL.*

Receptors **50 – 53** were not further tested for ability to bind PI(4,5)P$_2$. Receptor **54** (later dubbed Pleckstrin Homology Domain Mimetic, PHDM, Figure 1.28) was demonstrated to bind most strongly to IP$_3$ and was therefore chosen to be resynthesized and tested further with a series of *in vitro* assays and cellular studies (*58*).
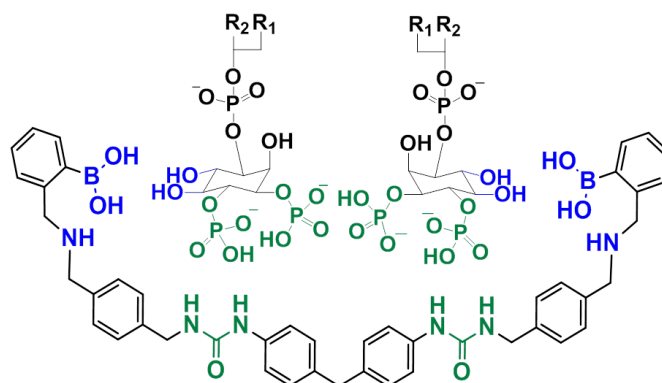
Figure 1.28: PHDM and PI(4,5)P₂, showing the proximity of the boronic acid to the vicinal alcohols, and of the urea to the phosphate groups. R1 = octadecanoyl. R2= 5Z, 8Z, 11Z, 14Z-eicosatetraenoyl.

PHDM was identified as having high affinity for the lipid PI(4,5)P$_2$ (K$_d$ = 17.6 ± 10.1 μM) as well as the corresponding IP$_3$ headgroup. In addition it was shown to bind much more strongly to PI(4,5)P$_2$ than to the other phosphoinositides, demonstrating considerable selectivity similar to that of the PLCδ1-PH domain. When considering that the PIPs are structurally very similar, this was a significant finding.

The biological activity of PHDM was then studied in NIH3T3 cells. After determining that the compound was not cytotoxic (up to 50 μM after 16 hours), cells which overexpressed GFP-tagged PLCδ1-PH domain were used to show that PHDM could compete effectively with this protein domain in the cell. The GFP-PLCδ1-PH domain binds to PI(4,5)P$_2$ and can be observed localised at the plasma membrane. When the cells are treated with PHDM, the fluorescence is displaced to the cytosol in a dose- and time-dependent manner as PHDM binds to PI(4,5)P$_2$ in place of the fluorescent protein domain. Other PI(4,5)P$_2$ dependent cellular processes including transferrin uptake and formation of actin stress fibres were disrupted by the presence of PHDM. Taken together, these findings indicate that PHDM is capable of entering the cell, binding to PI(4,5)P$_2$, and inhibiting protein-lipid interactions. It is therefore a powerful tool for the study of PI(4,5)P$_2$-dependent systems in the cell, and the many associated diseases.

1.5.3 Binding to PI(3,4,5)P$_3$

To date, no synthetic receptors have been developed specifically for either IP$_4$ or PI(3,4,5)P$_3$. The receptors (**32**-**34**) previously mentioned which were designed to bind IP$_3$ may also bind IP$_4$ (and other inositol phosphates) however only receptors **35** and **36** were examined for inositol phosphate selectivity. The zinc-DPA receptor **34** designed by Anslyn *et. al.* showed the highest binding affinity towards IP$_3$, likely due to the strong interaction between the zinc (II) and the anionic phosphate groups.

1.5.4 Previous methods used to design PI(3,4,5)P$_3$ receptors

One of the previous aims of this project included the use of a dynamic combinatorial library to generate a small library of receptors with the ability to bind PI(3,4,5)P$_3$. To this end, a small dynamic library of PI(3,4,5)P$_3$ receptors was formed. Dynamic combinatorial chemistry is a high-throughput means of identifying strong host-guest interactions, and has been employed as a tool in drug discovery, successfully identifying inhibitors for a number of enzymes and lectins (*109*),(*110*),(*111*),(*112*).

Dynamic combinatorial chemistry uses reversible interactions between monomers or 'building blocks' to generate a mixture of oligomers (*113*),(*114*) (Figure 1.29). The reversible nature of the interaction means that the formation of the most thermodynamically stable oligomers will be favoured. The library will reach an equilibrium state where the most stable oligomers will be present in higher amounts than those which are thermodynamically unstable. Addition of a guest molecule that binds to the oligomers (in this case, PI(3,4,5)P$_3$) will perturb the equilibrium, and the oligomer which binds most strongly to the templating molecule (generating the most thermodynamically stable host-guest complex) will be amplified at the expense of the other oligomers. Therefore there will be a greater amount of the amplified receptor in the mixture, and less of the other oligomers.

Mixture of monomers	Equilibrium distribution of oligomers	Addition of template causes re-equilibration

Oligomer which binds most strongly to template is amplified
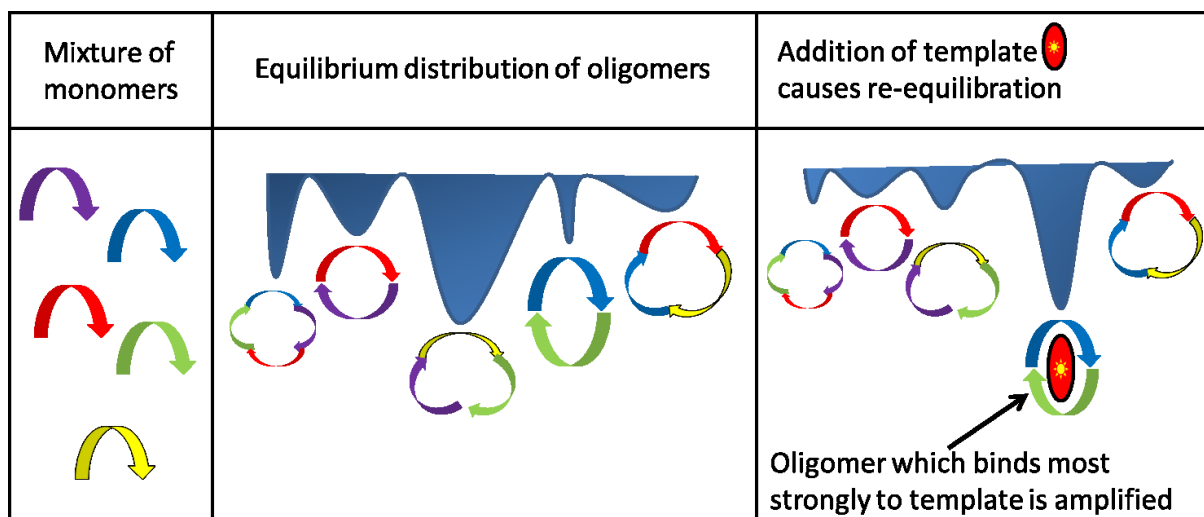
Figure 1.29: Principles of a dynamic combinatorial library. Monomers which reversibly react with each other form a mixture of oligomers. This mixture will reach an equilibrium distribution under a specific set of conditions. Upon addition of a templating molecule (which has the ability to bind to or interact with the oligomers), the equilibrium is perturbed, and the mixture will re-equilibrate. The oligomer which binds most strongly to the templating molecule will form the most thermodynamically stable complex, and therefore this oligomer will form at the expense of the others. Area in blue represents a free energy profile. Figure reproduced from reference (115).

The use of a dynamic library to screen for strong host-guest interactions must be carried out following a specific set of guidelines (*116*),(*117*). Briefly:

1. Building blocks reversibly interact with each other. Reversible covalent reactions (such as the formation of imines from aldehydes and amines) or specific noncovalent interactions (such as disulfide exchange or coordination chemistry) have been used in the past (*112*),(*118*),(*119*),(*120*).

2. The library of monomers must be free to reversibly interact with each other under the conditions of the library. For example, the use of imines is incompatible with aqueous conditions, since the presence of water will hydrolyse the oligomers and only a mixture of monomers will exist (*118*).

3. The library then needs to be 'frozen' in order to analyse the components. By quenching the reversible reaction (for example, irreversibly reducing imines to amines) the oligomers are then prevented from re-equilibrating so that their relative amounts may be quantified.

4. Analysis of the library must provide information on the quantity of each oligomer present. High performance liquid chromatography (HPLC) is often used for this purpose, since the area under the peaks for each compound is proportional to its amount. A disadvantage of the use of HPLC is that libraries with more components are more difficult to separate

effectively, and therefore it becomes more difficult to accurately quantify peak size. In addition, changes in peak size upon templating become more difficult to recognise (*121*).

In order to generate receptors for PI(3,4,5)P$_3$, a library was designed in which two phosphate-binding motifs would be joined by a spacer. Initial studies were carried out using a small library which would generate only four receptors, with the aim of expanding the library once proof of concept was established. Zinc-DPA was chosen as the phosphate-binding motif since dizinc-DPA receptors were previously shown to bind strongly to polyphosphorylated molecules. Four spacers with varied range and flexibility were chosen. Reversible imine formation was chosen as the reaction which would form the library. Imines form readily in anhydrous methanol, which PI(3,4,5)P$_3$ is also soluble in. The reversible reaction is rapidly quenched by the addition of sodium borohydride, allowing the resulting secondary amines to be quantified.

By allowing the primary amine to interact with the dialdehydes, an equilibrium mixture of imines was firstly established. After quenching the library was analysed by HPLC and the distribution of products was shown to be reproducible. The zinc-DPA was then mixed with individual aldehydes under the same conditions in order to identify the peaks in the library mixture.
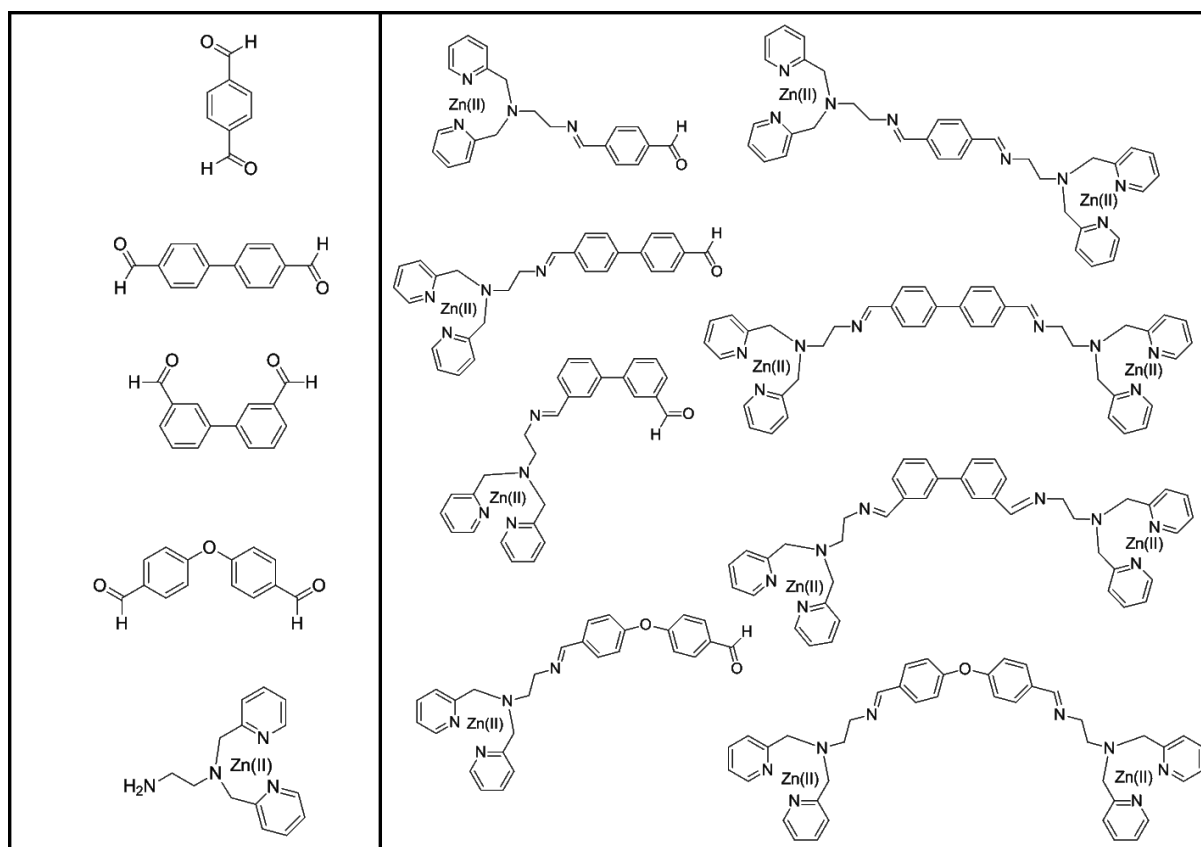
Figure 1.30: Left, four dialdehyde spacers and a primary amine attached to zinc-DPA, the phosphate recognition group. Right, the resulting mixture of imine products. Imines and diimines were observed in the equilibrium mixture (analysis by HPLC).

In the next stage, model polyphosphate compounds were applied to the library to perturb the equilibrium and in theory create a templating effect. Inositol hexakisphosphate (IP_6) was investigated, however it was insoluble in the methanolic mixture. Therefore after much optimisation the library was attempted in methanol with the template added under aqueous buffered conditions (final concentration of water present was 1 % v/v). Although the presence of water disfavours imine formation, it was shown that addition of IP_6 amplified the formation of one of the imine receptors. The library was then repeated using pyrophosphate as a smaller templating agent, and amplification of a different peak was then observed.
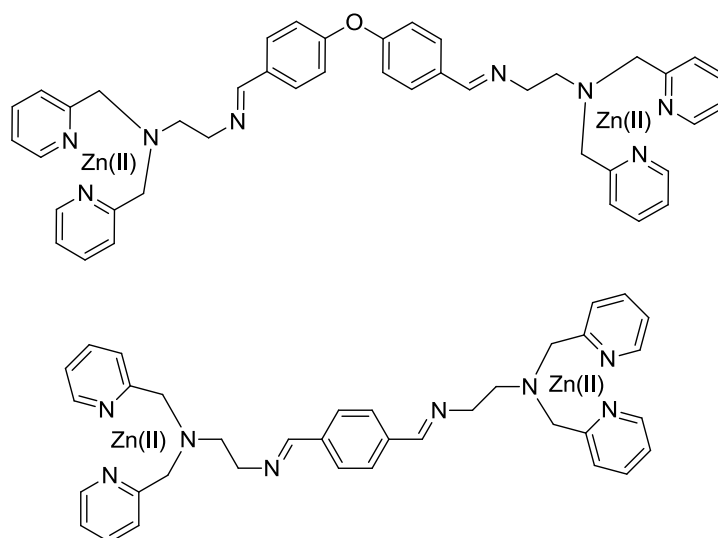
Figure 1.31: Top, imine amplified by addition of IP$_6$ to a dynamic library. Bottom, imine amplified by the addition of pyrophosphate to the same library.

The spacer of the receptor which was amplified by IP$_6$ was strikingly similar to that of PHDM which was demonstrated to bind strongly to PI(3,4,5)P$_3$. Using this information and the structure of PHDM, it was decided that the design of the PI(3,4,5)P$_3$ receptor would be based partly on the central spacer of PHDM, and include the zinc-DPA motifs incorporated into the dynamic library.

In order to assess whether the amplified receptors were indeed the ones which bound most strongly to IP$_6$ and pyrophosphate respectively, the individual receptors were synthesised. To be tested in aqueous conditions the imines were reduced to secondary amines, in order to prevent imine hydrolysis. Unfortunately the yields obtained of these products were extremely low, and scaled up reactions failed. Although imine formation was demonstrated by ^{1}H NMR spectroscopy, reduction by sodium borohydride was inefficient and isolation of the pure products was not possible. The receptors which were amplified by IP$_6$ and pyrophosphate were analysed using indicator displacement assays and both demonstrated strong binding affinities for their target molecules; however the receptor samples used were not of high purity. The design of PI(3,4,5)P$_3$ receptors was then continued using the information obtained from the libraries and receptors were synthesised using conventional methods.

1.6 Aims and objectives

The overall aim of this project was to design and synthesise novel small molecule receptors for PI(4,5)P_2 and PI(3,4,5)P_3. The receptors would be used to probe the signalling pathways dependent on these phospholipids by inhibiting protein-lipid interaction. Therefore, the receptors would be tested for binding to their target PIP in a range of biochemical assays.

This study built upon previous work by the Vilar and Woscholski groups, in which the compound known as 'PHDM' was found to bind to PI(4,5)P_2 with good affinity and selectivity. PHDM used a combination of boronic acid-diol and urea-phosphate interactions to bind its target and these functional groups were carried forward in the design of new PI(4,5)P_2 receptors. Two fluorescent receptors were designed with the aim of directly probing PI(4,5)P_2, both in biochemical assays and in cells.

Although no PI(3,4,5)P_3 receptors have been reported to date, the features of PHDM and other receptors known to bind inositol phosphates were combined to develop new receptors with the correct features to bind this PIP. These receptors possessed zinc(II)-dipicolylamine groups which are known to bind strongly to phosphates and, as discussed in the introduction, have been studied in the past in biological contexts.

Therefore the objectives of this project were to be:

1. Design and synthesis of novel PI(4,5)P_2-binding receptors based on the structure of PHDM, including two fluorescent receptors.
2. Design and synthesis of novel PI(3,4,5)P_3-binding receptors using the phosphate-binding zinc(II)-dipicolylamine group.
3. Evaluation of the binding affinity and specificity of each receptor for its target compared to other phosphoinositides, using indicator displacement assays.
4. Assessment of the capacity of the receptors to compete with protein domains for binding to PI(4,5)P_2 and PI(3,4,5)P_3, using competitive enzyme-linked immunosorbent assays and phosphatase assays.
5. Determination of ability to bind PI(4,5)P_2 and PI(3,4,5)P_3 in cells, by monitoring the phosphorylation of downstream effector Akt.
6. Application of fluorescent receptors to directly detect PI(4,5)P_2 in a series of biochemical assays, as well as in cells.

Chapter 2: Receptor design and Synthesis

A series of receptors were designed to target phosphatidylinositol (4,5) bisphosphate (PI(4,5)P$_2$) and phosphatidylinositol (3,4,5) trisphosphate (PI(3,4,5)P$_3$). Although very few synthetic PI(4,5)P$_2$ and PI(3,4,5)P$_3$-binding receptors have been previously reported (*105*),(*104*),(*102*),(*76*), binding to targets that contain diols (*122*),(*123*)and phosphates (*124*),(*73*) has been extensively studied. By building on this knowledge, new synthetic receptors were developed for both PI(4,5)P$_2$ and PI(3,4,5)P$_3$.

2.1 Designing new synthetic PI(4,5)P$_2$ receptors

Although PHDM shows many of the favourable characteristics required for a synthetic PI(4,5)P$_2$ receptor, it also has some drawbacks, the main one being poor solubility. We aimed to improve the binding properties and physical characteristics of PHDM by small modifications to the original compound. The receptors shown in Figure 2.1 were designed based on the recognition groups that proved successful for PHDM, namely methylamino boronic acid and urea groups (highlighted in red, see Figure 2.1). By synthesising two types of receptor with one and two arms respectively we intended to explore the possible cooperative binding of the recognition groups. We aimed to find out if the two-armed structure of PHDM is necessary for strong, specific interactions, or if one binding motif could be replaced by a reporter group (e.g. a fluorophore) without loss of binding affinity or specificity. Fluorescent receptors were designed with the aim of directly imaging PI(4,5)P$_2$ both in cells and in *in vitro* assays. Although the distance between the fluorophores and the boronic acid motifs made it unlikely that a change in fluorescence would be observed upon binding (i.e. that the fluorophore would act as an optical switch) our aim was to use these labelled receptors to probe cellular localisation of PI(4,5)P$_2$.
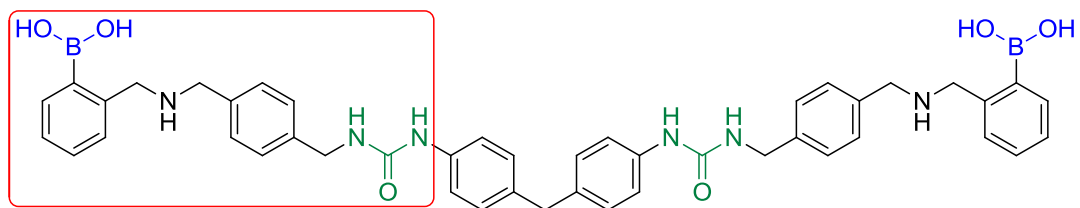
PHDM
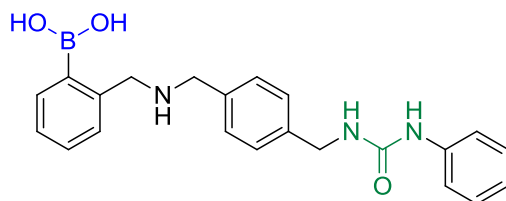
Receptor **3**
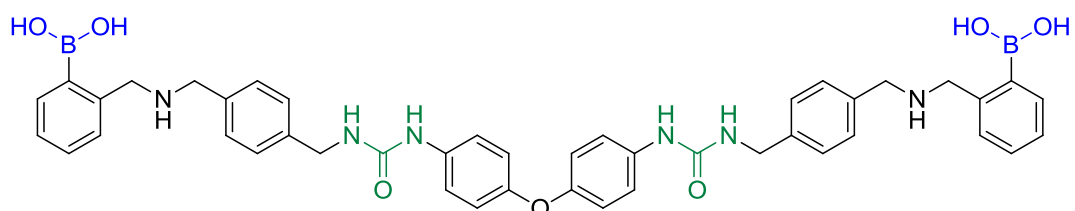
Receptor **4**
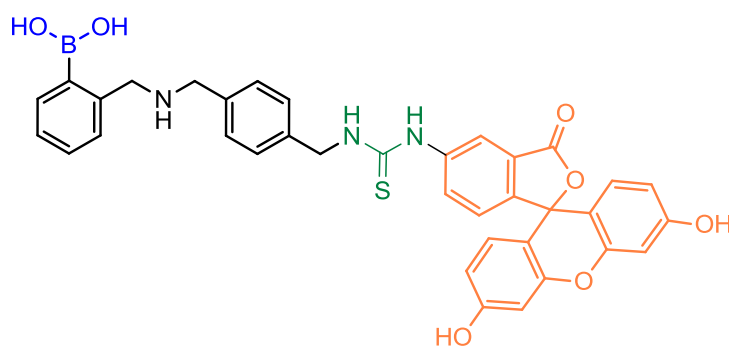
Receptor **5**
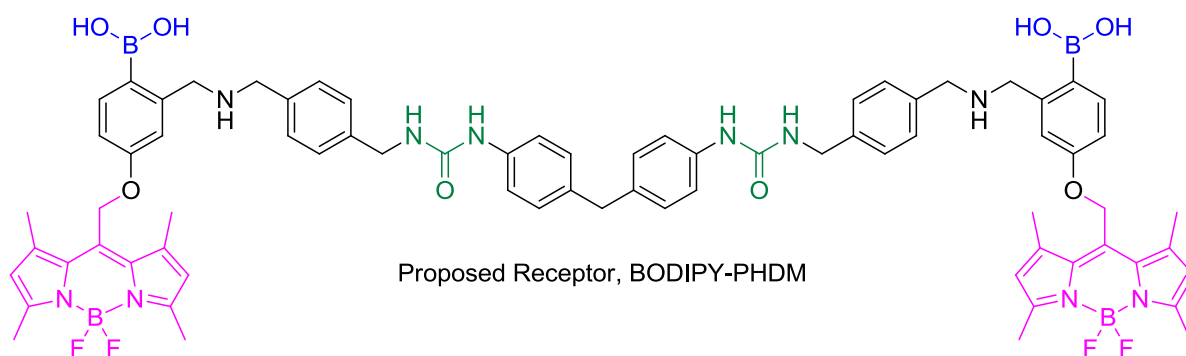
Proposed Receptor, BODIPY-PHDM

Figure 2.1: The structures of receptors designed to bind PI(4,5)P$_2$

2.2 Synthesis of PI(4,5)P₂ receptors

2.2.1 Receptor 3

Receptor **3** was synthesised in three steps following the synthetic route shown in Schemes 2.2, 2.3 and 2.4. This protocol is analogous to the one used to synthesise PHDM (*58*). An indirect reductive amination was carried out between 2-formylphenol boronic acid and mono-(di-*tert*-butoxycarbonyl, BOC) protected 1,4-methylenediamine using sodium borohydride as reducing agent. The use of the 2-substituted aldehyde ensured that the resulting secondary amine would be adjacent to the boronic acid on the phenyl ring, which is a requirement of the 'Wulff-type' boronic acids that bind well to adjacent alcohols (*91*).
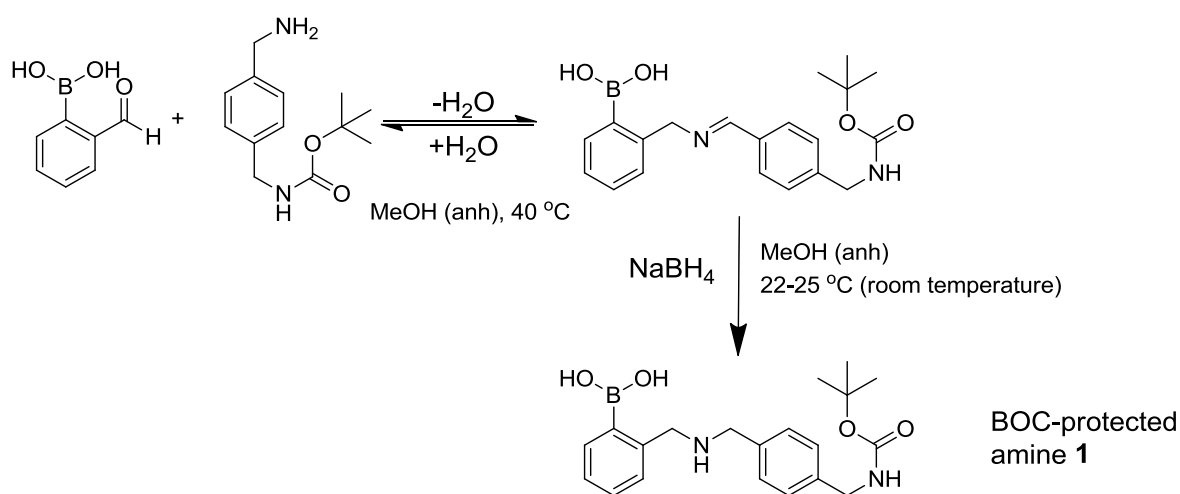
*Scheme 2.2: A reductive amination was carried out to form compound **1**. This is the first step in the synthesis of PHDM and receptors **3**, **4** and **5**.*

Conditions were strictly anhydrous with 3Å molecular sieves present in the dry methanol to absorb any water generated during imine formation. This assisted in driving the equilibrium towards formation of the product. After the imine was reduced to a secondary amine the product was purified by extensive washing with water and petroleum ether which removed triethylamine and unreacted starting materials. The BOC protecting group was then removed by trifluoroacetic acid (TFA, Scheme 2.3). Analysis by ^{1}H NMR spectroscopy showed that the singlet at 1.5 ppm (characteristic of the *tert*-butoxycarbonyl group) had disappeared, indicating that the deprotection was 100 % complete.
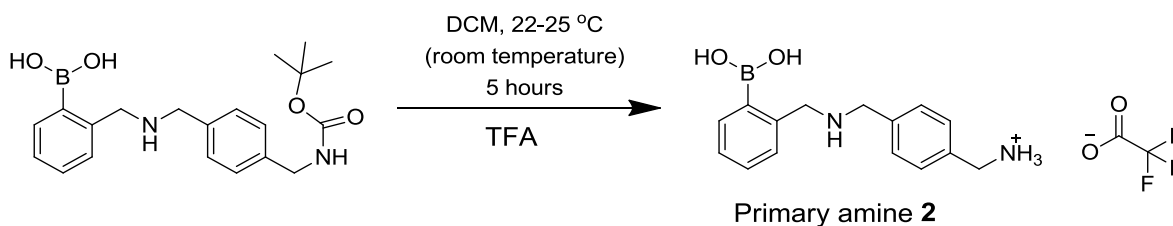
*Scheme 2.3: In the second step of this synthetic route, the BOC protecting group was removed by TFA to yield primary amine **2**.*

After removal of the solvent, ^{13}C NMR spectroscopy indicated the presence of some remaining trifluoroacetic acid (characteristic TFA peaks observed at δ = 159.7 and 113.4 ppm), probably present as trifluoroacetate counterions to the protonated amine. Compound **2** was used without further purification. The last step of the synthesis of compound **3** was carried out under similar conditions to that of PHDM. To deprotonate the primary amine **2** was stirred in the presence of triethylamine for 30 minutes before being used in the next step. Phenylisocyanate was reacted with the primary amine and form a urea which was directly attached to the phenyl ring (Scheme 2.4).
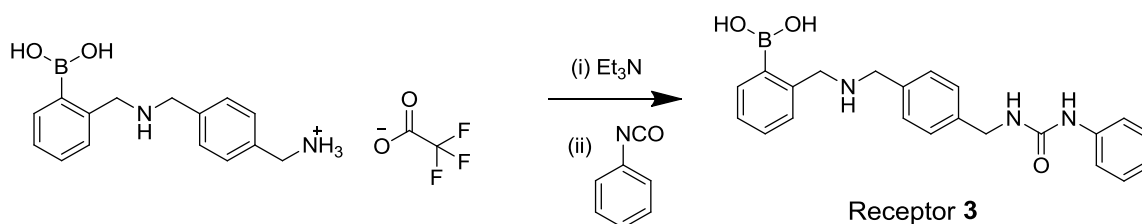
*Scheme 2.4: In the last step of compound **3** synthesis, phenylisocyanate was reacted with the primary amine to form a urea group.*

An excess of phenylisocyanate was used in order to ensure the reaction proceeded to completion. However this led to a complex mixture of products as indicated by TLC and 1H NMR. Results from similar syntheses indicated that the formation of a bisurea side product was likely, with the isocyanate reacting with the secondary amine adjacent to the boronic acid. Therefore for future reference, it is recommended that the secondary amine be protected with a protecting group such as fluorenylmethyloxycarbonyl (Fmoc) which is orthogonal to BOC- i.e. it is stable under acidic conditions but can be cleaved under basic conditions. This will likely provide a higher yield.

Receptor **3** was successfully purified by column chromatography. ^{1}H NMR spectroscopy of the resulting product showed the presence of three singlets with equal integration (2H each) in the aliphatic region associated with benzylic protons, which correspond to the three CH_2 groups present in **3**. IR spectroscopy showed a strong peak at 1658 cm^{-1} consistent with a C=O stretch, which indicated the presence of the urea. The formulation and purity of receptor **3** was confirmed by elemental analysis.

2.2.2 Receptor 4

Receptor **3** has only one "recognition arm" and therefore the binding to PI(4,5)P$_2$ is likely to be weaker than with PHDM. In order to compare the difference in binding affinity of receptors with one binding arm versus two arms, a symmetric analogue of PHDM was designed in which the central diphenyl spacer contained an oxygen molecule in place of the CH$_2$. The motivation to do this was to improve the water solubility of the resulting receptor without altering the recognition properties of PHDM. Receptor **4** was synthesised using the same procedure used for PHDM, as shown in Scheme 2.5.
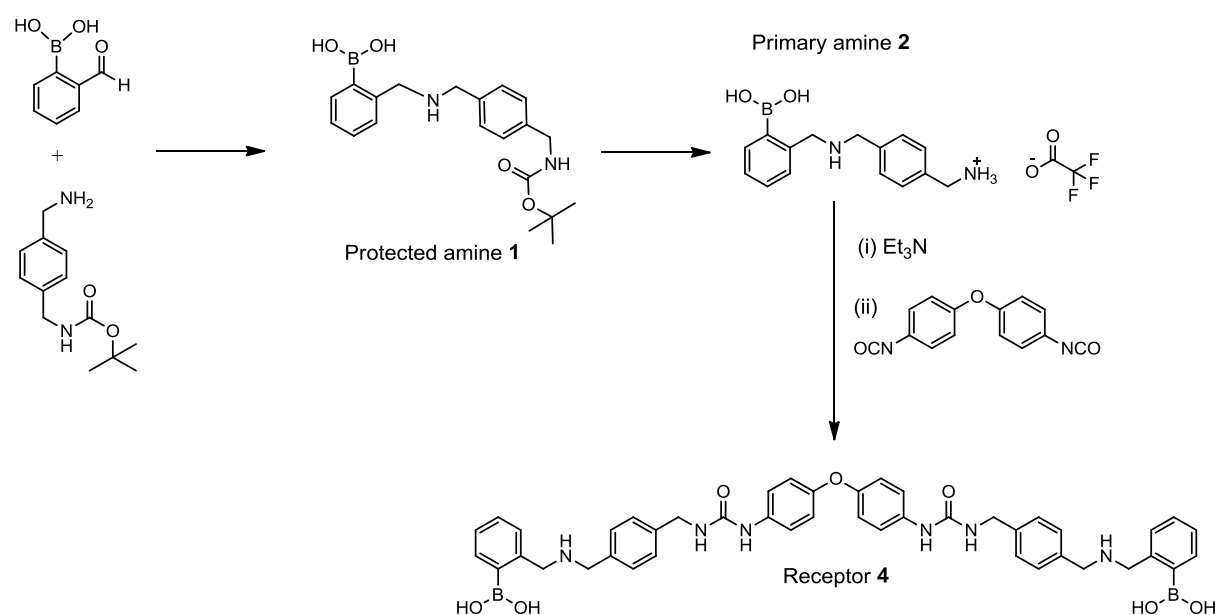
*Scheme 2.5: The synthesis of receptor **4**, an analogue of PHDM.*

In the final step (formation of the final di-urea product) amine **2** was reacted with diphenyl oxide 4,4'-diisocyanate in DMF for 24 hours. Addition of a few drops of water precipitated out a white solid. After extensive washing, analysis by ^{1}H NMR spectroscopy indicated this was indeed the product. Although the many peaks observed in the aromatic region overlap and are therefore difficult to assign, the aliphatic region showed three singlets of equal integration (all 4H), which correspond to the benzylic CH$_2$ groups. The ^{13}C NMR spectrum was also consistent with the proposed formulation. Mass spectrometry showed the presence of the doubly charged product [M+2H]$^{2+}$ at m/z = 397 a.m.u., and IR spectroscopy showed a strong peak at 1652 cm^{-1} which is consistent with the C=O stretch of the urea. The formulation and purity of compound **4** was confirmed by elemental analysis.

2.2.3 Receptor 5

Direct imaging of PI(4,5)P$_2$ is currently carried out using a number of methods. One of these is overexpression of a GFP-fusion protein domain- PLCδ1 PH, which binds to PI(4,5)P$_2$ (*58*), (*125*). We set out to design a receptor with a fluorescent label that would be taken up into the cell and be capable of binding to PI(4,5)P$_2$. In order to be able to detect PI(4,5)P$_2$ in normal cells, a fluorescent tag was incorporated onto the same binding motif used in receptors **3** and **4**.

To this aim, the basic structure of receptor **3** was retained and fluorescein was added in place of the terminal phenyl group via a thiourea group. To synthesise this, primary amine **2** was reacted with fluorescein isothiocyanate to generate receptor **5** as indicated in Scheme 2.6.
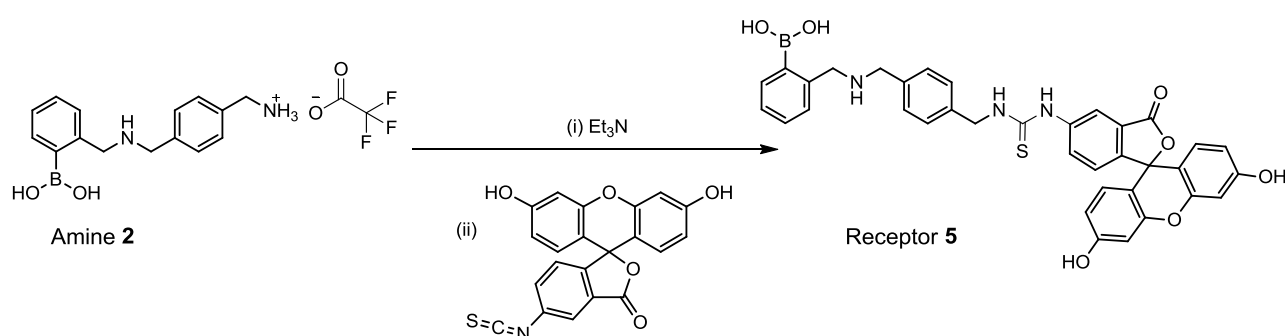
*Scheme 2.6: The synthesis of fluorescent receptor **5**.*

After 24 hours of reaction, the product was precipitated with water and the compound was purified by recrystallisation in methanol. The characteristic N=C=S stretch (ν = 2035 cm^{-1}) of fluorescein isothiocyanate was no longer present in the IR spectrum of the product and the formation of receptor **5** was confirmed by mass spectrometry, with [M+H]$^+$ observed at m/z = 660 a.m.u.. The ^{1}H NMR spectrum showed many overlapping peaks in the aromatic region with three distinct singlets appearing in the aliphatic region corresponding to three benzylic CH$_2$ groups. ^{13}C NMR spectroscopy correlated well with the expected product showing 16 quaternary, 15 CH and 3 CH$_2$ carbon peaks (assigned by 135DEPT NMR spectroscopy, see Appendix section 9.1.3). The formulation and purity of compound **5** was confirmed by elemental analysis.

2.2.4 Receptor BODIPY-PHDM

We set out to design a symmetric PI(4,5)P$_2$ receptor based on PHDM with the addition of a fluorescent tag for the purpose of direct PI(4,5)P$_2$ imaging. In order to preserve the binding properties of PHDM it was decided that such a fluorescent tag would be best placed *para* to the boronic acid, to minimise interference in the boronic acid-diol interaction and retain the flexibility of the linker. The boron dipyrromethene (BODIPY) fluorophore was chosen due to the synthetic versatility of these compounds as well as the useful and tunable optical properties they confer (*126*),(*127*). From the available starting materials, the synthetic route shown in Scheme 2.7 to a fluorescently tagged aldehyde was devised. This would then be followed by a reductive amination to generate a BOC-protected amine, followed by deprotection and reaction with 4,4'-methylenebis(phenyl isocyanate) as depicted in Scheme 2.8.
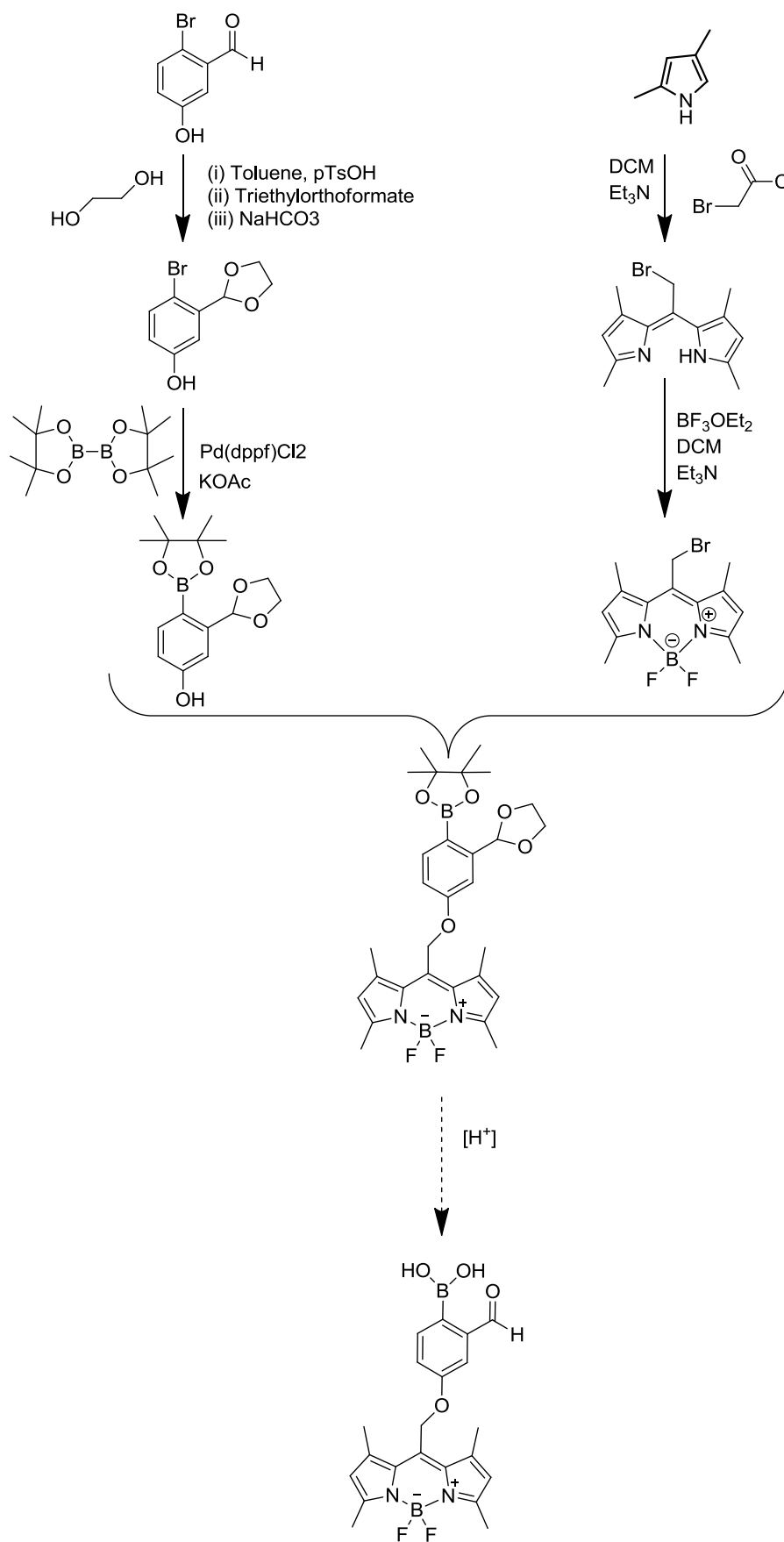
Scheme 2.7: Planned synthetic route to BODIPY aldehyde.
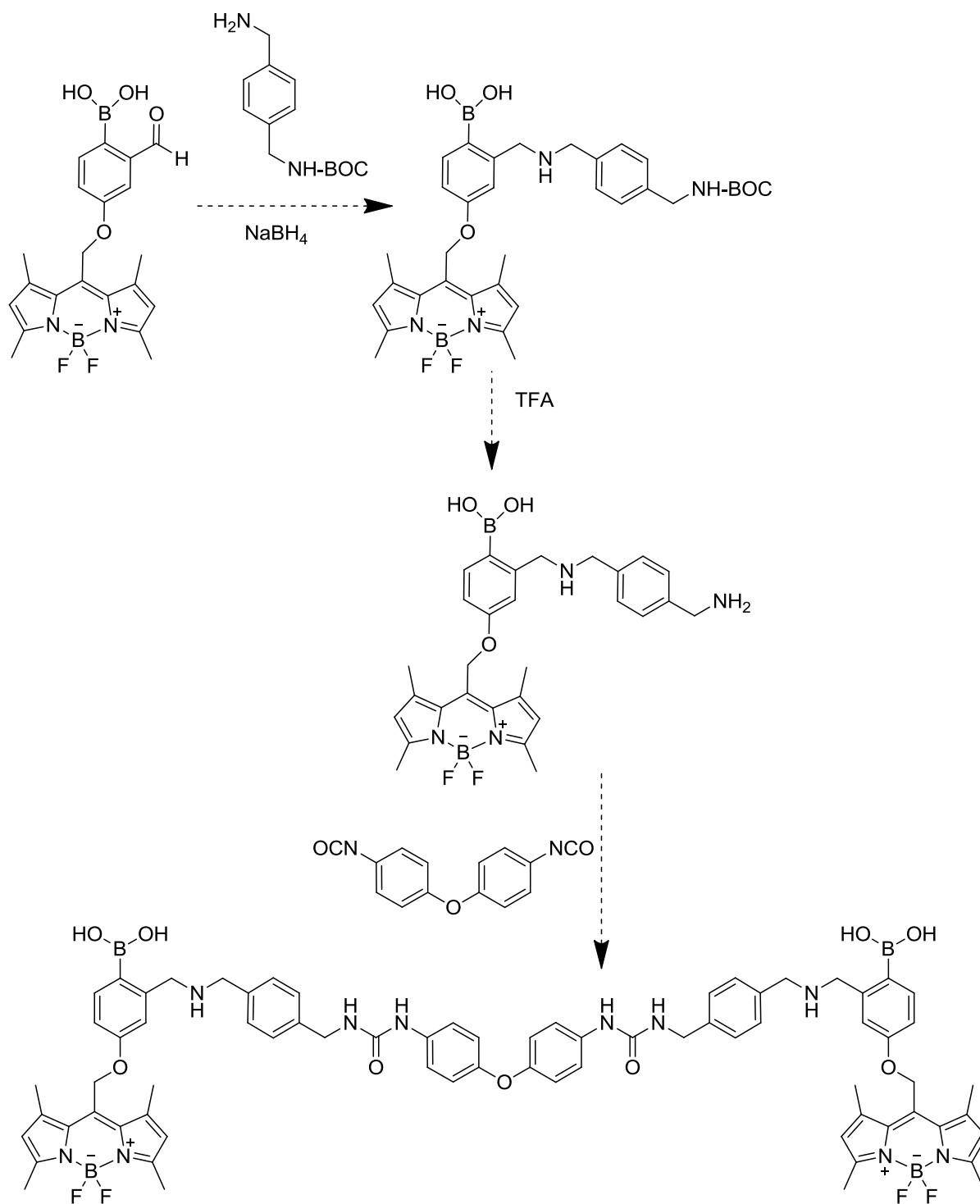
Scheme 2.8: Proposed synthetic scheme using BODIPY aldehyde to synthesise BODIPY-PHDM.

Compound **6** was synthesised according to a previously reported procedure (*126*).   Analysis by ^{1}H NMR spectroscopy showed a broad peak with a shoulder in the aliphatic region, which integrated to 12H; this was relative to two singlets at δ= 4.8 and 4.7 ppm, which when combined integrated to 2H and were assigned to the CH_2-Br protons. In the aromatic region a single peak integrated to 2H which corresponds to the pyrrole CH protons. After isolation of the product crystals of **6** were obtained which were suitable for X-ray crystallographic analysis. While most of the structure was in line with similar compounds, observation of the C-Br bond was disordered (see Appendix). This suggested that the sample contained an impurity in which the CH_2-Br was replaced by a methyl (CH_3) group, although it was not possible to separate these. The presence of the impurity was confirmed by mass spectrometry which contained a peak at m/z = 133 a.m.u., which corresponds to the doubly charged mass of the methyl structure.
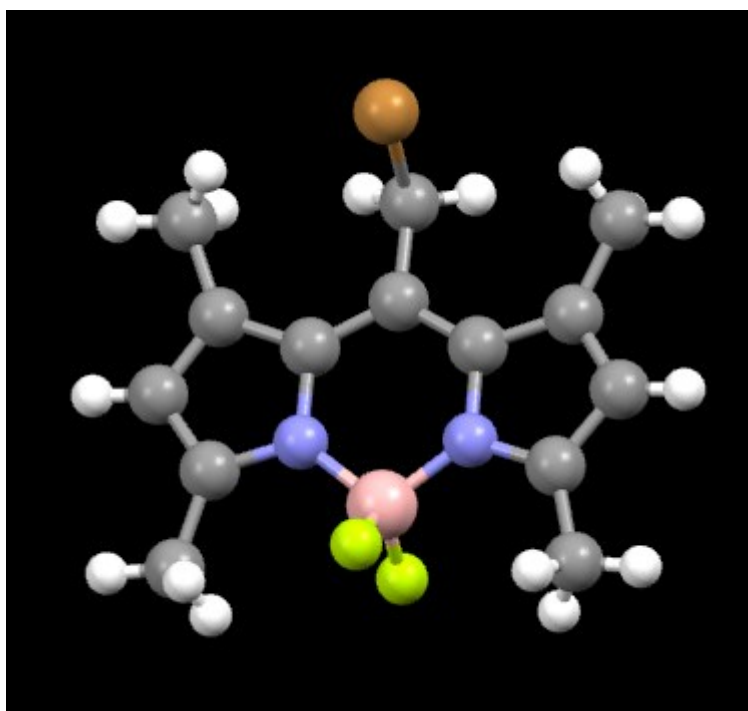
*Figure 2.9: Structure of compound **6** as determined by X-ray crystallography.*

2.2.4.2 Synthesis of 3-(1,3-dioxolan-2-yl)-4-(4,4,5,5-tetramethyl-1,3,2-dioxaborolan-2-yl)phenol, 7

Since BODIPY compound **6** contains several reactive features, it was decided to protect the aldehyde of starting material 2-bromo-5-hydroxy benzaldehyde by cyclisation with ethylene glycol. After

several attempts a protocol was optimised in which almost 100 % product formation was achieved. 2-bromo-5-hydroxy benzaldehyde and ethylene glycol were reacted in the presence of a catalytic amount of *para*-toluene sulfonic acid (*p*-TsOH) under anhydrous conditions for 24 hours. Solid sodium bicarbonate was added to quench the *p*-TsOH, preventing hydrolysis of the cyclic ester. ^{1}H NMR spectroscopy showed that the product was formed. The absence of a characteristic aldehyde peak between 10 and 11 ppm shows the starting material has been fully consumed, while the multiplets at 4.0 – 4.2 ppm corresponding to the cyclic 2CH_2 protons indicate that the cyclisation has taken place.

The protected aldehyde was then boronylated using a previously reported procedure for similar compounds (*128*). Dioxane was chosen as the solvent instead of the reported DMSO due to its lower boiling point which facilitated solvent removal. After 24 hours the catalyst and solvent were removed and the remaining dark solid was analysed firstly by ^{11}B NMR spectroscopy which showed that the new boron-containing product had formed (Figure 2.10).
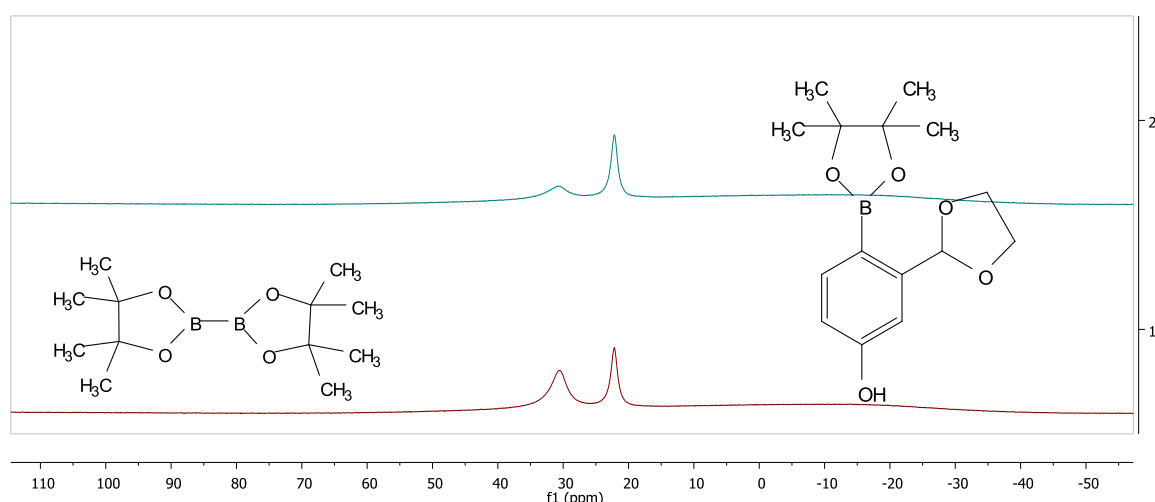
Figure 2.10: Top blue ^{11}B NMR spectrum shows reaction product. Lower red spectrum shows the same sample with added starting material in order to assign the peaks. Diboron pinacol ester δ = 30.7 ppm; Boronylated product δ = 22.2 ppm.

Analysis by ^{31}P NMR spectroscopy showed that the catalyst had been removed, since there was no visible phosphorus peak for [(Pd(dppf)Cl$_2$] (^{31}P NMR (162 MHz, d$_6$-DMSO) δ = 34.2 ppm). Recrystallisation from methanol afforded the product as a dark orange crystalline solid in 18 % yield. Analysis by ^{1}H NMR spectroscopy showed the presence of a singlet at 1.33 ppm which integrated to 12H and corresponded to the 4CH_3 protons of the pinacol ester.

2.2.4.3 Attempted synthesis of 10-((3-(1,3-dioxolan-2-yl)-4-(4,4,5,5-tetramethyl-1,3,2-dioxaborolan-2-yl)phenoxy)methyl)-5,5-difluoro-1,3,7,9-tetramethyl-5H-dipyrrolo[1,2-c:2',1'-f][1,3,2]diazaborinin-4-ium-5-uide

The next step in the synthesis of BODIPY-tagged aldehyde was coupling of compound **6** to the protected aldehyde via the phenolic OH as indicated in Scheme 2.11. Although the compound **6** sample contained an inseparable impurity, the reaction was attempted with this sample since it was assumed that the impurity would not react with the phenol.
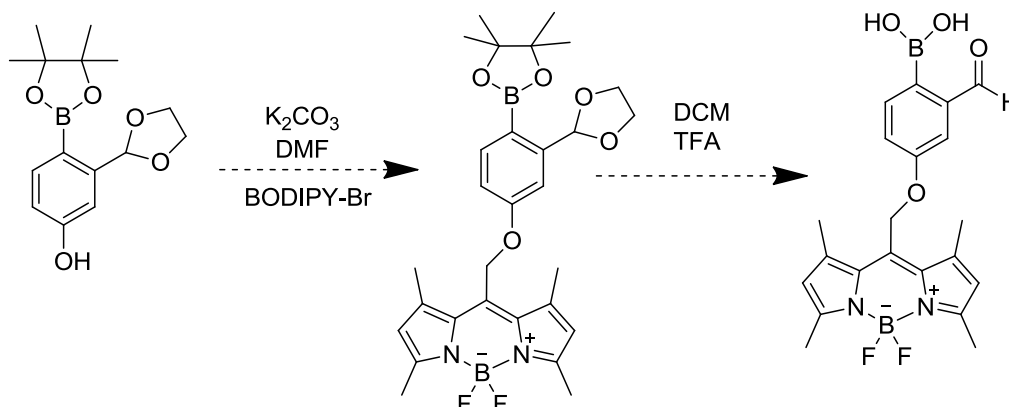
Scheme 2.11: Final step in the synthesis of fluorescently tagged aldehyde

Unfortunately although several sets of reaction and purification conditions were attempted, it was not possible to obtain a pure sample of this product. The progress of reactions was monitored using TLC (on silica, eluent = 5% CH_2Cl_2 and 95% n-hexane) as well as ^{1}H NMR spectroscopy (by observing the shift of the characteristic singlet integrating to 12H which corresponds to the 4CH_3 groups of pinacol). In some cases a small amount of product formation was observed however attempts to isolate this failed. It was decided that some reaction conditions would also be tested using commercially available bromoethylphthalimide, however unfortunately this compound also showed little reactivity towards the phenol. A summary of the conditions investigated is shown in Table 2.12.

*Table 2.12: Showing the reaction and purification conditions investigated. Some reaction conditions were also carried out with bromoethylphthalimide instead of compound **6**.*

Conditions used	Comments	Purification
Compound **6** Solvent: DMF (anhydrous) Base: K_2CO_3 Refluxed 24 hours under N_2	After 24 hours only a mixture of starting materials was observed by TLC.	None attempted.
Compound **6**, bromoethylphthalimide Solvent: DMF (anhydrous) Base: Bu_4NI, K_2CO_3 Refluxed 24 hours under N_2	Using compound **6** formation of product was observed in small amount (< 5 %) by TLC and ^{1}H NMR spectroscopy. After leaving reaction a further 12 hours this had not increased.	None attempted.
Compound **6**, bromoethylphthalimide Solvent: ACN (anhydrous) Base: K_2CO_3 and KI Refluxed for 72 hours under N_2.	Using bromoethylphthalimide formation of product was observed (5 – 10 %) by TLC and ^{1}H NMR spectroscopy. Could not isolate this by chromatography.	Chromatography: On silica using hexane and increasing proportions of DCM. On activated alumina using hexane and increasing proportions of DCM.
Bromoethylphthalimide only Solvent: None Base: K_2CO_3, 1,4-diazabicyclo[2.2.2]octane (DABCO) Grinding solid phase reagents for 6 hours.	No product formation was observed by TLC or ^{1}H NMR spectroscopy.	None attempted.

Due to low yielding reactions and lack of time it was reluctantly decided that attempts to synthesise this material would be suspended in order to begin further testing on the other receptors.

2.3 Designing new synthetic PI(3,4,5)P$_3$ receptors

To achieve maximum receptor-target interaction a PI(3,4,5)P$_3$ receptor should possess binding motifs capable of binding to up to four phosphate groups. Although boronic acids are capable of binding to phosphates via a dative bond between oxygen and boron, it was demonstrated that PHDM binds weakly to PI(3,4,5)P$_3$ (*58*). Therefore to design a receptor similar to PHDM that would target the more highly phosphorylated PI(3,4,5)P$_3$, the boronic acid was substituted for a stronger phosphate-binding motif. The success of Anh's IP$_3$/IP$_6$ receptor (**34**, Figure 1.22) and later, the SH2 domain mimetic (Figure 1.14) showed that zinc-DPA is a strong phosphate-binding motif capable of blocking protein-protein interactions (*76*),(*102*),(*59*). Therefore it was chosen to replace the boronic acid in the PI(3,4,5)P$_3$ receptors. For the first PI(3,4,5)P$_3$ receptor the central spacer and urea groups of PHDM (highlighted in red, see Figure 2.13) were retained and only the boronic acid binding motif was changed.
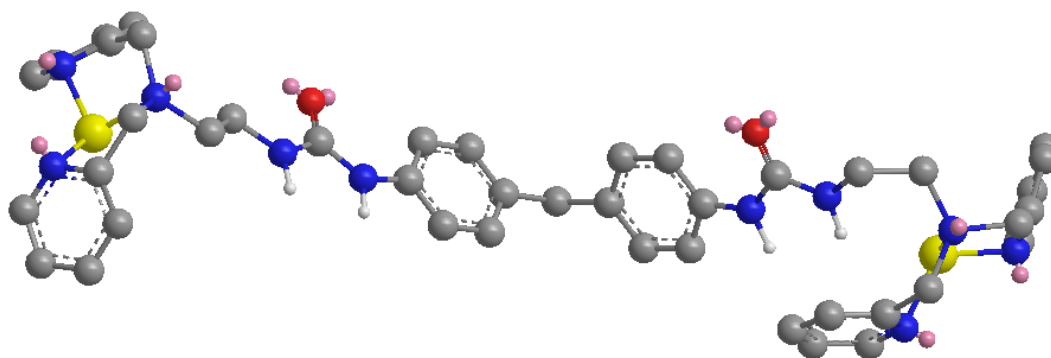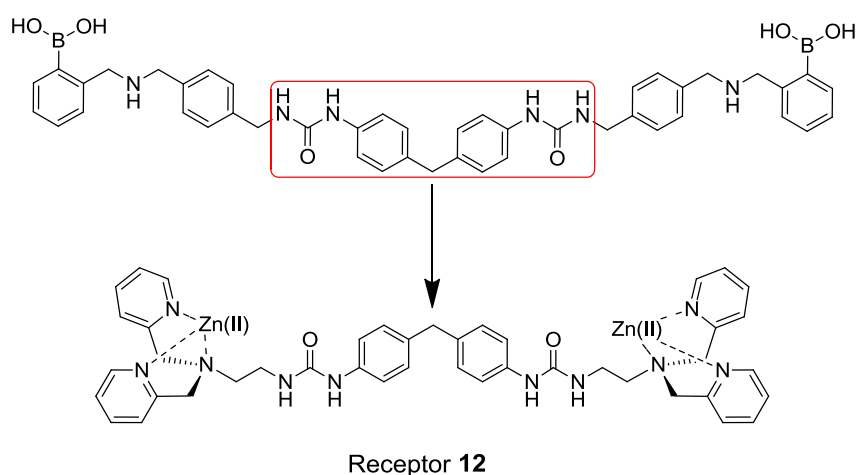
Receptor **12**

Figure 2.13: Top: to create a receptor for PI(3,4,5)P$_3$ the central section of PHDM was retained but the diol-binding motif was replaced by a phosphate-binding motif . Bottom: structure of receptor **12** *as drawn in ChemBio3D with energy minimisation. Distance between Zn ions 20.2 Å. Distance between Zn ion and proximal urea proton 4.8 Å, 2.4 Å.*

The second PI(3,4,5)P_3 receptor excluded the central 4,4'-methylene diphenyl spacer and connected the two zinc DPA motifs via a single central urea group (receptor **14**). The three adjacent phosphate-binding groups were spaced to maximise interaction with the three phosphates of PI(3,4,5)P_3. This smaller receptor was designed to test whether a large, nonpolar central spacer is a necessary module for PIP receptors. It may be that the hydrophobic nature of the central spacer assists in anchoring the receptor to the membrane and that by removing this component, the more polar **14** will not bind to PI(3,4,5)P_3 lipids as strongly as **12**.
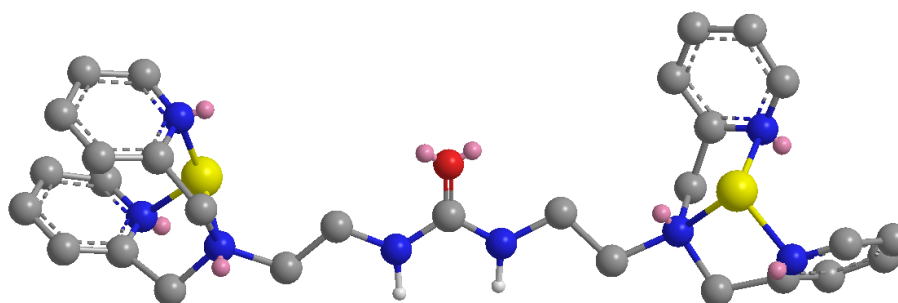
*Figure 2.14: Receptor **14**, a PI(3,4,5)P_3 receptor designed with three adjacent phosphate-binding groups and without the spacers incorporated into receptors **4** and **12**. Image drawn in ChemBio3D with energy minimisation carried out on structure. Distance between Zn ions 11.9 Å. Distance between Zn ion and proximal urea proton 5.1, 5.9 Å.*

Both of these receptors were designed to bind via a divalent metal ion which acts as a Lewis acid, accepting a lone pair of electrons from the oxygen of phosphates. Zinc (II) is the metal ion most commonly used to bind phosphates and has been successfully incorporated into a synthetic receptor for IP$_3$(*102*),(*88*). DPA preferentially coordinates to zinc over other metals including magnesium and calcium which are prevalent in biological systems (*88*),(*129*),(*130*). In addition zinc is not redox active and therefore it is expected that in the reducing conditions of the cell the metal will maintain it's +2 oxidation state, unlike other metal ions such as copper (II) which can be reduced to copper (I) (*131*).

2.4 Synthesis of PI(3,4,5)P$_3$ receptors

2.4.1 Synthesis of 1,1'-(methylenebis(4,1-phenylene))bis(3-(2-(bis(pyridin-2-ylmethyl)amino)ethyl)urea), 11

The first two steps in the synthesis of both the PI(3,4,5)P$_3$ receptors were carried out following a previously reported procedure (*132*). Bromoethylphthalimide and dipicolylamine were used in a two-step synthesis to yield DPA-ethylamine (amine **10**) which was used to form compounds **11** and **13**.
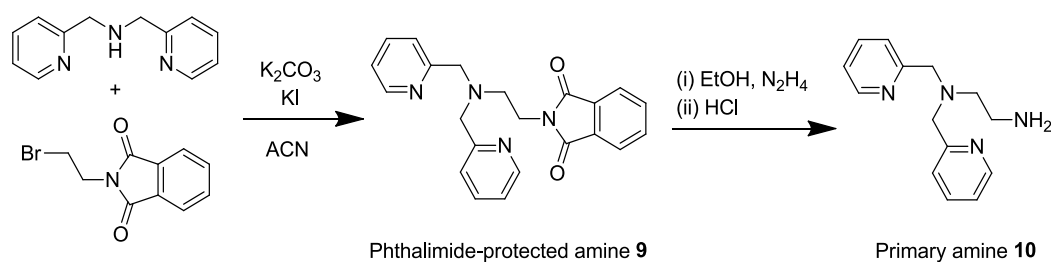
Scheme 2.15: Step 1 and 2 in the synthesis of both ligands for the PI(3,4,5)P$_3$ receptors.

Compound **9** was purified by chromatography using a small modification of the literature procedure (using silica with dichloromethane:methanol as eluent). A beige solid was isolated in good yield and analysis by NMR spectroscopy and mass spectrometry showed this to be the pure product **9**. The next step was to remove the phthalimide which was done following a literature procedure resulting in 100% removal of the phthalimide group. The literature procedure required that product **10** be purified by vacuum distillation. Although this was carried out, the yield was very low. After working up the primary amine as specified (without distillation), analysis by NMR spectroscopy and mass spectrometry indicated that the product was pure enough to be used in the next step directly. Therefore primary amine **10** was used without any further purification.
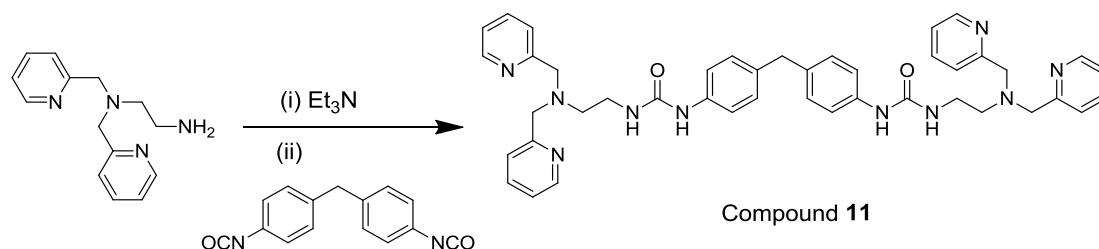
*Scheme 2.16: Formation of the final bis-DPA-bis-Urea ligand (compound **11**).*

The final step in the synthesis of compound **11** was to react the primary amine with the same diisocyanate spacer that formed the central core of PHDM as shown in Scheme 2.16. After stirring for six hours, the solvent was removed under reduced pressure to yield an orange oil. When this

was washed with cold anhydrous acetone, a tan precipitate formed. This was analysed by NMR

spectroscopy and shown to be the desired product **11**. In d_6-DMSO the protons of the urea group

were present (δ = 8.54 ppm; δ = 6.11 ppm) and the singlet corresponding to the CH_2 group between

the two phenyl groups (δ = 3.78 ppm) integrated to 2 protons relative to the CH_2-pyridine singlet

which had integration of 8 protons (δ = 3.38 ppm). The ESI(+) mass spectrum of the product showed

the molecular peak at m/z = 735 a.m.u. ([M+H]$^+$). Compound **11** was shown to be pure by elemental

analysis.

2.4.2 Synthesis of zinc(II) complex 12
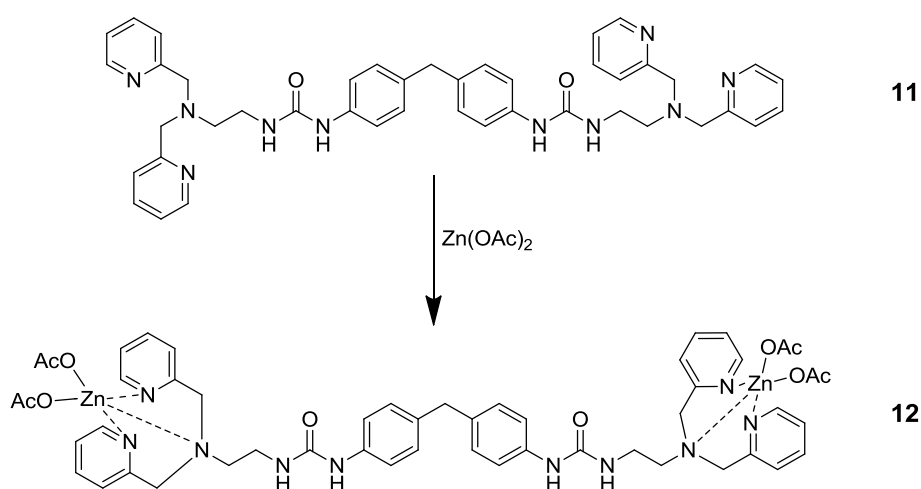
*Scheme 2.17: Addition of zinc acetate to ligand **11** forms complex **12**.*

In order to prepare the di-zinc (II) complex **12** (see Figure 2.17), the ligand was reacted with two

equivalents of zinc acetate. ^{1}H NMR spectroscopy showed that the zinc had been chelated by the

dipicolylamine. A singlet at δ = 2.0 ppm corresponds to the CH_3 groups of the acetate counterion and

the integration (12H) shows that two equivalents of zinc acetate are complexed to the ligand. In the

free ligand the CH_2 peaks vicinal to the pyridine in the dipicolylamine motif are free to rotate and are

therefore both chemically and magnetically equivalent, resulting in a singlet at 3.38 ppm in the ^{1}H

NMR spectrum. As the DPA coordinates to the metal, the structure becomes rigid. The lack of free

rotation of these CH_2 groups means that the ^{1}H NMR signal splits as the protons are no longer

magnetically equivalent (a representative spectrum is shown in Figure 2.20) (*133*). This splitting

indicated the formation of the final dizinc complex **12**. Since ligand **11** was shown to be pure by

elemental analysis, this was not carried out on compound **12**.

2.4.3 Synthesis of 1,3-bis(2-(bis(pyridine-2-yl methyl)amino)ethyl)urea, 13

In order to synthesise compound **13** the same primary amine starting material was used (amine **10**). As for the previous synthesis, the initial workup yielded the amine sufficiently pure to proceed without further purification. In order to form the urea **13**, carbonyldiimidazole (CDI) was used.
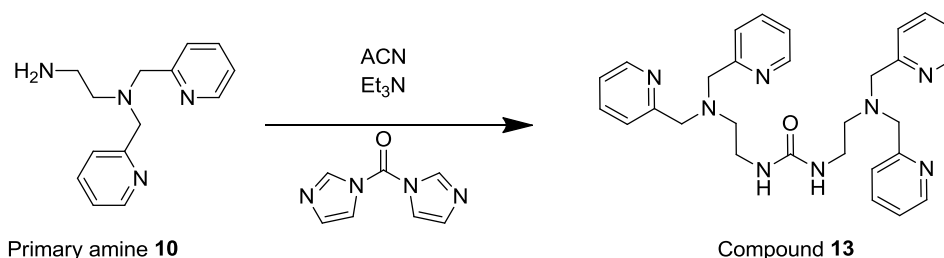
Scheme 2.18: The synthetic route to compound **13**.

Primary amine **10** was added to a solution of CDI in acetonitrile, and stirred for 48 hours to yield an orange oil which was purified by chromatography on silica. In some eluted fractions there remained some free imidazole mixed with the product as indicated by two singlets in the ^{1}H NMR spectra at δ= 7.7 ppm and δ=7.0 ppm with 1:2 integrations respectively. Flash chromatography using reverse phase (C18) silica was found to efficiently separate the imidazole from the product. The mixture was loaded onto a column equilibrated in 95% water containing 5% methanol. This solvent system was used to elute the imidazole while the ligand remained on the column. When the imidazole was removed the pure product was eluted using 95% methanol with 5% water. Analysis of the product by ^{1}H NMR spectroscopy confirmed that no imidazole remained and IR spectroscopy indicated the presence of the C=O stretch due to strong absorbance at 1592 cm^{-1}. Mass spectrometry also indicated that the desired product was present at m/z = 511 a.m.u. ([M+H]$^+$).

2.4.4. Synthesis of zinc complex 14
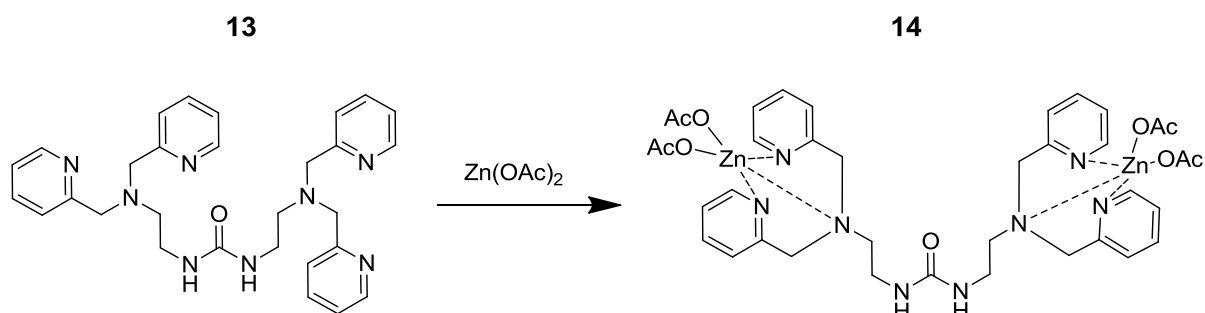
Scheme 2.19: Addition of zinc acetate to ligand **13** forms complex **14**.

Zinc(II) complex **14** was synthesised in the same way as complex **12** (Scheme 2.19). Two equivalents of zinc acetate in methanol were added to the ligand. After six hours, the solvent was removed and

the resulting solid was washed with acetone to yield the product as a pale yellow solid. The splitting of the CH$_2$ protons vicinal to the pyridine was again noted, consistent with the coordination of zinc(II) (Figure 2.20).
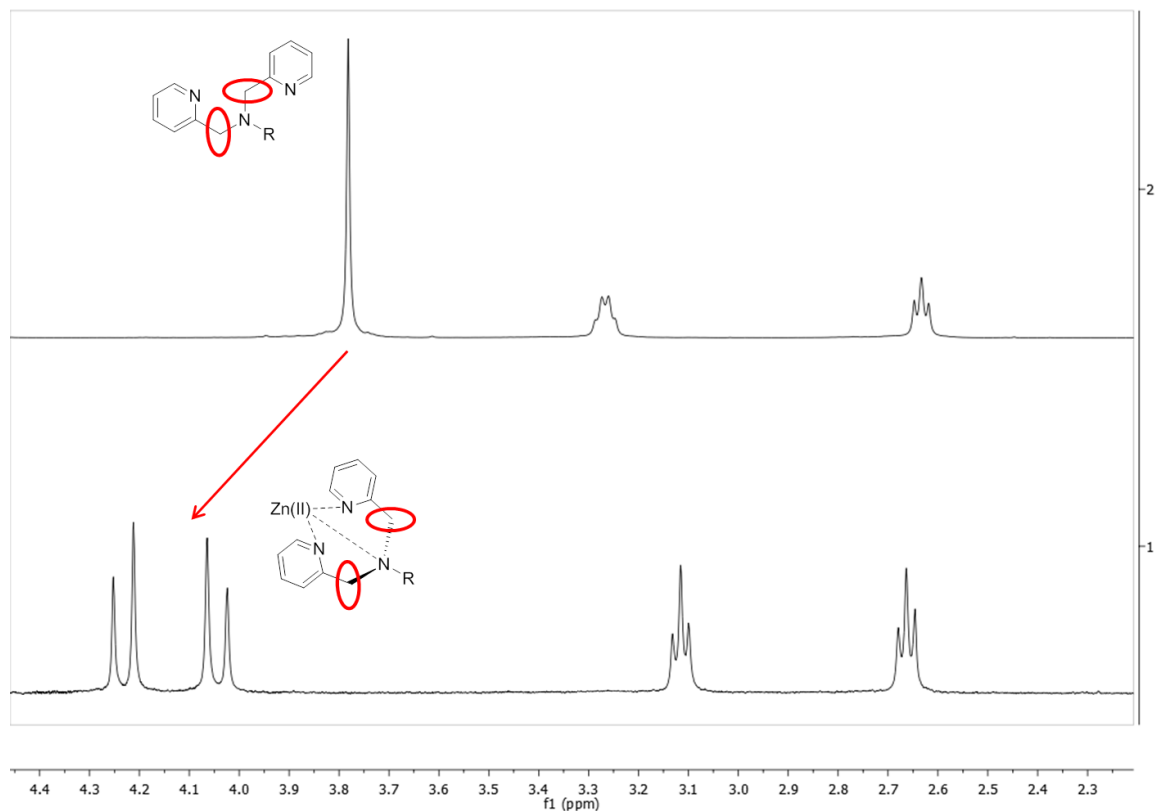
Figure 2.20: The ^{1}H NMR spectra of ligand **13** (top) and complex **14** (bottom) showing the aliphatic region. The singlet at 3.8 ppm splits into a doublet of doublets on complexation.

Chapter 3: Evaluation of PI(4,5)P₂ receptors

Receptors **3 - 5** were designed to bind to PI(4,5)P$_2$ in order to compete with PI(4,5P)$_2$-binding proteins and reduce downstream signalling. After synthesis the next stage was to assess how strongly the different receptors bind PI(4,5)P$_2$, and evaluate receptor specificity using all seven PIPs. A series of assays of increasing complexity were employed to firstly evaluate whether or not the receptors bind PI(4,5)P$_2$, then to establish if they are capable of binding in a competitive biological environment.

3.1 Receptors tested:

Receptors **3-5** possess the necessary binding motifs that target the chemical features of PI(4,5)P$_2$.
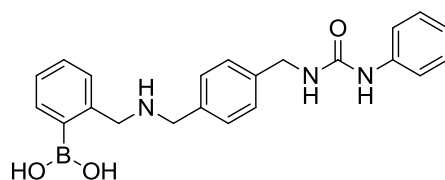
*Figure 3.1: Receptor **3**.*
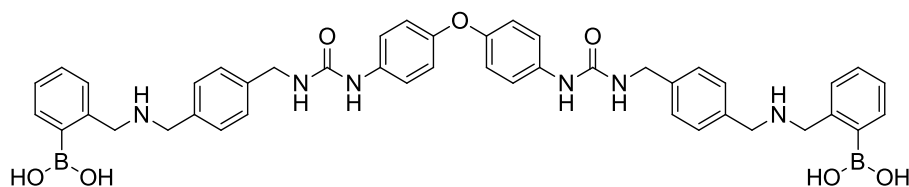
*Figure 3.2: Receptor **4**.*
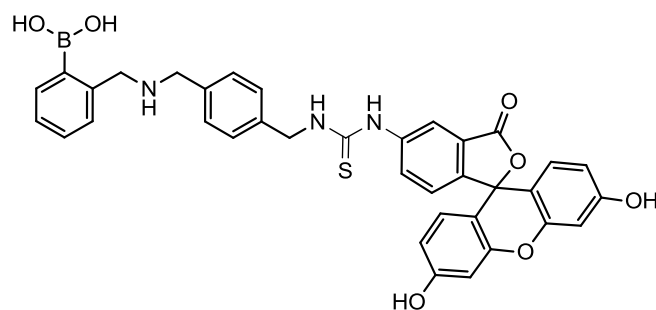
*Figure 3.3: Receptor **5**.*

3.2 Receptors were used in Indicator Displacement Assays (IDAs).

To evaluate binding of small molecule receptors to their targets, indicator displacement assays (IDAs) are commonly used (*134*),(*135*). Receptors bind to colourimetric dyes and this binding event alters the colour of the dye. Upon the addition of a more strongly binding target analyte, the dye is displaced from the receptor and returns to its original colour, and this process can be monitored by UV-Vis spectroscopy. IDAs are a useful method to determine which analytes bind to a receptor since any soluble molecule can be tested and binding affinities can also be calculated. In this instance the aim is to assess whether receptors **3** and **4** bind to PI(4,5)P$_2$ and its headgroup, IP$_3$.

3.2.1 Receptors 3 and 4 bind to Pyrocatechol Violet.

Firstly, the receptors were titrated with an appropriate indicator, to ensure that upon binding the UV-Vis spectrum changes by a detectable amount, so that the subsequent binding of the analyte can be monitored in this way. The indicator pyrocatechol violet (PV, structure shown in Figure 3.4) is often used due to its catechol moiety which is known to bind to boronic acids, causing a colour change (*93*), (*136*).
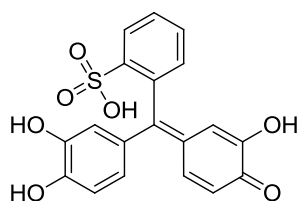
Figure 3.4: the structure of indicator pyrocatechol violet (PV).

A titration was set up to determine if the receptors under study bind to the indicator. Increasing concentrations of receptor were mixed with pyrocatechol violet at a constant concentration. The colour changed from yellow to red (Figure 3.5b), and this change was monitored by UV-Vis spectroscopy. The peak at 440 nm represents unbound PV and the peak at 500 nm represents the receptor-PV complex. The colour change as monitored by UV-Vis spectroscopy indicates that the receptors are both capable of binding to the dye.

a

b
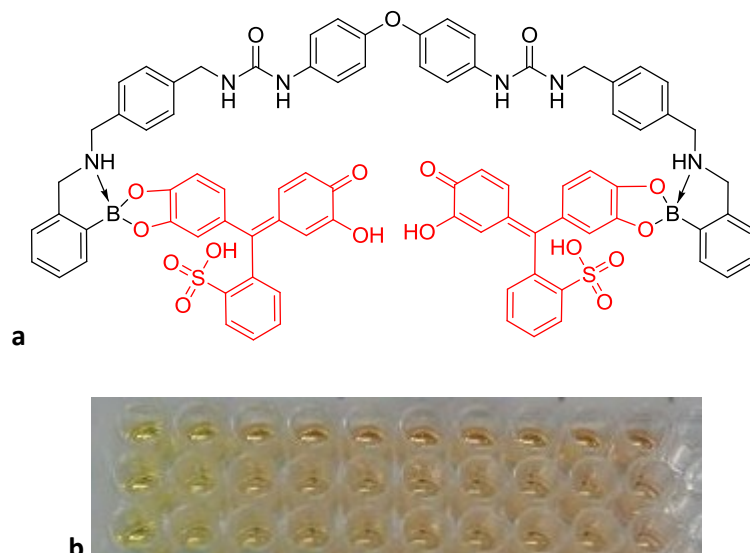
*Figure 3.5**a** Proposed binding mode between receptor **4** and PV. The indicator PV is red in colour when bound to receptor **4**. Figure 3.5**b**: The titration was carried out in 100 mM HEPES buffer at pH 7.4 using a constant concentration of PV (100 µM) and increasing the receptor concentration (0 →100 µM). Free PV is yellow in colour and as the concentration of receptor **4** is increased the complex shown in Figure **a** forms, the solution turns red (left →right, assay carried out in triplicate). Receptor **3**-PV complex is the same colour as diboronic acid receptor **4**-PV complex shown.*

a

b
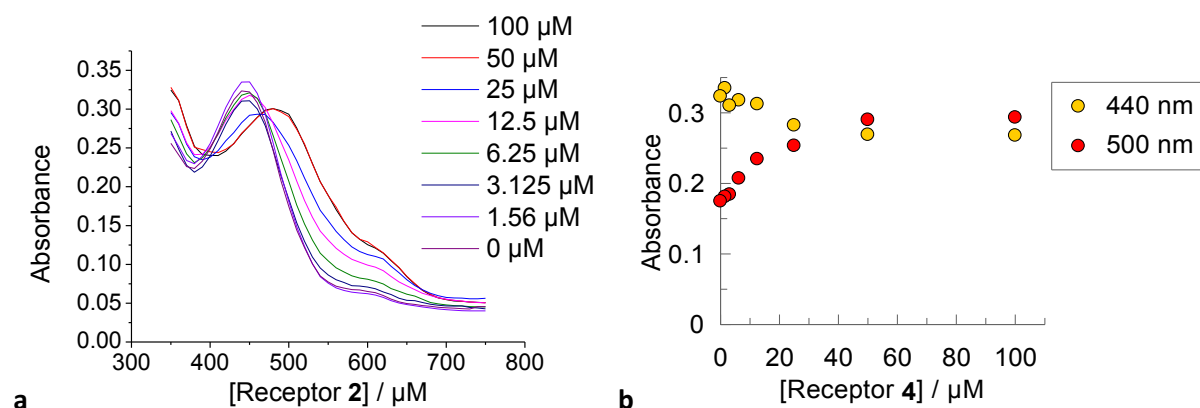
*Figure 3.6: Binding of receptor **4** to PV was monitored by UV-Vis spectroscopy. Figure **a**: The UV-Vis spectrum of 100 µM PV was monitored as receptor **4** concentration increased from 0 →100 µM. The intensity of the peak at 440 nm decreased, while the intensity at 500 nm increased. Figure **b**: Absorbance at 440 nm and 500 nm is plotted vs concentration of receptor **4**.*

The extent to which the receptors bind PV must be quantified, since different receptors will bind with different affinities and stoichiometries. In order to examine the stoichiometry of receptor-dye interaction, the method of continuous variation (commonly known as Job's plots) was carried out. The ratio of mole fractions (mole fraction = X) of the receptor and dye are varied with constant total mole fraction. The changing absorbance is plotted against the mole fraction of the receptor, and the maxima of the resulting plots indicate the ratio at which the maximum amount of receptor-PV complex is formed.
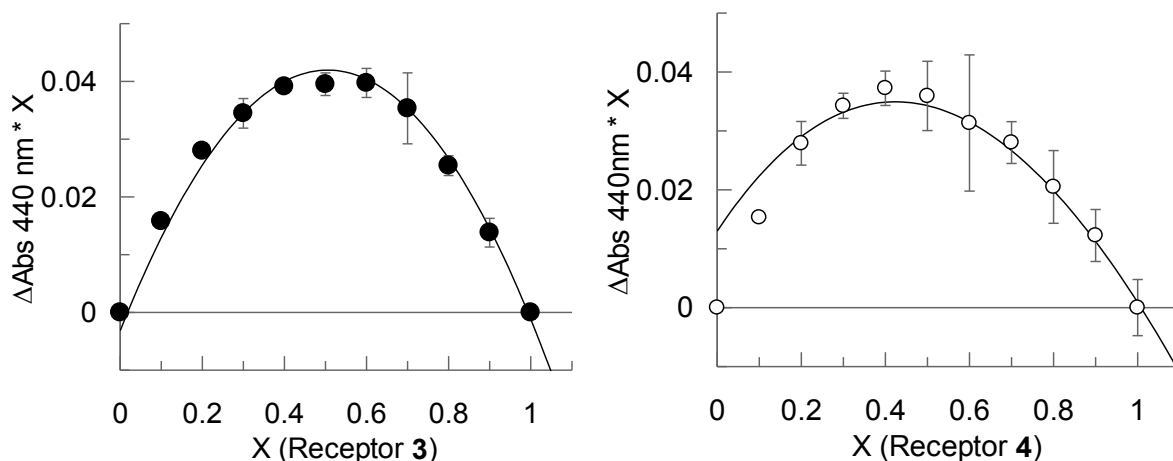
Figure 3.7: Determination of receptor-PV stoichiometry. The fractional change in absorbance at 440 nm is plotted against the mole fraction (X) of receptors 3 and 4. Total concentration is constant at 50 µM. The maxima of the plots indicate the mole fraction at which the maximum amount of receptor-PV complex has formed. Error bars represent standard deviation of the mean of two independent repeats carried out in triplicate (n=2).

Shown in Figure 3.7, the plot for receptor **3** has a maximum at X(receptor) = 0.5, X(PV) = 0.5 meaning it binds to PV with a 1:1 stoichiometry. The plot for receptor **4** reaches a maximum at 0.4 which suggests a stoichiometry of 2:3, or a mixture of 1:1 and 1:2. The latter is more probable since receptor **4** has two boronic acid motifs available to bind the catechol of PV; in addition, PV is known to be able to bind to two boronic acid moieties (*136*). This could give rise to both a 1:2 ratio in which the two boronic acids bind to two separate catechols, and a 1:1 or 2:2 ratio as shown in Figure 3.8, in which one diboronic acid receptor binds to one PV molecule, or two such receptors bind to two PV molecules.
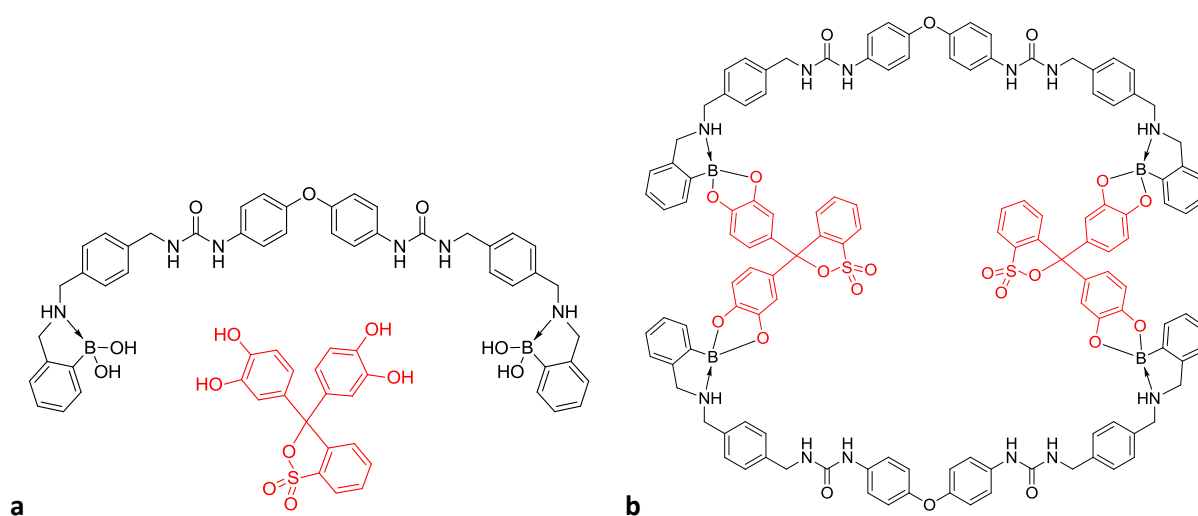
Figure 3.8: Potential binding stoichiometries between receptor 4 and PV. Figure a: Possible 1:1 binding between the two catechol motifs of PV and the two boronic acids of receptor 4. Figure b: Possible 2:2 binding between two PV moieties and two diboronic acids.

These stoichiometries are used to calculate the concentration of receptor-dye complex used in the next stage of the assay, so that excess dye is not present when the competing analyte is added.

3.2.2 Addition of target analytes to IDA.

In order to determine the binding constant between the receptors and their target analytes, the soluble headgroup IP$_3$ was added to a constant concentration of the receptor-indicator complexes (made up according to the stoichiometry determined). It was expected that the receptors would bind to the analytes and release the indicator, changing the colour of the solutions to that of free indicator. Spectroscopically this would be reflected by a decrease in intensity of the 500 nm peak in the UV-Vis spectrum and an increase in the 440 nm peak. However after addition of 2.5 equivalents of these analytes, no displacement was observed. Other analytes were tested including D-fructose, D-glucose, glucose-6-phosphate and adenosine triphosphate; none of these were capable of displacing the indicator. This means that under the conditions of the assay, the receptors bind to the indicator much more strongly than to any of the tested analytes.
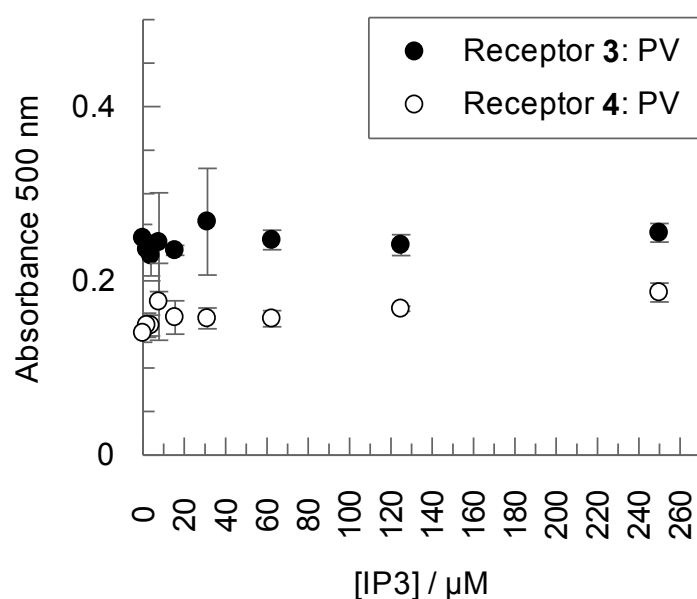
*Figure 3.9: IP$_3$ does not displace PV from either of the receptor-PV complexes. Increasing concentrations of IP$_3$ were added to a 1:1 ratio of receptor **3** and PV (100 µM each) and a 2:3 ratio of receptor **4** and PV (50 µM receptor **4**, 75 µM PV) in HEPES buffer at pH 7.4. The absorbance of the peak at 500 nm is not reduced, indicating that IP$_3$ is not binding to the receptors. Error bars represent standard deviation of two independent repeats carried out in duplicate (n=2).*

3.2.3 IDA conditions were modified.

The conditions of the assay were therefore altered in an attempt to observe the dye displacement that would indicate the receptors were binding their targets.

Several buffers were firstly tested, to ensure that this was not a source of interference. While the receptors bound to PV in PBS and HEPES and subsequent colour change from yellow to red was observed, only a small amount of binding took place in Tris buffer, as the change in colour was much less. Tris contains three hydroxymethyl groups which may form a 6-membered boronate ester in the presence of the boronic acid. Therefore PBS and HEPES were used to test the assay conditions.

Several examples of the use of boronic acid-based receptors in displacement assays use less polar methanolic conditions to enhance the binding between boronic acids and diols. The proportion of methanol used ranges from 50 % methanol, 50 % HEPES buffer (10 mM, pH 7.4, (*93*)) to 100 % methanol, buffered to pH 7.4 with *p*-toluene sulfonic acid and diisopropylethylamine (*136*). Therefore the receptor-PV titration was repeated using 75 % methanol with 25 % HEPES buffer (pH 7.4). Upon addition of boronic acid-based receptors **3** and **4** to the pyrocatechol violet, the colour of the solution changed from dark yellow to deep turquoise-blue.
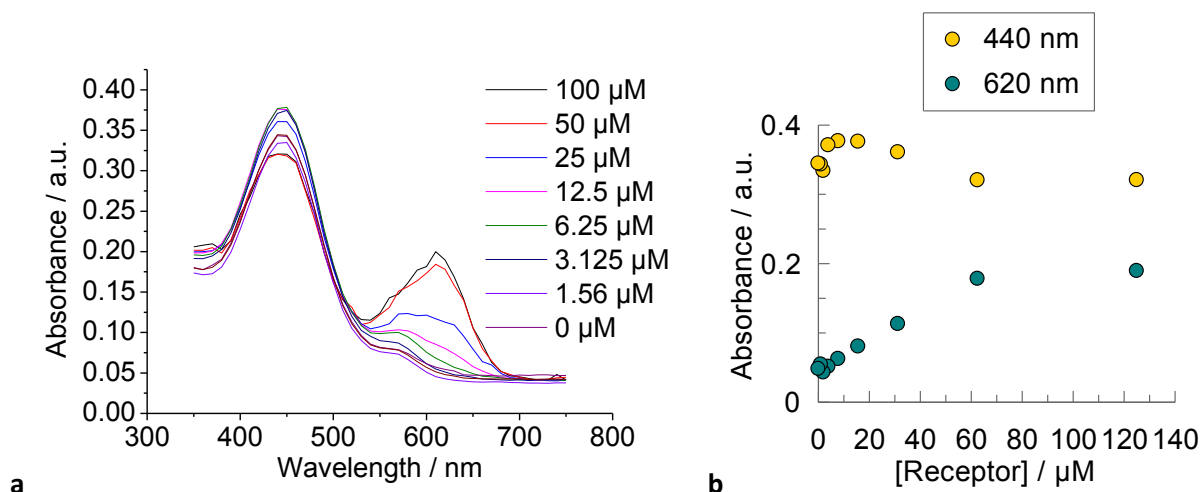
*Figure 3.10: Receptor **4** binds to PV in methanolic conditions. Figure **a**: The UV-Vis spectrum of PV changes upon addition of receptor **4** (0 → 100 µM) to pyrocatechol violet (50 µM) in 75 % methanol, 25 % HEPES (10 mM, pH 7.4). Figure **b**: Showing the absorbance values plotted against concentration of receptor **4** for the spectra shown.*

These data show that receptors **3** and **4** bind to pyrocatechol violet in a mixture of methanol and HEPES buffer. However in methanolic solution the addition of analytes led to the formation of a precipitate which prevented the use of UV-Vis spectroscopy to monitor the process. Several sets of conditions for this assay were investigated (summarised in Table 3.11), however the addition of analyte caused precipitation in all cases.

*Table 3.11: Methanolic conditions were attempted for displacement assays using receptors **3** and **4**.*

Methanol	Buffer	pH	Result
50%	50% HEPES	7.4	Precipitation observed
50%	50% PBS	7.4	Precipitation observed
90%	10% HEPES	7.4	Precipitation observed
90%	10% PBS	7.4	Precipitation observed
100%	*p*-TsOH/DIPEA	7.0	Precipitation observed

The precipitation that occurs upon addition of analytes may indicate that the receptors do in fact bind to the analyte, forming the insoluble product observed. However since this cannot be appropriately monitored by UV-Vis spectroscopy, another method of assessing the binding between receptors and PI(4,5)P$_2$ was sought.

3.3 Receptor 5 binds PI(4,5)P$_2$

3.3.1 Emission properties of receptor 5 in presence of PI(4,5)P$_2$

Several receptors with boronic acid binding motifs have been used as chemical sensors. Due to their particular structure some of these receptors can act as 'switch-on' or 'switch-off' probes for their targets which include fluoride and cyanide ions (*89*), (*90*). In order to test whether receptor **5** would act in a similar way, the fluorescence intensity of the receptor was measured in the presence and absence of PI(4,5)P$_2$-containing vesicles (1:1 molar ratio with Phosphatidylcholine, PC).
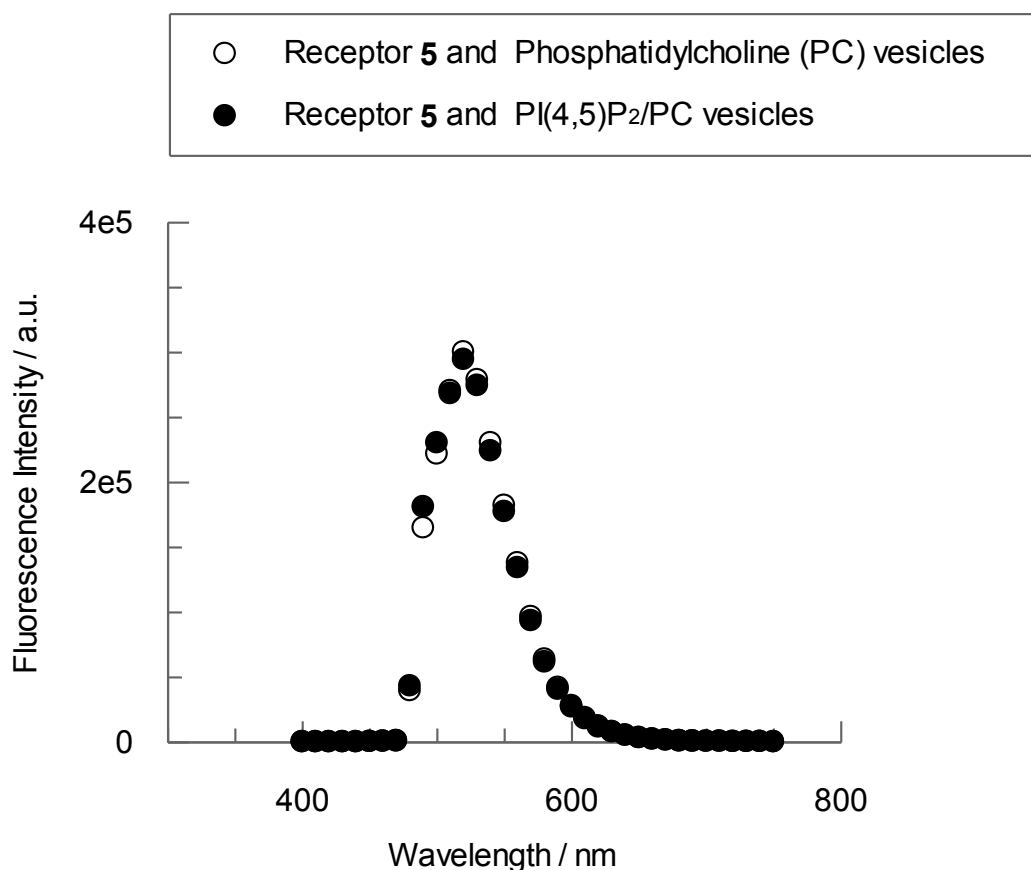
*Figure 3.12: Fluorescence of receptor **5** does not change in the presence of PI(4,5)P$_2$. The fluorescence intensity of receptor **5** (5 µM in PBS) was measured in the presence of PC:PI(4,5)P$_2$ (black circles; 100 µM PC with 100 µM PI(4,5)P$_2$) and with PC alone (white circles, 100 µM PC). Lipids prepared as vesicles, as described in Methods section. $\lambda_{excitation}$ = 485 nm.*
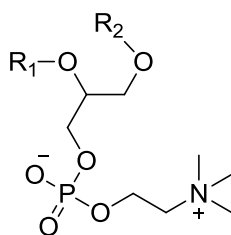
Figure 3.13 The structure of the zwitterionic phospholipid phosphatidylcholine (PC). R1 = octadecanoyl. R2= 5Z, 8Z, 11Z, 14Z-eicosatetraenoyl.

The fluorescence intensity and λ_{max} of receptor **5** are shown to be the same in the presence and absence of PI(4,5)P$_2$ (Figure 3.12). Since the fluorescent tag is not directly attached to the boronic acid of receptor **5**, it is likely that any binding event- which would change the boronic acid into a boronate ester- would be too far removed from the fluorophore to affect its fluorescence properties.

3.3.2 Receptor 5 binds immobilised PI(4,5)P$_2$

Lipids such as PI(4,5)P$_2$ are commonly quantified using PI(4,5)P$_2$-binding domains, such as the PLCδ1-PH domain (see section 3.4.1, enzyme-linked immunosorbent assay). Fluorescent receptor **5** has the potential to bind PI(4,5)P$_2$; by allowing receptor **5** to bind the immobilised lipid, it may be used to detect PI(4,5)P$_2$ by measurement of fluorescence intensity of bound receptor.

PI(4,5)P$_2$ was adsorbed onto a fluorescence microtiter plate and receptor **5** was allowed to bind. The unbound receptor was removed by washing and the fluorescence intensity of the remaining, bound receptor measured.
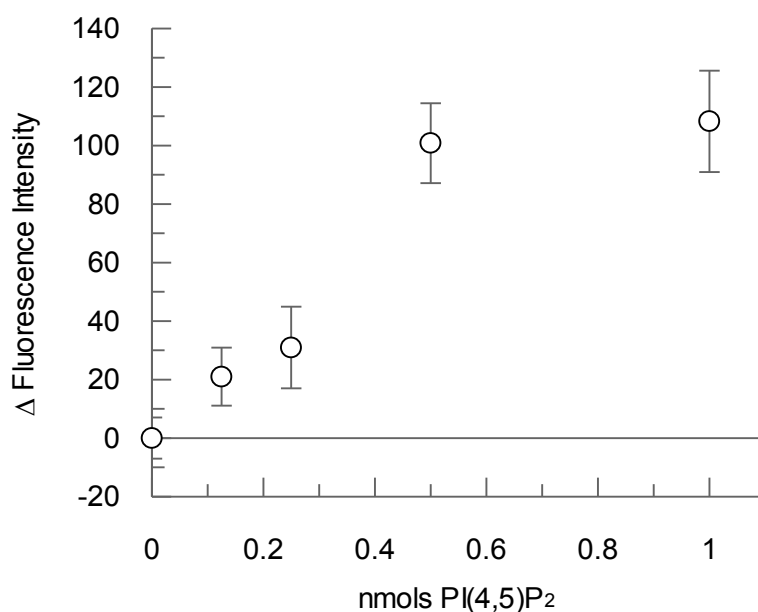
*Figure 3.14: Receptor **5** binds to increasing amounts of PI(4,5)P$_2$. After immobilising PI(4,5)P$_2$ onto a fluorescence microtiter plate, receptor **5** (10 µM) is allowed to bind. Assay carried out as described in*

Methods section. Error bars represent two independent experiments carried out in triplicate (n=2). $\lambda_{excitation}$ = 485 nm, $\lambda_{emission}$ = 525 nm.

The control (no PI(4,5)P$_2$) showed low fluorescence intensity, and for increasing amounts of PI(4,5)P$_2$ up to approximately 0.5 nmols, fluorescence intensity increases linearly. At a higher concentration the increase is no longer linear. As shown in Figure 3.13, receptor **5** is able to quantify increasing amounts of PI(4,5)P$_2$ linearly up to 0.5 nmols.

3.4 Receptors compete with PLCδ1-PH domain for PI(4,5)P$_2$ binding.

In order to determine whether the receptors can successfully compete with protein domains to bind PI(4,5)P$_2$, competitive ELISA (Enzyme-linked immunosorbent assays) were employed. ELISA are routinely used to quantify the binding of protein domains to their targets, and PI(4,5)P$_2$ has been quantified in this way using the PLCδ1-PH domain. Introducing a PI(4,5)P$_2$-binding receptor means the PLCδ1-PH domain has to compete with that receptor for binding sites. As a consequence, if the receptor has high affinity for PI(4,5)P$_2$ the amount of protein bound to the target decreases.

3.4.1 Calibration of ELISA

The detection of PI(4,5)P$_2$ by PLCδ1-PH domain was carried out according to previously described methods (Figure 3.14) (*58*). Firstly the binding of purified PLCδ1-PH domain to immobilised PI(4,5)P$_2$ was quantified. To be able to quantify inhibition of protein-lipid interactions, the absorbance response of the assay must be directly proportional to the amount of bound detection protein. Therefore the assay was optimised so that the absorbance output of the assay was linearly proportional to the bound detection protein.
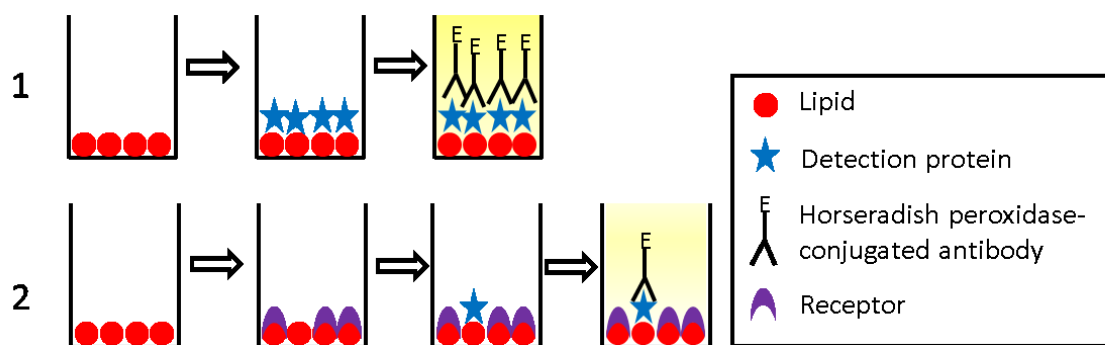
*Figure 3.15: The principles of a competitive ELISA. **1**: A lipid-binding protein (conjugated to GST) binds to an immobilised lipid. An anti-GST antibody binds to the protein and upon addition of an artificial substrate (TMB) the conjugated horseradish peroxidase generates a colourimetric product. When the reaction is stopped the absorbance at 450 nm of the generated product is proportional to amount of protein present. **2**: The receptor competes for lipid binding causing less protein to bind to the lipid, resulting in a reduction of the colourimetric output.*

To ensure that the assay had a linear response to increasing lipid, a single concentration of the detection protein domain GST-PLCδ1-PH was tested against increasing amounts of PI(4,5)P$_2$. This was followed by increasing the PLCδ1-PH domain while maintaining a constant amount of PI(4,5)P$_2$. The results of this are shown in Figure 3.15.
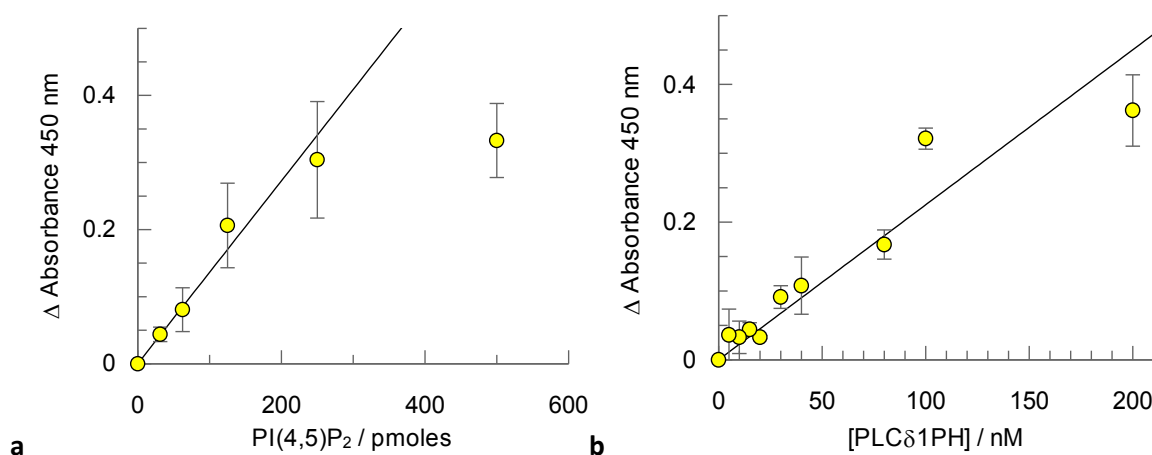
*Figure 3.16: Calibration of the ELISA assay. **a**: the increasing absorbance at 450 nm is plotted against the increase in PI(4,5)P$_2$ as detected using a constant concentration of PLCδ1-PH domain (50 nM). The absorbance becomes saturated at high lipid amounts, however the response is linear up to 125 pmols PI(4,5)P$_2$. Absorbance is normalised by subtracting the absorbance of 0 M lipid. **b**: the increasing absorbance at 450 nm is plotted against increasing concentration of PLCδ1-PH domain as added to a constant amount of PI(4,5)P$_2$ (100 pmols). The increase in absorbance is linear until 100 nm PLCδ1-PH domain. Absorbance is normalised by subtracting the absorbance of 0 M protein domain. Error bars represent standard deviation of two independent repeats carried out in triplicate (n=2). Linear portion of each plot has been fitted. Apparent dissociation constant of PLCδ1-PH domain was calculated using the method outlined by Orosz and Ovadi (137).*

K_d^{app} = 270 ± 65 nM.

As increasing PI(4,5)P$_2$ amounts were probed with the PLCδ1-PH domain (Figure 3.15**a**), the response was linear until 125 pmols PI(4,5)P$_2$. The increase in response was not linear above this point. Having established the linearity range for different amounts of PI(4,5)P$_2$, we employed a constant amount of PI(4,5)P$_2$ (100 pmol) in the presence of increasing PLCδ1-PH domain concentrations. As shown in Figure 3.15**b** this produced a linear response as increasing amounts of detection protein bound to the lipid on the plate surface. Under the conditions tested this was observed to be linear at concentrations up to 80 nM.

3.4.2 Receptors inhibit protein-lipid binding.

The optimised conditions were then applied so that detection of PI(4,5)P$_2$ was in the linear region, and the chemical receptors were tested for the ability to compete with the PLCδ1-PH domain.

As the amount of receptors incubated with PI(4,5)P$_2$ increased, the amount of protein domain detected is reduced (Figure 3.16). Receptor **4** achieved 50 % inhibition of protein-lipid binding at a lower concentration than receptors **3** and **5**. Although the receptors are much smaller than the protein domains, they effectively compete with the protein domains for PI(4,5)P$_2$ binding.
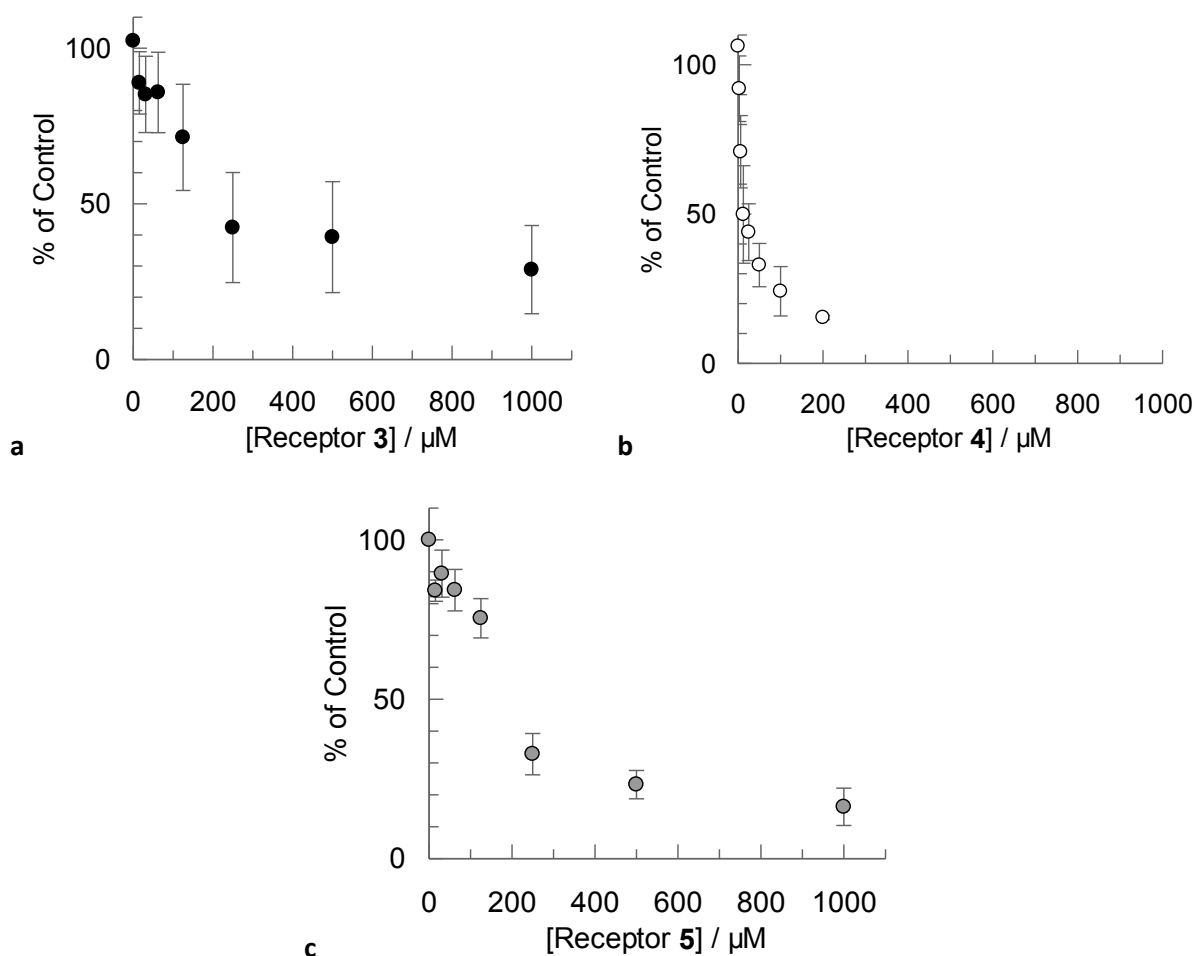
*Figure 3.17: Receptors **3** (plot **a**), **4** (plot **b**) and **5** (plot **c**) bind to PI(4,5)P$_2$. The absorbance as a percentage of control (no receptor, set at 100 %) is plotted against increasing receptor concentration. Decrease in absorbance correlates to reduced amount of bound protein detected, indicating that receptor **3** (black circle) and receptor **4** (open circle) compete with the protein domain for binding sites. Symmetric receptor **4** shows inhibition at a concentration 10-fold lower than monomeric receptor **3**. Assay was carried out as described in Methods section with receptors pre-incubated with PI(4,5)P$_2$, before detection with PLCδ1-PH domain as carried out previously. PI(4,5)P$_2$ amount was 100 pmols and protein was used at 50 nM concentration. Error bars for **a** and **b** represent the standard deviation of the mean of three independent repeats carried out in triplicate (n=3).Error bars for **c** represent the standard deviation of the mean of two independent repeats carried out in triplicate (n=2). Apparent dissociation constant was calculated using the method outlined by Orosz and Ovadi (137).*

K$_d$ (Receptor **3**) = 638 ± 120 µM; K$_d$ (Receptor **4**) = 87 ± 16 µM; K$_d$ (Receptor **5**) = 401 ± 59 µM (*137*).

The results in Figure 3.16 show that all three receptors are able to prevent binding of the detection protein to the immobilised PI(4,5)P$_2$, but also reveal that receptor **4** binds about 7-fold more potently than receptor **3**. Receptors **3** and **4** contain the same boronic acid and urea binding motifs, and the observed higher affinity of receptor **4** suggests that its two binding arms may be acting cooperatively, which greatly enhances the binding affinity. The lead molecule, PHDM, was

demonstrated to bind PI(4,5)P$_2$ in a similar assay with K$_d$ = 17.6 ± 10.1 μM (using the Cheng-Prusoff method) (*58*). The IC$_{50}$ of PHDM (approximately 10 μM) was similar to that of receptor **4** (7 μM).

Receptor **5** possesses boronic acid and thiourea groups in the same motif as receptor **3**, but with a fluorescent tag attached. The apparent binding affinity of receptor **5** towards PI(4,5)P$_2$ is calculated to be slightly higher than that of receptor **3**. Thiourea groups have been shown to interact with phosphates via hydrogen bonding with higher affinity than equivalent urea groups (*138*), which may be the origin of the stronger interaction of receptor **5** as compared to receptor **3**. Plot **c** also shows that the addition of a bulky fluorescent tag on the end of the molecule does not prevent the receptor from binding PI(4,5)P$_2$.

Taken together, these competitive ELISA results confirm that all three receptors bind to PI(4,5)P$_2$. Receptor **4** with its two binding sites interacts with higher affinity than the monomeric receptors **3** and **5**. Although the tested chemical receptors are much smaller in size than the PH domain of PLC (detection protein), they successfully competed with the protein for PI(4,5)P$_2$ binding sites on the plate surface.

3.5 Receptors bind to PI(4,5)P$_2$ and IP$_3$ and result in reduced enzyme turnover

Having shown that the chemical receptors were competing with the detection protein (PLCδ1-PH domain) for PI(4,5)P$_2$, the ELISA experiments provided evidence that the receptors are interacting with their intended target molecule PI(4,5)P$_2$. However the ELISA was not suitable to evaluate the affinity of the receptors for the headgroup of the PI(4,5)P$_2$ target, IP$_3$. Therefore we exploited the wider substrate specificity of the phosphoinositide phosphatase SopB to evaluate the specificity of the receptors.

By competing with the enzyme (SopB) for PI(4,5)P$_2$, the receptors would effectively restrict access to the substrate and thus turnover would be lowered. Therefore binding of the receptors to the SopB substrates would be observed as an apparent inhibition of the SopB catalytic activity.

3.5.1 Calibration of phosphatase assay using SopB with substrates PI(4,5)P$_2$ and IP$_3$.

To this end a phosphatase assay was carried out using the enzyme SopB. The activity of the purified enzyme SopB was firstly examined using both PI(4,5)P$_2$ and IP$_3$ as substrates (Figure 3.17). Phosphate release was measured using a phosphate detection reagent (*139*) which was calibrated against inorganic phosphate (see Methods).
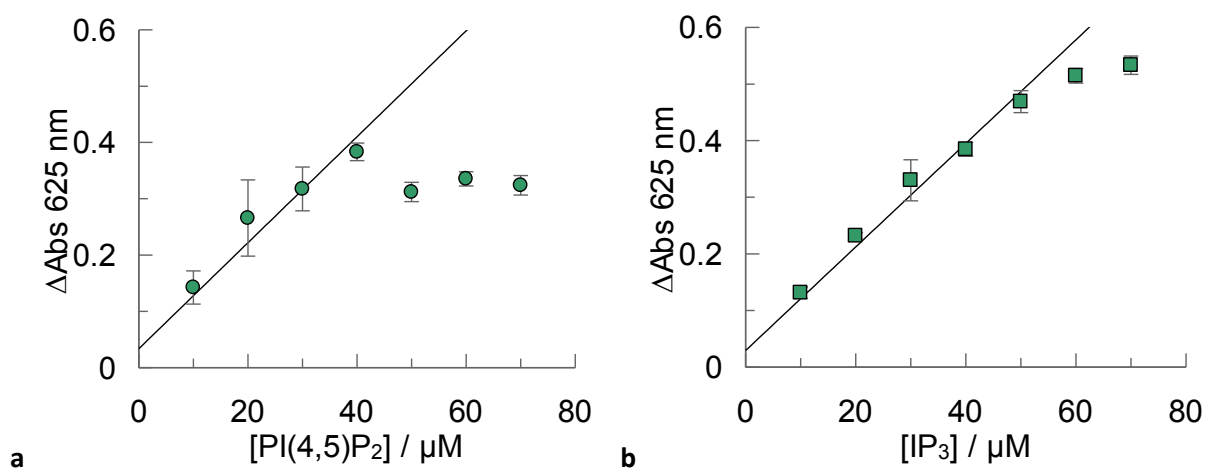
*Figure 3.18: Calibration of phosphatase assay conditions using SopB. Increasing concentrations of substrate (**a**, 1:1 PC:PI(4,5)P$_2$ (prepared as described in Method section); **b**, IP$_3$) were incubated with 2.4 µg/ml purified SopB at 37°C for 15 minutes, before the reaction was stopped by the addition of a phosphate detection reagent. Purification of phosphatase is detailed in Method section. Fitting is shown for linear portion of plots. Error bars represent standard deviation of two independent repeats carried out in triplicate (n=2). K$_m$ and V$_{max}$ determined using GraFit version 6.0.12.*

SopB dephosphorylates PI(4,5)P$_2$ with K$_m$ = 13.2 ± 5.7 µM and V$_{max}$ = 0.4 ± 0.1; the rate of dephosphorylation is linear up to approximately 30 µM PI(4,5)P$_2$. Using IP$_3$ as substrate, SopB has K$_m$ = 74.6 ± 9.3 µM and V$_{max}$ = 1.1 ± 0.1. The rate of reaction is linear until approximately 50 µM IP$_3$.

3.5.2 Receptors 3 and 4 inhibit enzyme-substrate interaction

Addition of the chemical receptors is expected to reduce the activity, so after choosing substrate concentrations in the linear range (Figure 3.17) the optimised conditions were used to test the ability of the chemical receptors to compete with SopB.

In the presence of receptors **3** and **4**, the binding between SopB and the phospholipid headgroup was inhibited. The IC_{50} values were determined for the inhibition of the phosphatase SopB by receptors **3** and **4**, with $PI(4,5)P_2$ and IP_3 as substrates.
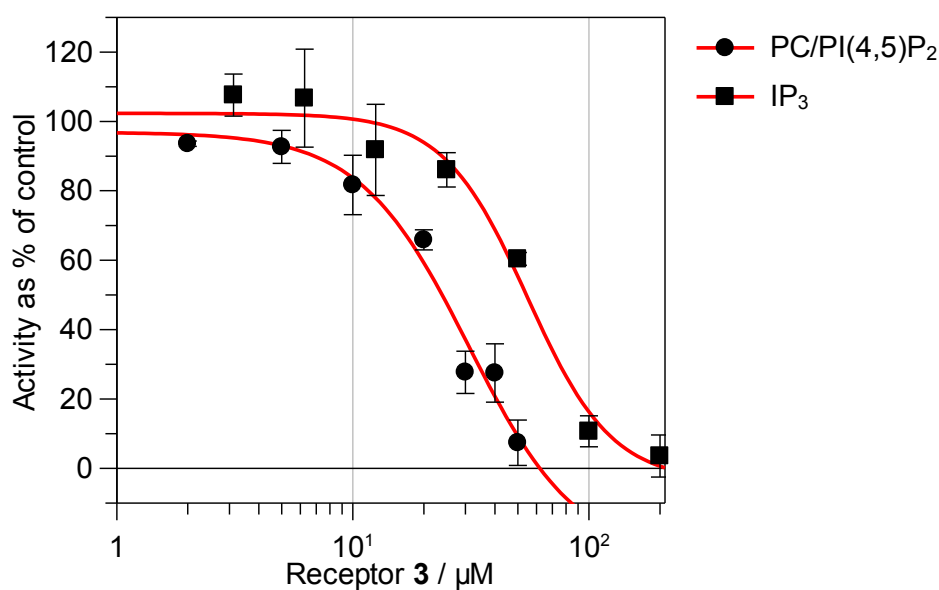
*Figure 3.19: Increasing concentrations of receptor **3** inhibit the activity of the phosphatase SopB (2.4 µg/ml). Circles show data for the lipid substrate (1:1 PC, $PI(4,5)P_2$; 30 µM), squares for the headgroup substrate IP_3 (30 µM). Substrates were incubated with receptor or vehicle control for 30 minutes before phosphatase was added to initiate reaction. All reactions were carried out at $37^{o}C$ for 15 minutes before stopping by addition of the phosphate detection reagent. Data is shown as % of vehicle control. Error bars represent standard deviation of three independent experiments carried out in triplicate (n=3). IC_{50} curves fitted using GraFit version 6.0.12.*

IC_{50} ($PC:PI(4,5)P_2$)= 30.95 ± 18.97 µM; IC_{50} (IP_3) = 54.94 ± 8.19 µM.

Figure 3.18 shows that as increasing amounts of receptor **3** bind to the substrate the enzyme activity decreases. Having demonstrated by ELISA that the receptor binds to $PI(4,5)P_2$, it is assumed that the receptor is blocking access to the substrate and that this is the mechanism of inhibition (not that the receptor is directly interacting with the protein). The IC_{50} value is approximately 2-fold lower for $PI(4,5)P_2$ which indicates a slightly higher binding affinity of receptor **3** for the lipid rather than the headgroup.
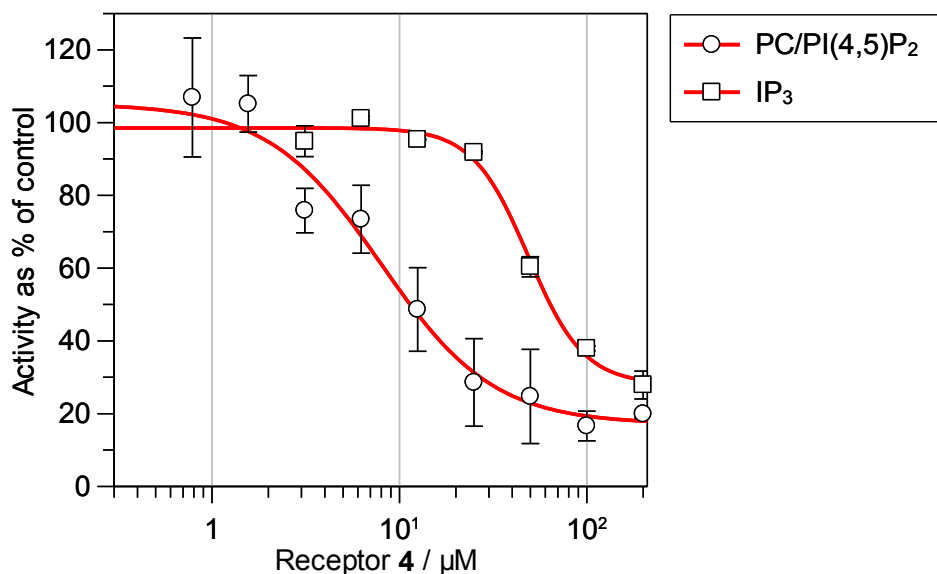
*Figure 3.20: Increasing concentrations of receptor **4** inhibit the activity of the phosphatase SopB (2.4 μg/ml). Circles show data for the lipid substrate (1:1 PC, PI(4,5)P$_2$; 30 μM), squares for the headgroup substrate IP$_3$ (30 μM). Substrates were incubated with receptor or vehicle control for 30 minutes before SopB (2.4 μg/ml) was added to initiate reaction. All reactions were carried out at 37°C for 15 minutes before stopping by addition of the phosphate detection reagent. Data is shown as % of vehicle control. Error bars represent standard deviation of three independent experiments carried out in triplicate (n=3). IC$_{50}$ curves fitted using GraFit version 6.0.12.*

IC$_{50}$ (PC:PI(4,5)P$_2$)= 7.98 ± 1.58 μM μM; IC$_{50}$ (IP$_3$) = 48.64 ± 3.60 μM.

Figure 3.19 shows that increasing concentrations of receptor **4** also inhibit the enzyme's activity by binding to the substrates. In this case the IC$_{50}$ value for the lipid is much lower than that for the headgroup, indicating that the receptor shows a clear preference for the PI(4,5)P$_2$ vesicles over the free IP$_3$.

*Table 3.21: The calculated IC$_{50}$ values of the inhibition of receptors **1** and **2**, in reactions with substrates PC/PI(4,5)P$_2$ vesicles and a solution of IP$_3$.*

IC$_{50}$	Substrate: PC/PI(4,5)P$_2$	Substrate: IP$_3$
Receptor **3**	30.95 ± 18.97 μM	54.94 ± 8.19 μM
Receptor **4**	7.98 ± 1.58 μM	48.64 ± 3.60 μM

For comparison all the IC$_{50}$ values obtained from phosphatase assays have been summarised in Table 3.20. Receptor **3** shows similar IC$_{50}$ values for both substrates, indicating only approximately 2-fold preference for the lipid over the headgroup. Receptor **4** shows a significantly higher affinity for the lipid with a 6-fold lower IC$_{50}$ value than that of the free IP$_3$. These data seem to support the possibility of receptor **4** possessing positive cooperativity when binding to lipid headgroups. After the first binding event the rest of the receptor is in close proximity to neighbouring PI(4,5)P$_2$

headgroups since they are arranged on a membrane, which facilitates binding of a second PI(4,5)P$_2$ by the dimeric receptor. This is in contrast to the IP$_3$ which is free in solution and thus binding of one IP$_3$ moiety does not facilitate binding of a second.

3.5.3 Receptor 5 inhibits enzyme-substrate interaction.

Receptor **5** was also tested for the ability to block protein-lipid interaction. Since the binding affinity as tested by ELISA was similar to that of receptor **3** (and to preserve material for future cell and microscopy experiments) a single concentration was tested. At 200 µM receptor **3** showed total inhibition of the phosphatase's activity, so 200 µM of receptor **5** was tested against PI(4,5)P$_2$ and IP$_3$.
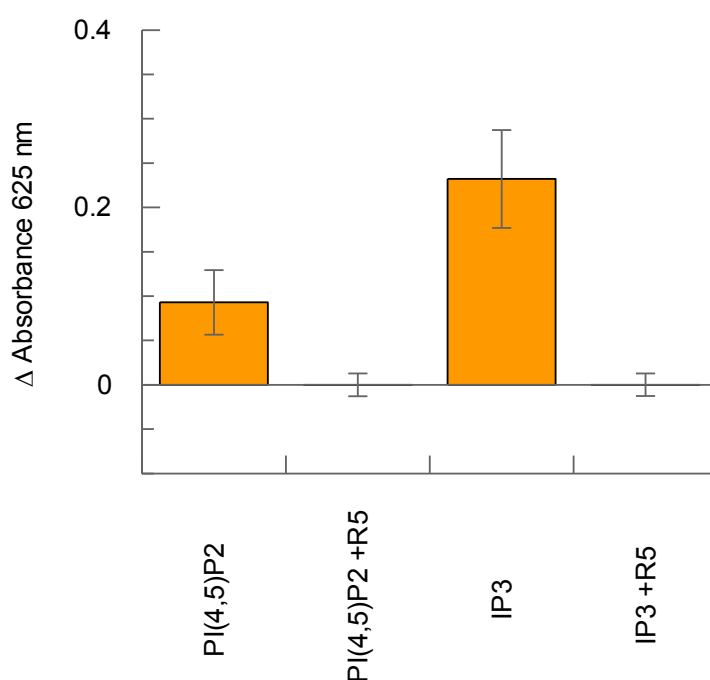
*Figure 3.22: Turnover of SopB is inhibited in the presence of 200 µM receptor **5**. Substrates were incubated with receptor or vehicle control for 30 minutes before SopB (2.4 µg/ml) was added to initiate reaction. Lipid substrate (1:1 PC, PI(4,5)P$_2$; 30 µM) and IP$_3$ (30 µM) were incubated with 2.4 µg/ml SopB at 37°C for 15 minutes prior to stopping by addition of phosphate detection reagent. Error bars represent standard deviation of two independent experiments carried out in triplicate (n=2).*

Figure 3.21 shows that with PI(4,5)P$_2$ and IP$_3$ as substrates, 200 µM of receptor **5** inhibits completely the activity of the phosphatase. The same inhibition was observed using 200 µM receptor **3**, suggesting these two receptors have similar efficacy.

3.6 Receptors bind with different affinities to each of the seven PIPs.

As previously mentioned SopB is known to dephosphorylate all of the phosphatidylinositol phosphates and is therefore a useful tool for testing the specificity of receptors **3** and **4** towards different PIPs (*58*). The phosphatase assay was carried out with each PIP as substrate. The activity in the presence of receptor is plotted as a % of the activity of the vehicle control for each PIP (set at 100%).
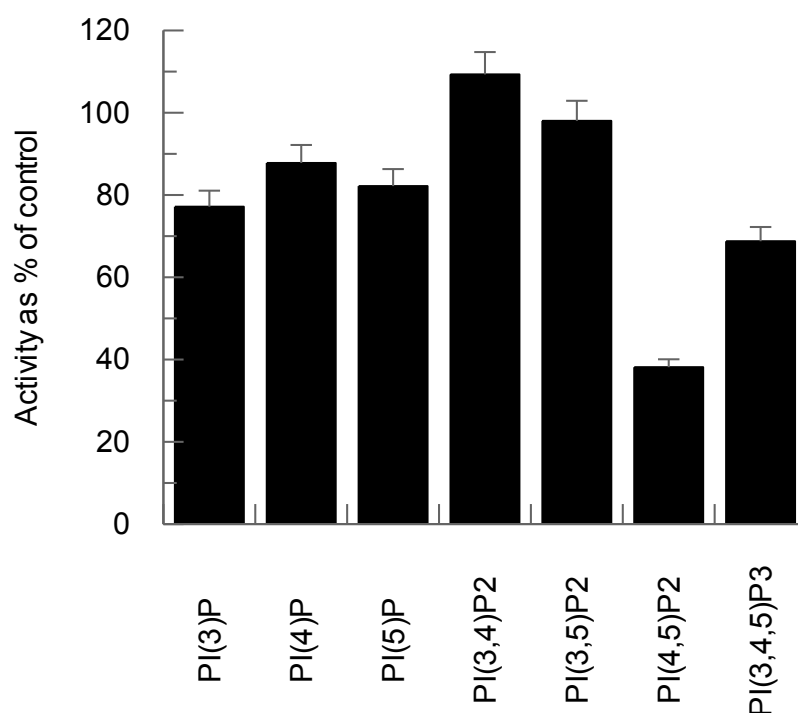
*Figure 3.23: Binding specificity of receptor **3**. Each PIP is used as 1:1 PC, PIP mix at 30 μM, and receptor **3** (25 μM) was incubated with substrates for 30 minutes prior to reaction. Substrates are then incubated with SopB (2.4 μg/ml) for 15 minutes at $37^{o}C$ before the reaction was stopped by addition of phosphate detection reagent. Turnover was calculated for each PIP (Abs[+Enzyme] – Abs[-Enzyme]) with vehicle control and in the presence of receptor **3** at 25 μM. Activity is stated using turnover(+receptor) as a percentage of turnover(vehicle control). Error bars represent standard deviation of two independent experiments carried out in triplicate (n=2).*

Receptor **3** binds with highest affinity to $PI(4,5)P_2$ at a concentration near the IC_{50} (Figure 3.22). Some inhibition is also observed for the monophosphorylated lipids PI(3)P, PI(4)P and PI(5)P as well as $PI(3,4,5)P_3$. The bisphosphorylated lipids $PI(3,4)P_2$ and $PI(3,5)P_2$ are not inhibited by receptor **3** at this concentration.

These results suggest that the receptor has a distinct but modest selectivity for $PI(4,5)P_2$ over the other PIPs. This may be due to the preferential binding of the boronic acid to the cis-diol (in the 2 and 3 positions); combined with the urea interacting with the 4- or 5-phosphate. The adjacent phosphate monoesters on $PI(4,5)P_2$ have been shown to share bridging protons by hydrogen

bonding (2); this, combined with the difference in charge density between monophosphoinositides and bisphosphoinositides at a membrane surface is likely to change the orientation of the phosphate monoesters of PI(4,5)P$_2$ relative to those of PI(4)P and PI(5)P.
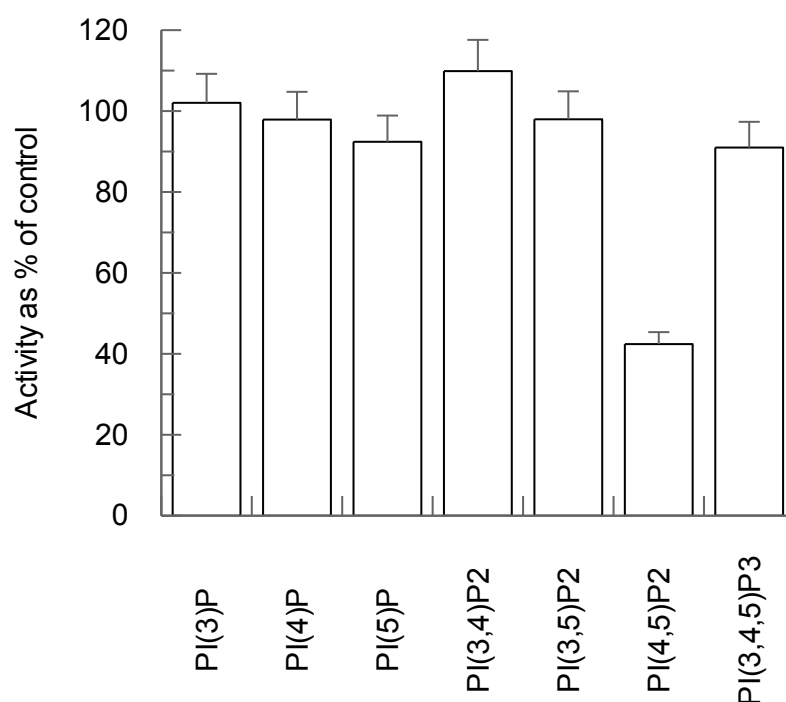
*Figure 3.24: Binding specificity of receptor **4**. Each PIP is used as 1:1 PC, PIP mix at 30 µM, and receptor **4** (10 µM) was incubated with substrates for 30 minutes prior to reaction. Substrates are then incubated with SopB (2.4 µg/ml) for 15 minutes at 37°C before the reaction was stopped by addition of phosphate detection reagent. Turnover was calculated for each PIP (Abs[+Enzyme] – Abs[-Enzyme]) with vehicle control and in the presence of diboronic acid receptor **4** at 10 µM. Activity is stated using turnover(+receptor) as a percentage of turnover(vehicle control). Error bars represent standard deviation of two independent experiments carried out in triplicate (n=2).*

Receptor **4** shows a definite selectivity for PI(4,5)P$_2$ (Figure 3.23) which is consistent with the results from the similar molecule PHDM (*58*). Unlike receptor **3**, it shows very little or no inhibition of the other PIPs which suggests that the use of the dimeric structure over monomeric enhances selectivity for PI(4,5)P$_2$. Receptor **5** was not tested for selectivity in this assay to preserve material for cellular work, however it is expected that it will have a similar binding profile to receptor **3**, due to the similarity in structure and PI(4,5)P$_2$ binding (as established using the competitive ELISA) of these two molecules.

3.7 Receptors bind to ATP with low affinity

Receptors **3** and **4** were designed to bind to diol and phosphate-containing molecules, including PI(4,5)P$_2$ and IP$_3$. However there are many other diol and phosphate-containing molecules present in the cell which could interfere with the binding between our chemical receptors and their targets (*93*), (*140*), (*92*). The most abundant of these is adenosine triphosphate (ATP) which exists in high concentrations in the cell. ATP contains a purine connected to a ribose moiety which has three consecutive phosphate groups attached.
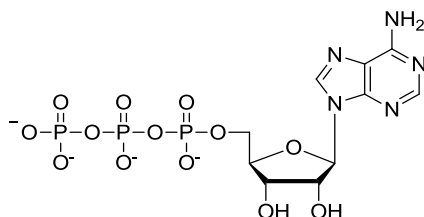
*Figure 3.25: Adenine triphosphate (ATP) contains a central ribose sugar which possesses a 1,2-diol which could interfere with the binding of receptors **3** and **4** to PI(4,5)P$_2$.*

The central ribose has a 1,2-diol that has the potential to bind to the boronic acid and phosphates which could interact with the urea of the receptors via hydrogen bonding (Figure 3.24). In order to test whether the receptors bind to ATP, a phosphatase assay was set up based on the ability of ATPase to remove a phosphate from ATP to generate ADP; this process can be followed using phosphate detection reagent.

Increasing concentrations of ATP were tested to find the range where the response is linear. Then, increasing concentrations of enzyme were tested against a single ATP concentration to ensure that the enzymatic response is linear (Figure 3.25). A concentration in the linear region was chosen so that inhibition would be readily observed as a decrease in absorbance.
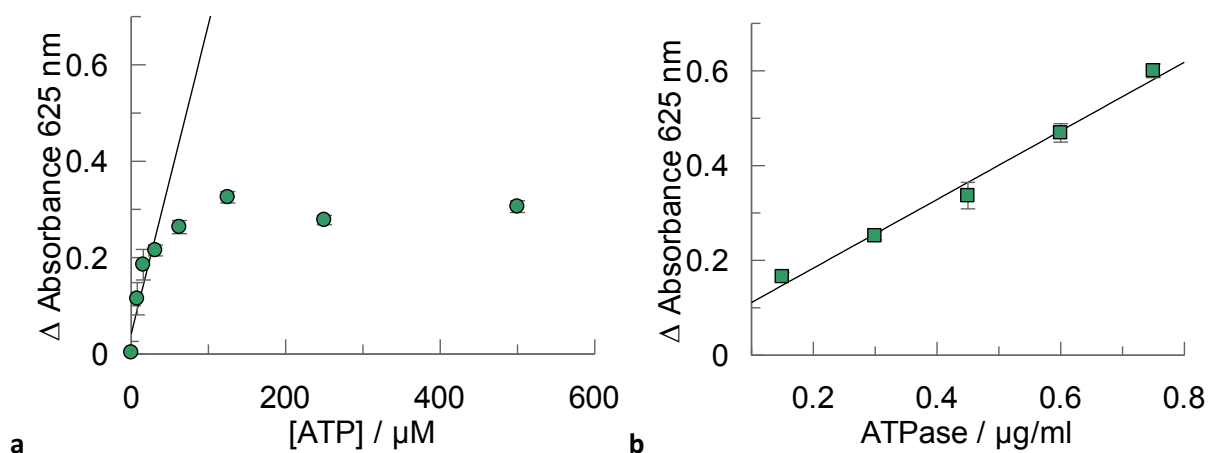
Figure 3.26: Calibration of ATPase assay. ***a:*** *Commercially available ATPase (0.15 μg/ml) was incubated with increasing concentrations of ATP for 15 minutes at 37°C before the reaction was stopped with phosphate detection reagent. The increase is linear until approximately 30 μM ATP (linear fit shown); above this concentration the enzyme reaches saturation.* ***b:*** *ATP (15 μM) was incubated with increasing concentrations of ATPase for 15 minutes at 37°C before the reaction was stopped by addition of phosphate detection reagent. The change in absorbance increases linearly up to 0.75 μg/ml ATPase. Error bars represent standard deviation of two independent experiments carried out in triplicate (n=2).*

Using the optimised conditions, receptors **3** and **4** were tested for binding to ATP in the ATPase assay. In a similar fashion to the phosphatase assays, it is expected that the receptors binding to the substrate ATP would result in a subsequent inhibition of the ATPase activity (measured by phosphate detection reagent).

Increasing concentrations of receptors **3** and **4** were added to ATP and preincubated for 30 minutes before addition of the enzyme to facilitate binding of the chemical receptors to ATP. The reaction was stopped after 15 minutes by addition of the phosphate detection reagent. The change in absorbance was plotted as a % of the vehicle control (2% DMSO v/v).
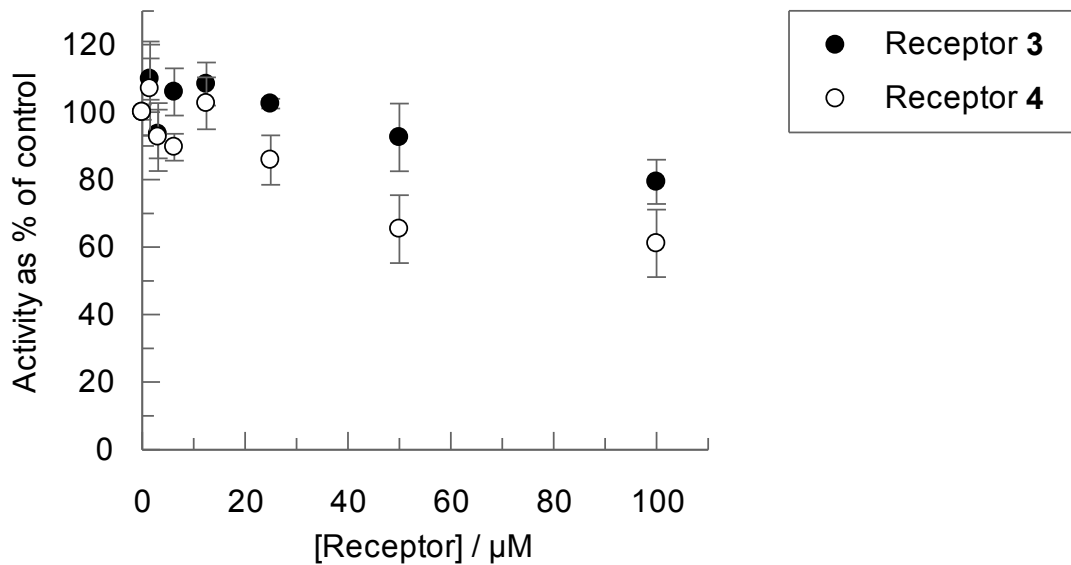
*Figure 3.27: Receptors **3** and **4** inhibit ATPase reaction by a small amount. ATP (15 µM) was incubated with increasing concentrations of receptor for 30 minutes before ATPase (0.15 µg/ml) was added to initiate reaction. Enzyme was incubated with the substrate for 15 minutes at 37°C before addition of phosphate detection reagent. Activity is stated using turnover (+receptor) as a percentage of turnover (vehicle control). Error bars represent standard deviation of two independent experiments carried out in triplicate (n=2).*

A decrease in activity is observed in the presence of high concentrations of **3** and **4**, although the reaction is not fully inhibited (Figure 3.26). Receptor **3** (100 µM) reduces the activity to around 80% of the control while the same concentration of receptor **4** reduces activity to approximately 60%. These data suggest that the receptors do bind to ATP. However even with an excess of receptors **3** and **4** over ATP there is still at least 60 % activity which suggests that the binding affinity is not strong- in comparison, 100 µM of both receptors completely inhibited the activity of the SopB by binding to PI(4,5)P_2 and IP_3. This suggests that the receptors could still be capable of binding to PI(4,5)P_2 and IP_3 even in the presence of ATP.
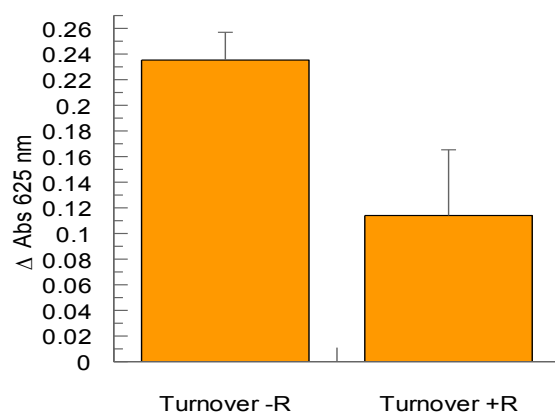
*Figure 3.28: A single concentration of receptor **5** was tested for binding to ATP. ATP (15 µM) was incubated with Receptor **5** for 30 minutes before ATPase (0.15 µg/ml) was added to initiate reaction. Enzyme was incubated with the substrate for 15 minutes at 37°C before addition of phosphate detection reagent. Receptor **5** (500 µM) reduces the activity to approximately 45 % of the vehicle control. Error bars represent standard deviation of two independent experiments carried out in triplicate (n=2).*

A single concentration of receptor **5** was tested (Figure 3.27). At this very high concentration (500 µM) the activity of ATPase is reduced to approximately 45 % of the control. The relatively low inhibition observed indicates that the receptors bind to ATP but with low affinity.

3.8 Receptors have no direct effect on the enzymes SopB and ATPase.

Small molecules that contain boronic acid motifs are known to inhibit certain types of enzyme (*141*), (*142*), (*100*). The boron can accept lone pairs of electrons from nucleophiles, including the side chains of certain amino acid residues such as lysine, histidine and serine. Enzymes which have any of these residues in their active site can potentially form a complex with boronic acids and the activity of the enzyme is therefore inhibited.

The ELISA assays show that the receptors bind to PI(4,5)P$_2$ and are capable of blocking protein-lipid interaction. This is thought to be the mechanism by which the phosphatase reaction is inhibited, however to test if the receptors are directly inhibiting the enzyme an artificial substrate was used.

When *o*-methyl fluorescein phosphate (OMFP) is dephosphorylated the fluorescent product OMF is generated (Figure 3.28). By measuring the increase in fluorescence intensity, the progress of the reaction can be monitored. If the receptors were directly inhibiting the enzyme, the rate of reaction would decrease. However if the receptors are binding to the substrate, there should be no change in the reaction rate when OMFP is used, since there are no diol binding sites available for the receptors to bind.
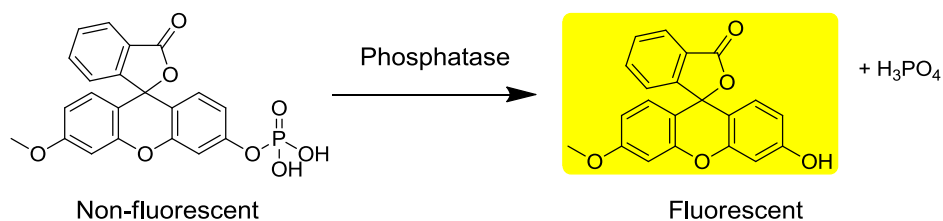
Figure 3.29: SopB removes the phosphate from OMFP to generate fluorescent OMF.

Increasing concentrations of enzyme were tested against a single OMFP concentration to ensure that the reaction rate was not in the range of saturation (Figure 3.30).
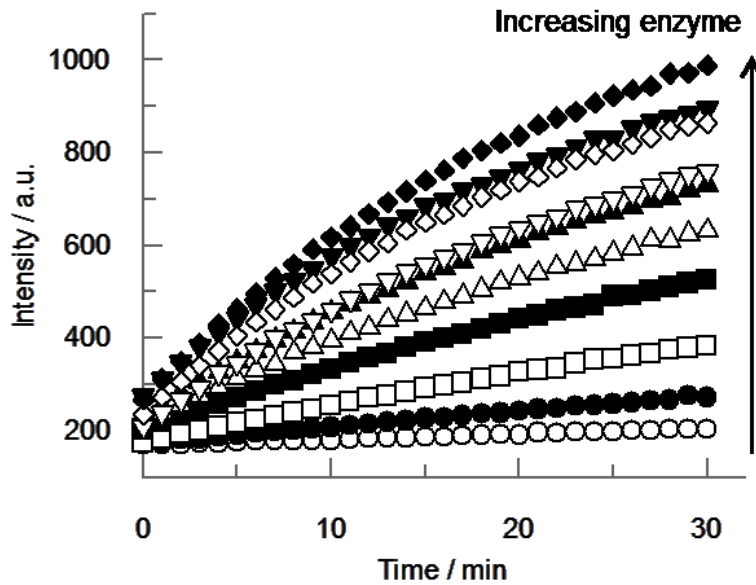
Figure 3.30: SopB dephosphorylates OMFP to generate fluorescent OMF. The fluorescence intensity of enzymatically generated OMF is plotted vs time for increasing enzyme concentrations (0 → 10.6 μg/ml). OMFP (50 μM) was added to initiate reaction and fluorescence intensity was monitored (Excitation 485 nm, Emission 525 nm).

At high enzyme concentrations the increase in fluorescence intensity is linear for the first ten minutes, and starts to plateau after around 15 minutes. Therefore the rate was calculated as the change in intensity over ten minutes.
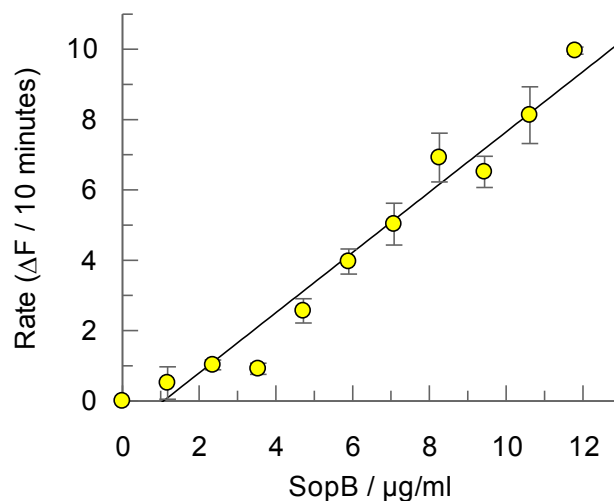
Figure 3.31: Increase in fluorescence over 10 minutes increases linearly with increasing SopB concentration (up to 11.8 μg/ml). Substrate (50 μM) was added to the initiate reaction and fluorescence intensity was monitored (Excitation 485 nm, Emission 525 nm). Control contained no enzyme in order to measure background hydrolysis of OMFP; this was subtracted from each data point. Error bars represent standard deviation of three independent experiments carried out in triplicate (n=3).

The rate of reaction increased linearly up to 11.8 µg/ml SopB (Figure 3.30). Then the enzyme was tested against increasing concentrations of the substrate in order to determine the linear range (Figure 3.31).
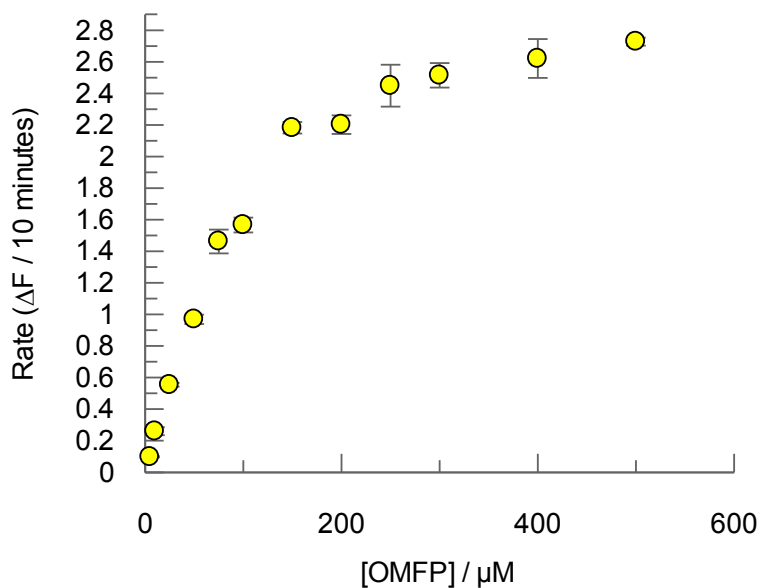
Figure 3.32: Increase in fluorescence (over 10 minutes) vs substrate concentration. Substrate was added to SopB (2.36 μg/ml) to initiate reaction and fluorescence intensity was monitored (Excitation 485 nm, Emission 525 nm). Error bars represent standard deviation of three independent experiments carried out in triplicate (n=3). K_m and V_{max} determined using GraFit version 6.0.12.

 K_m = 107.6 ± 11.0 µM, V_{max} = 3.4 ± 0.1.

The reaction rate was then measured in the presence of receptors **3** and **4** (100 µM each). Controls were set up which contained no enzyme in order to calculate the rate of background hydrolysis of OMFP. The latter was subtracted from the reaction rate of the enzyme.
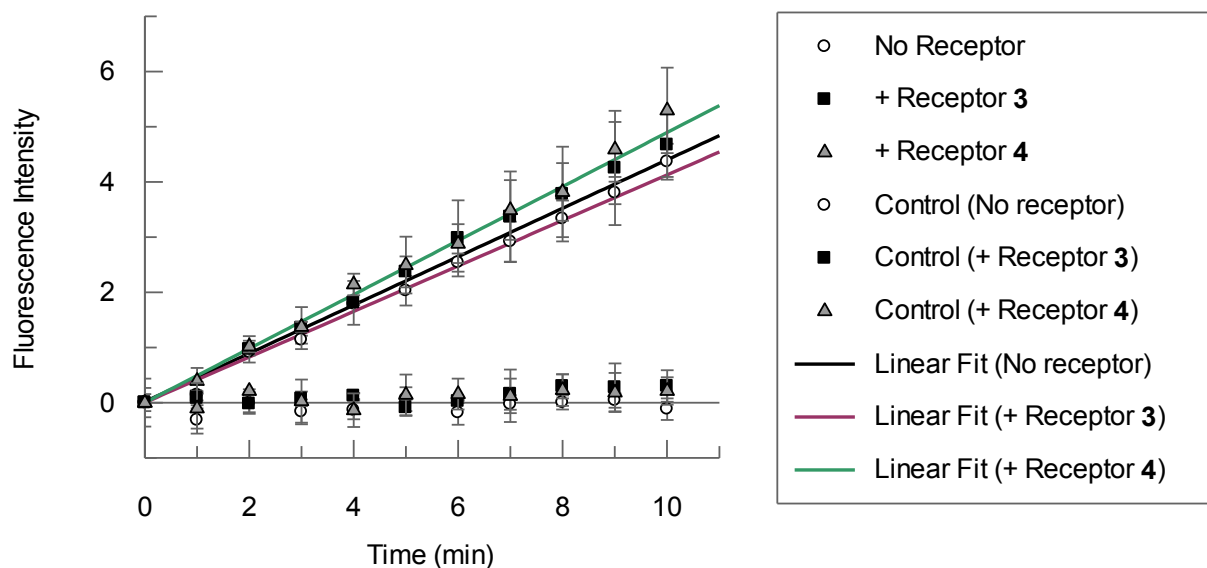
*Figure 3.33: SopB is not inhibited by receptor **3** or receptor **4**. The rate of enzymatic hydrolysis of OMFP to OMF by SopB (2.36 μg/ml) is unchanged in the presence of receptor **3** (100 μM, squares) or receptor **4** (100 μM, triangles). OMFP (50 μM) was added to initiate reaction and fluorescence intensity was monitored (Excitation 485 nm, Emission 525 nm). Controls contained no enzyme in order to measure background hydrolysis of OMFP. Error bars represent standard deviation of three independent experiments carried out in triplicate (n=3).*

As discussed above, at 100 μM, both receptors inhibited the dephosphorylation of $PI(4,5)P_2$ and IP_3. At the same concentration these receptors did not inhibit the dephosphorylation of OMFP. Since OMFP lacks the diol motif, receptors are unlikely to bind strongly and therefore any inhibition observed would likely be due to the receptors directly interacting with the enzyme. Since no inhibition is observed, it is assumed the receptors are not directly interacting with the enzyme (Figure 3.32).

The same process was repeated with ATPase. Firstly, the activity of the enzyme on OMFP was tested by increasing first the enzyme concentration in the presence of 50 μM OMFP, then by increasing the OMFP concentration in the presence of 0.15 μg/ml ATPase (Figure 3.33).
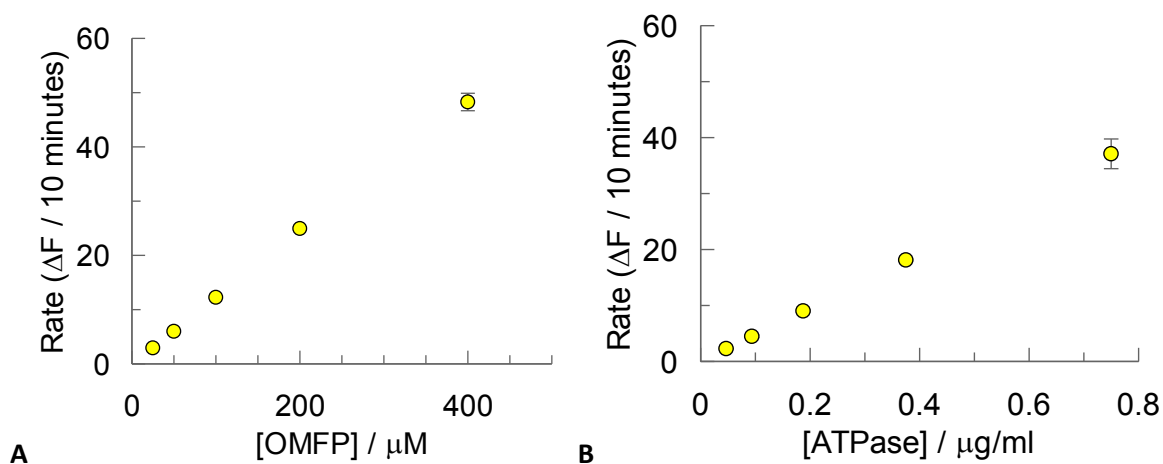
*Figure 3.34: Calibration of ATPase activity on the artificial substrate OMFP. **a**: Increasing concentrations of OMFP were added to ATPase (0.15 μg/ml) to initiate reaction. Controls were set up for each concentration of OMFP without enzyme to monitor background hydrolysis of OMFP. **b**: OMFP (50 μM) was added to increasing amounts of enzyme. For **a** and **b**, Excitation = 485 nm, Emission = 525 nm. Error bars represent standard deviation of two independent experiments carried out in triplicate (n=2).*

In order to test whether the receptors inhibit the enzyme, receptors **3** and **4** (100 μM) were incubated with the enzyme before the OMFP was added to initiate the reaction. Fluorescence intensity was monitored over 10 minutes.
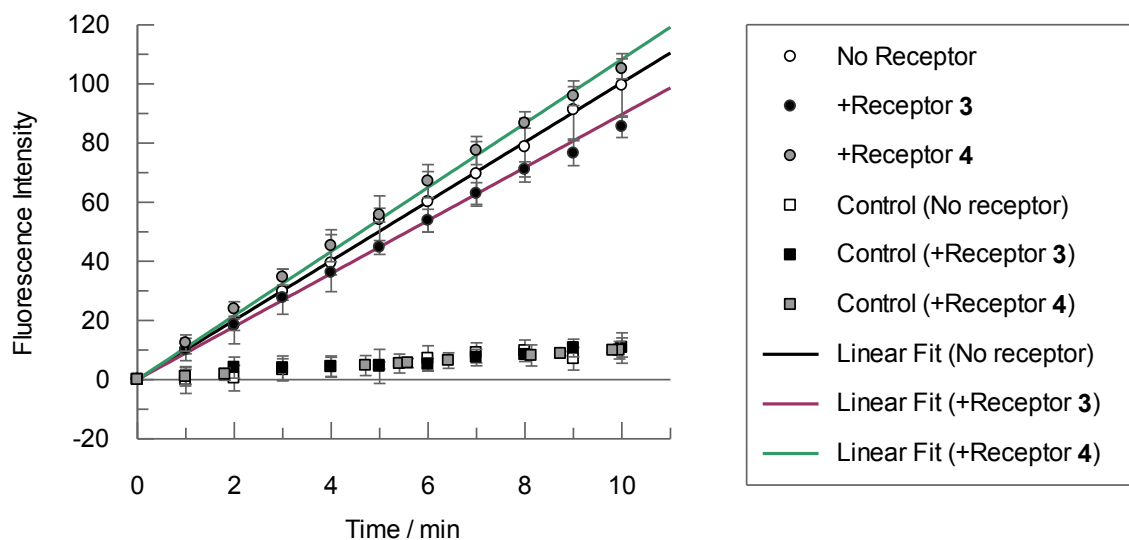
*Figure 3.35: ATPase is not inhibited by receptor **3** or receptor **4**. The rate of enzymatic hydrolysis of OMFP to OMF by ATPase (0.15 μg/ml) is unchanged in the presence of receptor **3** (100 μM, squares) or receptor **4** (100 μM, triangles). OMFP (50 μM) was added to initiate reaction and fluorescence intensity was monitored (Excitation 485 nm, Emission 525 nm). Controls contained no enzyme in order to measure background hydrolysis of OMFP. Error bars represent standard deviation of two independent experiments carried out in triplicate (n=2).*

The rate of dephosphorylation of OMFP was not affected by the presence of the receptors (3.34). These data confirm that, receptors **3** and **4** have no direct effect on the enzyme. The receptors have only a negligible inhibitory effect on the reaction between ATP and ATPase which can be attributed to the low affinity binding of the receptors to ATP.

3.9 Summary: PI(4,5)P$_2$ receptors

3.9.1 Displacement assays using receptors 3 and 4 failed

Although binding of the receptors to the dye PV was demonstrated (Figure 3.5), the addition of analytes proved problematic. In aqueous buffered conditions the presence of IP$_3$ induced no colour change (a change in colour would indicate that the receptors were binding to IP$_3$), even when large excesses of IP$_3$ over PV were present (Figure 3.9). The assays were also attempted in methanol-buffer mixtures (Figure 3.10) however addition of the IP$_3$ induced a precipitate that prevented the use of UV-Vis to monitor the assay.

3.9.2 Receptor 4 binds more strongly to PI(4,5)P$_2$ than receptors 3 and 5

By means of a competitive ELISA, receptors **3**-**5** were shown to bind to PI(4,5)P$_2$ (Figure 3.16). The presence of the receptors inhibits the interaction of the PLCδ1-PH domain with PI(4,5)P$_2$ by blocking access to the lipid headgroup. Monomeric receptor **3** binds with approximately 7-fold lower affinity than symmetric receptor **4**, which may be due to the diboronic acid structure of receptor **4** which has two binding sites. Interactions between boronic acid and diols are reversible, so when one of these bonds is hydrolysed, receptor **4** can still bind via the other boronic acid. The free boronic acid will remain close to the PI(4,5)P$_2$ layer and the likelihood of binding again to the lipid headgroup is high. In contrast, if the bond between the boronic acid of receptors **3** or **5** and PI(4,5)P$_2$ is hydrolysed, the receptor can diffuse away from the membrane surface into the bulk solution, where the probability of binding to the lipid headgroup is reduced. Receptor **5** has a slightly higher binding affinity than receptor **3** which may be attributable to the presence of a thiourea (receptor **5**) in place of a urea (receptor **3**).

3.9.3 Receptor 4 shows preference for PI(4,5)P$_2$ over IP$_3$; receptor 3 exhibits little preference

Phosphatase assays using the enzyme SopB were used to compare the binding strengths of both receptors for PI(4,5)P$_2$ as part of a membrane, and IP$_3$ free in solution. While receptor **3** showed a small preference for PI(4,5)P$_2$ over IP$_3$ (Figure 3.18), receptor **4** displayed a marked preference for the lipid over the headgroup (Figure 3.19). This may be due to the symmetric nature of receptor **4** which is more suited to binding two headgroups simultaneously, which is favoured when the headgroups are prearranged at a membrane rather than free in solution (see Figure 3.35).
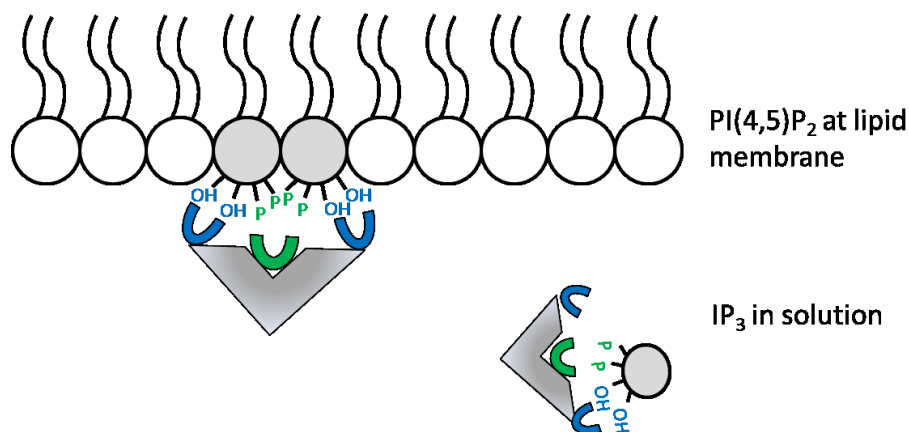
*Figure 3.36: A schematic representation of receptor **4** binding to two molecules of PI(4,5)P$_2$ at the membrane, and to a single IP$_3$ molecule in solution.*

3.9.4 Receptors 3 and 4 show good selectivity for PI(4,5)P$_2$ over other PIPs

The selectivity of receptors **3** and **4** was tested using SopB, which is able to dephosphorylate all PIPs, in a phosphatase assay. Both receptors decreased the enzyme activity and therefore must have interacted strongly with PI(4,5)P$_2$. Receptor **3** showed a small amount of binding to the monophosphoinositides PI(3)P, PI(4)P and PI(5)P and also to PI(3,4,5)P$_3$ (Figure 3.22). Receptor **4** did not bind to any of the other PIPs (Figure 3.23). Receptor **5** was not tested in this way due to lack of material, however it is expected that it will have similar specificity to receptor **3** due to its similar structure.

3.9.5 Receptor 5 can detect PI(4,5)P$_2$

Although receptor **5** does not experience any change in fluorescence upon binding (Figure 3.12), the receptor can be used to probe immobilised PI(4,5)P$_2$. Figure 3.13 revealed that the increase in PI(4,5)P$_2$ is observed as an increasing fluorescence intensity up to approximately 0.5 nmols. Although the detection limit of receptor **5** (0.1 nmol, Figure 3.13) is lower than that of PLCδ1-PH domain (approx. 30 pmol), the receptor shows potential as a future PI(4,5)P$_2$ detection tool. By increasing the affinity of the receptor for PI(4,5)P$_2$, a lower detection limit may be achieved.

3.9.6 Receptors 3-5 bind with low affinity to ATP

ATP contains a central ribose which possesses a 1,2-diol, and phosphate groups (Figure 3.24). These functional groups are known to interact with boronic acids and ureas, and therefore receptors **3-5** have the potential to bind ATP. This was tested using a phosphatase assay employing ATP and ATPase. The turnover of the enzyme remained high, even at high receptor concentrations, indicating that the receptors to not bind the substrate strongly (Figure 3.26).

3.9.7 Receptors do not directly inhibit SopB or ATPase

Finally, both receptors were tested for the ability to inhibit the enzymes SopB and ATPase directly, by interaction with the enzyme rather than the substrate. In the presence of receptors **3** and **4**, the enzymatic reaction with an artificial substrate was unaffected, suggesting that the enzymes are not inhibited by the receptors (Figures 3.32 and 3.34).

Chapter 4: Evaluation of PI(3,4,5)P$_3$ receptors

Metal-based receptors **12** and **14** were designed to bind PI(3,4,5)P$_3$ (Chapter 2.3). Receptor **16** (Figure 4.3) was designed and synthesised by Dr. K. Damodaran as an ATP-binding receptor. Its structure suggests it may be able to bind one or more phospholipids so it was also tested. Due to the presence of the two strongly phosphate-binding zinc-DPA motifs, it is possible they will also bind to other phosphorylated PIPs. To examine which PIPs these receptors bind to and establish their affinity and selectivity, indicator displacement assays were employed. Competitive ELISA were carried out using the PI(3,4,5)P$_3$-binding GRP1-PH domain to evaluate the ability of the receptors to block protein-lipid interactions. The ability of the receptors to compete with the enzyme PTEN was established by phosphatase assays.
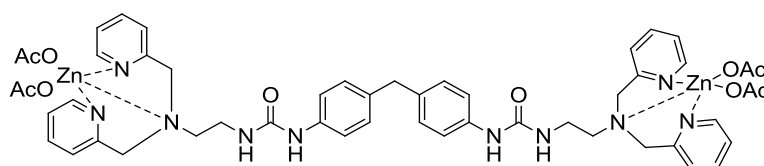
*Figure 4.1: Receptor **12***
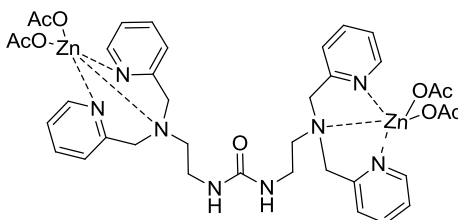
*Figure 4.2: Receptor **14***
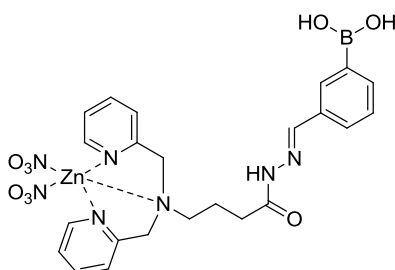
*Figure 4.3: Receptor **16***

4.1 Receptors were used in Indicator Displacement Assays (IDAs).

Firstly, the binding of receptors to the seven phospholipids was explored. As previously described, IDAs are a simple and effective method of determining binding affinity between receptors and analytes (*143*). The ability of each receptor to bind the various PIPs was examined.

4.1.1 Receptors bind to anionic dye.

Pyrocatechol violet (PV) was chosen as the indicator for the IDAs due to its large bathochromic shift upon binding to metal complexes (*144*). All three receptors bind to PV changing the colour from yellow to blue-green, a process which was readily monitored by UV-Vis spectroscopy (see Figure 4.4 and Appendix, Figure 9.13).
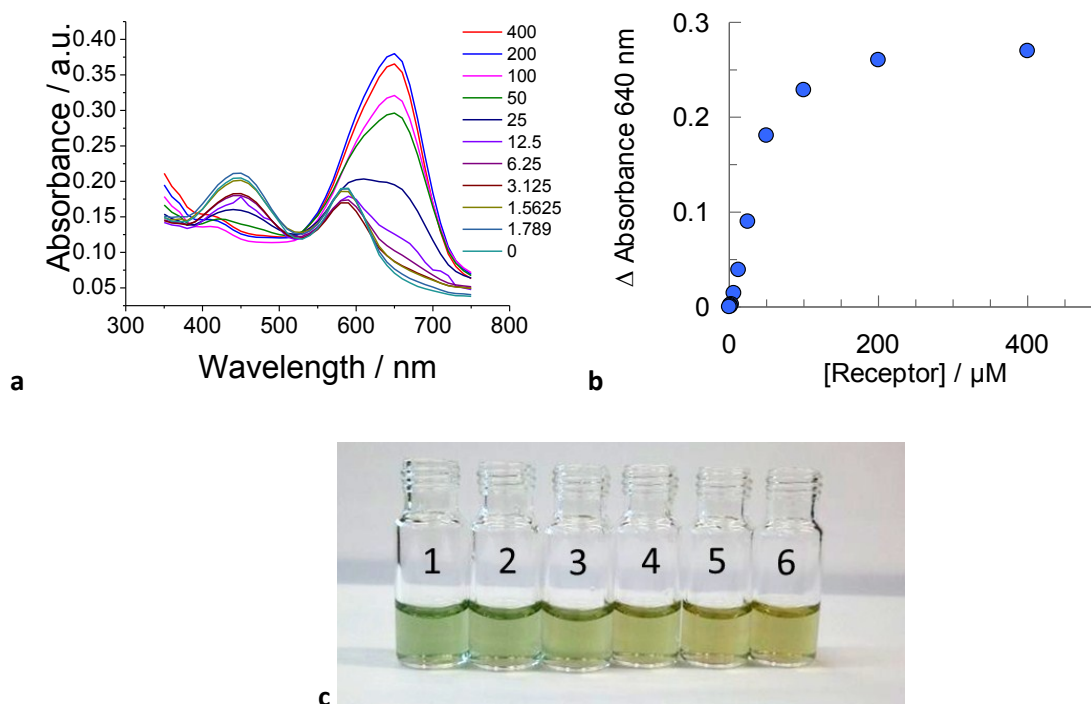
*Figure 4.4: Receptor **12** binds to PV. Figure a: The changes in the UV-Vis spectrum of PV (constant concentration at 50 μM) upon addition of increasing concentrations of receptor **12** (0 – 400 μM). Titration was carried out in HEPEs buffer (100 mM) at pH 7.4. As the receptor concentration increases, the peak at 640 nm increases in intensity and at the one at 440 nm decreases in intensity. Figure b: a plot of change in absorbance of the peak at 640 nm vs. receptor concentration. Figure c: Far left, a 1:2 mixture of receptor **12** and PV. Vials 1-6 contain increasing concentrations of IP$_4$. Upon binding IP$_4$ to the receptor the dye is released, returning to its original yellow colour. Dye concentration in all samples was 100 μM and receptor concentration was 50 μM. IP$_4$ concentrations: 1= 0 μM, 2 = 6.25 μM, 3 = 12.5 μM, 4 = 25 μM, 5 = 50 μM, 6 = 100 μM.*

For the next stage of the assay, stoichiometric ratios of the receptor-dye complexes were required, so that no excess receptor was present; if this was the case then upon addition of the analyte, the colour change would not be proportional to the displacement of the dye. To determine the stoichiometry of receptor-PV interaction, Job's plots (continuous variation plots, Figure 4.5) were carried out with all three receptors with PV.
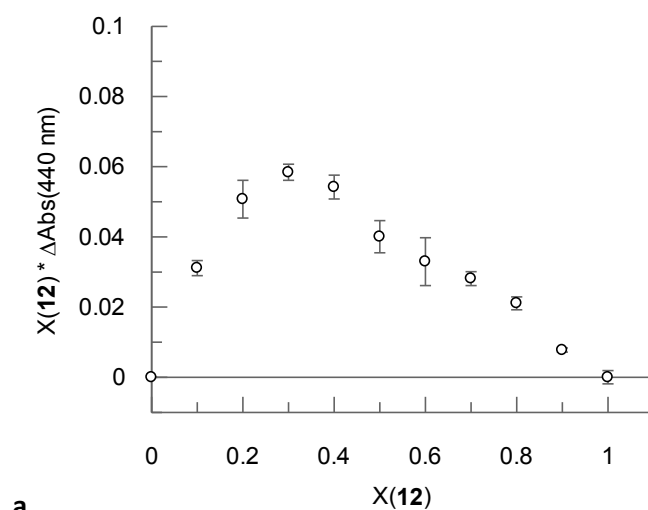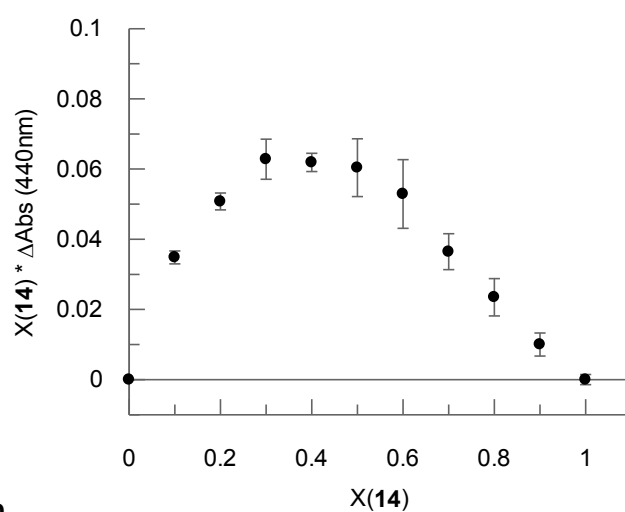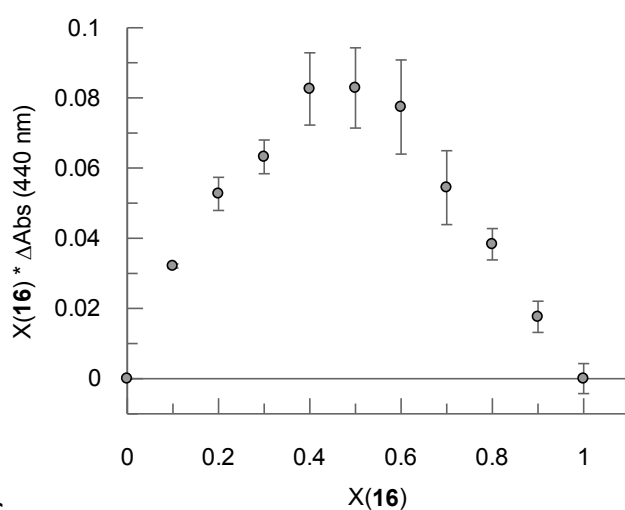
*Figure 4.5: Job's plot for receptors **12** (plot a), **14** (plot b) and **16** (plot c) and PV. Change in absorbance is plotted against the mole fraction of receptor as the ratio of receptor to dye is varied Total concentration is 100 μM and assay was carried out in 100 mM HEPES, pH 7.4. Error bars represent standard deviation of three independent experiments carried out in triplicate (n=3). Indicated stoichiometry is shown in Table 4.6.*

Table 4.6: Maxima of Job's Plot for each receptor:dye complex and indicated stoichiometry

Receptor	Maximum of Job's Plot	Stoichiometry (Receptor: dye)
12	X(**12**) = 0.3	1:2
14	X(**14**) = 0.3	1:2
16	X(**16**) = 0.5	1:1

The maxima of the plots indicated the receptor-PV stoichiometry for each receptor and results are summarised in Table 4.6. The dizinc-DPA based receptors each bound to two PV moieties. Receptor **16** had a 1:1 binding ratio to PV however no information was obtained on the mechanism of this interaction. The zinc-DPA motif may interact with the sulfate group while the boronic acid binds to the catechol, or only one of these interactions may be the source of binding.

4.1.2 Inositol phosphates and phosphoinositides bind to receptors.

To measure the ability of the receptors to bind to inositol phosphates and phosphoinositides, these polyphosphates were added to a solution of the receptor-dye complex. The receptor-dye complexes are blue-green in buffered aqueous conditions; when polyphosphates were added the dye was released by the receptor and returned to its original yellow colour (see Figure 4.7). This process was monitored by UV-Vis spectroscopy.

By using displacement assays we can compare the binding of each receptor to all the PIPs, and therefore evaluate the selectivity of the receptor. These were added to a solution of each receptor-PV complex, and the magnitude of displacement was measured. Analytes which bind more strongly will displace the PV from the receptor-PV complex and the absorbance at 640 nm will decrease. The phospholipid phosphatidylserine (PS) was included as due to its anionic nature it could potentially also bind the receptors.
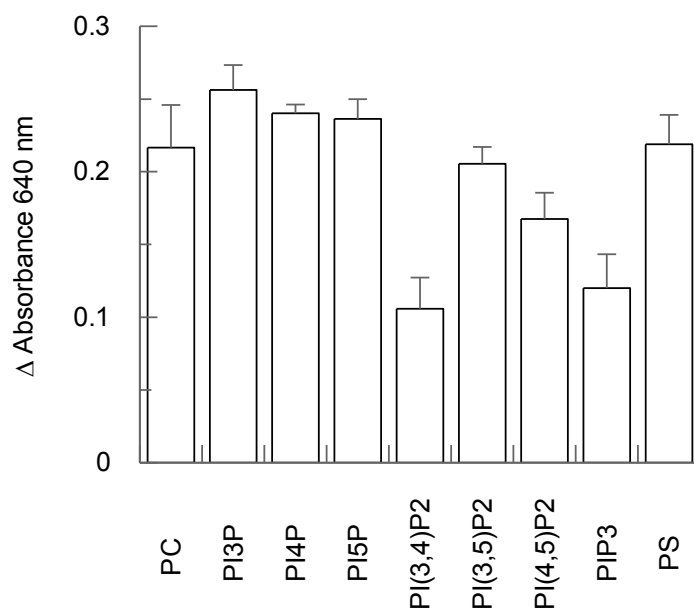
*Figure 4.7: The binding specificity of receptor **12**. Absorbance at 640 nm was measured upon addition of each PIP (1:1 PC, PIP; 25 μM) to a 1:2 mixture of receptor **12** (25 μM) and PV (50 μM). Background (absorbance of 50 μM free PV) has been subtracted to give ΔAbsorbance. This assay shows that receptor **12** binds to PI(3,4)P$_2$ and PI(3,4,5)P$_3$ most strongly. Error bars represent standard deviation of three independent experiments carried out in triplicate (n=3).*

The specificity plot (Figure 4.8) shows that receptor **12** binds preferentially to PI(3,4,5)P$_3$ and PI(3,4)P$_2$, suggesting that the receptor binds via the 3- and 4- phosphates present in both of these PIPs. Although dizinc complexes are known to interact strongly with polyphosphates, in this case the distance between the two zinc-DPA motifs makes it more likely that the two adjacent phosphates are interacting with one zinc-DPA and one urea, respectively.
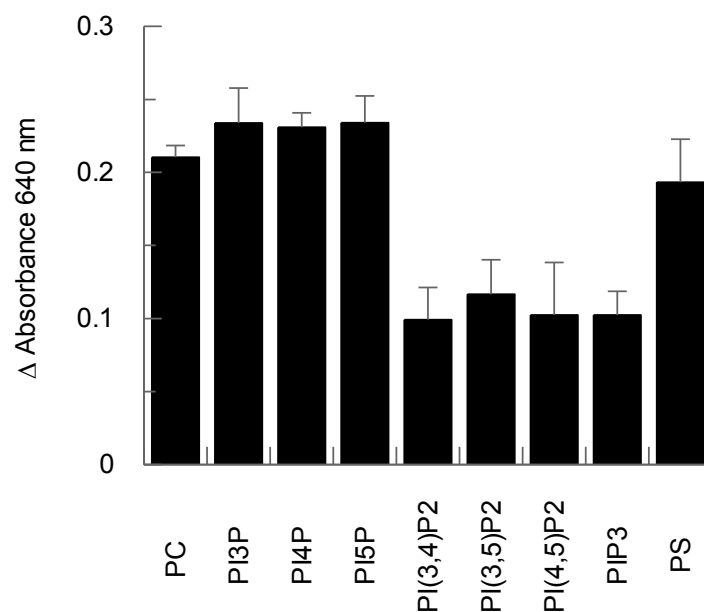
*Figure 4.8: The binding specificity of receptor **14**. Absorbance at 640 nm was measured upon addition of each PIP (1:1 PC, PIP; 25 μM) to a 1:2 mixture of receptor **14** (25 μM) and PV (50 μM). Background (absorbance of 50 μM free PV) has been subtracted to give ΔAbsorbance. This assay shows that receptor **14** binds to polyphosphorylated PI(3,4)P$_2$, PI(3,5)P$_2$, PI(4,5)P$_2$ and PI(3,4,5)P$_3$ equally. Error bars represent standard deviation of three independent experiments carried out in triplicate (n=3).*

Receptor **14** shows very little binding to monophosphorylated PIPs (Figure 4.9). While it binds to bis- and tris-phosphorylated PIPs, it exhibits little selectivity between each of them. Since receptor **14** has two flexible linkers about the central urea, it is plausible that these arms can move to accommodate the target polyphosphate. In contrast, receptor **12** has a more rigid core which restricts movement of the zinc-DPA motifs, preventing the receptor from interacting strongly with some of the PIPs.
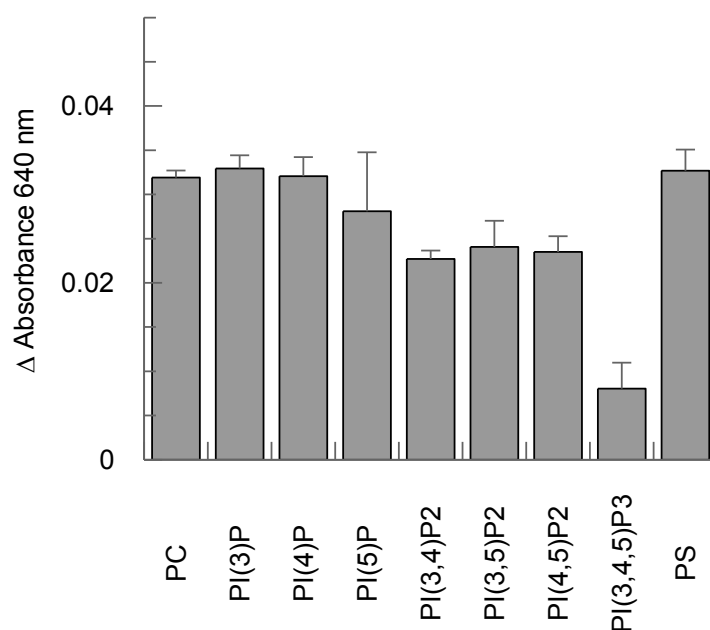
*Figure 4.9: The binding specificity of receptor **16**. Absorbance at 640 nm was measured upon addition of each PIP (1:1 PC, PIP; 25 μM) to a 1:2 mixture of receptor **16** (25 μM) and PV (25 μM). Background (absorbance of 25 μM free PV) has been subtracted to give ΔAbsorbance. This assay shows that receptor **16** binds to PI(3,4,5)P$_3$ most strongly. Error bars represent standard deviation of two independent experiments carried out in triplicate (n=2).*

Receptor **16** shows preferential binding to PI(3,4,5)P$_3$ (Figure 4.10). This is probably due to the ability of both the Zn-DPA and boronic acid groups to strongly bind phosphates, as well as the hydrazide linker which can interact via hydrogen bonding. Although the boronic acid was expected to be capable of binding to 1,2-diols the results show that the binding to diol-containing PI(4,5)P$_2$ is weak.

4.2 Receptors compete with GRP1-PH domain for PI(3,4,5)P₃ binding.

In order to test whether the receptors were capable of competing with the protein domain currently used for detecting PI(3,4,5)P₃, competitive ELISA were employed in the same manner as for the evaluation of PI(4,5)P₂ binding (see Chapter 3). However instead of the PLCδ1-PH domain which selectively binds PI(4,5)P₂, the PI(3,4,5)P₃-specific GRP1-PH domain was used (See Methods section 8.8).

4.2.1 Calibration of PI(3,4,5)P₃ detection using the GRP1-PH domain probe

Prior to testing the binding characteristics of the chemical receptors the optimal binding conditions of PLCδ1-PH domain for PI(4,5)P₂ were established. The assay was optimised to respond linearly to changes in both the lipid (Figure 4.11a) and the protein domain (Figure 4.11b).

a

b
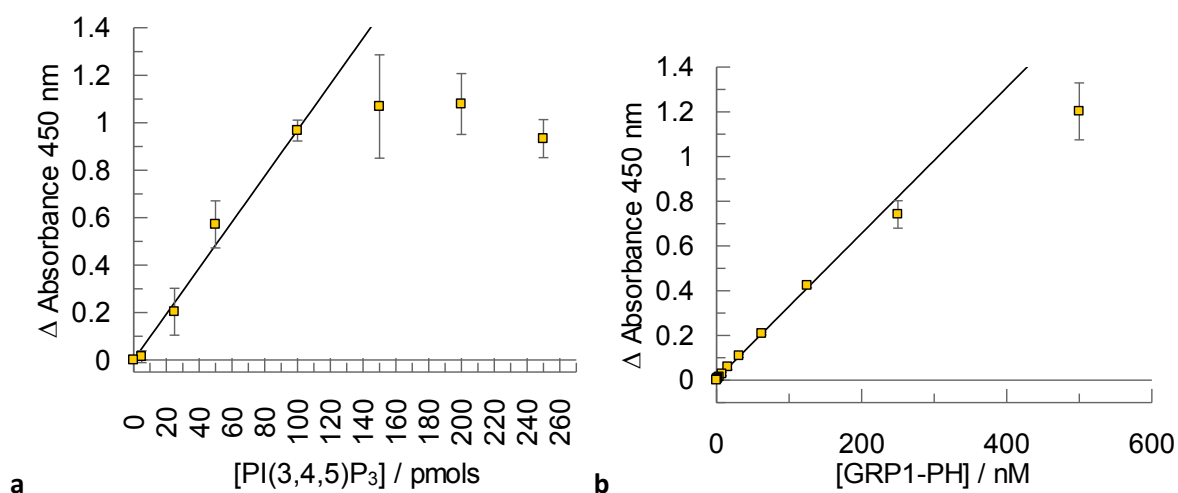
*Figure 4.10: Calibration of ELISA. Figure **a**: Absorbance at 450 nm increases as increasing concentrations of lipid are bound by the PI(3,4,5)P₃-binding domain GRP1-PH domain (100 nM). Background (absorbance at 0 M lipid) subtracted to give Δ absorbance at 450 nm. Figure **b**: Absorbance at 450 nm increases as increasing concentrations of GRP1-PH domain detect a single concentration of PI(3,4,5)P₃ (50 pmols). Background (absorbance at 0 M protein) subtracted to give Δ absorbance at 450 nm. Error bars represent standard deviation of two independent repeats carried out in triplicate (n=2). Apparent dissociation constants were calculated using the method of Orosz and Ovadi (137).*

K_d^{app} = 769 ± 177 nM.

The data presented in Figure 4.11**a** shows that the lipid could be linearly detected up to 100 pmols of PI(3,4,5)P₃ by 100 nM GRP1-PH domain; and that 50 pmols of PI(3,4,5)P₃ exhibit a linear response with up to 250 nM protein domain (Figure 4.11**b**). Therefore conditions using 50 pmols of PI(3,4,5)P₃ and 65 nM GRP1-PH domain were chosen to ensure that any inhibition by the receptors would be observed as a proportional decrease in colourimetric response in the following experiments.

4.2.2 Receptors inhibit protein-lipid binding.

Competitive ELISAs were set up in order to test the ability of receptors **12**, **14** and **16** to inhibit protein-lipid interactions. PI(3,4,5)P$_3$ -receptor mixtures were adsorbed onto the ELISA plate surface. The protein domain was then added to compete with the receptors, and the amount of bound protein was detected with enzyme-linked antibodies. The calculated apparent dissociation constant of GRP1-PH domain was used to determine the dissociation constant of each receptor for PI(3,4,5)P$_3$.

a

b

c
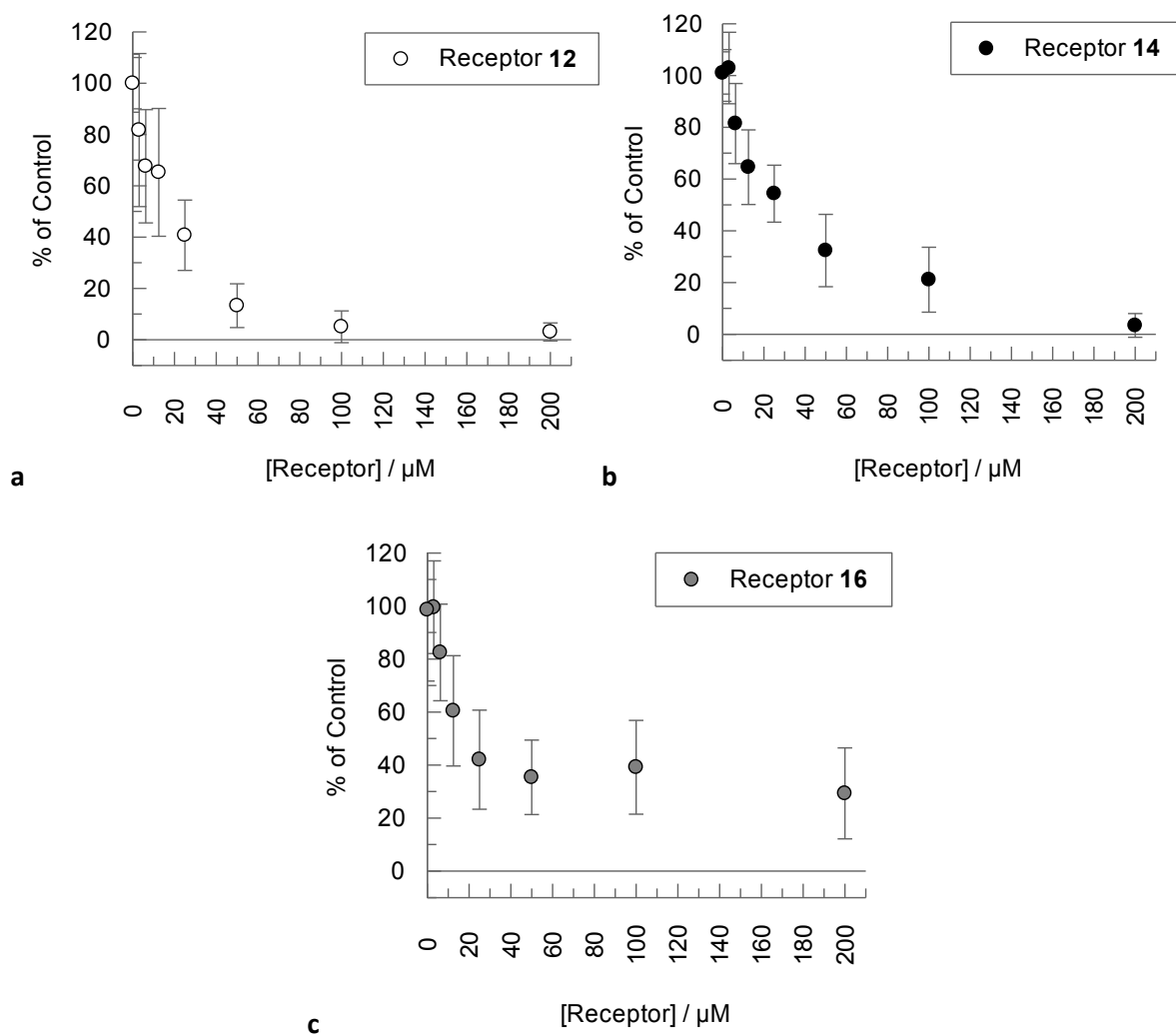
*Figure 4.11: Receptors **12** (a), **14** (b) and **16** (c) bind to PI(3,4,5)P$_3$. Absorbance at 450 nm is plotted as a percentage of the control (no receptor present). As concentration of receptor increases, the amount of protein detected decreases, suggesting that the receptor is successfully competing with the protein. PI(3,4,5)P$_3$ is used at 50 pmols and GRP1-PH domain at 65 nM. Assay was carried out using procedure described in Method section. Error bars represent standard deviation of three independent experiments carried out in triplicate (n=3). Apparent dissociation constant was calculated using the method outlined by Orosz and Ovadi (137).*

K_d^{app} (Receptor **12**) = 43.1 ± 3.6 µM.

K_d^{app} (Receptor **14**) = 50.8 ± 4.1 µM.

K_d^{app} (Receptor **16**) = 193.9 ± 71.7 µM.
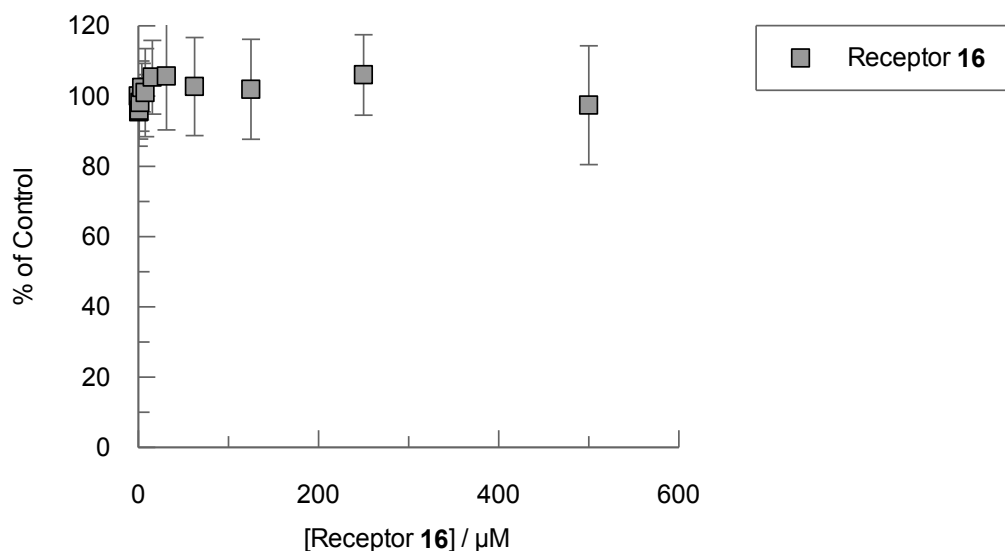
*Figure 4.12: Receptor **16** does not bind to PI(4,5)P$_2$. Absorbance at 450 nm is plotted as a percentage of the control (no receptor present). PI(4,5)P$_2$ is used at 100 pmols and PLCδ1-PH domain was 50 nM. Assay was carried out using procedure described in Method section. Error bars represent standard deviation of two independent experiments carried out in triplicate (n=2).*

As Figure 4.11 shows, from all the tested compounds receptor **12** inhibits the protein-lipid interaction to the greatest extent, followed closely by **14**. Both these receptors reduce the level of protein detected down to background levels. In contrast, receptor **16** initially binds strongly but only reduces the detected protein to around 30 % of the control, indicating that the GRP1-PH domain, at 65 nM concentration, is still able to compete with the larger concentration of receptor and bind to the lipid. Since it contains a boronic acid motif, receptor **16** was also tested for binding to PI(4,5)P$_2$ (which has been shown to bind to boronic acid-containing receptors) using the same procedure used to test receptors **3**, **4** and **5** (Section 3.4.2). However as shown in Figure 4.13, even at high concentrations receptor **16** was unable to block protein-lipid interactions; this correlates with the lack of PI(4,5)P$_2$ binding previously indicated by the IDA (Figure 4.10).

This pattern shows that the dizinc compounds are more effective than receptor **16**, which contains only one zinc-DPA motif. In receptors **12** and **14** the two zinc-DPA groups seem to act cooperatively, which is a more effective way of competing with a protein domain that possesses only a single binding site. Although the boronic acid is capable of interacting with phosphates, this is not a strong bond and is easily broken.

Since phosphate is present in cells at high concentrations, the ability of these receptors to bind PI(3,4,5)P_3 in the presence of phosphate was examined. To this end, phosphate ($KHPO_4$) was used to compete with PI(3,4,5)P_3 for receptor binding. It was expected that if the receptors interacted well with phosphate anions in solution, they would no longer to bind PI(3,4,5)P_3 and therefore the binding of GRP1-PH domain would be uninhibited.

Competitive ELISAs were carried out using the same conditions as Figure 4.12 except for washing with PBST (phosphate buffered saline with Tween-20) instead of TBST. Inhibition of protein-lipid binding by receptors **14** and **16** was greatly reduced (Figure 4.14).
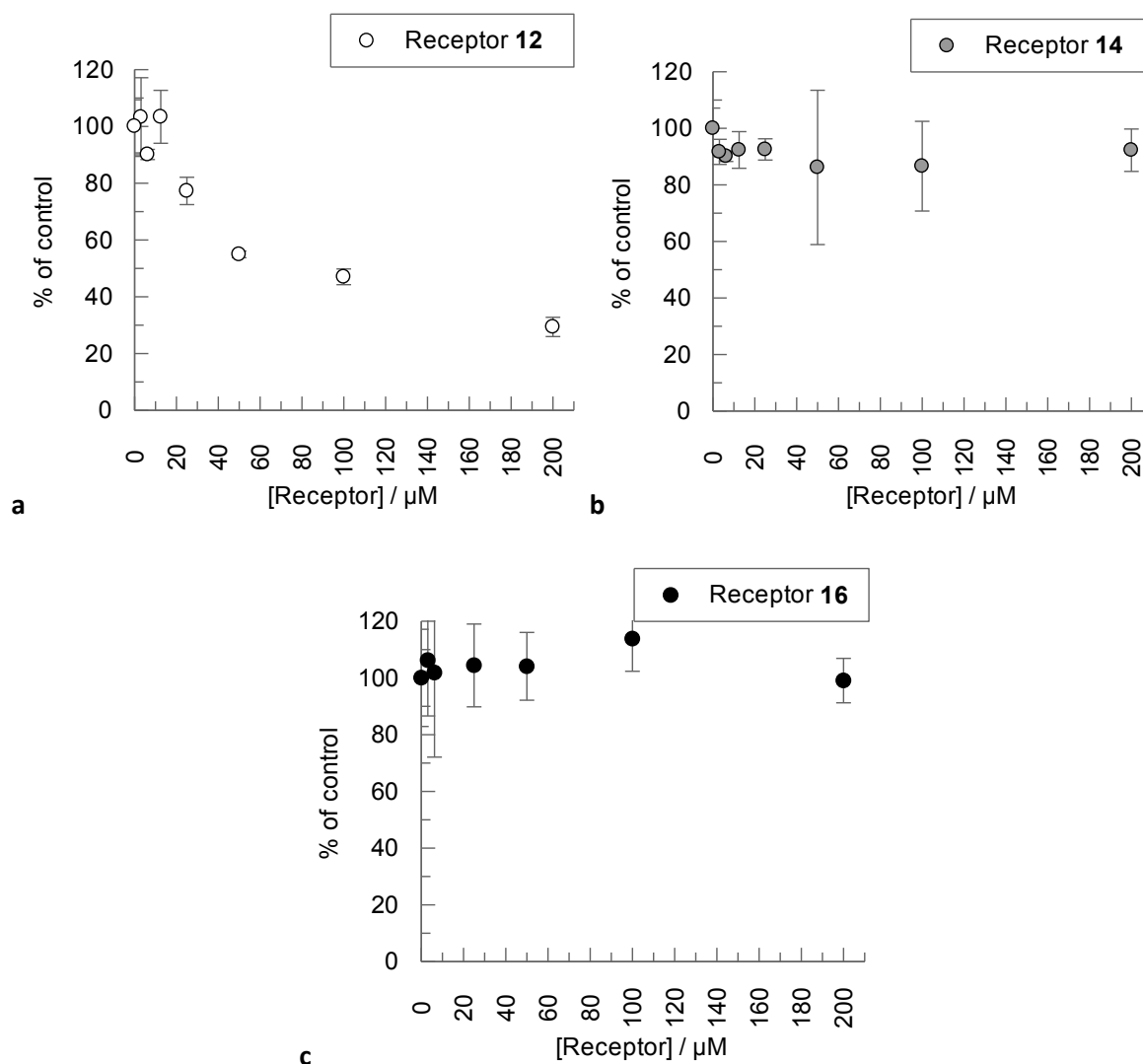
Figure 4.13: Binding of receptors 12 (a), 14 (b) and 16 (c) is decreased in the presence of phosphate. Absorbance at 450 nm is plotted as a percentage of the control (0 M receptor present). PI(3,4,5)P_3 is used at 50 pmols and GRP1-PH domain at 65 nM. Assay was carried out using procedure described in Method section, except PBST was used in every washing step instead of TBST. Error bars represent standard deviation of two independent experiments carried out in triplicate (n=2).

As shown in Figure 4.13, the presence of phosphate decreases the inhibition observed for all receptors. Receptor **12** alone is still able to bind PI(3,4,5)P$_3$ and prevent the GRP1-PH domain from binding. However the IC$_{50}$ value has shifted and to inhibit protein-lipid binding by 50 % in the presence of phosphate requires around 10-fold more receptor **12** than under phosphate-free conditions.

The ability of receptors **14** and **16** to inhibit protein-lipid binding is removed completely in the presence of KHPO$_4$. The receptors must therefore bind to the phosphate in solution, allowing the GRP1-PH domain to bind the immobilised PI(3,4,5)P$_3$. Therefore it is possible that in cells (which contain high concentrations of phosphate and many phosphorylated species) receptors **14** and **16** will be unable to bind PI(3,4,5)P$_3$, or block protein-lipid interactions.

4.3 Phosphatase assay: PI(3,4,5)P$_3$ substrate

Receptors **12**, **14** and **16** have been shown by indicator displacement assays to directly bind PI(3,4,5)P$_3$; competitive ELISAs were then employed to show that the receptors could block the interaction between lipid headgroups and protein domains. In a cellular environment downstream effectors such as Akt would be prevented from binding the lipid, and this should therefore attenuate the downstream signalling pathway. By reducing available PI(3,4,5)P$_3$ the receptors act as mimetics of PTEN, an enzyme which reduces PI(3,4,5)P$_3$ levels at the plasma membrane. The enzyme PTEN is a 3-phosphatase and dephosphorylates the 3'-position of PI(3,4,5)P$_3$ generating PI(4,5)P$_2$.

The chemical receptors can bind PI(3,4,5)P$_3$, blocking access to the lipid and lowering the amount of PI(3,4,5)P$_3$ that is available to downstream effectors. By sequestering PTEN's substrate the receptors can also act as an inhibitor of dephosphorylation. To examine this, a phosphatase assay was carried out in the presence of the receptors.

4.3.1 Calibration of PTEN dephosphorylation of PI(3,4,5)P$_3$.

The dephosphorylation of PI(3,4,5)P$_3$ by PTEN can be monitored by use of the phosphate detection reagent used previously. In order to be able to observe inhibition of this reaction by the chemical receptors, the assay was calibrated in order to determine the concentrations of enzyme and substrate which provided a linear response.

The response of the purified PTEN to increasing concentrations of PI(3,4,5)P$_3$ was determined; then the enzyme concentration was increased for a given substrate concentration (Figure 4.15).
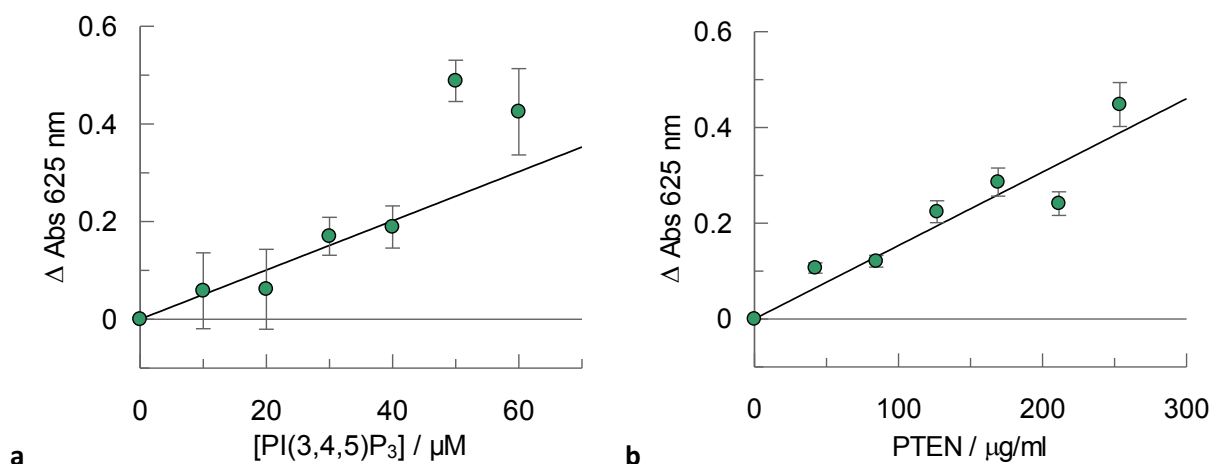
Figure 4.14: Calibration of phosphatase assay using PI(3,4,5)P₃ and PTEN. Figure **a**: Increasing concentrations of PC:PI(3,4,5)P₃ (1:1 ratio prepared as described in Methods section) were incubated with 126.9 μg/ml purified PTEN for 20 minutes at 37°C before the reaction was stopped by addition of phosphate detection reagent. Purification of PTEN is detailed in Methods section. Figure **b**: Increasing concentrations of PTEN were incubated with 30 μM PI(3,4,5)P₃ for 20 minutes at 37°C before the reaction was stopped using phosphate detection reagent. Error bars represent standard deviation of two independent experiments carried out in triplicate (n=2). Linear fit shown.

4.3.2 Receptors 12, 14 and 16 reduce PTEN turnover

The next aim was to show that when binding to lipids in this way, the chemical receptors would inhibit the action of enzymes by blocking access to the substrate. To examine this, the receptors were incubated with PI(3,4,5)P₃ before the application of the enzyme PTEN. The plots in Figure 4.16 show that the enzyme is inhibited by all three receptors to varying degrees. Receptor **12** has the lowest IC$_{50}$ of 8.5 μM while receptors **14** and **16** both show IC$_{50}$ of approximately 20 μM.
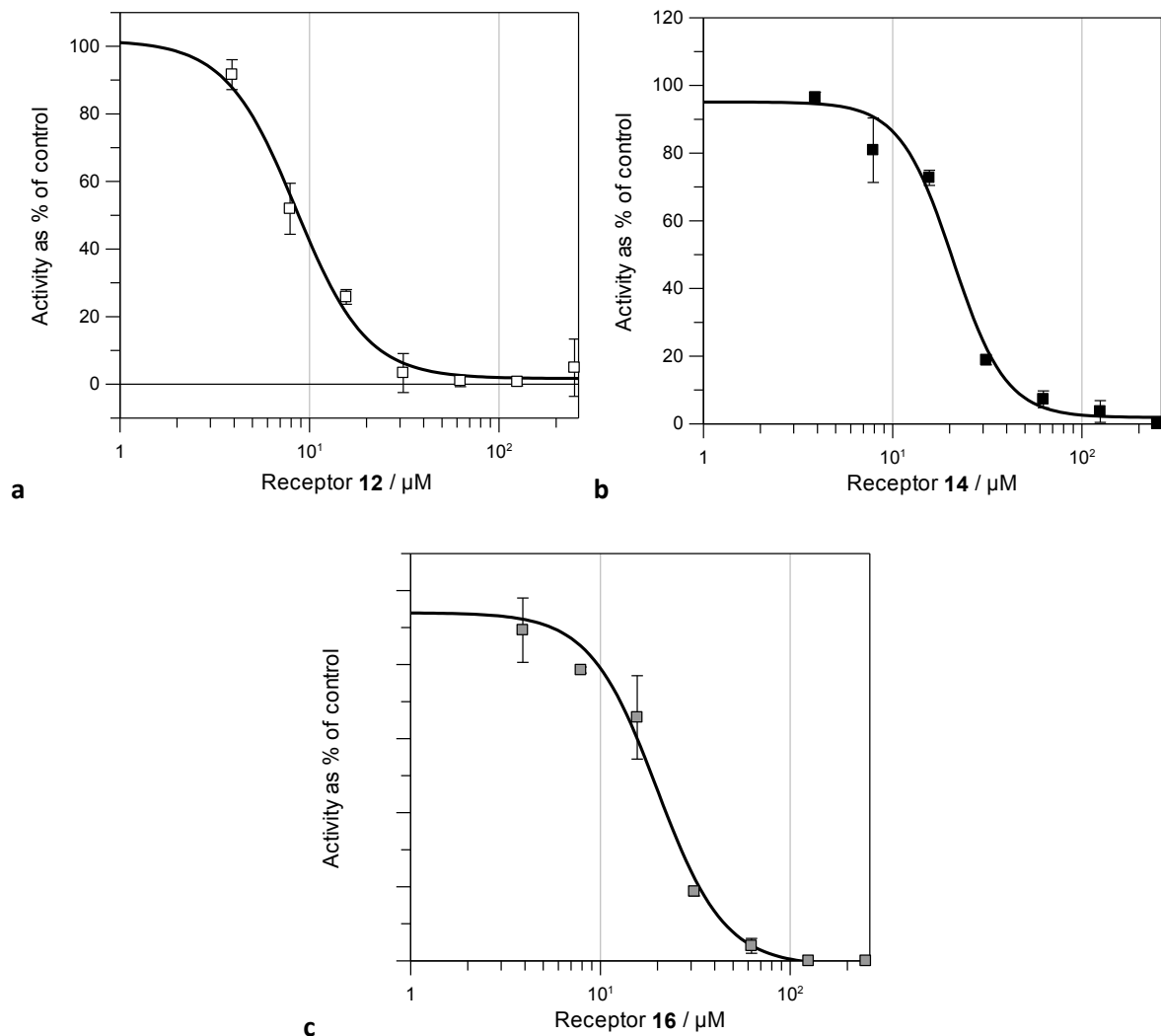
*Figure 4.15: Inhibition of the phosphatase activity of PTEN (126.9 μg/ml) by receptors **12** (a), **14** (b) and **16** (c). Receptors were incubated with mixed 1:1 PC-PI(3,4,5)P$_3$ (30 μM) vesicles for 15 minutes, followed by addition of the enzyme. After 20 minutes at 37°C the enzyme reaction was stopped by addition of phosphate detection reagent. Turnover in the presence of receptor was stated as a percentage of the turnover of a control containing no receptor. Error bars represent standard deviation of two independent experiments carried out in triplicate (n=2).*

Receptor **12** IC$_{50}$ = 8.5 ± 0.7 μM;

Receptor **14** IC$_{50}$ = 20.8 ± 1.5 μM;

Receptor **16** IC$_{50}$ = 19.9 ± 2.1 μM.

4.4 Zinc-based receptors inhibit PTEN directly

To test whether the receptors directly inhibit PTEN, the artificial substrate OMFP was employed (Figure 3.29). The increase in fluorescence due to enzymatic dephosphorylation was monitored over 25 minutes in the presence of receptors **12**, **14** and **16** and compared to the rate of increase of fluorescence in the absence of receptors (vehicle control).
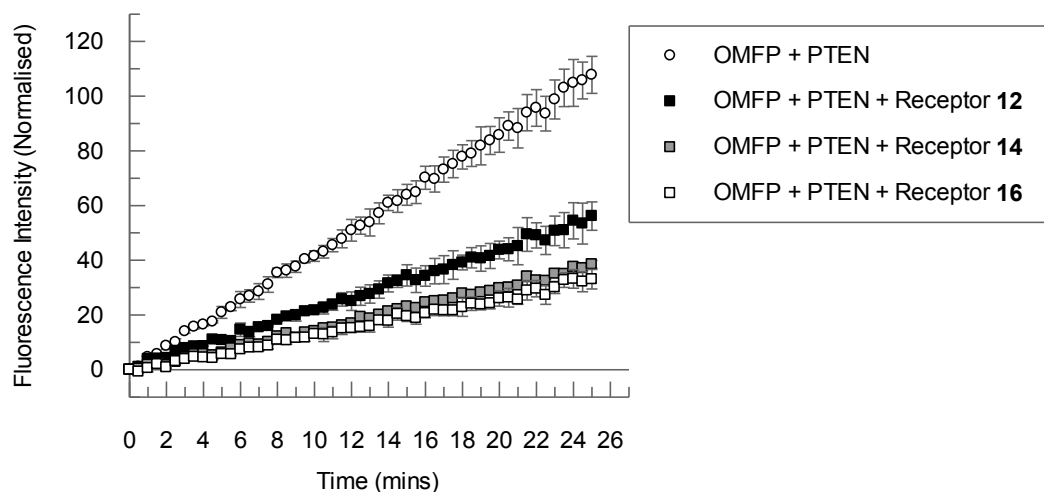
*Figure 4.16: Receptors **12, 14** and **16** (15 µM) inhibit enzyme activity. The increase in fluorescence intensity over time as PTEN (84.6 µg/ml) dephosphorylates OMFP (50 µM). Reaction carried out with no receptor (Control) and in the presence of 15 µM **12, 14** and **16**. Error bars represent standard deviation of two independent experiments carried out in triplicate (n=2).*

As shown in Figure 4.17, the rate of OMFP hydrolysis is reduced in the presence of all three receptors. Since the OMFP substrate possesses a terminal phosphate it was thought that the receptors may be inhibiting the reaction by binding to the substrate. Therefore different substrate concentrations were used to test whether the inhibition was due to substrate binding or a direct effect on the protein. If the inhibitory effect is overcome by addition of large excesses of OMFP (more than 10x receptor concentration), it is likely that the inhibition is due to the receptors binding to the substrate. Conversely, if the inhibition is independent of concentration then the effect is probably due to direct inhibition of the enzyme.

The rate of dephosphorylation (change in fluorescence intensity over time) was measured for four different concentrations of OMFP, with the receptor and enzyme concentrations remaining constant. Since divalent metal ions are known to inhibit some phosphatases, free zinc (II) was also tested (IC_{50} of zinc towards PTEN was determined to be 13.6 ± 1.3 µM, see Appendix Figure 9.11). It is possible that the zinc present in receptors **12**, **14** and **16** is the origin of inhibition of PTEN activity.
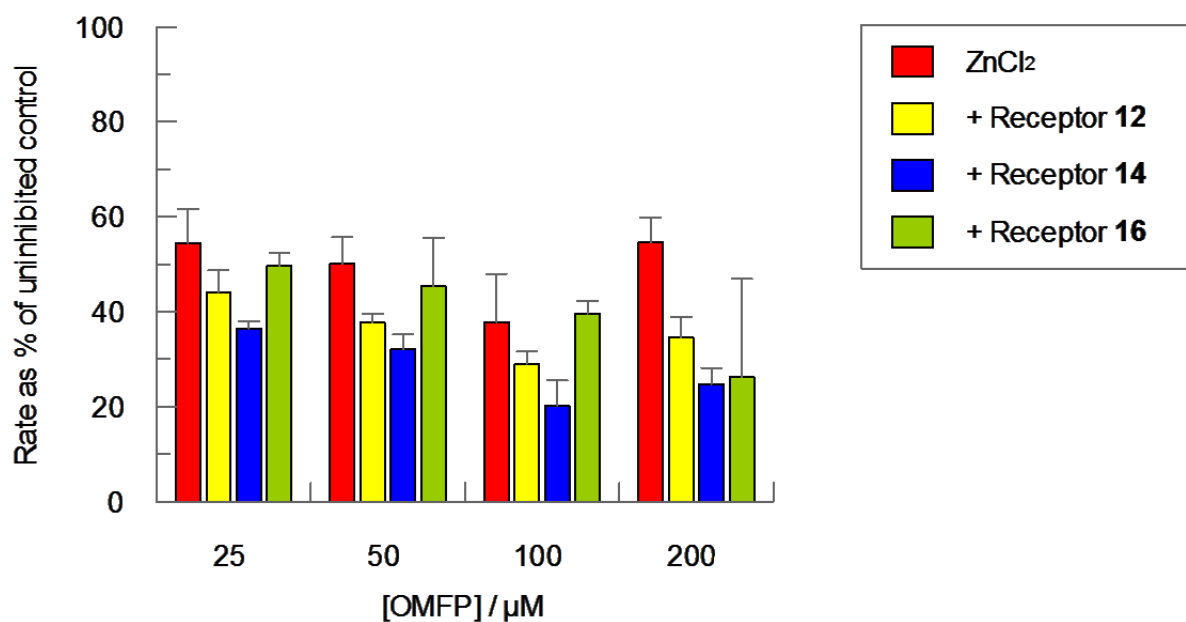
Figure 4.17: Rate of dephosphorylation of OMFP over 10 minutes, expressed as % of control for increasing OMFP concentrations. All receptors and zinc used at 15 µM each, PTEN used at 84.6 µg/ml. Error bars represent standard deviation of two independent experiments carried out in triplicate (n=2).

The data in Figure 4.18 show that all the receptors appear to inhibit the enzyme activity. The same pattern of inhibition is observed at all substrate concentrations, indicating that the inhibition is independent of substrate concentration. If the mechanism of inhibition was via the receptors binding to the substrate, this effect would decrease as substrate concentration increased. Therefore the receptors must be directly inhibiting the enzyme.

All three receptors show similar levels of inhibition to zinc (II). However the inhibition does not appear to be independent of the ligands. Receptors **12** and **14** possess two equivalents of zinc (II) each and yet show the same amount of inhibition as one equivalent of free zinc (II), and as receptor **16**. If the receptors were releasing their chelated zinc (II) into solution it would be expected that 15 µM receptors **12** and **14** would have twice the inhibitory effect of 15 µM free zinc (II).

This could be due to one of two reasons. Firstly, that the zinc (II) is existing in equilibrium between being free in solution, and coordinated by DPA. Therefore partial inhibition is observed due to the free zinc (II). Secondly, that the coordinated zinc is inhibiting the enzyme via a free coordination site. Therefore only one receptor molecule (containing two coordinated zinc (II)) is required for inhibition.

4.5 Summary: PI(3,4,5)P$_3$ receptors

4.5.1 Receptors 12, 14 and 16 show variable specificity

Indicator displacement assays indicated that receptor **12** showed binding specificity towards PI(3,4)P$_2$ and PI(3,4,5)P$_3$ (Figure 4.8). This pattern suggests the receptor binds both the phosphates on the 3- and 4- positions of these lipids. The PH domain of Akt has similar selectivity, binding also to PI(3,4)P$_2$ and PI(3,4,5)P$_3$, therefore this receptor is a potential mimetic of the Akt-PH domain.

Receptor **14** showed a preference for polyphosphorylated PIPs, but no selectivity between these (Figure 4.9). The small distance between the zinc-DPA motifs and the flexible nature of the linker between these is likely to contribute to its promiscuous binding.

Receptor **16** bound preferentially to PI(3,4,5)P$_3$, showing only weak interaction with other PIPs (Figure 4.10). Although it was expected that **16** would bind with good affinity to PI(4,5)P$_2$ due to the possibility of forming a cyclic boronate ester this was not the case. This is likely due to the nature of the boronic acid group: receptors **3**, **4** and **5** all have methyl-amino groups adjacent to the boronic acid which form a tetrahedral boronate, which is known to interact more strongly with diols at physiological pH (*122*), (*145*) than the trigonal boronic acid. Receptor **16** does not have this functional group next to the boronic acid.

4.5.2 Dizinc receptors fully inhibit protein-lipid interaction in phosphate-free conditions

Competitive ELISA showed that receptor **12** bound strongly to immobilised PI(3,4,5)P$_3$, blocking the PH domain of GRP1. Receptor **14** showed slightly lower affinity binding; however both of these receptors were capable of completely blocking protein-lipid interaction at high concentrations. Receptor **16** also displayed strong PI(3,4,5)P$_3$ binding although even at higher concentrations this receptor was unable to completely inhibit protein-lipid binding. This receptor showed no binding to PI(4,5)P$_2$ when tested using this method, even at high concentrations.

When phosphate buffer was used instead of Tris buffer, the larger phosphate concentrations competed with the lipid for receptor binding sites. Receptors **14** and **16** were unable to inhibit protein-lipid interactions under these conditions, while the IC$_{50}$ of receptor **12** was reduced by around 10-fold. Since cells typically contain many phosphorylated species it is unlikely that receptors **14** and **16** will bind their targets. Receptor **12** shows more resilience in the presence of 10 mM phosphate, since some protein-lipid inhibition is still observed.

4.5.3 Receptors inhibit dephosphorylation of PI(3,4,5)P$_3$ and OMFP by PTEN

Phosphatase assays using PTEN showed that these receptor were potent inhibitors of the dephosphorylation of PI(3,4,5)P$_3$, in particular receptor **12** which had the lowest IC$_{50}$. However, the

use of the artificial substrate OMFP showed that the zinc present in the receptors was having a direct inhibitory effect on the enzyme. Therefore the mechanism of the inhibition is not clear- it may be that the receptors do indeed bind the substrate, while the zinc simultaneously inhibits the enzyme. A small variation in the IC_{50} values would seem to indicate that receptor-PI(3,4,5)P$_3$ binding is responsible for part of the inhibition. However in reactions carried out with the artificial substrate OMFP, the pattern of inhibition was the same at all OMFP concentrations. This suggested that the enzyme is inhibited directly, since any substrate-binding inhibition would be overcome at higher substrate concentrations.

4.5.4 Metal ions inhibit a number of phosphatases

Divalent metal ions can interact with proteins in several ways as detailed in a review by Meggers (*146*). Firstly, their versatile geometry can direct the shape of ligands and form uniquely shaped inhibitors that can fit into the active site of an enzyme and act as a competitive inhibitor. One example of this is the vanadyl complex VO-OHpic which is a potent and selective inhibitor of PTEN (IC_{50} = 35 nM ± 2.0 nM) (*147*) over other phosphatases. The vanadium is chelated by two 3-hydroxypicolinate ligands and the resulting complex fits well into the active site of PTEN, but not other similar phosphatases; the resulting complex is much more potent and selective than merely delivering the vanadate to the active site of the enzyme. Secondly, metals can interact directly with amino acid residues present in the active sites of enzymes. This is a common mode of action affecting enzymes which possess active site residues such as cysteine or histidine, since the sulfur or nitrogen in the side chains of these residues can coordinate to metal ions. Several metal ions including zinc are known to inhibit protein tyrosine phosphatases and many inhibitors have been designed with metal cores (*148*). Both the enzymes PTEN and SopB both contain the sequence CX$_{(5)}$R (*147*), and it is likely that the cysteine residue coordinates to the zinc ion of the receptors.

That receptors **12**, **14** and **16** inhibit phosphatases limits their usefulness in enzymatic assays. Instead of mimicking the function of PTEN, they have been shown to inhibit that important tumour suppressor, with no more potency than free zinc itself. However they have also been demonstrated to bind to PIPs by means of IDAs and competitive ELISA. Receptor **12** was shown to bind most strongly to PI(3,4,5)P$_3$ with specificity similar to that of the Akt-PH domain (*22*); in addition it was also able to bind PI(3,4,5)P$_3$ in a competitive phosphate-containing environment. Receptor **16** showed specificity towards PI(3,4,5)P$_3$ only, similar to the GRP1-PH domain (*22*). Therefore as PH domain mimetics receptors **12** and **16** may yet prove useful in binding studies using non-enzymatic methods such as ELISA.

Chapter 5: Evaluation of receptors in cancer cells

Receptors **3**-**5** and **12**, **14** and **16** have all been shown to inhibit protein-lipid interaction, therefore it is expected that firstly, PI(4,5)P$_2$-binding receptors will inhibit the activity of PI3K and reduce the amount of PI(3,4,5)P$_3$ generated; and secondly that PI(3,4,5)P$_3$-binding receptors will prevent the recruitment of Akt to the plasma membrane. The level of Akt phosphorylated on serine residue 473 (pSer 473) was used as a marker of interaction of the receptors with endogenous PI(4,5)P$_2$ and PI(3,4,5)P$_3$.

5.1 PI3K-Akt signalling pathway

As shown in Figure 5.1, the activated form of Akt regulates several downstream pathways which control cell growth and proliferation and inhibit apoptosis. Therefore when this pathway is overactivated (for example, when PTEN is mutated and cannot regulate the action of PI3K) cell growth is uncontrolled and tumours can form (*31*), (*5*), (*30*). This is a notorious pathway involved in many types of cancer and efforts have been focused on reducing the activation of the PI3K-Akt pathway, mainly by inhibiting the action of PI3K.
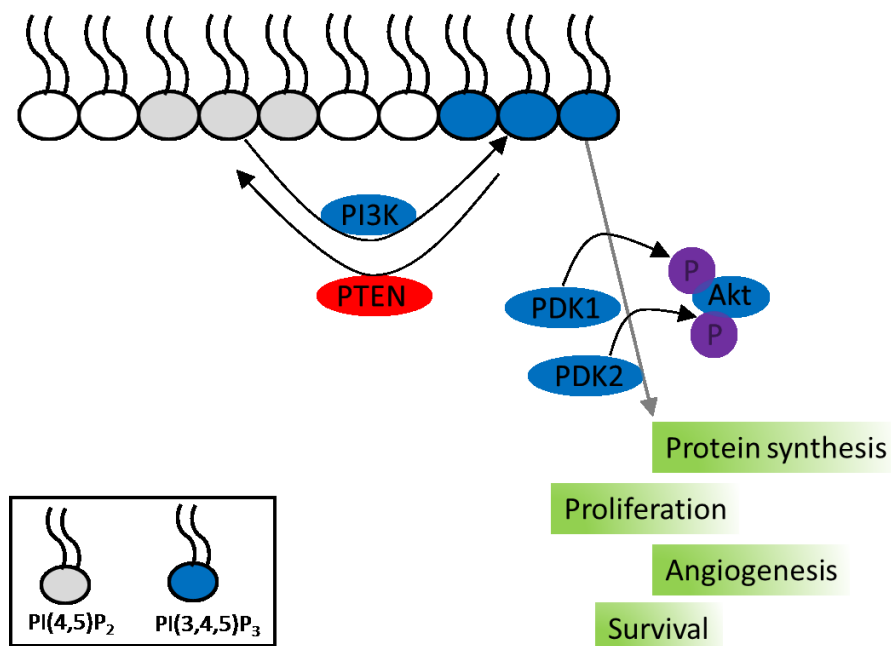
*Figure 5.1: A schematic of the Akt pathway. Activation of receptor tyrosine kinases activates PI3K, which catalyses the phosphorylation of PI(4,5)P$_2$ to PI(3,4,5)P$_3$. The latter recruits Akt to the plasma membrane where it is phosphorylated twice on the Serine 473 and Threonine 308 positions. Phosphorylated Akt regulates several downstream signalling pathways which control a number of cellular processes including cell survival and proliferation (*35*). In several types of cancer the pro-life, anti-apoptotic signalling pathway of Akt is overactivated causing tumour formation (*31*).*

In previous studies it was established that PHDM was able to enter cells and bind to PI(4,5)P$_2$ (*58*). This binding had a number of effects on PI(4,5)P$_2$-dependent cellular functions: PHDM inhibited transferrin endocytosis, actin fibre formation, and reduced the number of mitochondria by approximately 40 % (*58*). PHDM also reduced the phosphorylation of Akt by binding PI(4,5)P$_2$ and inhibiting the synthesis of PI(3,4,5)P$_3$ by PI3K. This prevented Akt from being recruited to the membrane and therefore it was not phosphorylated. The levels of phosphorylated Akt were probed by Western blot and were shown to decrease with increasing PHDM concentrations (personal communication, Dr. L. Mak).

Since receptors **3**-**5** and **12**, **14** and **16** have been shown to bind to PI(4,5)P$_2$ or PI(3,4,5)P$_3$ by *in vitro* assays, they were all tested for the ability to inhibit the phosphorylation of Akt. It was expected that by binding to these phospholipids the receptors would be capable of reducing Akt phosphorylation.

5.2 Stimulation with insulin activates PI3K-Akt pathway in HCT116 cells

Since the phosphorylation of Akt was to be stimulated by the addition of insulin, the response of the cells to different concentrations of insulin was analysed. It was expected that the receptors would reduce the phosphorylation of Akt, therefore a concentration of insulin was chosen where this effect could be observed as a decrease in intensity under the conditions of the experiment. Therefore, cells were starved overnight before treatment with various concentrations of insulin.
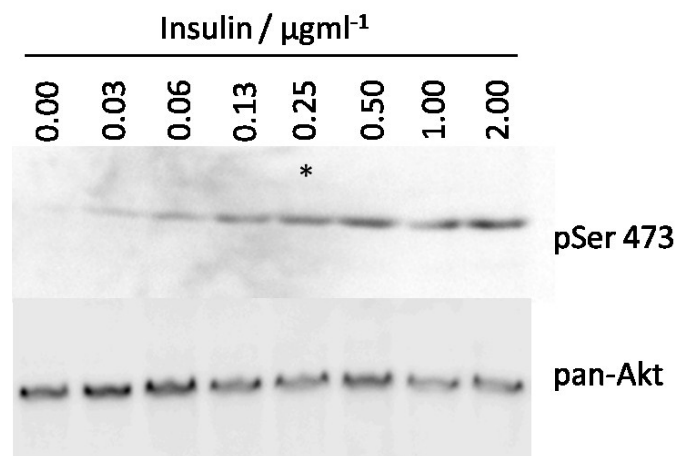
Figure 5.2: Increasing concentrations of insulin stimulate phosphorylation of Akt. HCT116 cells were starved overnight and stimulated with increasing concentrations of insulin (15 mins, 37 °C). Cells were lysed and proteins separated using SDS-PAGE. After transferring to nitrocellulose membrane, the proteins were probed with pSer 473 or pan-Akt antibody. Data shown is representative of two independent experiments. Starred concentration (0.25 μgml^{-1}) was used to stimulate cells in later experiments.

Figure 5.2 shows that as the concentration of insulin increases, the intensity of the phosphorylated Akt band of the Western blot also increases. The increase in intensity is linear up to around 0.5 µg/ml insulin, after which the band becomes saturated. Therefore in order to be able to observe a decrease in intensity after application of the receptors, it was decided that the cells would be stimulated with 0.25 µg/ml insulin.

5.3 Receptors 3 – 5 decrease amount of phosphorylated Akt in HCT116 cells

After determining the concentration range where Akt phosphorylation increases linearly with rising insulin concentrations, receptors **3-5** were applied to serum-starved HCT116 endothelial cells, before stimulating the cells with insulin. In addition, increasing amounts of insulin were applied to cells containing vehicle control to ensure that the presence of 2 % DMSO did not affect the response of the cells to the concentration of insulin used.

After the cells were lysed and proteins separated by SDS-PAGE the proteins were transferred to nitrocellulose membrane by Western blot, and these membranes were probed with antibodies detecting the phosphorylated serine 473 residue of Akt. The amount of total Akt was also determined by probing with pan-Akt antibody.
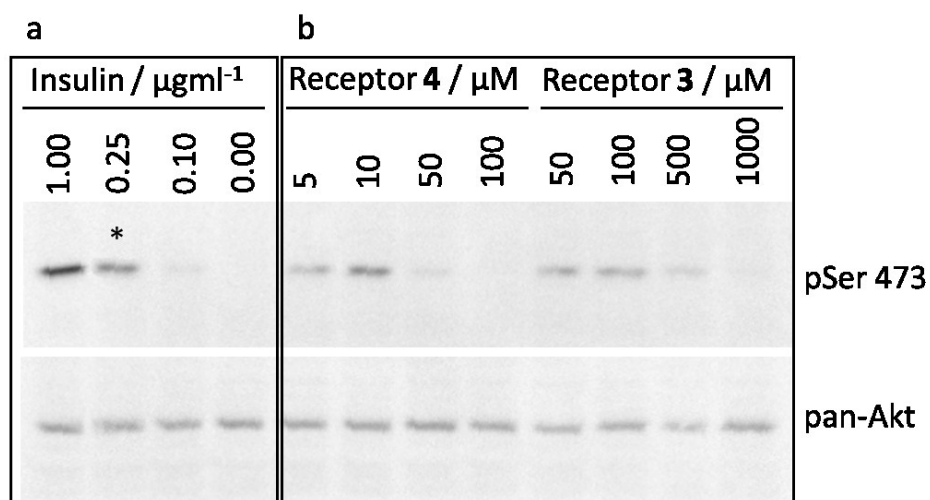
*Figure 5.3: Increasing concentrations of receptors **3** and **4** reduce the phosphorylation of Akt on serine 473. HCT116 cells were starved of serum overnight, before incubation with vehicle (part **a**) or receptor **3** and **4** (part **b**). This was followed by stimulation with insulin (concentrations as indicated). Cells were lysed and proteins separated using SDS-PAGE. After transferring to nitrocellulose membrane, the proteins were probed with pSer 473 or pan-Akt antibody. Data shown is representative of two independent experiments. Part **a**: HCT116 cells were incubated with DMSO (2 % v/v, 15 mins, 37 ^{o}C), which was followed by stimulation with insulin (concentrations as indicated). Part **b**: Starved HCT116 cells were incubated with receptors **3** and **4** for 15 minutes at 37 ^{o}C. The cells were then stimulated with insulin (0.25 µg/ml, 15 mins, 37 ^{o}C). The appropriate control (lane 2) on part **a** is highlighted with a star, and the concentration of insulin employed is in the linear range.*
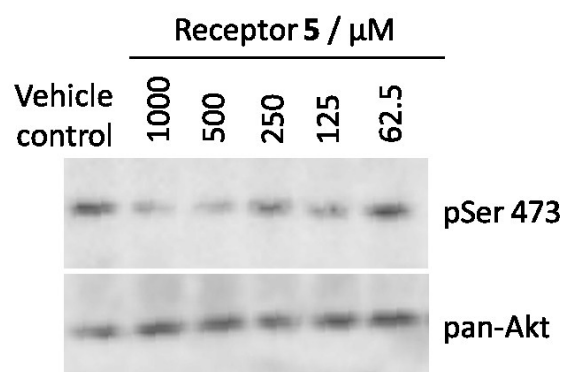
*Figure 5.4: Increasing concentrations of receptor **5** reduce the phosphorylation of Akt on serine 473. HCT116 cells were starved, treated with receptor **5** and insulin and analysed for phosphorylated Akt content as described in Figure 5.3. Data shown is representative of two independent experiments.*

Figures 5.3 and 5.4 show that increasing the concentration of receptors **3**, **4** and **5** decreases the level of phosphorylated Akt in cells, while the total Akt remains unaffected. This suggests that the Akt pathway is inhibited in the presence of these receptors, since the phosphorylation of Akt is an indicator of the activation of this pathway. Receptor **4** is more potent than receptors **3** and **5**, which is consistent with its higher affinity and specificity towards PI(4,5)P$_2$. These results are consistent with the data obtained for the original PHDM molecule which was also shown to interrupt various PI(4,5)P$_2$ controlled cellular processes.

5.4 Receptors 12, 14, 16 have no effect on phosphorylated Akt level in HCT116 cells

Receptor **12** has been shown to bind to PI(3,4)P$_2$ and PI(3,4,5)P$_3$ which are also the targets of Akt, so this compound has potential to block phospholipid-Akt interactions and reduce Akt phosphorylation. Receptors **14** and **16** bind to other phospholipids as well, however since PI(4,5)P$_2$ is the main phosphoinositide component of the plasma membrane (*1*),(*3*) it is supposed that these receptors have a high probability of interacting with PI(4,5)P$_2$.   As shown by receptors **3-5** in Figures 5.3 and 5.4, the presence of PI(4,5)P$_2$ –binding receptors decreases phosphorylated Akt levels, presumably by inhibiting the synthesis of PI(3,4,5)P$_3$.
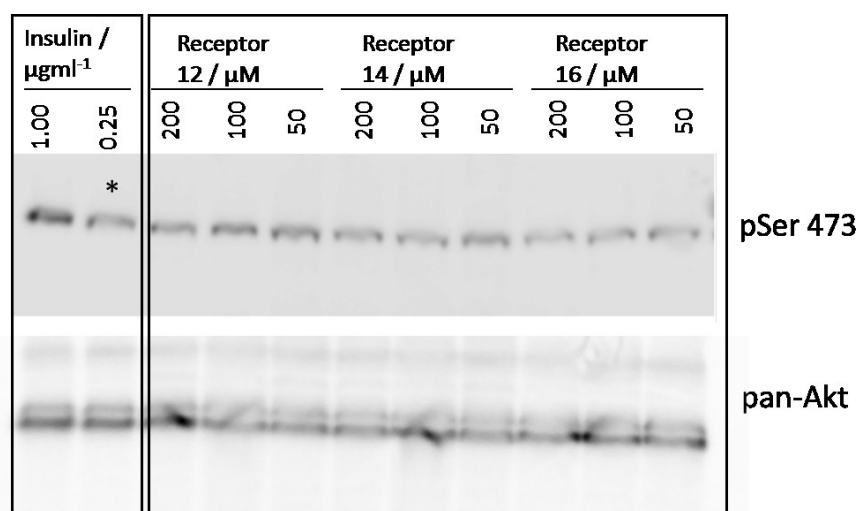
*Figure 5.5: Increasing concentrations of receptors **12, 14** and **16** have little effect on the phosphorylation of Akt on serine 473. HCT116 cells were starved of serum overnight before incubation with receptor for 15 minutes at 37°C. After stimulation with insulin (0.25 µg/ml, 15 mins, 37°C) cells were lysed and proteins separated using SDS-PAGE. After transferring to nitrocellulose membrane, the proteins were probed with pSer 473 or pan-Akt antibody. Data shown is representative of two independent experiments. Lane two (*) indicates vehicle control (DMSO only).*

The changes in phosphorylated Akt levels that were shown with receptors **3**-**5** (Figures 5.3 and 5.4) were not observed on addition of receptors **12**, **14** and **16**. One explanation for this lack of effect could be that due to the highly polar nature of the zinc complexes, they may not cross the plasma membrane efficiently enough to have an effect. Therefore an experiment was set up in which the ligands were incubated with the cells, followed by an ionophore compound which is known to transport zinc into cells. It was hypothesised that the ligands would form zinc complexes inside the cell, and there they would have the potential to bind to phosphoinositides and block protein-lipid interaction.

Insulin / μgml^{-1}	1	0.25	0	0.25	0.25	0.25	0.25	0.25	0.25	0.25	0.25	0.25
DMSO	-	-	-	+	-	-	-	-	-	-	-	-
Ligand	-	-	-	-	-	-	11	11	13	13	15	15
Na-Pyrithione	-	-	-	-	+	-	+	-	+	-	+	-
Zn-Pyrithione	-	-	-	-	-	+	-	+	-	+	-	+
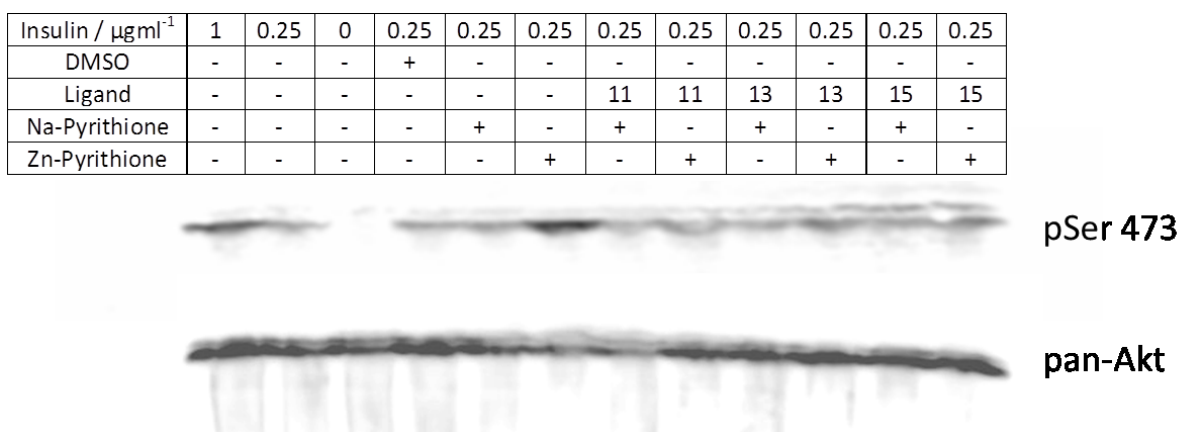
*Figure 5.6: Compounds **11**, **13** and **15** have little effect on phosphorylation of Akt when incubated separately to zinc pyrithione. HCT116 cells were starved of serum overnight before incubation with ligand (100 μM) or vehicle control (30 mins, 37 ^{o}C). The medium was removed by aspiration and replaced with fresh medium to which sodium pyrithione (50 μM) or zinc pyrithione (50 μM) was added, and incubated at 37 ^{o}C for 15 minutes. After stimulation with insulin (0.25 μg/ml, 15 mins, 37 ^{o}C) the cells were lysed and proteins separated using SDS-PAGE. After transferring to nitrocellulose membrane, the proteins were probed with pSer 473 or pan-Akt antibody. Data shown is representative of two independent experiments.*

As shown in Figure 5.6 above, application of the ionophore zinc pyrithione has an insulin mimetic effect on cells, increasing the levels of phosphorylated Akt. The control compound sodium pyrithione shows no activation of phosphorylated Akt and confirms that the zinc ion, and not the pyrithione ligand, is the source of this effect.

In the presence of ligands **11**, **13** and **15** the phospho Akt levels are comparable to the vehicle control. No decrease in phospho Akt is observed which would indicate that the zinc complexes are binding to PI(4,5)P$_2$ or PI(3,4,5)P$_3$; however the activation observed in the presence of zinc pyrithione has also been reduced. This suggests that the ligands are interacting with the zinc once inside the cells, however they do not appear to be capable of binding PI(4,5)P$_2$ or PI(3,4,5)P$_3$ intracellularly.

5.5 Summary:

Receptors **3**, **4** and **5** were capable of reducing the levels of phosphorylated Akt with potency that directly reflected the binding strength of each receptor for PI(4,5)P$_2$. Receptor **3** which had the strongest binding affinity for PI(4,5)P$_2$ exhibited the most potent effect on the level of phosphorylated Akt. At 50 µM this receptor reduced phosphorylated Akt levels almost completely, which is comparable to the effectiveness of original compound PHDM (personal communication, Dr. L. Mak). The binding affinity of receptors **4** and **5** for PI(4,5)P$_2$ were approximately 5 – 7 fold lower than that of receptor **3**; this lower binding affinity was reflected in cells where receptors **4** and **5** required almost 10-fold higher concentrations to achieve similar reduction of phosphorylated Akt.

Addition of receptors **12**, **14** and **16** had no observed effect on phosphorylated Akt levels. Considering that this might be due to a lack of uptake of the metal complexes, rather than lack of efficacy, the metal-free ligands (compounds **11**, **13** and **15**) were employed. Cells were exposed to these compounds before a zinc ionophore was added. The ionophore delivered zinc into the cells and when zinc pyrithione was used alone an increase in phosphorylated Akt level was observed- consistent with the insulinomimetic effect of zinc. In the presence of compounds **11**, **13** and **15** no such increase was observed, indicating that the metal-free ligands are capable of forming a complex with zinc inside the cells, preventing cells from its insulinomimetic effect. However, no decrease in phosphorylated Akt was observed, indicating that the zinc complexes are not competing with Akt for binding to PI(4,5)P$_2$ or PI(3,4,5)P$_3$ once inside the cell.

Another possibility is that the generation of PI(3,4,5)P$_3$ in cells is too transient to be affected by the receptors. Activation of PI3K increases PI(3,4,5)P$_3$ levels very rapidly, and Akt is recruited to the PH domain in this time. However the action of PTEN and other phosphatases is also rapid, so that PI(3,4,5)P$_3$ levels increase only transiently. It may be that the receptors do not bind quickly enough to the membrane to be effective against Akt.

5.6 Probing PI(4,5)P$_2$ in NIH3T3 cancer cells

Examination of pSer 473 levels indicated that receptor **5** was able to reduce levels of phosphorylated Akt in HCT116 cells. This fluorescent receptor was then used to probe the distribution of PI(4,5)P$_2$ in NIH3T3 cells by microscopy.

As shown in Figure 5.4, a high concentration of receptor **5** is required to observe changes in levels of phosphorylated Akt. Therefore a lower concentration was chosen for imaging purposes, enabling the receptor to be directly imaged without disturbing the signalling pathways which are activated by phosphorylated Akt.

5.6.1 Receptor 5 is taken up by live cells

Having established that receptor **5** binds to PI(4,5)P$_2$ and is capable of crossing the cell membrane, we next examined its cellular localisation by fluorescence microscopy. Firstly, a solution of the receptor was added to live cells, which were then costained with DAPI and fixed before mounting onto microscopy slides.
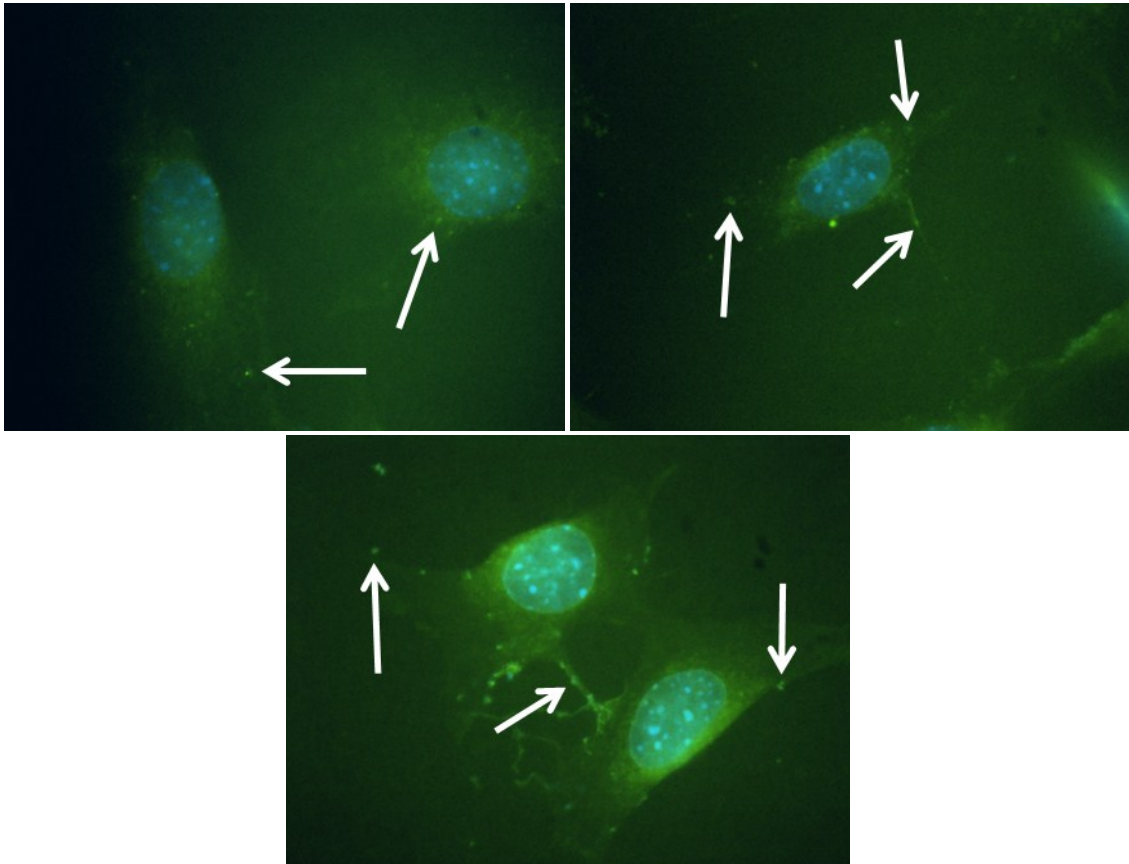
*Figure 5.7: Receptor **5** accumulates in the cytosol of live cells. NIH3T3 cells were starved of serum overnight, and the next day fresh starvation medium containing receptor **5** (10 µM) was added. After 15 minutes the medium containing receptor **5** was removed and the cells were washed thoroughly with PBS. After co-staining with DAPI the cells were fixed. DAPI is shown in blue and fluorescein in green.*

The images show that the receptor accumulates in small, highly localised areas within the cytosol (selected areas are indicated with white arrows). Although the majority of PI(4,5)P$_2$ is at the plasma membrane, this would appear as a continuous perimeter around the cells. Instead, there are small bright areas of fluorescence observed which may be endosomes or other small organelles. It is possible that upon addition of receptor **5**, the cells begin to internalise the receptor and this is the cause of the localisation that is observed.

5.6.2 Addition of receptor 5 to fixed cells

One benefit of using a fluorescent receptor is that accumulation of the compound into fixed cells can be monitored over time. After fixing cells with 4 % PFA, cells were incubated with receptor **5** (10 µM in PBS) over an increasing amount of time. The cells were thoroughly washed and after DAPI staining the fluorescence intensity of the coverslips was scanned.
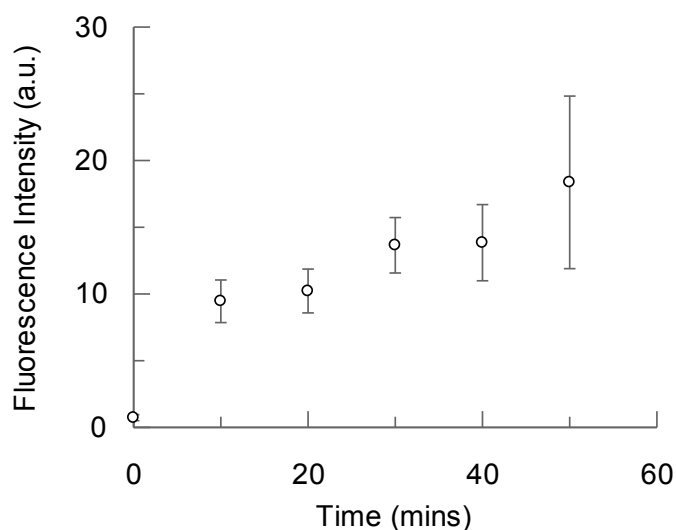
*Figure 5.8: Accumulation of receptor **5** in fixed cells over time. NIH3T3 cells starved overnight before fixing. The cells were then incubated with 10 µM receptor **5** in PBS for increasing times, and the fluorescence intensity of the coverslip was scanned and averaged (λ_{ex} = 485, λ_{em} = 525). After removal of the coverslip the fluorescence intensity of the empty wells was also measured and subtracted. Error bars represent standard deviation of two experiments perfomed in duplicate (n=2).*

Figure 5.8 shows that the receptor passes into cells within the first 10 minutes of incubation. After this time accumulation of the receptor increases more slowly.

5.6.3 Receptor 5 accumulates in fixed cells

Next, the receptor was added to cells which had already been fixed by 4 % PFA. After fixation the cells were incubated firstly with a solution of receptor **5** (10 μM, 2% v/v DMSO), then washed and incubated with DAPI.
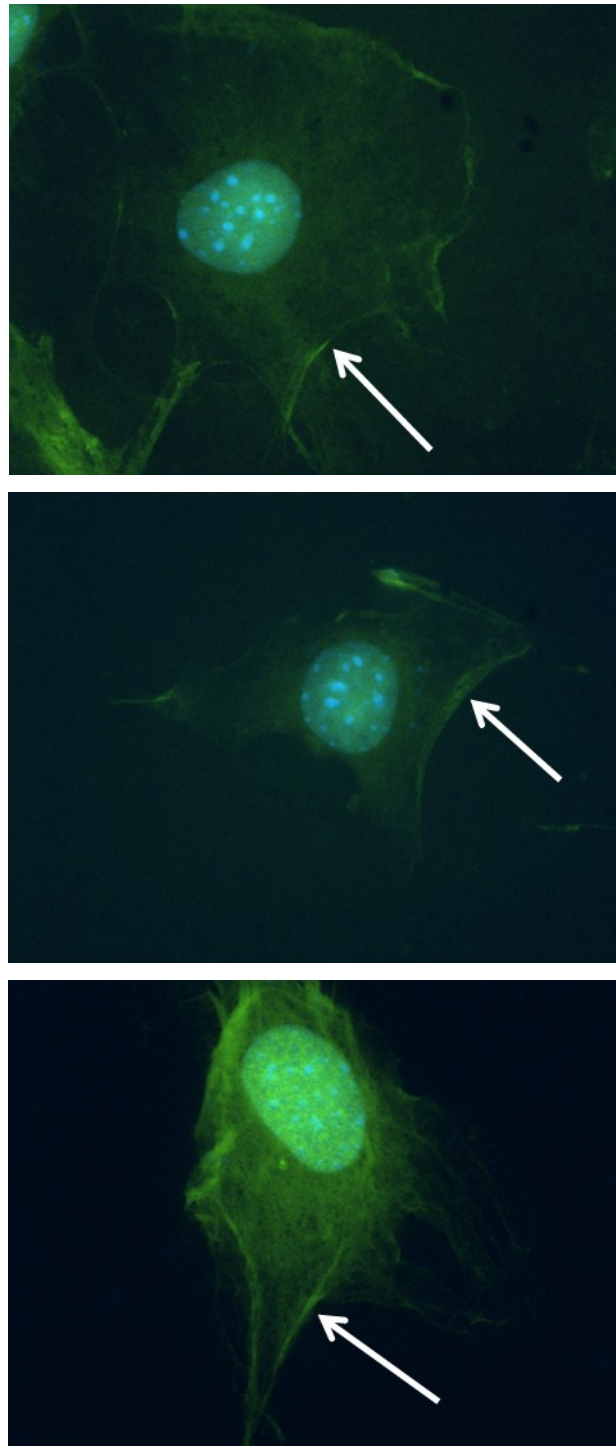
*Figure 5.9: Receptor **5** accumulates in fixed cells. NIH3T3 cells were starved of serum overnight, and the next day fixed. Cells were then incubated with receptor **5** (10 μM, 15 minutes) and co-stained with DAPI. DAPI is shown in blue and fluorescein in green.*

Figure 5.9 shows higher fluorescence intensity in a perimeter around the cells (indicated with white arrows), and none of the spots of high intensity which were observed in Figure 5.7. In order to identify this area of high intensity as the plasma membrane, co-staining experiments are required. If the fluorescence due to receptor **5** co-localises with that of plasma membrane markers, then the receptor can be positively identified as accumulating at the plasma membrane.
In addition, much of the receptor is also visible in the nucleus of the cells. $PI(4,5)P_2$ is known to localise in both the plasma membrane and the nucleus, so it is possible that the receptor is accumulating in these locations due to binding its target phospholipid (*26*),(*149*).

The images of cells in Figure 5.9 resemble those obtained by *Mak et. al*. which show accumulation of the $PI(4,5)P_2$-binding probe (PLCδ1 PH domain) at the plasma membrane with very low fluorescence intensity in the cytoplasm (*58*). However, while receptor **5** is also present in some areas of the nucleus (Figure5.11), the PLCδ1-PH domain was not observed inside the nucleus.
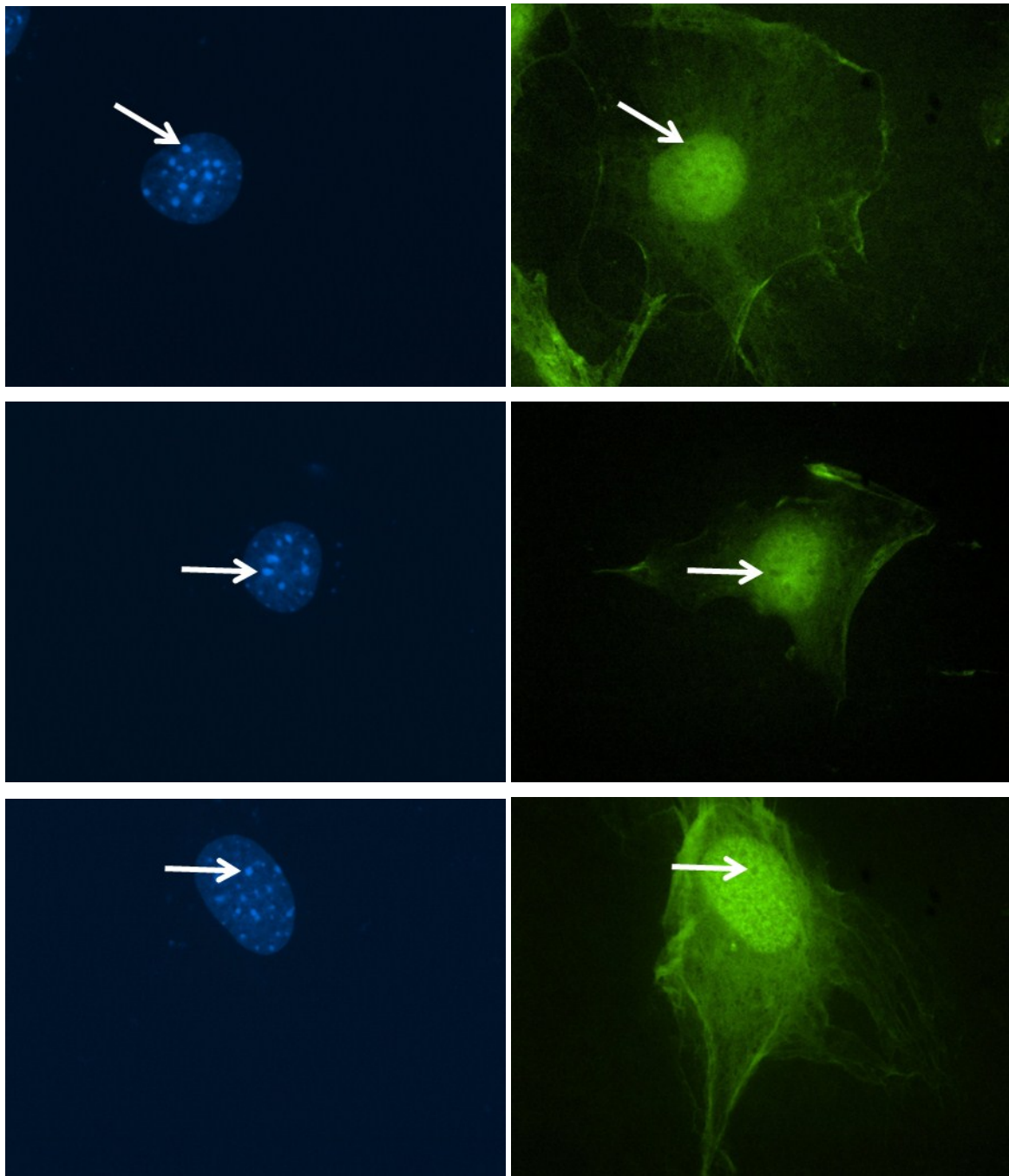
*Figure 5.10: Receptor **5** accumulates in fixed cells and is present in the nucleus. NIH3T3 cells were starved of serum overnight, and the next day washed and fixed. Cells were then incubated with receptor **5** (10 µM, 15 minutes) and co-stained with DAPI. Fluorescence channels are shown separately. DAPI is shown in blue (left) and fluorescein in green (right). Selected areas indicate high intensity DAPI stain and low intensity fluorescein stain.*

By examining the distribution of fluorophores separately (shown in Figure 5.10), it is observed that although the receptor was observed in the nucleus it did not co-localise with DAPI. Bright blue spots on the DAPI images coincide with dark spots on the FITC image.

This is consistent with work previously carried out by Stallings *et. al.*, where the nucleus was stained with DAPI, the PLCδ1-PH domain was expressed as a GFP (green fluorescent protein) conjugate, and PI(4,5)P$_2$ was detected using an anti-PI(4,5)P$_2$ antibody (*150*). PI(4,5)P$_2$ is observed in the areas which are not strongly stained by DAPI.

Receptor **5** has been shown to localise both in the nucleus and in a perimeter around the cell which could be the plasma membrane. These are the same areas where PI(4,5)P$_2$ and the PI(4,5)P$_2$-binding PLCδ1-PH domain have been shown to localise (Figure 5.10). This suggests that the receptor may be binding to PI(4,5)P$_2$ in fixed cells. If this receptor is shown to bind PI(4,5)P$_2$, it could be used in the future as a PI(4,5)P$_2$ imaging agent similar to GFP-conjugated binding domains and fluorophore-conjugated antibodies.

5.7 Summary

Firstly receptor **5** was incubated with live cells, which were then co-stained with DAPI and fixed. The resulting images showed that the receptor did not accumulate at the plasma membrane, but was observed in small localised areas of the cytoplasm. PI(4,5)P$_2$ has a role in endocytosis, so it is possible that the receptor co-localises with PI(4,5)P$_2$ and is then internalised into an endocytic vesicle; these are then transported away from the membrane causing the resulting image of the cell to possess small areas of fluorescence as observed in Figure 5.7.

Measuring the fluorescence intensity of fixed cells after exposure to receptor **5** for increasing amounts of time indicated that around 50% of the receptor accumulated in the cells in the first ten minutes of incubation. After fixing with PFA, receptor **5** was incubated with the cells, followed by DAPI staining. The images obtained showed that the receptor accumulated in the nucleus of the cells and in a perimeter around the cytosol, which may be the plasma membrane. Since PI(4,5)P$_2$ exists mainly at the plasma membrane the visibility of this component would be in line with expectations (*18*). It is also known that PI(4,5)P$_2$ exists in the nucleus where it has signalling functions that are distinct from those of plasma membrane PI(4,5)P$_2$ (*149*).

Although further work with this receptor is required, the images obtained are a good indication that receptor **5** is co-localising with PI(4,5)P$_2$ in the nucleus and also possibly at the plasma membrane.

- After application of receptor **5** to live cells, co-staining with plasma membrane markers.
- After application of receptor **5** to live cells, co-staining with endosome markers would indicate whether the receptor is indeed being taken up in this way.

- When receptor **5** is applied to fixed cells, addition of $PI(4,5)P_2$-binding protein domains (e.g. GST-PLCδ1 PH domain and subsequent addition of fluorescent anti-GST antibody), may enable us to observe whether receptor **5** is displaced from the plasma membrane by the more strongly-binding protein domain. If the fluorescence of receptor **5** is displaced from the plasma membrane to the cytosol, it would indicate that receptor **5** is interacting specifically with $PI(4,5)P_2$.

- This may also be achieved by the use of a combination of receptors **4** and **5**, since receptor **4** has a much higher affinity for $PI(4,5)P_2$ than receptor **5**.

Chapter 6: Summary & Conclusion

The phosphoinositides PI(4,5)P_2 and PI(3,4,5)P_3 are key players in cell signalling pathways, the most important being the Akt pathway. The amount and localisation of these PIPs are tightly controlled, and their deregulation has been linked to a number of diseases including cancer and Lowe Syndrome (*151*),(*34*). The ability to manipulate PIP levels has been identified several times as a potential therapeutic measure. Chemical perturbation of PIP levels can affect downstream events such as phosphorylation of Akt. Previously, PIP levels in cells have been manipulated by selective inhibition of the enzymes which generate them. For example, PI(3,4,5)P_3 levels can be reduced by inhibition of PI3K (*54*), or increased by inhibition of PTEN (*147*).

The aim of this project was to use synthetic receptors which bind to PI(4,5)P_2 and PI(3,4,5)P_3 to inhibit protein-phospholipid interactions. In this way the effective concentration of the free PIP can be reduced. Small molecule receptors were designed to bind to PI(4,5)P_2 and PI(3,4,5)P_3 were synthesised (Chapter 2). The PI(4,5)P_2 receptors **3**, **4** and **5** used boronic acid and urea functional groups to bind to their target; receptor **4** was a symmetric analogue of receptor **3**, with two binding 'arms'; and receptor **5** had a similar structure to receptor **3** but incorporated a fluorescein moiety (Figures 3.1, 3.2, 3.3). The PI(3,4,5)P_3 receptors made use of the zinc-DPA functionality which is well-known to bind strongly to phosphates. Receptor **12** used a similar central spacer to that of lead molecule PHDM, to attempt to replicate the success of that compound. The boronic acid groups were replaced with two phosphate-binding Zn-DPA motifs in order to better target PI(3,4,5)P_3 over other PIPs (Figure 4.1). Receptor **14** also possessed two Zn-DPA motifs however these were linked only by two short alkyl chains and a urea group (Figure 4.2). Receptor **16** which was originally designed as an ATP receptor was made up of a Zn-DPA motif linked via a hydrazide to a boronic acid. Due to the presence of the boronic acid, receptor **16** was tested for binding to PI(4,5)P_2 which has a diol motif, since these two functional groups are known to interact (Figure 4.3).

The binding of receptor **4** to PI(4,5)P_2 is assumed to be with 1:2 stoichiometry. When the PI(4,5)P_2 molecules are arranged at a membrane, a single receptor can bind two adjacent headgroups. Although the two phospholipids are separate and distinct molecules, they are prearranged such that the receptor can interact with more than one headgroup at a time. Receptors **3**, **4** and **5** were all shown by competitive ELISA to inhibit the interaction between PI(4,5)P_2 and the binding domain PLCδ1-PH. It was observed that receptor **4** binds to PI(4,5)P_2 with much higher affinity than receptors **3** and **5** (Figure 3.16).

This pattern was reflected in the results of the phosphatase assay, where the dephosphorylation of PI(4,5)P$_2$ by SopB was inhibited by receptors **3**, **4** and **5**. It was observed that receptor **4** had a much lower IC$_{50}$ value than receptor **3** (Figures 3.18, 3.19). The fact that receptor **4** shows much higher inhibitory effect than receptor **3** is consistent with the model of a cooperative effect, in which one binding event increases the likelihood of a second. In addition receptor **4** has displayed selectivity for the membrane-bound PI(4,5)P$_2$ over IP$_3$, which is free in solution (Figure 3.19). This also lends weight to the evidence of a cooperative effect between the two binding arms: if the receptor had high affinity for PI(4,5)P$_2$ due to its overall structure, this would also be the case for IP$_3$. It has been previously demonstrated by James *et. al.* that receptors with two boronic acids (and possessing an appropriate spacer) exhibited cooperativity in binding saccharides with more than one cis-diol, resulting in strong 1:1 binding (*152*). These diboronic acids had a distinctly higher binding affinity than monoboronic acids. This work also demonstrated the importance of using an appropriate spacer, since not all of the diboronic acids displayed enhanced affinity for the saccharides.

The ability of receptors **3**, **4** and **5** to bind PI(4,5)P$_2$ inhibits protein-lipid interactions. In cells, this is thought to affect downstream processes including the synthesis of PI(3,4,5)P$_3$ by PI3K, and subsequent recruitment of Akt to the plasma membrane, which is required for Akt phosphorylation. These downstream effects can be measured by probing the levels of phosphorylated Akt in cells using specific antibodies. Receptor **4**, which had the highest binding affinity for PI(4,5)P$_2$, was shown to completely prevent phosphorylation of Akt when incubated with HCT116 cells at 50 µM (Figure 5.3), the conventional PI3K inhibitor LY294002 has also been shown to completely prevent PI(3,4,5)P$_3$ synthesis also at 50 µM (*153*). Therefore receptor **4** has similar potency to this compound; although other PI3K inhibitors are commonly used which are much more potent such as Wortmannin (IC$_{50}$ in neutrophils 5 nM, (*154*)). Receptors **3** and **5** required almost 10x higher concentration to achieve the same inhibition as receptor **4** (Figures 5.3 and 5.4), which is consistent with their lower binding affinities as determined by competitive ELISA (Figure 3.16). Manipulation of PIP levels has thus far been achieved by inhibition of PIP-metabolising enzymes, however the results presented in Section 5.3 show this can be achieved in cells by directly interacting with the phospholipids. In order to be certain that the reduction in pSer 473 is not due to direct inhibition of PI3K by receptors **3**, **4** and **5**, assays of PI3K activity in the presence of these receptors are currently being carried out.

Receptor **5** was used to quantify the amount of PI(4,5)P$_2$ adsorbed onto a microtiter plate (Section 3.3). This has been previously achieved by the use of the PI(4,5)P$_2$-binding PLCδ1-PH domain in an overlay assay or an ELISA (Figure 3.15). However the use of a single reagent such as receptor **5** has

many advantages over protein domains. Conventional PI(4,5)P$_2$ quantification by overlay assay (*24*) or ELISA (*25*) requires the expression and purification of the appropriate protein, followed by application of one or more antibodies and a substrate reagent which is then used to detect the bound protein. However PI(4,5)P$_2$ detection by a small molecule such as receptor **5** is a single step process which requires only the fluorescent receptor to be synthesised and purified. The linear range of detection of adsorbed PI(4,5)P$_2$ by receptor **5** (up to 0.5 nmols, Figure 3.13)) was higher than that achieved by the PLCδ1-PH domain in an ELISA (up to 0.25 nmols, Figure 3.15). To improve this detection limit the use of a two-armed fluorescent receptor (such as the attempted BODIPY-PHDM receptor described in section 2.1), which in theory should have a higher binding affinity (closer to that of receptor **4**), is proposed.

Receptor **5** was also used to probe PI(4,5)P$_2$ in cells. On application of the receptor to fixed cells, it was observed to accumulate at the plasma membrane (Figure 5.9) and in the nucleus (Figure 5.10) where most PI(4,5)P$_2$ is known to localise. The images obtained were consistent with those of Mak *et. al.* (*58*) and Stallings *et. al.* (*150*) which also showed the presence of PI(4,5)P$_2$ at the plasma membrane and in the nucleus where DAPI was absent. Having shown receptor **5** to be capable of binding and quantifying PI(4,5)P$_2$ it is assumed that the observation of fluorescence at the plasma membrane is due to the receptor binding the PI(4,5)P$_2$ present there. Receptor **5** has potential as a small molecule PI(4,5)P$_2$ detection tool that can be readily used on fixed cells. Currently, PI(4,5)P$_2$ is often visualised using a detection protein (such as GST-PLCδ1-PH domain) which is then detected by a fluorophore-conjugated antibody (*58*),(*26*). However this method requires permeabilisation of the membrane with a detergent so that the protein and antibodies can enter the cell; receptor **5** has the advantage of crossing the plasma membrane without the need for detergent and the membrane remains intact.

As introduced in Section 1.4 metal complexes, especially Lewis acids such as zinc(II), are often used as receptors for anions including phosphate. The zinc-DPA motif has in particular been incorporated into receptors for biologically relevant phosphorylated species. Receptors **12**, **14** and **16** were developed using this binding motif on different molecular scaffolds. Each of these receptors displayed different selectivity for the various PIPs (Figures 4.8, 4.9 and 4.10), with receptor **12** displaying similar selectivity to Akt by binding PI(3,4)P$_2$ and PI(3,4,5)P$_3$ most strongly, and receptor **16** mimicking GRP1 by binding PI(3,4,5)P$_3$ with highest affinity.

The aim of this work was to use these metal complexes not only for recognition of PI(3,4,5)P$_3$, but also to inhibit protein-lipid interactions in the same way as PHDM: by mimicking PI(3,4,5)P$_3$-binding protein domains. Inhibition of protein-PI(3,4,5)P$_3$ interactions has been demonstrated by Miao *et.*

al., who developed small molecules capable of inhibiting the binding of PI(3,4,5)P$_3$-binding domains (*56*). These small molecules (PITs) targeted the PH domains, preventing association with PI(3,4,5)P$_3$. Akt recruitment was inhibited with IC$_{50}$ values between 13 and 30 μM and as a consequence phosphorylation of Akt was reduced, resulting in apoptosis.

Receptors **12**, **14** and **16** were shown to bind with good affinity to PI(3,4,5)P$_3$ and in this way the interaction between PI(3,4,5)P$_3$ and the binding protein GRP1 was inhibited (Figure 4.12). These receptors inhibit with IC$_{50}$ between 10 and 28 μM, a similar range to the family of PI(3,4,5)P$_3$- PH domain interaction inhibitors known as PITs. Therefore it was assumed that they would have the potential to induce apoptosis as demonstrated by Miao *et. al.* using the PITs (*56*).

The zinc(II) complexes were shown to directly inhibit PTEN, with similar efficacy to that of free zinc (Figures 4.16, 9.11). Firstly it was proposed that the receptors could be binding to the substrate OMFP via the phosphate group. However the inhibition was demonstrated to be independent of the substrate concentration, indicating that the receptors do not interact strongly with OMFP. This is consistent with results obtained in the IDA which show that all three of the receptors bind poorly to monophosphorylated species (Figures 4.8, 4.9 and 4.10); although competitive ELISA in the presence of phosphate (Figure 4.12) indicates that at high concentrations, the phosphate will interact with the receptors. It was then concluded that the receptors were directly interacting with the enzyme, resulting in inhibition.

The main mechanism of binding of these receptors to their target is the interaction of phosphate groups with zinc. If the zinc was not part of the receptor, no binding would take place. The differential binding of the three receptors to the seven PIPs demonstrated in IDAs (Figures 4.8, 4.9, 4.10) and the inhibition of protein-lipid binding shown in competitive ELISA (Figure 4.12) are strong indications that the zinc remains chelated to the DPA. Since the ELISA was carried out under similar conditions to the phosphatase assay, it is unlikely that the zinc has been removed from DPA. The IC$_{50}$ of zinc for PTEN was determined as approximately 13 μM (Figure 9.11); when 15 μM of each receptor was applied to the enzyme, almost 50 % inhibition was observed in each case (Figure 4.18). Therefore if only free zinc were capable of inhibiting the enzyme, 50 % of the zinc would need to be removed from chelation of receptors **12** and **14**, and 100 % from receptor **16**. This demonstrates that the enzyme may be inhibited by the zinc even as the metal is chelated by DPA.

Zinc is known to inhibit phosphatases including PTP-like phosphatases, and the IC$_{50}$ of zinc chloride was determined for PTEN, SopB and ATPase (Figure 9.11) (*148*),(*155*). However, zinc-DPA complexes have been previously used to monitor dephosphorylation by PTP1B (compounds **23a** and **23b**, Figure

1.13) and as protein mimetics (SH2 domain mimetic, Figure 1.14), although interestingly neither of these were used in the presence of a functioning enzyme. These zinc-DPA complexes were employed solely as sensors for their phosphorylated targets (*82*),(*59*). Having developed receptors **12**, **14** and **16** which have differential selectivity for certain PIPs, these compounds can be used in conjunction with non-enzymatic techniques such as those previously mentioned (Figures 1.13 and 1.14) as well as indicator displacement assays or ELISA. Since PTEN is closely involved in the metabolism of PI(3,4,5)P_3 it would be extremely difficult to distinguish between the PI(3,4,5)P_3-binding (PTEN mimetic) and phosphatase inhibiting (PTEN inhibitor) effects of these receptors in the presence of the enzymes.

After establishing that receptors **12**, **14** and **16** inhibited protein-PI(3,4,5)P_3 interactions, they were examined for ability to reduce the phosphorylation of Akt in cells. Even at high concentrations, the zinc(II) complexes caused no reduction in the level of phosphorylated Akt. This is either due to the receptors not being taken up by the cells, or to the receptors not inhibiting protein-PI(3,4,5)P_3 interactions. The latter may be due to the different selectivities displayed by each receptor in the IDAs (Figure). In addition to binding to PI(3,4,5)P_3, receptor **12** also binds PI(3,4)P_2; receptor **14** binds all diphosphorylated PIPs and although receptor **16** bound only to PI(3,4,5)P_3 under the IDA conditions, it is also known to bind strongly to ATP (personal communication, Dr. K. Damodaran) which is present in high concentrations in the cell. Competitive ELISA in the presence of phosphate showed that the binding of receptors **14** and **16** to PI(3,4,5)P_3 was blocked in the presence of phosphate, while that of receptor **12** was reduced (Figure 4.14).

In order to test the former, the ligands **11**, **13** and **15** were applied to the cells, followed by zinc pyrithione. Zinc pyrithione is commonly used as an ionophore which can carry zinc across cell membranes. The aim of this was to form metallo-receptors **12**, **14** and **16** *in situ*, following a procedure developed by Aoki *et. al.* in which a zinc cyclen complex was formed inside cells (*156*). The results obtained showed that the level of phosphorylated Akt was similar to the control. This may indicate that the complexes were formed (since the insulinomimetic effect of zinc was negated in the presence of ligands) but since no inhibition was observed, it is unlikely that the receptors are binding PI(3,4,5)P_3 in cells. It is possible that the receptors are binding nonspecifically to one or more of the many phosphorylated species in the cell. Another explanation could be that the zinc complexes are binding PI(3,4,5)P_3 (reducing phosphorylated Akt) as well as inhibiting PTEN (increasing PI(3,4,5)P_3 and therefore increasing phosphorylated Akt). These two modes of action have opposing (but not necessarily equal) effects on the level of phosphorylated Akt. From the current data, the activity of these zinc-based receptors in cells remains inconclusive. By firstly

inhibiting PTEN with the much more potent VO-OHpic (*50*) and then applying the receptors (as zinc complexes or as ligand/zinc pyrithione separately), more information might be obtained. The enzyme would be strongly and selectively inhibited, so any binding of the receptors to PI(3,4,5)P$_3$ should be readily observed as a decrease in phosphorylated Akt levels.

Further work

Further work on design of a molecule to inhibit protein-PI(4,5)P$_2$ interactions would include development of receptor **4**, which showed strong and specific interactions. This work showed that using a single binding motif reduced the affinity for PI(4,5)P$_2$ as well as the selectivity for the phospholipid over IP$_3$. Therefore a receptor using three sets of binding arms, arranged around a tripodal scaffold as used by Anslyn *et. al.* could lead to even stronger binding affinity. In addition one of the benzyl positions may be appended to a fluorophore to create a fluorescent PI(4,5)P$_2$ probe with strong binding affinity.
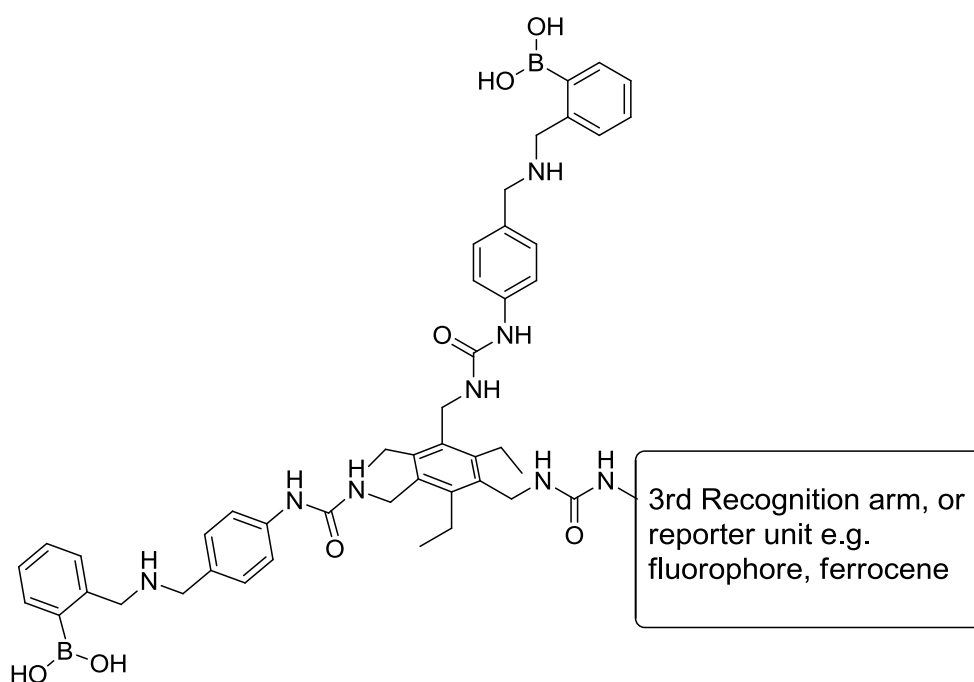
Figure 6.1: Possible tripodal receptor type based on PHDM.

In addition, the ability of the receptors to bind phosphate could be enhanced by addition of functional groups that bind to phosphate with higher affinity than that of the urea. Thiourea and guanidinium groups have both been shown to interact with anions more strongly than urea groups, and the urea group could be replaced with either of these (Figure 6.2 **A** and **B**). The secondary amine group could also be further functionalised, for example with the side chain of arginine (Figure 6.2 **C**).
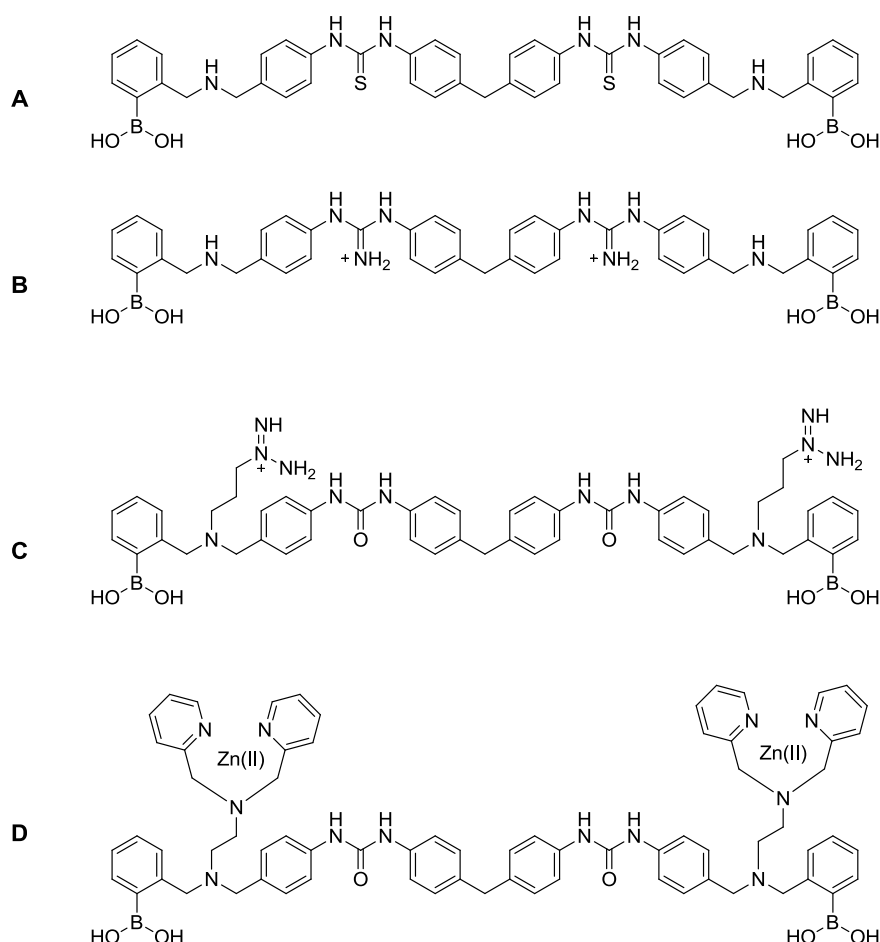
*Figure 6.2: Possible next generation of PI(4,5)P$_2$ receptors. **A**: Urea is replaced with neutral thiourea, which interacts with phosphate more strongly than urea. **B**: Urea is replaced with positively charged guanidinium groups, which could strongly increase the affinity for negatively charged PIPs. **C**: PHDM could be functionalised with the side chain of arginine which possesses a guanidinium group, to increase the phosphate-binding potential of the receptor. **D**: PHDM may also be functionalised with zinc-DPA motifs, known to bind phosphate with very high affinity. This should be approached with caution due to the side-effects of the presence of zinc demonstrated in this thesis.*

Incorporation of a positive charge in the form of the guanidinium groups would very likely increase the affinity of the receptor for phosphorylated targets (since the hydrogen bonding interactions and then supplemented with electrostatic interaction), however this may have some negative effects.

Firstly, the use of functional groups which bind phosphate very strongly may increase the affinity of the receptor for all phosphorylated PIPs, resulting in loss of selectivity. Secondly, incorporation of a charged moiety could reduce its cell permeability.

Another motif which could be added to the receptor is zinc-DPA (Figure 6.2**D**). Although zinc-DPA motifs are known to bind phosphate with very high affinity, this work has demonstrated that the presence of zinc can have unintended consequences such as inhibition of CX_5R type phosphatases including PTEN.
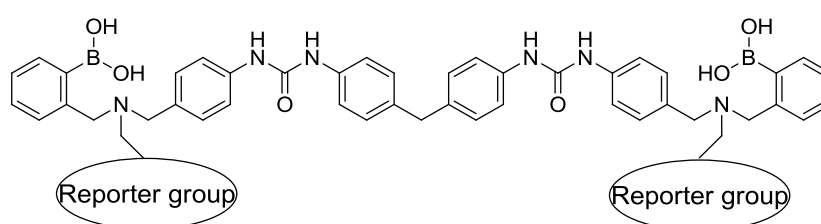
Figure 6.3: Functionalisation of PHDM with a reporter group (e.g. fluorophore, ferrocene, biotin) at the secondary amine.

Receptor **4** was also shown to have a much higher affinity for $PI(4,5)P_2$ over IP_3. Since the original set of compounds (Figure 1.26) were tested for binding to IP_3 and not $PI(4,5)P_2$, it may be beneficial to revisit these compounds as $PI(4,5)P_2$ receptors.

Receptor **16** was isolated from a dynamic library of zinc-DPA and boronic acid components which were designed to bind to ATP via the phosphate and diol groups. Replacing the zinc-DPA component with another boronic acid would create a dynamic library of diboronic acid compounds (Figure 6.4). Addition of IP_3 or $PI(4,5)P_2$ as a templating molecule could accelerate the formation of the most strongly-binding diboronic acid product. The library is quenched by a change in pH, which is compatible with the use of biological phosphorylated molecules. Even a small library would give some information on structure-activity relationship that would be beneficial for the design of future $PI(4,5)P_2$ receptors.
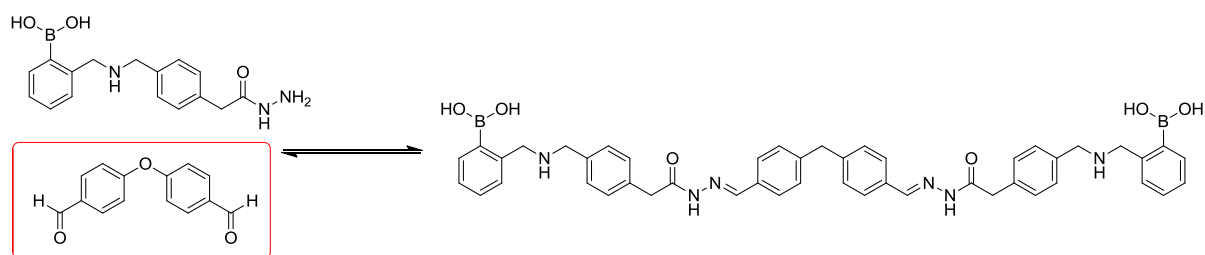
Figure 6.4: Reversible formation of a hydrazone analogue of PHDM. This reaction is suitable for application in a dynamic library, with a number of dialdehydes (highlighted in red above). The library would select for the receptor which binds most strongly to the target (PI4,5)P$_2$ or IP$_3$).

The use of this library would also provide some information on the role of the urea groups in binding PI(4,5)P$_2$ and IP$_3$. In a hydrazone library the urea groups would be replaced with hydrazides, which have a lesser ability to hydrogen bond than urea (since they possess only one hydrogen bond donor group versus two of urea (*157*)). If these receptors failed to bind PI(4,5)P$_2$ and IP$_3$ with the same affinities as the urea-containing molecules, it would indicate that the presence of a phosphate binding group with strong interactions with phosphate is a vital component of receptors targeting PI(4,5)P$_2$ and IP$_3$.

The PI(4,5)P$_2$-binding receptors have been shown to attenuate the phosphorylation of Akt. Having established that the receptors bind PI(4,5)P$_2$ *in vitro* (and therefore prevent downstream proteins and enzymes from binding) it is suggested that this is the mechanism by which phosphoAkt is reduced. However in order to ensure that the receptors are not acting as PI3K inhibitors (which would also reduce phosphoAkt in cells) *in vitro* assays are currently being carried out. Unlike the phosphatase enzymes which dephosphorylate OMFP, PI3K does not have an artificial substrate that can be used to assess whether the receptors are interacting with the PIP or the enzyme. However since PI3K can also phosphorylate PI and PI(4)P (receptors **3** and **4** do not bind PI(4)P), these will be used as control substrates. It is expected that the phosphorylation of PI(4,5)P$_2$ will be reduced in the presence of receptors **3** and **4**. If the phosphorylation of PI and PI(4)P are unaffected in the presence of receptors **3** and **4**, then it can be assumed that the receptors are not directly inhibiting the enzyme. Enzymatic products (PI(3)P, PI(3,4)P$_2$ and PI(3,4,5)P$_3$) can be extracted using standard techniques such as the Bligh and Dyer method, and then quantified by means of ELISA or overlay assay.

$$PI \xrightarrow{PI3K} PI(3)P \qquad \text{Probed using FYVE domain}$$

$$PI(4)P \xrightarrow{PI3K} PI(3,4)P_2 \qquad \text{Probed using Akt-PH domain}$$

$$PI(4,5)P_2 \xrightarrow[\text{Inhibited by}]{PI3K} PI(3,4,5)P_3 \qquad \text{Probed using Akt-PH domain or}$$
$$\text{PI(4,5)P}_2 \text{ receptor?} \qquad\qquad\qquad \text{GRP1-PH domain}$$
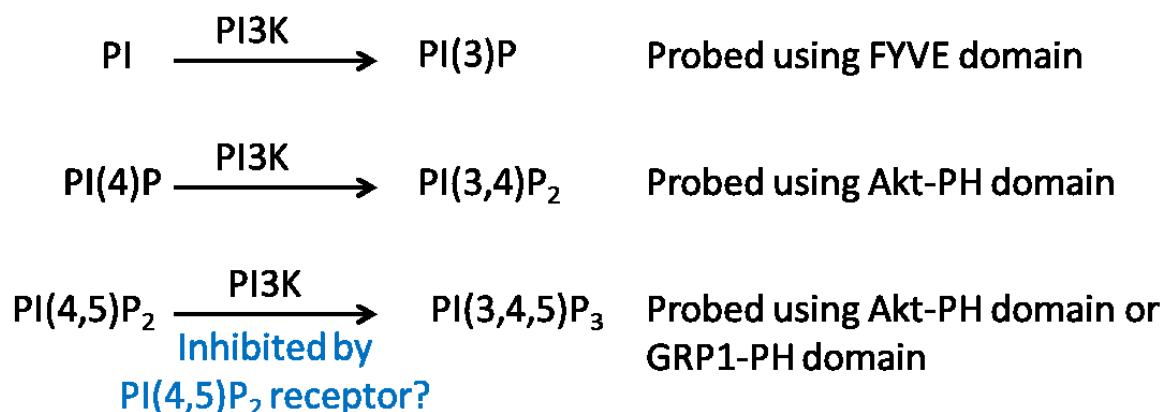
*Figure 6.5: Experiments underway to determine the effect of PHDM and receptors **3** and **4** on PI3K. If the receptors directly act on PI3K, all three of the above reactions will be inhibited. However if the receptors do not directly interact with PI3K, only the third reaction (phosphorylation of PI(4,5)P₂ to PI(3,4,5)P₃) will be disrupted.*

Receptor **5** showed promise as a tool for detection of PI(4,5)P$_2$ *in vitro* as well as in fixed cells. To further characterise the activity of this receptor in live cells it would be beneficial to carry out the experiments detailed in section 5.7. Firstly, the cells should be co-stained in order to identify which compartments the receptor accumulates in. In addition, to positively identify that receptor **5** was binding to PI(4,5)P$_2$ at the plasma membrane of fixed cells, the GST-PLCδ1-PH domain could be applied at the same time. The PH domain would be expected to displace the receptor, and the fluorescence would therefore be diffused in the cytoplasm rather than accumulated at the plasma membrane. It would be interesting to carry out the same experiment using receptor **4** as the displacing molecule.

While PI(4,5)P$_2$ is constitutively present in the plasma membrane of cells, PI(3,4,5)P$_3$ is present only for a short time after stimulation, and the total amount of PI(3,4,5)P$_3$ is still very low overall. When seeking to attenuate the Akt pathway, PI(4,5)P$_2$ could be a better target for small molecule receptors than PI(3,4,5)P$_3$. By reducing the amount of PI(4,5)P$_2$ available to proteins, the amount of PI(3,4,5)P$_3$ generated is lower, and hence the activity of the Akt pathway is reduced.

However, receptor **12** showed promise as a mimic of the Akt-PH domain. Its ability to bind PI(3,4)P$_2$ and PI(3,4,5)P$_3$ in competitive conditions (such as in the presence of Mg^{2+} or ATP) could be determined by competitive ELISA. In addition, the use of enhanced DPA motifs which possess acetamido groups adjacent to the nitrogen of the pyridines (*158*) would provide additional coordination sites for the zinc (II), preventing the metal from binding amino acid residues at enzyme active sites. This could prevent or reduce the ability of zinc to inhibit phosphatases, so compounds of this type would be more useful as substrate-binding receptors.

Chapter 7: Synthesis

7.1 Materials and Reagents

2-Formylphenyl boronic acid was purchased from Sigma-Aldrich and recrystallized from ethanol before use. 1-(N-BOC-aminomethyl)-4-(aminomethyl)benzene, sodium borohydride, phenylisocyanate, 4,4'-bis(isocyanatophenyl)oxide, triethylorthoformate, 1-(2-pyridinyl)-N-(2-pyridinylmethyl)methanamine, N-(2-Bromoethyl)phthalimide, fluorescein isothiocyanate, 4,4'-methylenebis(phenyl isocyanate), 1,1'-carbonyldiimidazole, zinc acetate were all purchased from Sigma-Aldrich and used without further purification. Hydrazine monohydrate was purchased from Alfa Aesar.

Powdered molecular sieves (3Å) were purchased from VWR and activated by heating at 200°C for 30 minutes under vacuum. Celite was purchased from Sigma-Aldrich. TLC plates (Silica gel 60, aluminium back) were purchased from Merck. Reversed-phase TLC plates (C18 silica, glass back) were purchased from Sigma-Aldrich. Sodium bicarbonate, hydrochloric acid (12M) and sodium hydroxide were purchased from VWR.

Prepacked C18 silica cartridges used for reverse-phase chromatography were purchased from Buchi and used as part of Buchi Isocratic Pump System. Modules used: Pump Controller, C-610; Pump Manager, C-615; Pump Module C-601 with 4-way Injection/Purge device.

7.2 Solvents

Anhydrous triethylamine, anhydrous dichloromethane and anhydrous dimethylformamide were purchased from Sigma-Aldrich as Sure-Seal products and handled under nitrogen atmosphere without further purification. Glacial acetic acid was purchased from Sigma-Aldrich. Trifluoroacetic acid was purchased from VWR. Methanol was purified by Innovative Technology Inc. PureSolv solvent purification system.

HPLC grade methanol and water were purchased from VWR. Reagent grade petroleum ether (40-60) and acetonitrile were purchased from VWR and used without further purification. Reagent grade dichloromethane and methanol were purchased from Sigma-Aldrich and used without further purification. Deuterated solvents (CDCl$_3$, MeOD, d$_6$-DMSO) were purchased from Sigma-Aldrich.

7.3 Analysis

^{1}H NMR spectra were recorded at 400 MHz on Bruker Avance 400 Ultrashield instruments. ^{13}C NMR spectra were recorded at 101 MHz on Bruker Avance 400 Ultrashield instruments or at 500 MHz on Bruker Avance 500 Ultrashield at 298 K unless otherwise specified. NMR are referenced to tetramethylsilane (TMS) as standard.   ^{1}H NMR spectra are assigned where unambiguous with the aid of HMQC and COSY experiments (both carried out on Bruker Avance 400 Ultrashield instruments except where specified), and ^{13}C are assigned as C, CH, CH_2 or CH_3 according to data from 135DEPT experiments. Coupling constants (J) measured in Hertz.

Mass spectra were obtained by J. Barton at Imperial College on a Micromass LCT Premier instrument.

IR were recorded on a Perkin Elmer Spectrum 100 FT-IR instrument.

Elemental analyses were performed by A. Dickerson at the University of Cambridge.

Crystal structure was resolved by A. White at Imperial College London.

Synthesis of (2-(((4-(((tert-butoxycarbonyl)amino)methyl)benzyl)amino)methyl)phenyl)boronic acid, **1** (*58*).
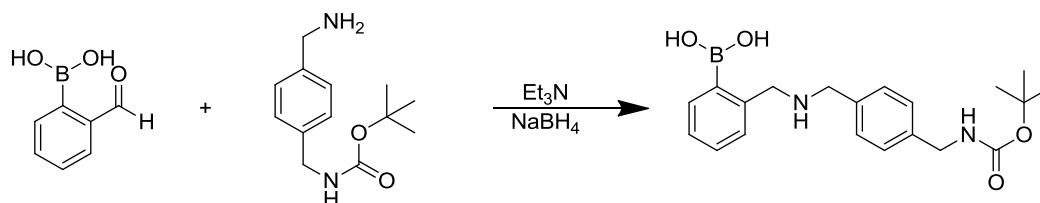
Synthesised following previously reported procedure(*58*). A flask containing activated 3 Å molecular sieves and 2-formylphenyl boronic acid (672 mg, 4.48 mmol) was purged and filled with nitrogen. A solution of 1-(N-BOC-aminomethyl)-4-(aminomethyl)benzene (1.12 g, 4.48 mmol) in anhydrous methanol and triethylamine (6.20 ml, 44.8 mmol) was added. The reaction mixture was stirred vigorously at 40 °C for two hours. After cooling to room temperature solid sodium borohydride (508 mg, 13.4 mmol) was added, and the reaction was stirred for a further two hours at room temperature. After this time the crude reaction mixture was filtered through celite and concentrated under reduced pressure until approximately 5 ml reaction mixture remained. The crude was treated with triethylorthoformate (2.23 ml, 13.4 mmol) and three drops of glacial acetic acid with stirring at room temperature for six hours. The solvent was then removed under reduced pressure to yield an off-white solid which was washed with petroleum ether, water, and again with petroleum ether and dried to yield protected amine **1** as a white solid (1.48 g, 3.99 mmol, 89 %).

^{1}H NMR (400 MHz, CDCl$_3$): 7.49 (d, 1H, Ar*H*, J= 4.8), 7.40 (dd, 4H, Ar*H*, J= 7.3, J= 25.8), 7.24-7.16 (m br, 1H, Ar*H*), 7.09 (m br, 1H, Ar*H*), 4.27 (s, 2H, C*H$_2$*), 3.99 (s, 2H, C*H$_2$*), 3.87 (s, 2H, C*H$_2$*), 1.47 (s, 9H, 3C*H$_3$*). ^{13}C NMR (101 MHz, CDCl$_3$): 156.3 (*C*), 150.1 (*C*), 139.3 (*C*), 139.0 (*C*), 129.9 (*C*H), 128.8 (*C*H), 127.8 (*C*H), 127.5 (*C*H), 126.3 (*C*H), 122.8 (*C*H), 78.2 (*C*), 52.8 (*C*H$_2$), 48.1 (*C*H$_2$), 43.6 (*C*H$_2$), 28.7 (*C*H$_3$). One quaternary carbon not observed. ESI-MS m/z: 371 ([M+H]$^+$ 100 %), 393 ([M+Na]$^+$ 5 %). HRMS: Observed [M+H]$^+$, 371.2144. C$_{20}$H$_{28}$N$_2$O$_4$B requires 371.2412, Δ 0.5 ppm. IR: v_{max}/cm^{-1}: 3327, 1686, 1365, 1168.

Synthesis of (2-(((4-(aminomethyl)benzyl)amino)methyl)phenyl)boronic acid,
2 (58).
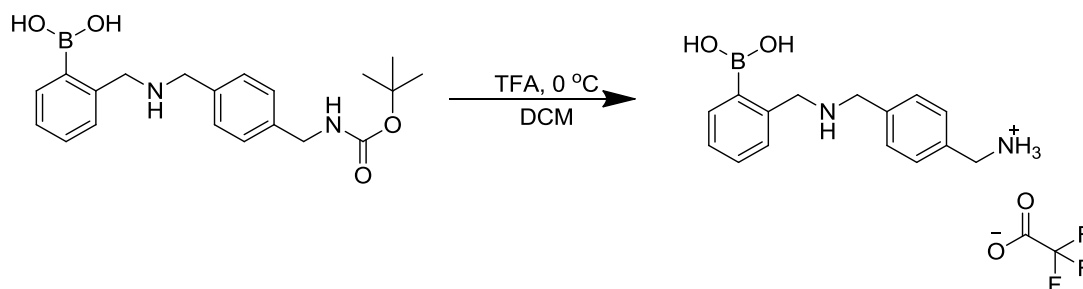
Synthesised following previously reported procedure(*58*). A solution of compound **1** (0.24 g, 0.65 mmol) in dichloromethane was cooled in an ice bath. When the solution had reached 0 °C, trifluoroacetic acid (3.74 ml, 39.9 mmol) was added dropwise to the stirred solution. After one hour at 0 °C the ice bath was removed and the reaction mixture stirred at room temperature for a further 24 hours. After this time the solvent was removed under reduced pressure, and analysis by ^{1}H NMR spectroscopy showed 100 % removal of the BOC protecting group. The product appeared as colourless oil after drying on a high vacuum for 24 hours. Analysis by ^{13}C NMR spectroscopy showed the presence of some remaining trifluoroacetic acid. This was allowed to remain and the product was used directly in the next step of the synthesis of compound **3** (0.25 g, 0.65 mmol).

^{1}H NMR (400 MHz, MeOD): 7.70 (s, br, 1H, Ar*H*), 7.66-7.57 (m, 4H, Ar*H*), 7.53-7.46 (m, 3H, Ar*H*), 4.33 (s, 2H, C*H*$_2$), 4.29 (s, 2H, C*H*$_2$), 4.20 (s, 2H, C*H*$_2$). ^{13}C NMR (101 MHz, MeOD): 159.7 (TFA, *C*OOH), 156.2, 150.1, 139.3, 139.0, 133.1, 130.5, 129.4, 128.9, 127.9, 126.9, 113.4 (TFA, *C*F$_3$) 49.9, 48.7, 40.8. ESI-MS m/z: 395 (100 %), 271 ([M+H]$^+$ 45 %). HRMS: Observed [M+H]$^+$, 271.1564. C$_{15}$H$_{20}$N$_2$O$_2$B requires 271.1618, Δ 19.9 PPM. IR: ν$_{max}$/cm^{-1}: 3024, 1661, 1379, 1129.

Synthesis of (2-(((4-((3-phenylureido)methyl)benzyl)amino)methyl)phenyl)boronic acid, 3.
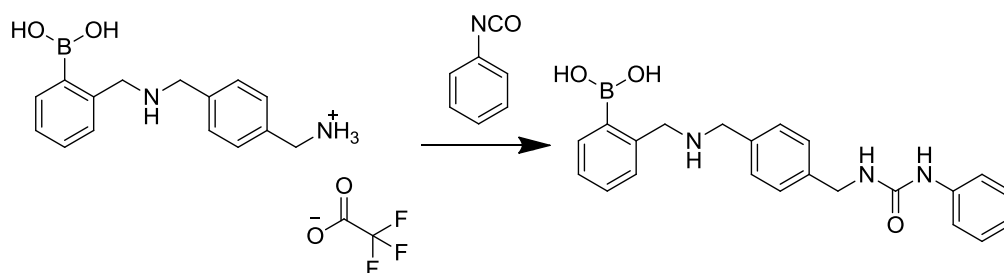
Primary amine **2** (227 mg, 0.84 mmol) was dissolved in anhydrous dichloromethane and stirred with anhydrous triethylamine (0.42 ml, 4.2 mmol) for 30 minutes. A solution of phenylisocyanate (100 mg, 0.84 mmol) in anhydrous dichloromethane was added dropwise over ten minutes to the amine solution. The reaction was left to stir at room temperature for 24 hours under a nitrogen atmosphere. The solvent was then evaporated under reduced pressure, yielding an off-white gum. After chromatography on silica using 1 % methanol in dichloromethane, the fractions were analysed by TLC and those containing single spots of Rf = 0.25 were combined and the solvent evaporated yielding a yellow oil. The oil was left under reduced pressure overnight to remove solvents, and water (20 ml) was added which initiated a white precipitate. The precipitate was filtered and dried to yield compound **3** (218 mg, 0.56 mmol, 67 % yield).

^{1}H NMR (400 MHz, d$_6$-DMSO): 8.92 (d, 2H, J = 5.2), 8.59 (t, 1H, J = 7.1), 8.06 (t, 2H, J = 7.1), 7.85 (d, 1H, J = 6.0), 7.51 (dd, 4H, J = 4.6), 7.44 – 7.35 (m, 3H), 4.31 (s, 2H), 4.20 (s, 2H), 4.06 (s, 2H). ^{13}C NMR (500 MHz, d$_6$-DMSO): 155.7 (*C*), 155.2 (*C*), 142.0 (*C*), 140.4 (*C*), 139.1 (*C*), 137.0 (*C*), 133.6 (*C*H), 129.2 (*C*H), 128.6 (*C*H), 128.2 (*C*H), 127.3 (*C*H), 125.8 (*C*H), 125.6 (*C*H), 121.8 (*C*H), 121.0 (*C*H), 119.8 (*C*H), 117.6 (*C*H), 49.3 (*C*H$_2$), 49.2 (*C*H$_2$), 42.5 (*C*H$_2$). ESI-MS m/z: 413 ([M+Na]$^+$, 5 %), 491 (100 %). IR: ν$_{max}$/cm^{-1}: 1658, 1598, 1511, 1232, 1202. Microanalysis: Observed: %C, 61.57; %H, 6.16; %N, 9.98. C$_{22}$H$_{24}$BN$_3$O$_3$·2.1H$_2$O requires: %C, 61.87; %H, 6.66; %N, 9.84.

Synthesis of (((((((((oxybis(4,1-phenylene))bis(carbonyl))bis(azanediyl)bis(methylene))bis(4,1-phenylene))bis(methylene))bis(azanediyl))bis(methylene))bis(2,1-phenylene))diboronic acid, **4.**
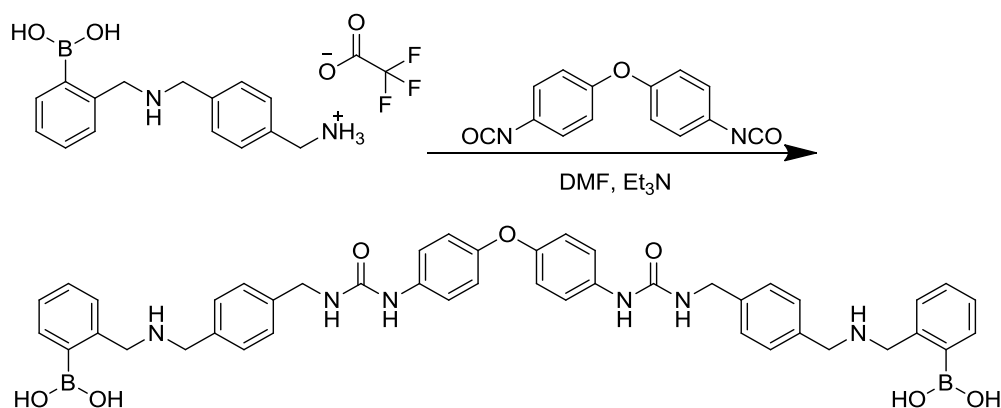
Amine **2** (90 mg, 0.33 mmol) was dried under vacuum and the flask was refilled with nitrogen. Anhydrous DMF was added (10 ml), followed by anhydrous triethylamine (457 μl, 3.3 mmol). A solution of diphenyl oxide 4,4'-diisocyanate (38 mg, 0.15 mmol) in anhydrous DMF (1 ml) was added dropwise to the vigorously stirred reaction mixture. After stirring at room temperature for 48 hours the DMF was evaporated under reduced pressure until approximately 5 ml remained. Upon dropwise addition of water (20 ml) a white precipitate formed. The precipitate was filtered and washed with water (3 x 10 ml) and dichloromethane (3 x 10 ml). Receptor **4** was yielded as a white solid (105 mg, 0.13 mmol, 89 % yield).

^{1}H NMR (400 MHz, d$_6$-DMSO): 7.50-7.40 (m, 10H, Ar*H*), 7.34 (d, 4H, Ar*H*, J = 9.2), 7.21-7.18 (m, 4H, Ar*H*), 7.10-7.07 (m, 2H, Ar*H*), 6.91 (d, 4H, Ar*H*, J = 9.2), 4.43 (s, 4H, C*H$_2$*), 3.99 (s, 4H, C*H$_2$*), 3.88 (s, 4H, C*H$_2$*). ^{13}C NMR (500 MHz, d$_6$-DMSO, 388 K): 155.5, 151.5, 149.4, 138.7, 138.2, 135.5, 129.5, 128.5, 127.6, 126.0, 122.4, 120.1, 119.6, 118.8, 114.8, 52.3, 47.5, 42.5. ESI-MS m/z: 397 ([M+2H]$^{2+}$, 100 %). IR: v$_{max}$/cm^{-1} 1652, 1551, 1498, 1217. Microanalysis: Observed: %C, 63.99; %H, 5.49; %N, 10.04. C$_{44}$H$_{50}$B$_2$N$_6$O$_9$ requires %C, 63.78; %H, 6.08; %N, 10.14.

Synthesis of (2-(((4-((3-(3',6'-dihydroxy-3-oxo-3H-spiro[isobenzofuran-1,9'-xanthen]-5-yl)thioureido)methyl)benzyl)amino)methyl)phenyl)boronic acid, **5**
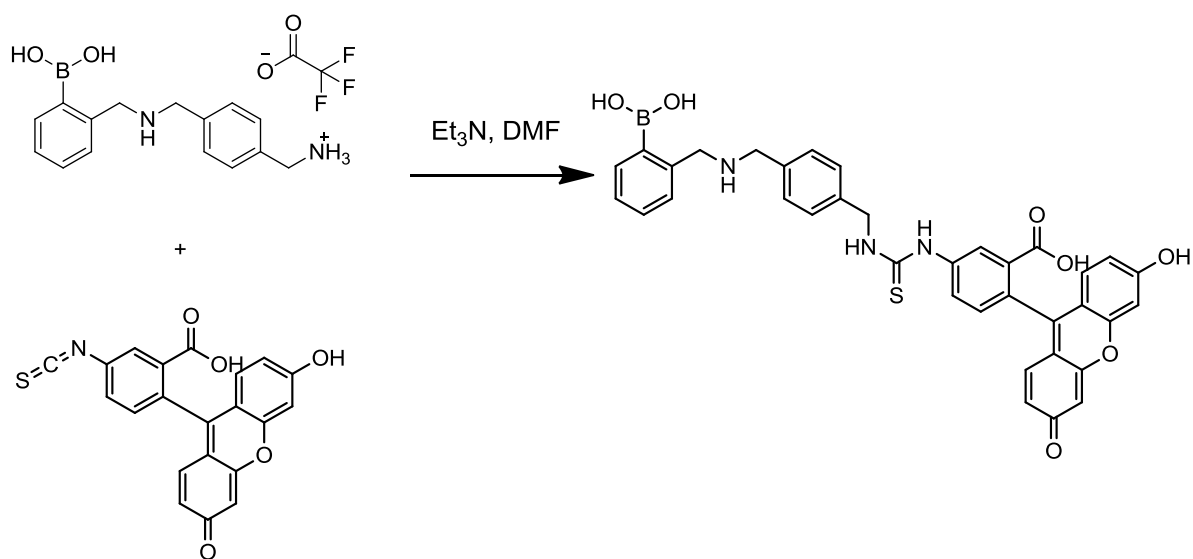
Amine **2** (24 mg, 0.064 mmol) was dried well under vacuum, and then stirred in anhydrous DMF with triethylamine for 30 minutes under nitrogen atmosphere. A solution of fluorescein isothiocyanate (FITC, 25 mg, 0.064 mmol) in DMF was added, and the reaction was stirred for 16 hours under nitrogen. The solvent was removed under reduced pressure, leaving a red-orange oil. After addition of water (10 ml) an orange solid precipitated. This solid was washed extensively with water (3 x 10 ml) and petroleum ether (3 x 10 ml) and recrystallized from hot methanol to yield pure receptor **5** (30 mg, 0.046, 72 % yield).

^{1}H NMR (400 MHz, d_6-DMSO): 7.94 (s, 1H), 7.68-7.46 (m, 2H), 7.39-7.11 (m, 6H), 7.01-6.75 (m, 4H), 6.66 (s, 1H), 6.09-6.04 (m, 2H), 5.97 (s, 1H), 2.89 (s, 2H, CH_2), 2.73 (s, 2H, CH_2), 2.41 (d, 2H, CH_2, J = 6.3). ^{13}C NMR (101 MHz, d_6-DMSO): 168.8 (*C*), 167.3 (*C*), 160.2 (*C*), 156.2 (*C*), 155.2 (*C*), 154.3 (*C*), 152.3 (*C*), 151.6 (*C*), 150.1 (*C*), 145.8 (*C*), 143.5 (*C*), 141.5 (*C*), 139.4 (*C*), 137.4 (*C*), 136.5 (*C*H), 131.0 (*C*H), 129.9 (*C*H), 129.6 (*C*H), 128.7 (*C*H), 127.7 (*C*H), 127.4 (*C*H), 126.8 (*C*H), 126.3 (*C*H), 125.5 (*C*H), 124.4 (*C*H), 122.8 (*C*H), 122.3 (*C*), 121.8 (*C*H), 113.1 (*C*H), 109.6 (*C*), 102.7 (*C*H), 52.9 (*C*H$_2$), 48.1 (*C*H$_2$), 43.6 (*C*H$_2$). ESI-MS m/z: 330 ([M+2H]$^{2+}$, 100 %) 660 ([M+H]$^+$, 15 %). HRMS: Observed [M+H]$^+$ 660.1981. C36H31N3O7SB requires 660.1976, Δ = 0.8 ppm. IR: ν$_{max}$/cm^{-1} 3059, 1678, 1594, 1256, 1177. Microanalysis: Observed: %C, 62.24; %H, 5.14; %N, 4.46. C$_{36}$H$_{32}$BN$_3$O$_8$S.H$_2$O requires %C, 62.16; %H, 4.93; %N, 6.04.

*Synthesis of 10-(bromomethyl)-5,5-difluoro-1,3,7,9-tetramethyl-5H-dipyrrolo[1,2-c:2',1'-f][1,3,2]diazaborinin-4-ium-5-uide, **6** (126).*
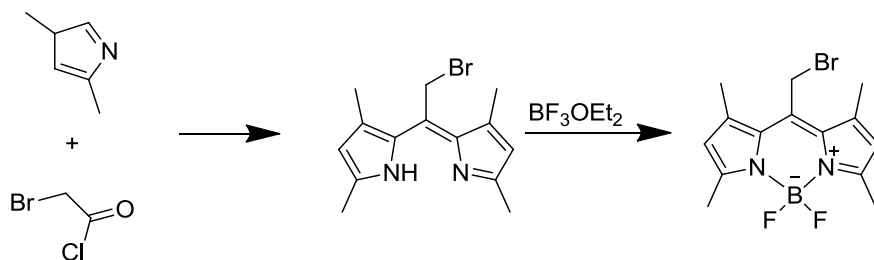
Compound **6** was synthesised according to a literature procedure (*126*). Bromoacetyl chloride (170 µl, 2.0 mmol) and 2,4-dimethylpyrrole (400 µl, 3.9 mmol) were dissolved in anhydrous DCM (10 ml) and stirred under nitrogen. The reaction was monitored by TLC (silica; hexane, ethyl acetate 10:1) and after two and a half hours the reaction appeared to be complete. A solution of boron trifluoride diethyl etherate (8 ml, 7.5 mmol) in anhydrous DCM (5 ml) and triethylamine (4 ml, 28.7 mmol) was added dropwise over 30 minutes, and the reaction was further stirred for a further four hours. The solvent was removed under reduced pressure yielding a black oily residue. The product was isolated by gravity chromatography on a silica column using hexane and ethyl acetate as eluent (10:1 [Lit, 6:1]) Rf = 0.3. The product was then purified by recrystallization from ethyl acetate and was obtained as a dark pink solid (299 mg 0.88 mmol, 22 % yield).

^{1}H NMR (400 MHz, CDCl$_3$): 6.11 (s, 2H, ArH), 4.81, 4.70 (both s, CH_2Br and CH_3), 2.57 & 2.55 (both s, combined 12H, CH_3). ^{13}C NMR (101 MHz, CDCl$_3$): 156.5, 141.1, 122.5, 113.4, 37.2, 15.9, 15.5, 14.8. ESI-MS m/z: 133 ([C$_{14}$H$_{17}$BF$_2$N$_2$+2H]$^{2+}$, 100%); 340, 342 ([M+H]$^+$, 10%).

*Synthesis of 4-bromo-3-(1,3-dioxolan-2-yl)phenol, **7**.*
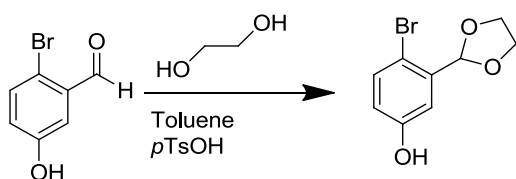
2-bromo-5-hydroxy benzaldehyde (1 g, 5.0 mmol) and ethylene glycol (3.5 ml, 50 mmol) were dissolved in anhydrous toluene in the presence of *p*-TsOH (5 mol %). The reaction mixture was refluxed for 24 hours with a Dean-Stark trap. After the addition of triethylorthoformate (3.5 ml, 5.0 mmol) the solution was further refluxed and 30 minutes later solid sodium bicarbonate was added (4.2 g, 50 mmol). After 30 minutes the solution was cooled and solids filtered off. The solvent was removed under reduced pressure and the ethylene glycol removed by drying well under vacuum for 16 hours. The product was obtained as pink-orange oil in high yield (1.20 g, 4.95 mmol, 99 % yield). The product was used without further purification.

^{1}H NMR (400 MHz, MeOD): 7.37 (d, 1H, Ar*H*, J = 8.9), 7.06 (d, 1H, Ar*H*, J = 3.1), 6.74 (dd, Ar*H*, 1H, J = 3.1, J = 8.7), 5.97 (s, 1H, ArC*H*), 4.17-4.10 (m, 2H, C*H*$_2$), 4.06-4.01 (m, 2H, C*H*$_2$). ^{13}C NMR (101 MHz, MeOD): 156.9 (C), 137.4 (C), 133.2 (*C*H), 117.6 (*C*H), 114.6 (*C*H), 110.9 (C), 102.2 (*C*H), 65.1 (*C*H$_2$). IR: v_{max}/cm^{-1} 3510, 2895, 1467, 1289, 1101.

Synthesis of 3-(1,3-dioxolan-2-yl)-4-(4,4,5,5-tetramethyl-1,3,2-dioxaborolan-2-yl)phenol, **8.**
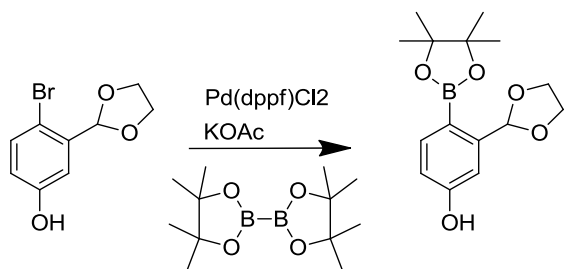
A solution of protected aldehyde **7** (1.2 g, 4.95 mmol) was dissolved in dioxane, along with potassium acetate (1.5 g, 15 mmol) and Pd(dppf)Cl$_2$ (204 mg, 0.25 mmol) was degassed by bubbling with nitrogen for 30 minutes followed by three freeze-pump-thaw cycles. Diboron pinacol ester (1.9 g, 7.5 mmol) was added and the solution heated at 80 ^{o}C under nitrogen atmosphere for 24 hours. After cooling, the solution was filtered through celite and the solvent removed under reduced pressure. The dark solid was extracted with methanol yielding an orange-brown solid. This solid was washed with water (3 x 10 ml) and diethyl ether (3 x 10 ml) leaving an orange solid which then recrystallised from methanol. This was analysed by ^{1}H NMR and ^{11}B NMR spectroscopy and shown to be the product (260 mg, 0.89 mmol, 18 % yield).

^{1}H NMR (400 MHz, (CD$_3$)$_2$CO): 7.61 (d, 1H, Ar*H*, J = 8.4), 7.14 (d, 1H, Ar*H*, J = 2.2), 6.84 (dd, 1H, Ar*H*, J = 8.3, J = 2.3), 6.35 (s, 1H, ArC*H*), 4.08-4.03 (m, 2H, C*H$_2$*), 3.98-3.93 (m, 2H, C*H$_2$*), 1.33 (s, 12H, C*H$_3$*).
^{13}C NMR (101 MHz, (CD$_3$)$_2$CO): 205.5, 159.6, 146.5, 137.3, 115.0, 112.6, 101.8, 83.0, 64.7, 24.3. ^{11}B NMR: 22.38.

Synthesis of N-phthalimido-N',N'-bis(2-pyridylmethyl)ethylenediamine, **9**
(*132*).
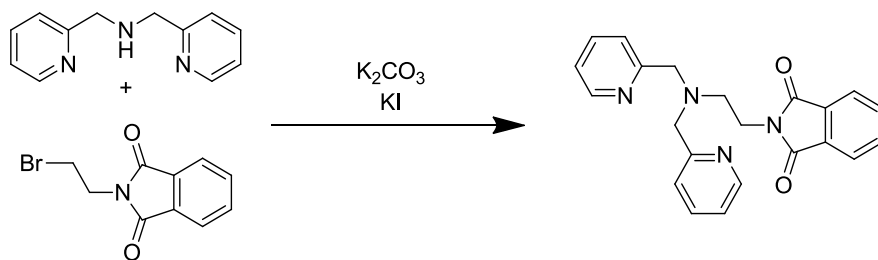
Compound **9** was prepared according to a literature procedure(*132*). Potassium carbonate (11.53 g, 83.0 mmol) and potassium iodide (4.62 g, 28.0 mmol) were added to a solution of 1-(2-pyridinyl)-N-(2-pyridinylmethyl)methanamine (5.00 ml, 28.0 mmol) in acetonitrile (50 ml), followed by N-(2-Bromoethyl)phthalimide (7.08 g, 28.0 mmol). The reaction mixture was refluxed for 24 hours. After this time the mixture was filtered and the solid removed under reduced pressure to yield dark brown crystalline solid. The solid was dissolved in dichloromethane, and the organic solution was washed with water (3 x 20 ml), with a saturated solution of sodium bicarbonate in water (3 x 20 ml) and finally with water (3 x 20 ml). The organic solvent was removed and to the resulting red solid was added hydrochloric acid (25 ml, 2M). The acidic solution was washed with dichloromethane (3 x 20 ml) and then basified by addition of solid sodium bicarbonate (5 g). A brown solid precipitated out and was extracted using dichloromethane (2 x 50 ml). The dichloromethane was evaporated and a brown crystalline solid remained. The product was isolated by chromatography on silica using dichloromethane and methanol (95:5) as eluent (Rf = 0.8) [Lit: 95:5 ethyl acetate and chloroform]. Compound **9** appeared as a tan solid (3.65 g, 9.82 mmol, 35 %).

^{1}H NMR (400 MHz, CDCl$_3$): 8.45 (d, 2H, Py*H*, J= 4.87), 7.79 (m, 4H, Ar*H*), 7.43 (td, 2H, Py*H*, J= 7.7, J= 1.8), 7.35 (d, 2H, Py*H*, J= 7.9), 7.17-7.12 (m, 2H, Py*H*), 3.86 (m, 6H, PyC*H*$_2$ and C*H*$_2$), 2.87 (t, 2H, C*H*$_2$, J= 5.9). ^{13}C NMR (101 MHz, CDCl$_3$): 168.2 (*C*), 159.4 (*C*), 149.1 (*C*H), 136.6 (*C*H), 134.8 (*C*H), 132.1 (*C*), 123.4 (*C*H), 122.9 (*C*H), 122.5 (*C*H), 59.9 (*C*H$_2$), 51.1 (*C*H$_2$), 36.0 (*C*H$_2$). ESI-MS m/z: 373 (100%, [M+H]$^+$), 395 (15%, [M+Na]$^+$). HRMS: Observed [M+H]$^+$, 373.1657. C$_{22}$H$_{20}$N$_4$O$_2$ requires [M+H]$^+$ 373.1665; Δ 2.1 ppm. IR: v$_{max}$/cm^{-1} 2817 (C-H), 1710 (C=O), 1394, 781, 722.

Synthesis of N,N-di(2-pyridinylmethyl)ethylenediamine, **10** (*132*).
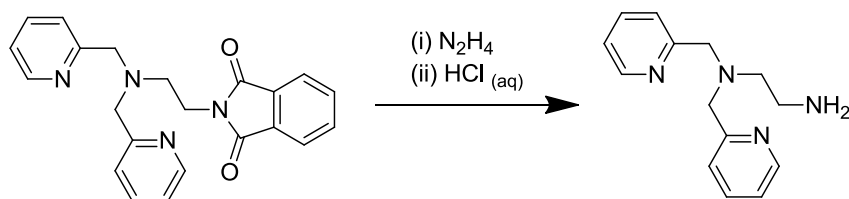
Compound **10** was synthesised following a literature procedure (*132*). Hydrazine monohydrate (0.14 ml, 2.73 mmol) solution was added to a solution of **9** (1.02 g, 2.73 mmol) in absolute ethanol. The mixture was refluxed for three hours, over which time a dense white precipitate formed. The ethanol was removed under reduced pressure. Hydrochloric acid (12 M, 0.85 ml) was added to the resulting white solid. This acidic solution was stirred at room temperature for 24 hours. The acid was removed under reduced pressure and to the resulting yellow oil a solution of sodium hydroxide was added. The pH was raised to 14 with aqueous sodium hydroxide (20 ml, 15 % w/v) and the aqueous solution was then extracted with dichloromethane (3 x 80 ml). The organic solvent was evaporated to yield compound **10** as yellow oil, which was used without further purification (257 mg, 1.06 mmol, 39 % yield).

^{1}H NMR (400 MHz, CDCl$_3$): 8.53 (m, 2H, Py*H*), 7.65 (td, 2H, Py*H,* J= 6.1, J= 2.0), 7.50 (dt, 2H, Py*H,* J= 7.9, J= 1.1), 7.15 (ddd, 2H, Py*H,* J= 7.6, J= 7.4, J= 1.2), 3.85 (s, 4H, PyC*H$_2$*), 2.79 (t, 2H, C*H$_2$*, J= 6.1), 2.66 (t, 2H, C*H$_2$*, J= 6.1). ^{13}C NMR (101 MHz, CDCl$_3$): 159.6 (C), 149.2 (*C*H), 137.0 (*C*H), 123.2 (*C*H), 122.6 (*C*H), 54.5 (*C*H$_2$), 53.4 (*C*H$_2$), 52.6 (*C*H$_2$). ESI-MS m/z: 243 ([M+H]$^+$ 100%). HRMS: Observed [M+H]$^+$, 243.1069. C$_{14}$H$_{19}$N$_4$ requires 243.1610; Δ 0.4 ppm. IR: v_{max} / cm^{-1}: 3354 (N-H), 2826 (C-H), 1590, 1433, 759.

Synthesis of 1,1'-(methylenebis(4,1-phenylene))bis(3-(2-(bis(pyridin-2-ylmethyl)amino)ethyl)urea), **11.**
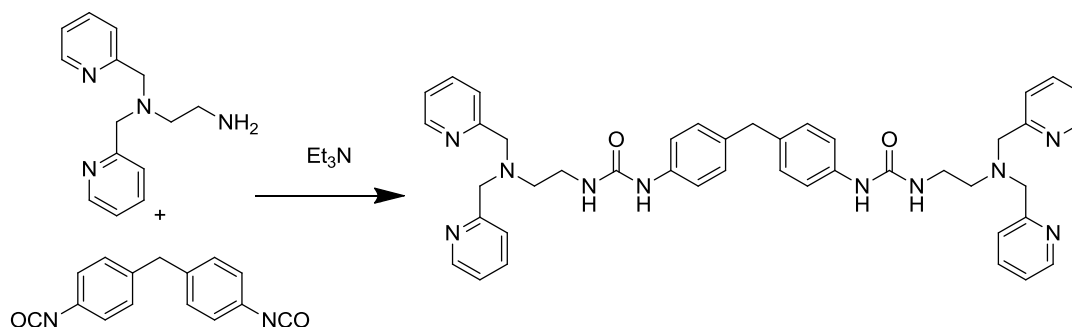
Anhydrous triethylamine (30 µl, 0.42 mmol) was added to a solution of 4,4'-methylenebis(phenyl isocyanate) (51.7 mg, 0.21 mmol) in anhydrous dichloromethane under a nitrogen atmosphere. A solution of compound **10** (100 mg, 0.42 mmol) in anhydrous dichloromethane was added dropwise at room temperature, and the reaction mixture was stirred overnight under nitrogen. The solvent was then removed under reduced atmosphere and the orange oil was washed with cold acetone (3 x 10 ml), aqueous sodium hydroxide (3 x 5 ml, 0.1M) and acetone again (3 x 10 ml). The remaining oil was dried under vacuum for 24 hours to obtain compound **11** as a beige solid (105 mg, 0.14 mmol, 68 % yield).

^{1}H NMR (400 MHz, d_6-DMSO): 8.54 (s, br, 2H, N*H* (urea)), 8.48 (d, 4H, Py*H,* J= 4.5), 7.72 (td, 4H, Py*H,* J= 7.6, J= 1.9), 7.59 (d, 4H, Py*H,* J= 7.6), 7.28 (d, 4H, Ar*H,* J= 8.6), 7.23 (m, 4H, Py*H*), 7.05 (d, 4H, Ar*H,* J= 8.6), 6.11 (t, br, 2H, N*H* (urea) J= 5.6), 3.78 (s, 8H, PyC*H$_2$*), 3.77 (s, 2H, ArC*H$_2$*Ar), 3.24 (m, 4H, C*H$_2$*), 2.56 (t, 4H, C*H$_2$*, J= 6.3). ^{13}C NMR (101 MHz, d_6-DMSO): 158.9 (*C*), 156.9 (*C*), 148.1 (*C*H), 137.3 (*C*), 135.7 (*C*H), 134.6 (*C*), 128.9 (*C*H), 123.6 (*C*H), 122.41 (*C*H), 119.2 (*C*H), 59.7 (*C*H$_2$), 54.0 (*C*H$_2$), 40.1 (*C*H$_2$), 37.1 (*C*H$_2$). ESI-MS m/z: 735 ([M+H]$^+$ 10 %), 757 ([M+Na]$^+$ 30 %), 368 ([M+2H]$^{2+}$ 100 %). HRMS: Observed [M+H]$^+$, 735.3895. $C_{43}H_{46}N_{10}O_2$ requires 735.3883, Δ 1.6 ppm. IR: v_{max} / cm^{-1}: 3315 (br, N-H str), 2932, 1591, 1543, 1309, 1231. Microanalysis: Observed %C, 68.21; %H, 6.47; %N, 18.01; $C_{43}H_{46}N_{10}O_2$.2H$_2$O requires %C, 68.60; %H, 6.43; %N, 18.60.

Synthesis of dizinc complex *12*
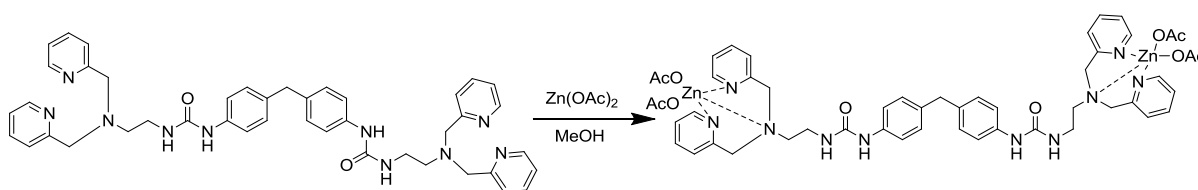
Compound **11** (187 mg, 0.26 mmol) was dissolved in methanol (10 ml). To this solution was added two equivalents of zinc acetate (112 mg, 0.51 mmol) in methanol (10 ml), and the mixture was heated at 40 $^{\circ}$C for 16 hours. The methanol was then removed under reduced pressure and the resulting yellow solid was washed with diethyl ether (3 x 10 ml) and dried under vacuum. Analysis by ^{1}H NMR spectroscopy showed that the singlet corresponding to the aliphatic protons vicinal to the pyridine had shifted and split into a doublet of doublets, indicating that complexation had taken place between the dipyridyl and the zinc. In addition, the ^{1}H NMR spectrum of the complex possessed a 12-proton singlet in the aliphatic region which corresponds to the acetate counterion. Receptor **12** was obtained as an orange solid (295 mg, 0.26 mmol, 100 % yield).

^{1}H NMR (400 MHz, d_6-DMSO): 8.76 (d, 4H, PyH, J = 4.7 Hz), 8.03 (t, 4H, PyH, J = 7.8), 7.59-7.53 (m, 8H, PyH), 7.23 (d, 4H, ArH, J = 9.0 Hz), 6.98 (d, 4H, ArH, J = 9.0 Hz), 4.30 (dd, br, 8H, PyCH_2 J = 15.0 Hz, J = 55.5 Hz), 3.82 (s, 2H, ArCH_2Ar), 3.29 (t, 4H, CH_2, J = 6.7 Hz), 2.82 (t, 4H, CH_2, J = 6.7 Hz), 1.98 (s, 12H, CH_3 (OAc)). ^{13}C NMR (101 MHz, d_6-DMSO): 179.6 (C), 156.7 (C), 155.1 (CH), 148.2 (CH), 140.5 (C), 137.2 (C), 135.9 (CH), 128.7 (CH), 124.5 (CH), 123.9 (CH), 57.1 (CH_2), 54.1 (CH_2), 40.1 (CH_2), 35.2 (CH_2), 21.7 (CH_3). IR: v_{max} / cm^{-1}: 3287, 1509, 1557, 1392, 1311.

Synthesis of 1,3-bis(2-(bis(pyridine-2-yl methyl)amino)ethyl)urea, **13.**
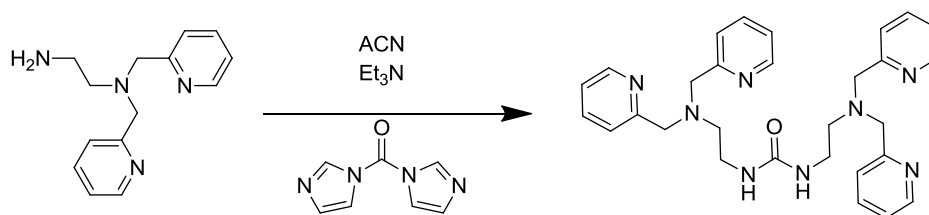
Compound **10** (1.45 g, 6.0 mmol) was stirred in anhydrous acetonitrile (10 ml) with anhydrous triethylamine (830 µl, 6.0 mmol) for 30 minutes. Then this mixture was added dropwise under nitrogen atmosphere to a solution of 1,1'-carbonyldiimidazole (434 mg, 3.0 mmol) in anhydrous acetonitrile. The reaction mixture was stirred at room temperature for 48 hours. The solvent was removed under reduced pressure and the crude dissolved in dichloromethane (20 ml). The organic solution was washed with water (3 x 10 ml) and then dried over sodium sulphate. The solvent evaporated to yield orange oil. Compound **13** was isolated by chromatography on silica gel, using 3 % methanol in chloroform as eluent (Rf = 0.2). Where traces of imidazole eluted with compound **13**, the imidazole was removed by reverse-phase chromatography. The mixture (100 mg) was loaded onto a pre-packed column containing C18 silica gel, pre-equilibrated with a mobile phase of 95 % water and 5 % methanol (HPLC grade). After washing for five minutes (25 ml eluent passed through column at 5 ml/min) analysis by TLC showed that the imidazole had been eluted. The mobile phase composition was then changed to 5 % water and 95 % methanol and after 1-2 minutes the pure product **13** was obtained as pale yellow oil (2.54 g, 4.98 mmol, 83 % yield).

^{1}H NMR (400 MHz, CDCl$_3$): 8.48 (d, 4H, PyH, J = 5.0), 7.57 (td, 4H, PyH, J = 7.8, J = 2.0), 7.42 (d, 4H, PyH, J = 7.8), 7.10 (m, 4H, PyH), 6.25 (s, 2H, NH), 3.78 (s, 8H, PyCH_2), 3.27 (q, 4H, CH_2, J = 5.4), 2.63 (t, 4H, CH_2, J = 5.9). ^{13}C NMR (101 MHz, d$_6$DMSO): 159.7 (C), 158.4 (C), 149.3 (CH), 136.9 (CH), 123.0 (CH), 122.4 (CH), 60.2 (CH$_2$), 54.7 (CH$_2$), 37.8 (CH$_2$). ESI-MS m/z: 256 (100 % [M+2H]$^{2+}$), 511 (45 % [M+H]$^+$), 533 (55 % [M+Na]$^+$). HRMS: Observed [M+H]$^+$ 511.2953. C$_{29}$H$_{35}$N$_8$O requires 511.2934, Δ 3.7 ppm. IR: ν$_{max}$ / cm^{-1}: 3115, 2931, 2837, 1592, 1434.

Synthesis of dizinc complex *14.*
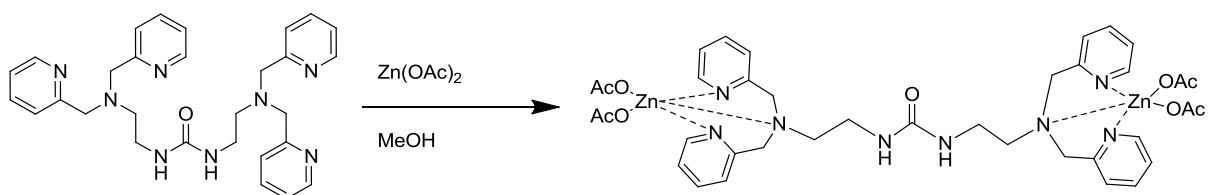
Compound **13** (347 mg, 0.70 mmol) was dissolved in methanol (5 ml). To this solution was added zinc acetate (299 mg, 1.40 mmol) in methanol (15 ml), and the mixture was heated at 40 $^{\circ}$C for six hours. The methanol was removed under reduced pressure to yield a beige solid, which was washed with cold acetone (3 x 5 ml). The resulting off-white solid was filtered and dried under vacuum. Analysis by ^{1}H NMR spectroscopy showed the splitting of the singlet that corresponds to the aliphatic protons vicinal to the pyridines, an indication that the zinc had formed a complex with the dipyridyl motif (614 mg, 0.70 mmol, 100%).

^{1}H NMR (400 MHz, CDCl$_3$): 8.52 (d, 4H, Py*H*, J = 5.0), 7.97 (td, 4H, Py*H*, J = 1.7, J = 7.8), 7.50 (t, 4H, Py*H*, J = 6.6), 7.46 (d, 4H, Py*H*, J = 7.8), 4.14 (dd, 8H, PyC*H$_2$*, J = 16.0, J = 75.1), 3.12 (t, 4H, C*H$_2$*, J = 6.6), 2.66 (t, 4H, C*H$_2$*, J = 6.6), 1.83 (s, 12H, C*H$_3$* (OAc)). ^{13}C NMR (101 MHz, CDCl$_3$): 148.5 (*C*H), 143.7 (*C*), 140.5 (*C*H), 140.7 (*C*), 124.5 (*C*H), 124.2 (*C*H), 34.7 (*C*H$_2$*), 56.9 (*C*H$_2$*) 53.3 (*C*H$_2$*), 23.1 (*C*H$_3$*). IR: ν_{max} / cm^{-1}: 3287, 2925, 2062, 1569, 1392. Microanalysis: Observed %C, 48.02; %H, 5.57; %N, 11.93. C$_{37}$H$_{46}$N$_8$O$_9$Zn$_2$.2H$_2$O requires: %C, 48.64; %H, 5.52; %N, 12.27.

Chapter 8: Biochemical assays

8.1 Materials

96-well fluorescence plates, Costar

96-well microtitre plates, Brand PureGrade

All PIPs, IP$_3$ and IP$_4$, Cell Signals

anti pan-Akt antibody (mouse monoclonal), Cell Signalling

anti-GST antibody (HRP conjugate), AbCam

anti-pAkt antibody (p-Serine 473, rabbit monoclonal), Novagen

ATP and ATPase, Sigma-Aldrich

Bovine serum albumin, Sigma-Aldrich

Fatty acid free Bovine serum albumin, Sigma-Aldrich

Bradford reagent, Sigma-Aldrich

Centrifugation filters, Millipore

DAPI, Merck

Glutathione Sepharose 4B beads, G.E. Healthcare

Goat anti-mouse antibody, BioRad

Goat anti-rabbit antibody, BioRad

LB broth and LB agar, Merck

Mammalian cell media, Sigma-Aldrich

MaxiSorp ELISA plates, Thermo Scientific

Milk powder, Merck

OMFP, Sigma Aldrich

ProLong Gold Antifade reagent, Invitrogen

TMB ELISA substrates, Thermo Scientific

Tween-20, Sigma-Aldrich

8.2 Buffers and Reagents

Bacterial lysis buffer: 2 mM EDTA, 1% Triton, 2mM DTT, 100 µg/ml trypsin inhibitor (from soyabean), 10 mM benzamidine-HCl, 2 mg/ml lysozyme, 0.5 mM AEBSF, 50 mM TrisHCl, pH 7.4.

GST affinity column equilibration buffer: 140 mM NaCl, 2.7 mM KCl, 50 mM TrisHCl, pH 7.4.

GST affinity column washing buffer 1: 140 mM NaCl, 2.7 mM KCl, 2mM DTT, 50 mM TrisHCl, pH 7.4.

GST affinity column washing buffer 2: 500 mM NaCl, 2.7 mM KCl, 2mM DTT, 50 mM TrisHCl, pH 7.4.

GST affinity column elution buffer: 20 mM Glutathione, 250 mM NaCl, 2 mM DTT, 100 mM TrisHCl, pH 7.4.

Phosphate detection reagent: 6 mM Malachite green oxalate, 19 mM ammonium molybdate, 77 mM bismuth (III) citrate, 17% (v/v) concentrated HCl. Reagent is 2x as required to stop enzyme reactions.

PBST: 140 mM NaCl, 2.7 mM KCl, 0.1 % Tween-20, 100mM $KHPO_4$, pH 7.4.

TBST: 140 mM NaCl, 2.7 mM KCl, 0.1 % Tween-20, 100 mM TrisHCl, pH 7.4.

ELISA blocking buffer: 3% w/v Essentially fatty acid free BSA in PBST or TBST, pH 7.4.

Cell growth medium: HCT116 cells grown in McCoy's 5A medium with glutamine and supplemented with 10% FCS. NIH/3T3 cells grown in DMEM supplemented with 10% BCS.

Cell starvation medium: DMEM low glucose medium, serum-free.

Mammalian cell lysis buffer: 62.5 mM TrisHCl, pH 6.8, 2 % w/v SDS, 10 % v/v Glycerol, 50 mM Dithiothreitol, 0.01 % w/v Bromophenol blue.

Western blot blocking buffer: TBST with 5 % w/v milk powder

Primary antibody dilution buffer: TBST with 5 % w/v BSA

Enhanced Chemiluminescence (ECL) detection solution: 1.25 mM luminol, 200 µM *p*-coumaric acid, 100 mM TrisHCl, pH 8.5. Hydrogen peroxide 30 % solution was added immediately prior to use (3.1 µl for 10 ml solution).

Buffer pH was adjusted using NaOH and HCl.

8.3 Methods

8.3.1 Calibration of phosphate detection reagent

The phosphate detection reagent was made up as described (based on literature formulation (*58*)) and calibrated using inorganic $KHPO_4$ in MilliQ water before being used in the assay. The phosphate detection reagent (100 µl per well) was added to increasing concentrations of phosphate (100 µl per well) in a standard 96-well microtitre plate. Absorbance was measured at 625 nm after five minutes.
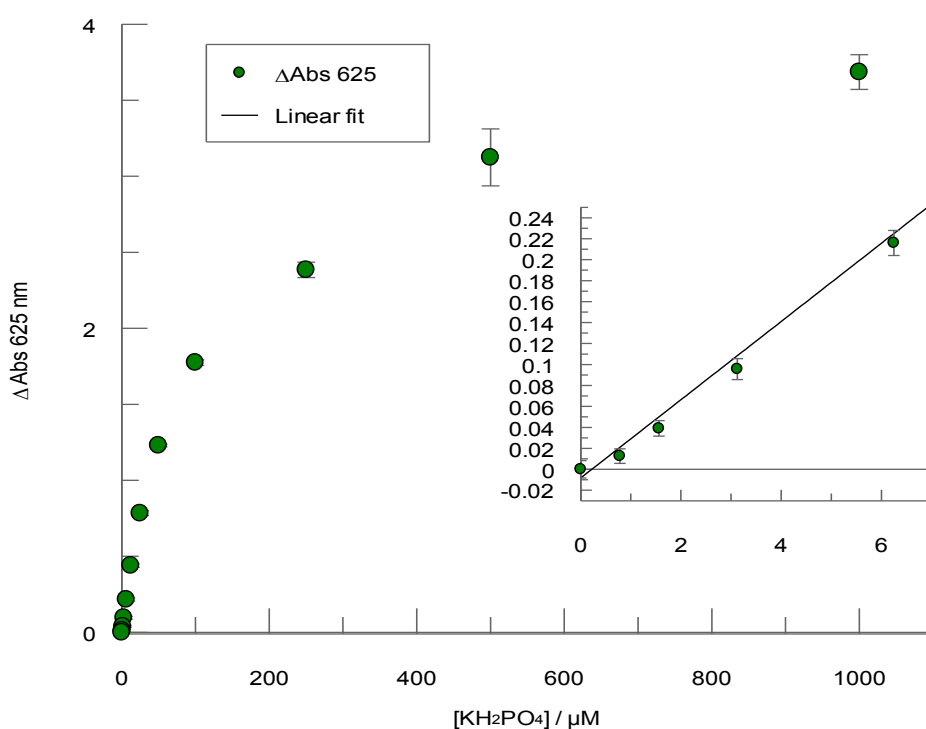
Figure 8.1: Calibration of phosphate detection reagent with increasing phosphate. Increase in absorbance at 625 nm of the phosphate detection reagent (100 µl) in the presence of increasing concentrations of $KHPO_4$ in MilliQ water (100 µl). Absorbance at 0M $KHPO_4$ was subtracted to give ΔAbsorbance. Inset: the concentration range (µM) in which the response of the dye to phosphate is linear. Linear fit shown. Error bars represent standard deviation of three independent repeats carried out in triplicate.

8.3.2 Calibration of protein detection

Protein concentration was determined using the Bradford method (*159*). Bradford reagent (200 µl, used as provided by manufacturer) was added to standard solutions of bovine serum albumin (BSA, 20 µl) in a standard 96-well microtitre plate. Absorbance was measured at 595 nm.
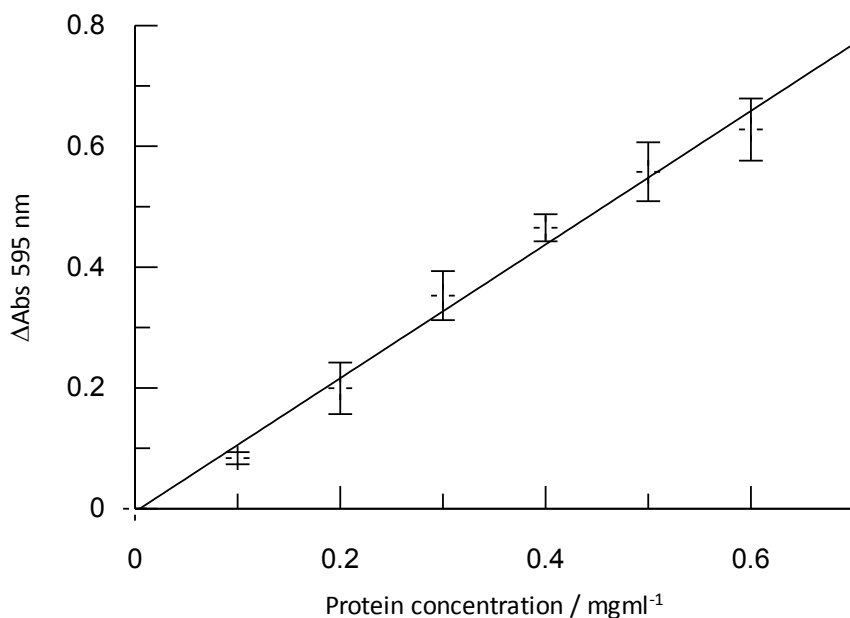
Figure 8.2: Calibration of Bradford reagent against BSA with linear fit. Bradford reagent (200 µl) was added to standard solutions of BSA (20 µl, 0 → 0.6 mg/ml) and absorbance was measured at 595 nm. Absorbance at 0 mg/ml BSA was subtracted to yield ΔAbsorbance. Error bars represent standard deviation of two independent repeats carried out in triplicate.

This standard plot was used to determine protein concentration.

8.3.3 Protein expression and purification

Akt-PH domain, PLCδ1-PH domain, SopB and PTEN were expressed as GST-fusion proteins according to the following protocol optimised by our group (*58*).

Plasmid DNA containing ampicillin resistance gene was added to DH5α E. Coli cells on ice (1 μl). After incubating on ice for 30 minutes the cells were heat shocked by incubating at 42 ^{o}C for 90 seconds, and were then returned to ice for two minutes. The cells were then spread onto agar plates containing ampicillin (Amp concentration = 100 μg/ml). The plates were incubated at 37 ^{o}C for 16 hours after which time bacterial colonies were observed. Single colonies were picked using a sterile tip and added to 10ml sterilised LB broth containing ampicillin each (100 μg/ml). After incubating for 16 hours at 37 ^{o}C the cloudy mixtures were added to 1L sterilised LB broth also containing ampicillin (100 μg/ml). The bacteria were allowed to grow until the optical density at 600 nm was in the range 0.5-0.6. Fresh ampicillin was then added (to a final concentration of 200 μg/ml) and expression was induced using isopropyl β-D-1-thiogalactopyranoside (IPTG, 1ml, 1M). The mixtures were incubated with shaking at 18 ^{o}C. After 24 hours the bacteria were collected by centrifugation at RCF = 4684g (4600 RPM) for 15 minutes. The supernatant was removed and the pellets frozen at -20 ^{o}C before purification.

The pellets were thawed and resuspended in lysis buffer (50 ml buffer per 1L LB preparation), and stirred for one hour at 4 ^{o}C. The cells were then lysed using a manual homogeniser followed by sonication (five cycles of one minute sonication followed by two minutes rest on ice). Cell debris was removed by centrifugation at RCF = 30753g (11500 RPM) and 4 ^{o}C for 60 minutes. The supernatant was then filtered onto a glutathione sepharose column (pre-equilibrated with column equilibration buffer, 20 ml) using a 0.45 μm syringe filter. After washing with buffers 1 and 2 (20 ml each), elution buffer containing fresh glutathione was added (5 ml) and incubated with the column at 4 ^{o}C overnight. After 16 hours the fractions were collected and protein concentration determined using Bradford assay. Fractions containing protein were combined and the protein was concentrated by ultracentrifugation (PH domains, 30 kDa filter; SopB and PTEN 80 kDa filter). The concentration of protein was determined by Bradford assay, and the purity was determined by staining on SDS-PAGE gel. Proteins were diluted x2 with glycerol and stored at -80 ^{o}C until required.

8.3.4 Phosphatase assays

To measure the activity of the phosphatases SopB and PTEN, and of ATPase, two methods were used. The first method is an endpoint assay which uses phosphoinositides, inositol phosphates and ATP as substrates, and measures the amount of phosphate released over a set period of time.   This is achieved by adding the phosphate detection reagent (calibrated against phosphate, Section 8.3.1) to the enzyme reaction which is stopped due to the acidic pH of the reagent. The second method is a continuous assay which uses the artificial substrate OMFP. OMFP is dephosphorylated to generate fluorescent OMF, and the fluorescence intensity can be measured continuously.

8.3.4.1 Phosphate release endpoint assay

Phosphate release assays were carried out for PTEN (substrate PC:PI(3,4,5)P_3), SopB (substrates IP$_3$ and all seven PIPs as PC:PIP mixtures) and ATPase (substrate ATP) by using a slight modification of a standard protocol (*139*),(*160*).

8.3.4.1 Sample preparation: lipid substrate

The phosphoinositide substrates were presented as 1:1 molar ratio of PIP and phosphatidylcholine (PC). The stock lipids were stored in chloroform. To make up samples the required amounts of PIP and PC were mixed in a glass vial (3ml size) and the solvent removed under flowing nitrogen for one hour. When the solvent was removed a film of lipid was observed. Water was then added to make solutions up to the required concentration and upon vortexing the mixture became cloudy. After bath sonication for 10 minutes the solutions were clear, and were used thus as substrate solutions. Fresh vesicle solutions were made up immediately before use and stored on ice until required.

8.3.4.2 Phosphatase activity

In each case, the substrate solutions were incubated with enzyme in a 96-well plate for 15 minutes at 37 $^{\circ}$C (100mM Tris, pH 7.4, 4 mM MgCl$_2$; total volume 100 µl per well using MilliQ water). The reaction was stopped by addition of a phosphate detection reagent based on malachite green (100 µl per well). Control wells included the same concentration of substrate, and the enzyme was added after the phosphate detection reagent (so that no reaction could take place, but that all the components were accounted for when the absorbance was read). Colour was allowed to develop for five minutes and absorbance was read at 625 nm. Turnover of the enzyme was calculated as the absorbance of the reaction wells minus absorbance of enzyme control wells (ΔAbsorbance at 625 nm). Each substrate was tested for linearity of response against the corresponding enzyme and vice versa.

8.3.4.3 Inhibition of phosphatase activity

For each assay, concentrations of enzyme and substrate were chosen which provided a linear response to the phosphate detection reagent (see Table 8.1). Receptors were incubated with a constant concentration of substrate for 30 minutes before addition of constant amount of enzyme (total volume 100 µl, 100 mM Tris pH 7.4, 4 mM $MgCl_2$, 2 % v/v DMSO where required). Controls were included which contained the relevant amount of receptor and substrate, and the enzyme was added after the phosphate detection reagent so that no reaction could take place. Absorbance was read at 625 nm and the turnover of the enzyme was the absorbance of the reaction wells minus absorbance of enzyme control wells (ΔAbsorbance at 625 nm). Turnover was plotted as % of vehicle control. IC_{50} values were calculated using 4-parameter fitting with GraFit version 6.0.12.

Table 8.1: Enzyme and substrate concentrations used in phosphate release assay IC_{50} measurements.

Enzyme	Enzyme Concentration	Substrate	Substrate Concentration
SopB	2.4 µg/ml	PC:PI(4,5)P_2	30 µM
SopB	2.4 µg/ml	IP_3	30 µM
ATPase	0.15 µg/ml	ATP	15 µM
PTEN	126.9 µg/ml	PC:PI(3,4,5)P_3	30 µM

8.3.4.4 Continuous phosphate release assay

This assay was carried out according to a previously described method (*161*). Ortho-methylfluorescein phosphate (OMFP) was used as an artificial substrate for SopB, PTEN and ATPase. When the phosphatases act on OMFP they generate OMF which is fluorescent. OMFP stocks were made up to 20 mM in DMSO and stored at -20 ^{o}C.

OMFP (in MilliQ water with 2 % DMSO) was added to enzyme solutions to initiate the reaction (total volume 100 μl, final concentrations 100 mM Tris and 4 mM $MgCl_2$, constant 2 % v/v DMSO) in 96-well fluorescence microtitre plates. Increase in fluorescence was measured (λex = 485 nm, λem = 525 nm) over time. Control solutions contained no enzyme in order to determine the background level of fluorescence due to OMFP hydrolysis to OMF. Rate of reaction was calculated as the change in fluorescence intensity over 10 minutes.

8.3.4.5 Enzyme inhibition- continuous phosphate release assay

Enzyme inhibition using a single concentration of receptors **3**, **4**, **12**, **14** and **16** was tested using the following method. Receptors were added to the buffered enzyme solution (concentrations indicated in Table 8.2; final concentrations 100 mM Tris, 4 mM $MgCl_2$, pH 7.4, 2 % v/v DMSO) and incubated at room temperature for 15 minutes. OMFP (50 μM) was then added to initiate the reaction and the fluorescence intensity was monitored over 30 minutes.

Table 8.2: Receptor and enzyme concentrations for inhibition assay using OMFP substrate. Receptors were incubated with enzyme and upon addition of OMFP (50 μM) fluorescence intensity was measured for 30 minutes.

Inhibitor	Receptor concentration (final concentration in 100 μl)	Enzyme	Enzyme concentration (final concentration in 100 μl)
Receptor **3**	100 μM	SopB	2.36 μg/ml
Receptor **4**	100 μM	SopB	2.36 μg/ml
Receptor **3**	100 μM	ATPase	0.15 μg/ml
Receptor **4**	100 μM	ATPase	0.15 μg/ml
Receptor **12**	15 μM	PTEN	84.6 μg/ml
Receptor **14**	15 μM	PTEN	84.6 μg/ml
Receptor **16**	15 μM	PTEN	84.6 μg/ml

To calculate IC_{50} values, increasing concentrations of zinc chloride and receptors **12**, **14** and **16** were added to the enzymes (enzyme concentrations as Table 8.2, 100 mM Tris, 4 mM $MgCl_2$, pH 7.4, 2 % v/v DMSO) in a 96-well fluorescence microtitre plate and incubated at room temperature for 15 minutes. OMFP was added to initiate the reaction and fluorescence intensity was measured over 30

minutes. Rate of reaction was calculated as change in fluorescence intensity over 10 minutes. IC_{50} values were calculated using 4-parameter fitting with GraFit version 6.0.12.

8.3.6 Detection of immobilised PI(4,5)P$_2$

Fluorescent receptor **5** was used to detect immobilised PI(4,5)P$_2$ using the following method. Increasing amounts of PI(4,5)P$_2$ were coated onto the bottom of a 96-well ELISA plate (MaxiSorp) by incubating in methanol (50 μl) overnight at 4 ^{o}C. After 16 hours the methanol was allowed to evaporate at room temperature for one hour. The lipid was washed with TBST (3 x 200 μl, pH 7.4). Receptor **5** (50 μl, 5 μM, 2 % v/v DMSO) in methanol was then incubated for one hour at room temperature, and unbound receptor was removed by washing the wells with TBST (3 x 200 μl, pH 7.4). The fluorescence intensity of the plate was measured (λ_{ex} = 485, λ_{em} = 525 nm).

8.3.7 Enzyme-linked immunosorbent assay (ELISA)

Lipids were coated onto the bottom of a 96-well ELISA plate (MaxiSorp) by incubating in methanol (50 µl) overnight at 4°C. After 16 hours the methanol was allowed to evaporate at room temperature for one hour. The wells were then washed with buffer (PI(4,5)P_2 system used PBST; PI(3,4,5)P_3 system used TBST; washed 3 x 200 µl, 5 minutes each). The lipid was incubated with a solution of blocking buffer containing the relevant lipid-binding protein domain as GST fusion protein. After one hour at room temperature the wells were again washed with buffer (200 µl, 3 x 5 minutes each). The wells were then incubated with a solution containing buffer and HRP-conjugated anti-GST antibody (1:10,000). After a further round of washing (3 x 200 µl, 5 minutes each) a solution of TMB reagent (100 µl per well) was added and allowed to develop for five minutes, turning blue in colour. The reaction was then stopped by addition of sulfuric acid (100 µl per well, 2M) and the absorbance of the resulting yellow solutions was measured at 450 nm.

ELISA assays were optimised by analysing the linear response of increasing lipid against a single concentration of protein, and increasing protein against a single lipid concentration. In this way we can be sure that decrease in absorbance at 450 nm is linearly proportional to inhibition.

8.3.7.1 Determination of binding affinity of receptors towards PI(4,5)P_2 and PI(3,4,5)P_3:

Competitive ELISAs were carried out according to the protocol above, but with the following modification.

Receptor-lipid mixtures were made up in methanol (containing constant concentration of 2% DMSO or H_2O). The mixtures were laid onto the plate overnight at 4°C and the solvents were allowed to evaporate at room temperature the next day. The ELISA protocol above was then followed exactly from (including) the first washing step.

Receptors **3**, **4**, **5** and **16** (increasing concentrations) were incubated with PI(4,5)P_2 (100 pmols) which was probed with the PLCδ1-PH domain (50 nM); receptors **12**, **14** and **16** (increasing concentrations) were incubated with PI(3,4,5)P_3 (50 pmols) which was probed with GRP1-PH domain (65 nM, expressed and purified by Dr. Lok Hang Mak, Woscholski group).

8.3.8 Cell culture

HCT116 wild type cells and NIH/3T3 cells were cultured in 10 cm sterile plates in a humidified incubator at 37°C with 5% CO_2 atmosphere. Cells were handled in a laminar flow hood. HCT116 cells were grown in McCoy's 5A medium supplemented with glutamine and 10% serum. NIH3T3 cells were grown in Dulbecco's Modified Eagle Medium (DMEM) supplemented with 10 % serum. When cells reached approximately 80% confluency the medium was removed by aspiration, and the cells washed with sterile PBS (1 x 10 ml). Trypsin (1 ml, 0.25%) was added to detach the cells which were then resuspended in medium and split 1:10 (NIH3T3) or 2:10 (HCT116) three times per week or as required into fresh medium.

8.3.8.1 Determination of phospho-Akt

HCT116 cells were grown on 6 cm plates until 80% confluency. The cells were starved overnight in starvation medium containing no serum (in incubator at 37°C with 5% CO_2 atmosphere), and before experiments were carried out the medium was replaced with fresh starvation medium. Solutions of receptors were added to the medium (using up to 2 % (v/v) DMSO) and incubated for 15 minutes before stimulation with insulin for a further 15 minutes. Where compounds were solutions in DMSO, controls contained the same volume of DMSO (2 % v/v). Cells were then washed three times with cold PBS and detached using lysis buffer (300 µl), and the lysate boiled for 5 minutes at 95°C.

8.3.8.2 Western blot

Cell lysate (20 µl) was run on SDS gels (stacking gel 5 % polyacrylamide, running gel 10 %) at 200 V for 45 minutes, along with protein ladders. The gels were then transferred onto nitrocellulose membrane using 200 V and 350 mA for 60 minutes at 4°C. The membrane was washed twice with TBST and blocked using milk powder (5 % w/v) in TBST for one hour at room temperature. After washing three times with TBST (5 mins each, with gentle agitation) the membrane was incubated overnight (minimum 16 hours) with primary antibody (1:5000 dilution) in TBST with 5 % (w/v) BSA at 4°C. The membrane was washed another three times with TBST and incubated with secondary antibody (1:2000 dilution) for one hour at room temperature in TBST with milk powder (5 % w/v) before a further three washes were carried out. The blot was incubated in ECL detection solution for 2 minutes prior to imaging by chemiluminescent detection.

8.3.8.3 Fluorescence microscopy

NIH/3T3 cells were cultured as described. In preparation for experiment, cells were split into 24-well plates containing coverslips and grown in a humidified incubator at 37°C and 5 % CO2 atmosphere until approximately 80 % confluent. Cells were starved overnight in serum-free medium before experiments were carried out.

8.3.8.4 Sample preparation- live cells

Medium was removed by aspiration and fresh starvation (serum-free) medium was added to the cells before procedures were carried out. Receptor **5** was added to the medium and incubated for 15 minutes at 37°C before the medium was removed. The cells were washed with PBS (3 x 500 µl) before paraformaldehyde (PFA) was added (300 µl, 4 %, 15 mins, room temperature). After removal of PFA the wells were washed with PBS (3 x 500 µl). A solution of 4',6-Diamidino-2-Phenylindole (DAPI) in blocking buffer (200 µl, 1:1000 DAPI in 3 % BSA in PBS) was incubated (10 minutes, room temperature), and after this time the wells were washed with PBS (3 x 500 µl).

8.3.8.5 Sample preparation- fixed cells

Medium was removed by aspiration and fresh starvation (serum-free) medium was added to the cells before procedures were carried out. The cells were washed twice with PBS before paraformaldehyde (PFA) was added (300 µl, 4 %, 15 mins, room temperature). After removal of PFA the wells were washed with PBS (3 x 500 µl). Receptor **5** was added to the medium and incubated for 15 minutes at room temperature before the medium was removed. After washing with PBS (3 x 500 µl) cells were incubated with DAPI (200 µl, 1:1000 DAPI in 3 % BSA in PBS, 10 mins, room temperature) and after this time the wells were washed with PBS (3 x 500 µl).

8.3.8.6 Imaging cells

Coverslips were mounted onto glass slides using ProLong Gold Antifade and sealed with nail varnish. Cells were observed using a Nikon TE 2000 fluorescence microscope using a 100x lens. DAPI filter excitation wavelength range was 340 – 380 nm and emission wavelength 435-485 nm. FITC filter excitation wavelength range was 465 – 495 nm and emission wavelength 515 – 555 nm. Images were digitised using Hamamatsu CCD camera for each fluorophore and combined using IPLab software (Version 3.65 with Multiprobe extension). Images shown were all taken with the same exposure time (DAPI, 20 ms; FITC, 300 ms).

1.	Lietha, D. (2011) Phosphoinositides – The Seven Species : Conversion and Cellular Roles. In *Encyclopedia of Life Sciences (ELS)*, pp 1–11, John Wiley & Sons, Inc., Chichester.

2.	Kooijman, E. E., King, K. E., Gangoda, M., and Gericke, A. (2009) Ionization properties of phosphatidylinositol polyphosphates in mixed model membranes., *Biochemistry 48*, 9360–71.

3.	Di Paolo, G., and De Camilli, P. (2006) Phosphoinositides in cell regulation and membrane dynamics., *Nature 443*, 651–7.

4.	Falkenburger, B. H., Jensen, J. B., Dickson, E. J., Suh, B.-C., and Hille, B. (2010) Phosphoinositides: lipid regulators of membrane proteins., *J. Physiol. 588*, 3179–85.

5.	Halstead, J. R., Jalink, K., and Divecha, N. (2005) An emerging role for PtdIns(4,5)P2-mediated signalling in human disease., *Trends Pharmacol. Sci. 26*, 654–60.

6.	Kwiatkowska, K. (2010) One lipid, multiple functions: how various pools of PI(4,5)P(2) are created in the plasma membrane., *Cell. Mol. Life Sci. 67*, 3927–46.

7.	Doughman, R. L., Firestone, a J., and Anderson, R. a. (2003) Phosphatidylinositol phosphate kinases put PI4,5P(2) in its place., *J. Membr. Biol. 194*, 77–89.

8.	Vivanco, I., and Sawyers, C. L. (2002) The phosphatidylinositol 3-Kinase AKT pathway in human cancer., *Nat. Rev. Cancer 2*, 489–501.

9.	Hunzicker-Dunn, M. E., Lopez-Biladeau, B., Law, N. C., Fiedler, S. E., Carr, D. W., and Maizels, E. T. (2012) PKA and GAB2 play central roles in the FSH signaling pathway to PI3K and AKT in ovarian granulosa cells., *Proc. Natl. Acad. Sci. U. S. A. 109*, E2979–88.

10.	Zhang, S. Q., Tsiaras, W. G., Araki, T., Wen, G., Minichiello, L., Klein, R., and Neel, B. G. (2002) Receptor-Specific Regulation of Phosphatidylinositol 3-Kinase Activation by the Protein Tyrosine Phosphatase Shp2, *Mol. Cell. Biol. 22*, 4062–4072.

11.	Eck, M. J., Dhe-paganon, S., Nolte, R. T., and Shoelson, S. E. (1996) Structure of the IRS-1 PTB Domain Bound to the Juxtamembrane Region of the Insulin Receptor, *Cell 85*, 695–705.

12.	Filippakopoulos, P., Müller, S., and Knapp, S. (2009) SH2 domains: modulators of nonreceptor tyrosine kinase activity., *Curr. Opin. Struct. Biol. 19*, 643–9.

13.	Patel, S. (2013) Exploring novel therapeutic targets in GIST: focus on the PI3K/Akt/mTOR pathway., *Curr. Oncol. Rep. 15*, 386–95.

14.	Djiougue, S., Kamdje, A. H. N., Vecchio, L., Kipanyula, M. J., Farahna, M., Aldebasi, Y., and Etet, P. F. S. (2013) Insulin resistance and cancer : the role of insulin and IGFs, *Endocr. Relat. Cancer 20*, R1–R17.

15.	Bader, A. G., Kang, S., Zhao, L., and Vogt, P. K. (2005) Oncogenic PI3K deregulates transcription and translation., *Nat. Rev. Cancer 5*, 921–9.

16.	Kutateladze, T. G. (2012) Molecular Analysis of Protein-Phosphoinositide Interactions. In *Phosphoinositides and Disease* (Falasca, M., Ed.), pp 111–126, Springer Netherlands, Dordrecht.

17.   Lemmon, M. a. (2003) Phosphoinositide recognition domains., *Traffic 4*, 201–13.

18.   Heo, W. Do, Inoue, T., Park, W. S., Kim, M. L., Park, B. O., Wandless, T. J., and Meyer, T. (2006) PI(3,4,5)P3 and PI(4,5)P2 lipids target proteins with polybasic clusters to the plasma membrane., *Science 314*, 1458–61.

19.   Rosenhouse-Dantsker, A., and Logothetis, D. E. (2007) Molecular characteristics of phosphoinositide binding., *Pflugers Arch. 455*, 45–53.

20.   Essen, L., Perisic, O., Katan, M., Wu, Y., Roberts, M. F., and Williams, R. L. (1997) Structural Mapping of the Catalytic Mechanism for a Mammalian Phosphoinositide-Specific Phospholipase C, *Biochemistry* 1704–1718.

21.   Lemmon, M. A., Ferguson, K. M., O'Brien, R., Sigler, P. B., and Schlessinger, J. (1995) Specific and high-affinity binding of inositol phosphates to an isolated pleckstrin homology domain., *Proc. Natl. Acad. Sci. U. S. A. 92*, 10472–6.

22.   Ferguson, K. M., Kavran, J. M., Sankaran, V. G., Fournier, E., Isakoff, S. J., Skolnik, E. Y., Lemmon, M. a, Lietzke, S. E., Bose, S., Cronin, T., Klarlund, J., Chawla, a, Czech, M. P., and Lambright, D. G. (2000) Structural basis for discrimination of 3-phosphoinositides by pleckstrin homology domains., *Mol. Cell 6*, 385–94.

23.   C, P. P., Essen, L., Perisic, O., Katan, M., Wu, Y., Roberts, M. F., and Williams, R. L. (1997) Structural Mapping of the Catalytic Mechanism for a Mammalian Phosphoinositide-Specific Phospholipase C, *Biochemistry* 1704–1718.

24.   Dowler, S., Kular, G., and Alessi, D. R. (2002) Protein Lipid Overlay Assay, *Sci. Signal. 2002*, pl6–pl6.

25.   Hornbeck, P. (2001) Enzyme-linked immunosorbent assays. In *Current Protocols in Immunology*, p Unit 2.1, John Wiley & Sons, Inc.

26.   Hammond, G. R. V, Schiavo, G., and Irvine, R. F. (2009) Immunocytochemical techniques reveal multiple, distinct cellular pools of PtdIns4P and PtdIns(4,5)P(2)., *Biochem. J. 422*, 23–35.

27.   Howes, A. L., Arthur, J. F., Zhang, T., Miyamoto, S., Adams, J. W., Dorn, G. W., Woodcock, E. a, and Brown, J. H. (2003) Akt-mediated cardiomyocyte survival pathways are compromised by G alpha q-induced phosphoinositide 4,5-bisphosphate depletion., *J. Biol. Chem. 278*, 40343–51.

28.   Berman, D. E., Dall'Armi, C., Voronov, S. V, McIntire, L. B. J., Zhang, H., Moore, A. Z., Staniszewski, A., Arancio, O., Kim, T.-W., and Di Paolo, G. (2008) Oligomeric amyloid-beta peptide disrupts phosphatidylinositol-4,5-bisphosphate metabolism., *Nat. Neurosci. 11*, 547–54.

29.   Niciu, M. J., Ionescu, D. F., Mathews, D. C., Richards, E. M., and Zarate, C. a. (2013) Second messenger/signal transduction pathways in major mood disorders: moving from membrane to mechanism of action, part II: bipolar disorder., *CNS Spectr.* 1–10.

30. Zhang, S., and Yu, D. (2010) PI(3)king apart PTEN's role in cancer., *Clin. Cancer Res. 16*, 4325–30.

31. Cully, M., You, H., Levine, A. J., and Mak, T. W. (2006) Beyond PTEN mutations: the PI3K pathway as an integrator of multiple inputs during tumorigenesis., *Nat. Rev. Cancer 6*, 184–92.

32. Wishart, M. J., and Dixon, J. E. (2002) PTEN and myotubularin phosphatases: from 3-phosphoinositide dephosphorylation to disease., *Trends Cell Biol. 12*, 579–85.

33. Li, J. (1997) PTEN, a Putative Protein Tyrosine Phosphatase Gene Mutated in Human Brain, Breast, and Prostate Cancer, *Science (80-.). 275*, 1943–1947.

34. Attree, O., Olivos, I. M., Okabe, I., Bailey, L. C., Nelson, D. L., Lewis, R. A., McInnes, R. R., and Nussbaum, R. L. (1992) The Lowe's Oculocerebrorenal Syndrome gene encodes a protein highly homologous to inositol polyphosphate-5-phosphatase., *Lett. to Nat. 358*, 239–242.

35. Fresno Vara, J. A., Casado, E., de Castro, J., Cejas, P., Belda-Iniesta, C., and González-Barón, M. (2004) PI3K/Akt signalling pathway and cancer., *Cancer Treat. Rev. 30*, 193–204.

36. Pirruccello, M., and De Camilli, P. (2012) Inositol 5-phosphatases: insights from the Lowe syndrome protein OCRL., *Trends Biochem. Sci.*, Elsevier Ltd *37*, 134–43.

37. Erneux, C., Edimo, W. E., Deneubourg, L., and Pirson, I. (2011) SHIP2 multiple functions: a balance between a negative control of PtdIns(3,4,5)P_3 level, a positive control of PtdIns(3,4)P_2 production, and intrinsic docking properties., *J. Cell. Biochem. 112*, 2203–9.

38. Xie, J., Erneux, C., and Pirson, I. (2013) How does SHIP1/2 balance PtdIns(3,4)P2 and does it signal independently of its phosphatase activity?, *Bioessays* 1–11.

39. Morgan, T. M., Koreckij, T. D., and Corey, E. (2010) Targeted therapy for advanced prostate cancer: Inhibition of the PI3K/Akt/mTOR pathway, *Curr. Cancer Drug Targets 9*, 237–249.

40. Farooq, a, Walker, L. J., Bowling, J., and Audisio, R. a. (2010) Cowden syndrome., *Cancer Treat. Rev.*, Elsevier Ltd *36*, 577–83.

41. Farese, R. V. (2001) Insulin-Sensitive Phospholipid Signaling Systems and Glucose Transport. Update II, *Exp. Biol. Med. 226*, 283–295.

42. Lizcano, J. M., and Alessi, D. R. (2002) The insulin signalling pathway., *Curr. Biol. 12*, R236–8.

43. Xu, X., Müller-Taubenberger, A., Adley, K. E., Pawolleck, N., Lee, V. W. Y., Wiedemann, C., Sihra, T. S., Maniak, M., Jin, T., and Williams, R. S. B. (2007) Attenuation of phospholipid signaling provides a novel mechanism for the action of valproic acid., *Eukaryot. Cell 6*, 899–906.

44. Teo, R., King, J., Dalton, E., Ryves, J., Williams, R. S. B., and Harwood, A. J. (2009) PtdIns(3,4,5)P(3) and inositol depletion as a cellular target of mood stabilizers., *Biochem. Soc. Trans. 37*, 1110–4.

45.   Galanopoulou, A. S., Gorter, J. a, and Cepeda, C. (2012) Finding a better drug for epilepsy: the mTOR pathway as an antiepileptogenic target., *Epilepsia 53*, 1119–30.

46.   Mikoshiba, K. (2007) IP3 receptor/Ca2+ channel: from discovery to new signaling concepts., *J. Neurochem. 102*, 1426–46.

47.   Williams, R. S. B., Cheng, L., Mudge, A. W., and Harwood, A. J. (2002) A common mechanism of action for three mood-stabilizing drugs., *Nature 417*, 292–5.

48.   Loi, M. (2006) Lowe syndrome., *Orphanet J. Rare Dis. 1*, 16.

49.   Georgiades, S. N., Mak, L. H., Angurell, I., Rosivatz, E., Firouz Mohd Mustapa, M., Polychroni, C., Woscholski, R., and Vilar, R. (2011) Identification of a potent activator of Akt phosphorylation from a novel series of phenolic, picolinic, pyridino, and hydroxamic zinc(II) complexes., *J. Biol. Inorg. Chem. 16*, 195–208.

50.   Rosivatz, E., Matthews, J. G., Mcdonald, N. Q., Mulet, X., Ho, K. K., and Lossi, N. ASmall-Molecule Inhibitor for Phosphatase and Tensin Homologue Deleted on Chromosome 10 (PTEN) *1*.

51.   Gunn, R. M., and Hailes, H. C. (2008) Insights into the PI3-K-PKB-mTOR signalling pathway from small molecules., *J. Chem. Biol. 1*, 49–62.

52.   Sasaki, T., Sasaki, J., Sakai, T., Takasuga, S., and Suzuki, A. (2007) Metabolism and Functions of Phosphoinositides: The Physiology of Phosphoinositides, *Biol. Pharm. Bull. 30*, 1599–1604.

53.   Leslie, N. R., Biondi, R. M., and Alessi, D. R. (2001) Phosphoinositide-regulated kinases and phosphoinositide phosphatases., *Chem. Rev. 101*, 2365–80.

54.   McNamara, C. R., and Degterev, A. (2011) Small-molecule inhibitors of the PI3K signaling network, *Future Med. Chem. 3*, 549–565.

55.   Berrie, C. P., and Falasca, M. (2000) Patterns within protein / polyphosphoinositide interactions provide specific targets for therapeutic intervention, *J. Fed. Am. Soc. Exp. Biol. 14*, 2618–2622.

56.   Miao, B., Skidan, I., Yang, J., Lugovskoy, A., Reibarkh, M., Long, K., Brazell, T., Durugkar, K. a, Maki, J., Ramana, C. V, Schaffhausen, B., Wagner, G., Torchilin, V., Yuan, J., and Degterev, A. (2010) Small molecule inhibition of phosphatidylinositol-3,4,5-triphosphate (PIP3) binding to pleckstrin homology domains., *Proc. Natl. Acad. Sci. U. S. A. 107*, 20126–31.

57.   Falasca, M., Chiozzotto, D., Godage, H. Y., Mazzoletti, M., Riley, a M., Previdi, S., Potter, B. V. L., Broggini, M., and Maffucci, T. (2010) A novel inhibitor of the PI3K/Akt pathway based on the structure of inositol 1,3,4,5,6-pentakisphosphate., *Br. J. Cancer*, Nature Publishing Group *102*, 104–14.

58.   Mak, L. H., Georgiades, S. N., Rosivatz, E., Whyte, G. F., Mirabelli, M., Vilar, R., and Woscholski, R. (2011) A small molecule mimicking a phosphatidylinositol (4,5)-bisphosphate binding pleckstrin homology domain., *ACS Chem. Biol. 6*, 1382–90.

59. Drewry, J. a, Duodu, E., Mazouchi, A., Spagnuolo, P., Burger, S., Gradinaru, C. C., Ayers, P., Schimmer, A. D., and Gunning, P. T. (2012) Phosphopeptide selective coordination complexes as promising SRC homology 2 domain mimetics., *Inorg. Chem. 51*, 8284–91.

60. Bicker, K. L., Sun, J., Lavigne, J. J., and Thompson, P. R. (2012) Boronic acid functionalized peptidyl synthetic lectins: Combinatorial library design, peptide sequencing, and selective glycoprotein recognition, *ACS Comb. Sci. 13*, 232–243.

61. Menting, J. G., Whittaker, J., Margetts, M. B., Whittaker, L. J., Kong, G. K.-W., Smith, B. J., Watson, C. J., Záková, L., Kletvíková, E., Jiráček, J., Chan, S. J., Steiner, D. F., Dodson, G. G., Brzozowski, A. M., Weiss, M. a, Ward, C. W., and Lawrence, M. C. (2013) How insulin engages its primary binding site on the insulin receptor., *Nature 493*, 241–5.

62. Chinai, J. M., Taylor, A. B., Ryno, L. M., Hargreaves, N. D., Morris, C. a, Hart, P. J., and Urbach, A. R. (2011) Molecular recognition of insulin by a synthetic receptor., *J. Am. Chem. Soc. 133*, 8810–3.

63. Rock, F. L., Mao, W., Yaremchuk, A., Tukalo, M., Crépin, T., Zhou, H., Zhang, Y.-K., Hernandez, V., Akama, T., Baker, S. J., Plattner, J. J., Shapiro, L., Martinis, S. a, Benkovic, S. J., Cusack, S., and Alley, M. R. K. (2007) An antifungal agent inhibits an aminoacyl-tRNA synthetase by trapping tRNA in the editing site., *Science 316*, 1759–61.

64. Whyte, G. F., Vilar, R., and Woscholski, R. (2013) Molecular recognition with boronic acids—applications in chemical biology, *J. Chem. Biol. DOI 10.100*.

65. Kubik, S. (2010) Anion recognition in water., *Chem. Soc. Rev. 39*, 3648–63.

66. Kubik, S. (2012) Chapter 7: Receptors for biologically relevant anions. In *Anion Coordination Chemistry* (Bowman-James, K., Bianchi, A., and Garcia-Espana, E., Eds.) First., pp 363–464, Wiley-VCH.

67. Dydio, P., Lichosyt, D., and Jurczak, J. (2011) Amide- and urea-functionalized pyrroles and benzopyrroles as synthetic, neutral anion receptors., *Chem. Soc. Rev. 40*, 2971–85.

68. Xiao, K. P., Buhlmann, P., Nishizawa, S., and Umezawa, Y. (1997) Strong Hydrogen Bond-Mediated Complexation of H2P04- by Neutral Bis-Thiourea Hosts, *Tetrahedron 53*, 1647–1654.

69. Amendola, V., Fabbrizzi, L., and Mosca, L. (2010) Anion recognition by hydrogen bonding: urea-based receptors., *Chem. Soc. Rev. 39*, 3889–915.

70. Jose, D. A., Kumar, D. K., Ganguly, B., and Das, A. (2005) Urea and thiourea based efficient colorimetric sensors for oxyanions, *Tetrahedron Lett. 46*, 5343–5346.

71. Hughes, M. P., Shang, M., and Smith, B. D. (1996) High Affinity Carboxylate Binding Using Neutral Urea-Based Receptors with Internal Lewis Acid Coordination, *J. Org. Chem. 61*, 4510–4511.

72. Quinlan, E., Matthews, S. E., and Gunnlaugsson, T. (2007) Colorimetric recognition of anions using preorganized tetra-amidourea derived calix[4]arene sensors., *J. Org. Chem. 72*, 7497–503.

73. Bazzicalupi, C., Bencini, A., and Lippolis, V. (2010) Tailoring cyclic polyamines for inorganic/organic phosphate binding., *Chem. Soc. Rev. 39*, 3709–28.

74. Bazzicalupi, C., Bencini, A., Giorgi, C., Valtancoli, B., Lippolis, V., and Perra, A. (2011) Exploring the binding ability of polyammonium hosts for anionic substrates: selective size-dependent recognition of different phosphate anions by bis-macrocyclic receptors., *Inorg. Chem. 50*, 7202–16.

75. Houk, R. J. T., Tobey, S. L., and Anslyn, E. V. (2005) Abiotic Guanidinium Receptors for Anion Molecular Recognition and Sensing, *Anion Sens.* 199–229.

76. Niikura, K., Metzger, A., and Anslyn, E. V. (1998) Chemosensor Ensemble with Selectivity for Inositol-triphosphate, *J. Am. Chem. Soc. 120*, 8533–8534.

77. Fabbrizzi, L., and Poggi, A. (2012) Anion recognition by coordinative interactions: metal-amine complexes as receptors., *Chem. Soc. Rev.*

78. Janowski, V., and Severin, K. (2011) Carbohydrate sensing with a metal-based indicator displacement assay., *Chem. Commun. (Camb). 47*, 8521–3.

79. Caltagirone, C., Mulas, A., Isaia, F., Lippolis, V., Gale, P. a, and Light, M. E. (2009) Metal-induced pre-organisation for anion recognition in a neutral platinum-containing receptor., *Chem. Commun. (Camb).* 6279–81.

80. Zhang, X., and Eldik, R. Van. (1995) A Functional Model for Carbonic Anhydrase: Thermodynamic and Kinetic Study of a Tetraazacyclododecane Complex of Zinc(II), *Inorg. Chem. 34*, 5606–5614.

81. Ojida, A., Mito-Oka, Y., Inoue, M.-A., and Hamachi, I. (2002) First artificial receptors and chemosensors toward phosphorylated peptide in aqueous solution., *J. Am. Chem. Soc. 124*, 6256–8.

82. Ojida, A., Mito-oka, Y., Sada, K., and Hamachi, I. (2004) Molecular recognition and fluorescence sensing of monophosphorylated peptides in aqueous solution by bis(zinc(II)-dipicolylamine)-based artificial receptors., *J. Am. Chem. Soc. 126*, 2454–63.

83. Sakamoto, T., Ojida, A., and Hamachi, I. (2009) Molecular recognition, fluorescence sensing, and biological assay of phosphate anion derivatives using artificial Zn(II)-Dpa complexes., *Chem. Commun. (Camb).* 141–52.

84. Kohira, T., Honda, K., Ojida, A., and Hamachi, I. (2008) Artificial receptors designed for intracellular delivery of anionic phosphate derivatives., *Chembiochem 9*, 698–701.

85. Das, P., Mahato, P., Ghosh, A., Mandal, A. K., Banerjee, T., Saha, S., and Das, A. (2011) Urea / thiourea derivatives and Zn(II)-DPA complex as receptors for anionic recognition — A brief account, *J. Chem. Sci. 123*, 175–186.

86. Ojida, A., Inoue, M., Mito-oka, Y., Tsutsumi, H., Sada, K., and Hamachi, I. (2006) Effective disruption of phosphoprotein-protein surface interaction using Zn(II) dipicolylamine-based artificial receptors via two-point interaction., *J. Am. Chem. Soc. 128*, 2052–8.

87.   Sakamoto, T., Ojida, A., and Hamachi, I. (2009) Molecular recognition, fluorescence sensing, and biological assay of phosphate anion derivatives using artificial Zn(II)-Dpa complexes., *Chem. Commun. (Camb).* 141–52.

88.   Ngo, H. T., Liu, X., and Jolliffe, K. a. (2012) Anion recognition and sensing with Zn(ii)-dipicolylamine complexes., *Chem. Soc. Rev. 41*, 4928–65.

89.   Feng, L., Wang, Y., Liang, F., Liu, W., Wang, X., and Diao, H. (2012) A specific sensing ensemble for cyanide ion in aqueous solution, *Sensors Actuators B Chem.*, Elsevier B.V. *168*, 365–369.

90.   Nishimura, T., Xu, S.-Y., Jiang, Y.-B., Fossey, J. S., Sakurai, K., Bull, S. D., and James, T. D. (2013) A simple visual sensor with the potential for determining the concentration of fluoride in water at environmentally significant levels., *Chem. Commun. (Camb). 49*, 478–80.

91.   Wulff, G. (1982) Selective binding to polymers via covalent bonds. The construction of chiral cavities as specific receptor sites., *Pure Appl. Chem. 54*, 2093–2102.

92.   Zhang, T., and Anslyn, E. V. (2006) A colorimetric boronic acid based sensing ensemble for carboxy and phospho sugars., *Org. Lett. 8*, 1649–52.

93.   Zhong, Z., and Anslyn, E. V. (2002) A colorimetric sensing ensemble for heparin., *J. Am. Chem. Soc. 124*, 9014–5.

94.   Tulinsky, a, and Blevins, R. a. (1987) Structure of a tetrahedral transition state complex of alpha-chymotrypsin dimer at 1.8-A resolution., *J. Biol. Chem. 262*, 7737–43.

95.   Adebodun, F., and Jordan, F. (1988) 11B Nuclear Magnetic Resonance studies of the structure of the transition-state analogue phenylboronic acid bound to chymotrypsin, *J. Am. Chem. Soc. 110*, 309–310.

96.   Zhong, S., Jordan, F., Kettner, C., and Polgar, L. (1991) Observation of tightly bound 11B nuclear magnetic resonance signals on serine proteases. Direct evidence fpr tetrahedral geometry around the boron in the putative transition-state analogues., *J. Am. Chem. Soc. 113*, 23–25.

97.   Baggio, R., Elbaum, D., Kanyo, Z. F., Carroll, P. J., Cavalli, R. C., Ash, D. E., and Christianson, D. W. (1997) Inhibition of Mn2+ 2-Arginase by Borate Leads to the Design of a Transition State Analogue Inhibitor , 2(S)-Amino-6-boronohexanoic Acid, *J. Am. Chem. Soc. 119*, 8107–8108.

98.   Kettner, C. A., and Shenvi, A. B. (1984) Inhibition of the Serine Proteases Leukocyte Elastase , Pancreatic Elastase, Cathepsin G, and Chymotrypsin by Peptide Boronic Acids, *J. Biol. Chem. 259*, 15106–15114.

99.   Adams, J. (2002) Development of the proteasome inhibitor PS-341., *Oncologist 7*, 9–16.

100. Teicher, B. A., Ara, G., Herbst, R., Palombella, V. J., and Adams, J. (1999) The Proteasome Inhibitor PS-341 in Cancer Therapy, *Clin. Cancer Res. 5*, 2638–2645.

101. Groll, M., Berkers, C. R., Ploegh, H. L., and Ovaa, H. (2006) Crystal structure of the boronic acid-based proteasome inhibitor bortezomib in complex with the yeast 20S proteasome., *Structure 14*, 451–6.

102. Oh, D. J., and Ahn, K. H. (2008) Fluorescent sensing of IP3 with a Trifurcate Zn(II)-containing chemosensing ensemble system., *Org. Lett. 10*, 3539–42.

103. Oh, D. J., Han, M. S., and Ahn, K. H. (2007) Metal-containing Trifurcate Chemosensing Ensemble for Phytate, *Supramol. Chem. 19*, 315–320.

104. Jung, J. Y., Jun, E. J., Kwon, Y.-U., and Yoon, J. (2012) Recognition of myo-inositol 1,4,5-trisphosphate using a fluorescent imidazolium receptor., *Chem. Commun. (Camb). 48*, 7928–30.

105. Aoki, S., Zulkefeli, M., Shiro, M., Kohsako, M., Takeda, K., and Kimura, E. (2005) A luminescence sensor of inositol 1,4,5-triphosphate and its model compound by ruthenium-templated assembly of a bis(Zn2+cyclen) complex having a 2,2'-bipyridyl linker, *Supramol. Chem.* 9129–9139.

106. Dowlut, M., and Hall, D. G. (2006) An improved class of sugar-binding boronic acids, soluble and capable of complexing glycosides in neutral water., *J. Am. Chem. Soc. 128*, 4226–7.

107. Mirabelli, M. (2007) PhD Thesis, Imperial College London.

108. Huang, F., Cheng, C., and Feng, G. (2012) Introducing ligand-based hydrogen bond donors to a receptor: both selectivity and binding affinity for anion recognition in water can be improved., *J. Org. Chem. 77*, 11405–8.

109. Bunyapaiboonsri, T., Ramström, H., Ramström, O., Haiech, J., and Lehn, J.-M. (2003) Generation of bis-cationic heterocyclic inhibitors of Bacillus subtilis HPr kinase/phosphatase from a ditopic dynamic combinatorial library., *J. Med. Chem. 46*, 5803–11.

110. Bunyapaiboonsri, T., Ramström, O., Lohmann, S., Lehn, J. M., Peng, L., and Goeldner, M. (2001) Dynamic deconvolution of a pre-equilibrated dynamic combinatorial library of acetylcholinesterase inhibitors., *Chembiochem 2*, 438–44.

111. Shi, B., Stevenson, R., Campopiano, D. J., and Greaney, M. F. (2006) Discovery of Glutathione S-Transferase Inhibitors Using Dynamic Combinatorial Chemistry approach to the discovery of small molecule ligands for large, *J. Am. Chem. Soc. 128*, 8459–8467.

112. Demetriades, M., Leung, I. K. H., Chowdhury, R., Chan, M. C., McDonough, M. a, Yeoh, K. K., Tian, Y.-M., Claridge, T. D. W., Ratcliffe, P. J., Woon, E. C. Y., and Schofield, C. J. (2012) Dynamic combinatorial chemistry employing boronic acids/boronate esters leads to potent oxygenase inhibitors., *Angew. Chem. Int. Ed. Engl. 51*, 6672–5.

113. Otto, S., Furlan, R. L. E., and Sanders, J. K. M. (2002) Dynamic combinatorial chemistry., *Drug Discov. Today 7*, 117–25.

114. Ramström, O., Bunyapaiboonsri, T., Lohmann, S., and Lehn, J.-M. (2002) Chemical biology of dynamic combinatorial libraries., *Biochim. Biophys. Acta 1572*, 178–86.

115. Otto, S., Furlan, R. L. E., and Sanders, J. K. M. (2002) Recent developments in dynamic combinatorial chemistry., *Curr. Opin. Chem. Biol. 6*, 321–7.

116. Huc, I., and Lehn, J. M. (1997) Virtual combinatorial libraries: dynamic generation of molecular and supramolecular diversity by self-assembly., *Proc. Natl. Acad. Sci. U. S. A. 94*, 2106–10.

117. Lehn, J.-M., and Eliseev, A. V. (2001) Dynamic Combinatorial Chemistry, *Sci. 291* , 2331–2332.

118. Belowich, M. E., and Stoddart, J. F. (2012) Dynamic imine chemistry., *Chem. Soc. Rev. 41*, 2003–24.

119. Joshi, G., and Anslyn, E. V. (2012) Dynamic thiol exchange with β-sulfido-α,β-unsaturated carbonyl compounds and dithianes., *Org. Lett. 14*, 4714–7.

120. Roberts, S. L., Furlan, R. L. E., and Sanders, J. K. M. (2003) Metal-ion induced amplification of three receptors from dynamic combinatorial libraries of peptide-hydrazones, *Org. Biomol. Chem. 9*, 1625–1633.

121. Ludlow, R. F., and Otto, S. (2010) The impact of the size of dynamic combinatorial libraries on the detectability of molecular recognition induced amplification., *J. Am. Chem. Soc. 132*, 5984–6.

122. Nishiyabu, R., Kubo, Y., James, T. D., and Fossey, J. S. (2011) Boronic acid building blocks: tools for sensing and separation., *Chem. Commun. (Camb). 47*, 1106–23.

123. Springsteen, G., and Wang, B. (2002) A detailed examination of boronic acid–diol complexation, *Tetrahedron 58*, 5291–5300.

124. Hargrove, A. E., Nieto, S., Zhang, T., Sessler, J. L., and Anslyn, E. V. (2011) Artificial receptors for the recognition of phosphorylated molecules., *Chem. Rev. 111*, 6603–782.

125. Szentpetery, Z., Balla, A., Kim, Y. J., Lemmon, M. a, and Balla, T. (2009) Live cell imaging with protein domains capable of recognizing phosphatidylinositol 4,5-bisphosphate; a comparative study., *BMC Cell Biol. 10*, 67.

126. Guo, B., Peng, X., Cui, A., Wu, Y., Tian, M., Zhang, L., Chen, X., and Gao, Y. (2007) Synthesis and spectral properties of new boron dipyrromethene dyes, *Dye. Pigment. 73*, 206–210.

127. Ulrich, G., Ziessel, R., and Harriman, A. (2008) The chemistry of fluorescent bodipy dyes: versatility unsurpassed., *Angew. Chem. Int. Ed. Engl. 47*, 1184–201.

128. Ishiyama, T., Murata, M., and Miyaura, N. (1996) Palladium(0)-Catalyzed Cross-Coupling Reaction of Alkoxydiboron with Haloarenes: A Direct Procedure for Arylboronic Esters, *J. Org. Chem. 60*, 7508–7510.

129. Komatsu, K., Kikuchi, K., Kojima, H., Urano, Y., and Nagano, T. (2005) Selective zinc sensor molecules with various affinities for Zn2+, revealing dynamics and regional distribution of synaptically released Zn2+ in hippocampal slices., *J. Am. Chem. Soc. 127*, 10197–204.

130. Hirano, T., Kikuchi, K., Urano, Y., and Nagano, T. (2002) Improvement and biological applications of fluorescent probes for zinc, ZnAFs., *J. Am. Chem. Soc. 124*, 6555–62.

131. Barthel, A., Ostrakhovitch, E. a, Walter, P. L., Kampkötter, A., and Klotz, L.-O. (2007) Stimulation of phosphoinositide 3-kinase/Akt signaling by copper and zinc ions: mechanisms and consequences., *Arch. Biochem. Biophys. 463*, 175–82.

132. Incarvito, C., Lam, M., Rhatigan, B., Rheingold, A. L., Qin, C. J., Gavrilova, A. L., and Bosnich, B. (2001) Bimetallic reactivity. Preparations, properties and structures of complexes formed by unsymmetrical binucleating ligands bearing 4- and 6-coordinate sites supported by alkoxide bridges, *J. Chem. Soc. Dalt. Trans.* 3478–3488.

133. Lee, H. G., Lee, J. H., Jang, S. P., Hwang, I. H., Kim, S.-J., Kim, Y., Kim, C., and Harrison, R. G. (2013) Zinc selective chemosensors based on the flexible dipicolylamine and quinoline, *Inorganica Chim. Acta*, Elsevier B.V. *394*, 542–551.

134. Hargrove, A. E., Zhong, Z., Sessler, J. L., and Anslyn, E. V. (2010) Algorithms for the determination of binding constants and enantiomeric excess in complex host : guest equilibria using optical measurements., *New J. Chem. 34*, 348–354.

135. Thordarson, P. (2011) Determining association constants from titration experiments in supramolecular chemistry., *Chem. Soc. Rev. 40*, 1305–23.

136. Zhang, X., You, L., Anslyn, E. V, and Qian, X. (2012) Discrimination and classification of ginsenosides and ginsengs using bis-boronic acid receptors in dynamic multicomponent indicator displacement sensor arrays., *Chemistry 18*, 1102–10.

137. Orosz, F., and Ovádi, J. (2002) A simple method for the determination of dissociation constants by displacement ELISA., *J. Immunol. Methods 270*, 155–62.

138. Amendola, V., Bonizzoni, M., Esteban-Gómez, D., Fabbrizzi, L., Licchelli, M., Sancenón, F., and Taglietti, A. (2006) Some guidelines for the design of anion receptors, *Coord. Chem. Rev. 250*, 1451–1470.

139. Maehama, T., Taylor, G. S., Slama, J. T., and Dixon, J. E. (2000) A sensitive assay for phosphoinositide phosphatases., *Anal. Biochem. 279*, 248–50.

140. Cabell, L. A., Monahan, M., and Anslyn, E. V. (1999) A Competition Assay for Determining Glucose-6-phosphate Concentration with a Tris-boronic acid Receptor, *Tetrahedron Lett. 40*, 7753–7756.

141. Baker, S. J., Tomsho, J. W., and Benkovic, S. J. (2011) Boron-containing inhibitors of synthetases., *Chem. Soc. Rev. 40*, 4279–85.

142. Philipp, M., and Bender, M. L. (1971) Inhibition of Serine Proteases by Arylboronic Acids, *Proc. Natl. Acad. Sci. 68*, 478–480.

143. Nguyen, B. T., and Anslyn, E. V. (2006) Indicator–displacement assays, *Coord. Chem. Rev. 250*, 3118–3127.

144. Morgan, B. P., He, S., and Smith, R. C. (2007) Dizinc enzyme model/complexometric indicator pairs in indicator displacement assays for inorganic phosphates under physiological conditions., *Inorg. Chem. 46*, 9262–6.

145. Hall, D. G. (2005) Structure, Properties, and Preparation of Boronic Acid Derivatives. Overview of Their Reactions and Applications. In *Boronic Acids: Preparation and Applications in Organic Synthesis and Medicine*, Wiley-VCH.

146. Meggers, E. (2009) Targeting proteins with metal complexes., *Chem. Commun. (Camb).* 1001–10.

147. Rosivatz, E., Matthews, J. G., Mcdonald, N. Q., Mulet, X., Ho, K. K., Lossi, N., Schmid, A. C., Mirabelli, M., Pomeranz, K. M., Erneux, C., Lam, E. W.-F., Vilar, R., and Woscholski, R. (2006) A Small-Molecule Inhibitor for Phosphatase and Tensin Homologue Deleted on Chromosome 10 (PTEN), *ACS Chem. Biol. 1*, 780–790.

148. Lu, L., and Zhu, M. (2011) Metal-Based Inhibitors of Protein Tyrosine Phosphatases, *Anticancer Agents Med. Chem. 11*, 164–171.

149. Bunce, M. W., Bergendahl, K., and Anderson, R. a. (2006) Nuclear PI(4,5)P(2): a new place for an old signal., *Biochim. Biophys. Acta 1761*, 560–9.

150. Stallings, J. D., Tall, E. G., Pentyala, S., and Rebecchi, M. J. (2005) Nuclear translocation of phospholipase C-delta1 is linked to the cell cycle and nuclear phosphatidylinositol 4,5-bisphosphate., *J. Biol. Chem. 280*, 22060–9.

151. Bridges, D., and Saltiel, A. R. (2012) Phosphoinositides and Disease. In *Current Topics in Microbiology and Immunology 362* (Falasca, M., Ed.), pp 61–85, Springer Netherlands, Dordrecht.

152. Sandanayake, K. R. A. S., James, T. D., and Shinkaia, S. (1996) Molecular design of sugar recognition systems by sugar-di boronic acid macrocyclization, *Pure Appl. Chem. 68*, 1207–1212.

153. Vlahos, C. J., Matter, W. F., Hui, K. Y., and Brown, R. F. (1994) A Specific Inhibitor of Phosphatidylinositol 3-Kinase, 2-(4-Morpholinyl)-8-phenyl-4H-1-benzopyran-4-one (LY294002), *J. Biol. Chem. 269*, 5241–5248.

154. Arcaro, A., and Wymann, M. P. (1993) Wortmannin is a potent phosphatidylinositol 3-kinase inhibitor : the role of phosphatidylinositol 3,4,5-trisphosphate in neutrophil responses, *Biochem. J. 296*, 297–301.

155. Krstić, D., Krinulović, K., and Vasić, V. (2005) Inhibition of Na+/K(+)-ATPase and Mg(2+)-ATPase by metal ions and prevention and recovery of inhibited activities by chelators., *J. Enzyme Inhib. Med. Chem. 20*, 469–76.

156. Masanori Kitamura, Toshihiro Suzuki, Ryo Abe, Takeru Ueno, S. A. (2011) 11B NMR Sensing of d-Block Metal Ions in Vitro and in Cells Based on the Carbon-Boron Bond Cleavage of Phenylboronic Acid-Pendant, *Inorg. Chem. 50*, 11568–11580.

157. Kobayashi, A., Dosen, M., Chang, M., Nakajima, K., Noro, S., and Kato, M. (2010) Synthesis of metal-hydrazone complexes and vapochromic behavior of their hydrogen-bonded proton-transfer assemblies., *J. Am. Chem. Soc. 132*, 15286–98.

158. Lee, J. H., Park, J., Lah, M. S., Chin, J., and Hong, J.-I. (2007) High-affinity pyrophosphate receptor by a synergistic effect between metal coordination and hydrogen bonding in water., *Org. Lett. 9*, 3729–31.

159. Bradford, M. M. (1976) A rapid and sensitive method for the quantitation of microgram quantities of protein utilizing the principle of protein-dye binding., *Anal. Biochem. 72*, 248–54.

160. Cariani, L., Thomas, L., Brito, J., and del Castillo, J. . (2004) Bismuth citrate in the quantification of inorganic phosphate and its utility in the determination of membrane-bound phosphatases, *Anal. Biochem. 324*, 79–83.

161. Mak, L. H., Vilar, R., and Woscholski, R. (2010) Characterisation of the PTEN inhibitor VO-OHpic., *J. Chem. Biol. 3*, 157–63.

Chapter 9: Appendix

9.1 2-dimensional and 135DEPT NMR

9.1.1 ^{13}C and 135 DEPT, Compound 3
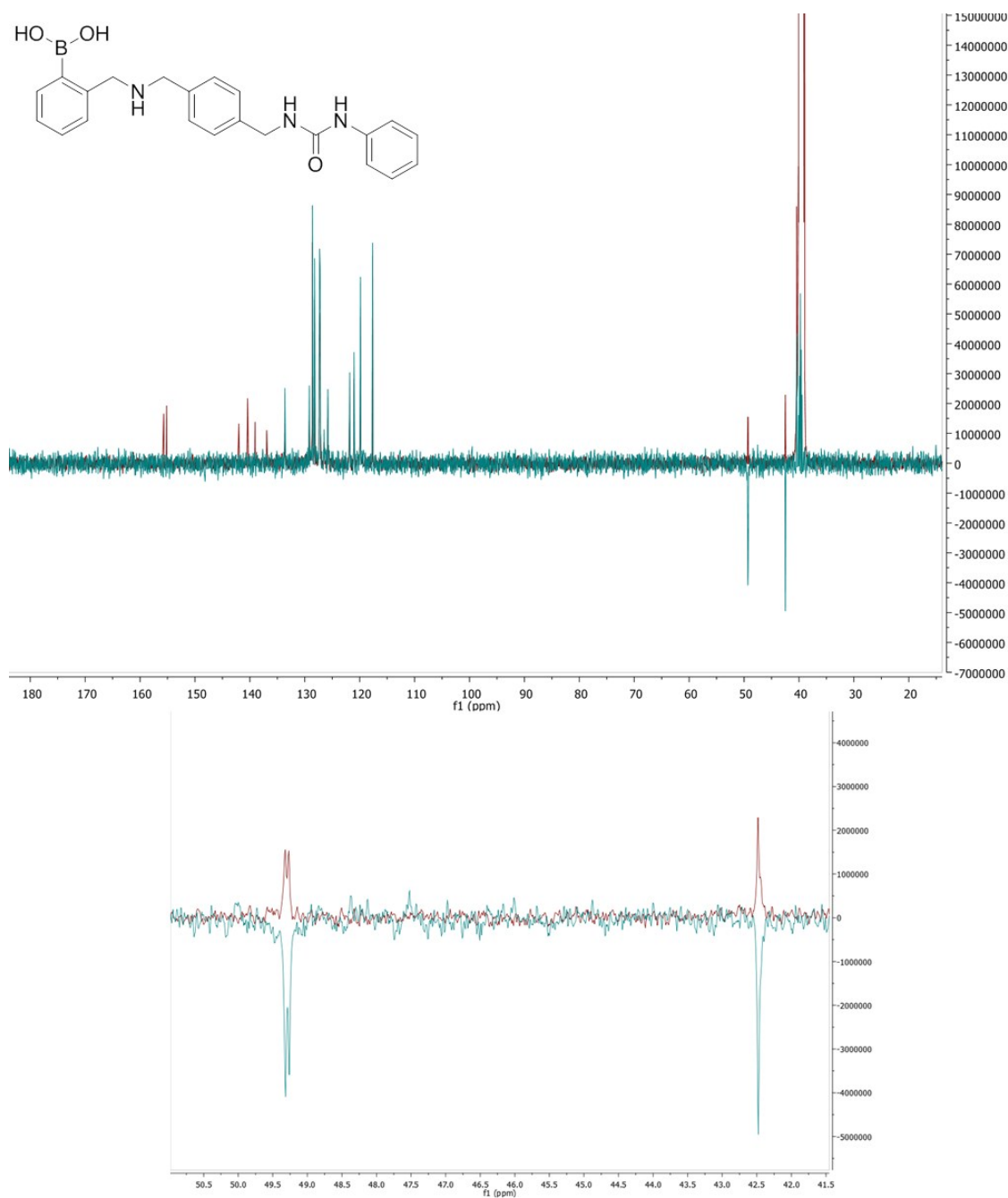

Figure 9.1: Top, ^{13}C spectrum of compound **3** (red) overlaid with 135DEPT of **3** (blue). Bottom, expansion benzylic protons showing two CH_2 peaks close together at 49.3 and 49.2 ppm. Spectra indicate the presence of six C, eleven CH and three CH_2 carbons.
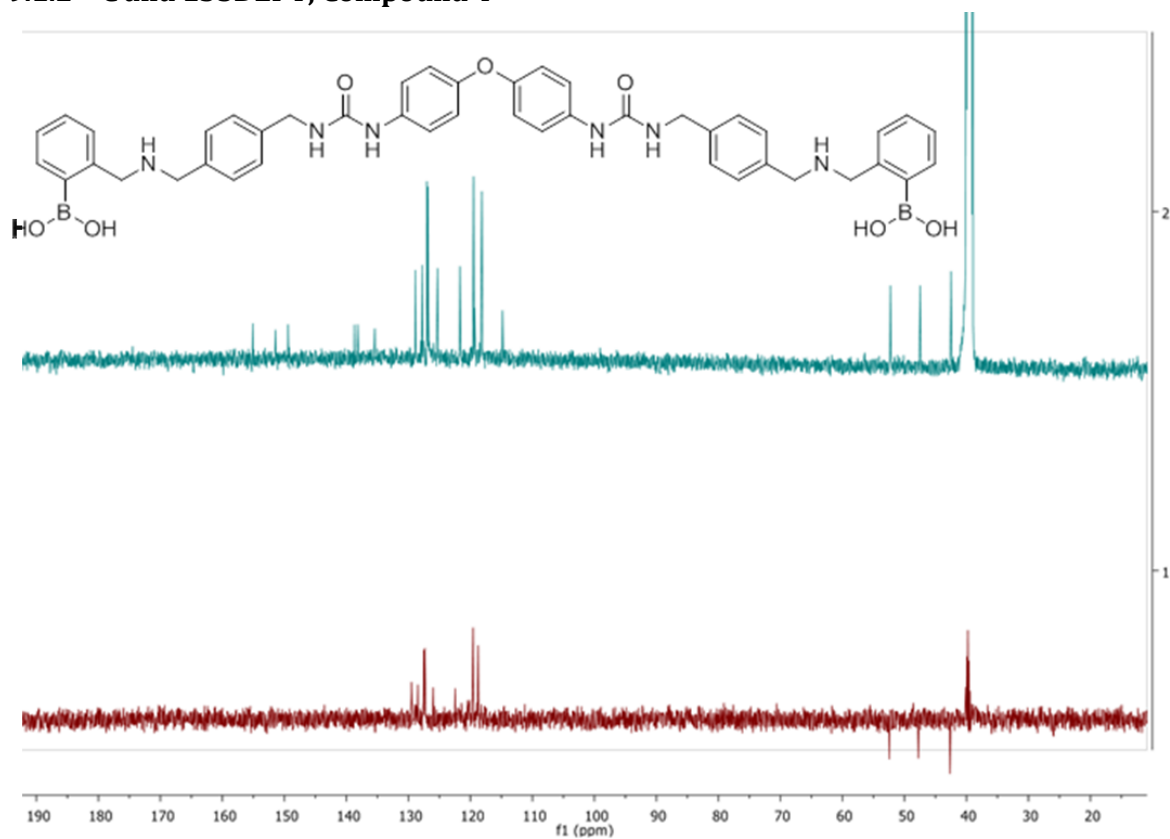
9.1.2 ^{13}C and 135DEPT, Compound 4

*Figure 9.2: Top, ^{13}C NMR spectrum of compound **4** taken at 388 K. Bottom, 135DEPT of compound **4** taken at 298K. The two spectra do not overlap due to difference in acquisition temperature. However the ^{13}C spectrum is observed to have seven more peaks in the aromatic region (seven removed peaks correspond to quaternary C, remaining eight are CH$_2$ carbons) than the 135DEPT spectrum. Three peaks are present in the benzylic region of the ^{13}C spectrum and correspond to three negative peaks in the same region of the 135DEPT spectrum.*
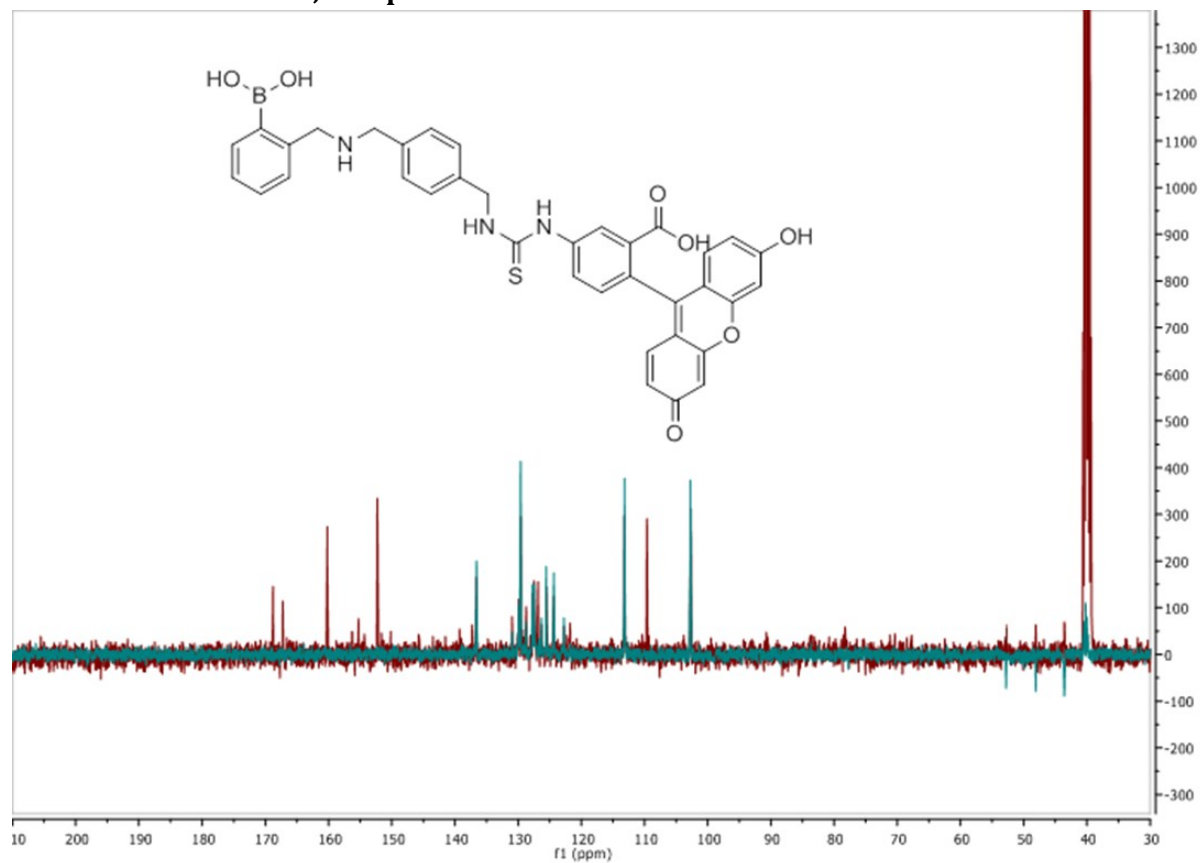
9.1.3 ^{13}C and 135DEPT, Compound 5

Figure 9.3: ^{13}C NMR (red) and 135DEPT (blue) of compound **5**.
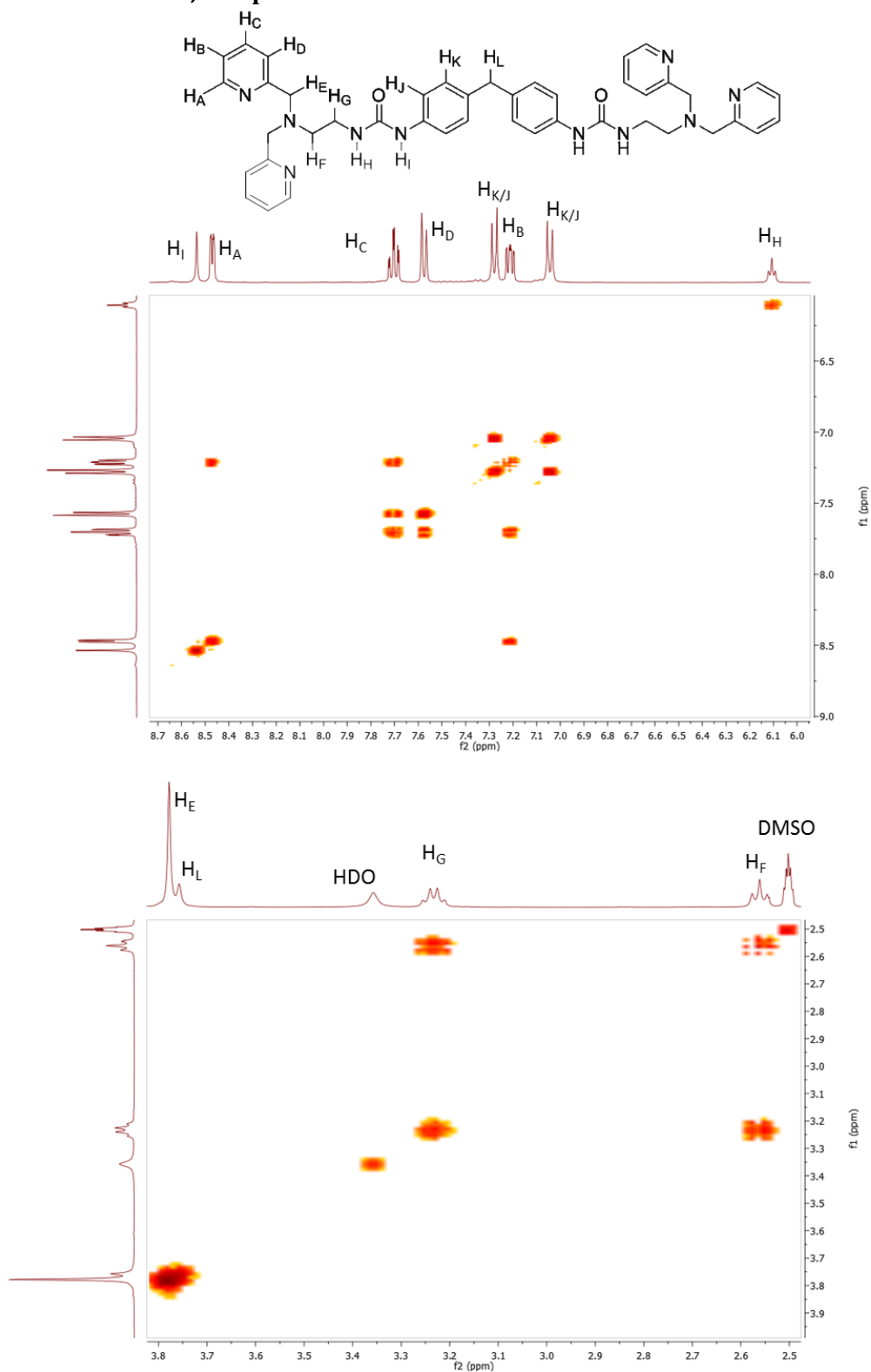
9.1.4 ¹H-¹H COSY, compound 11

Figure 9.4: Expansions of *¹H-¹H COSY crosspeaks for compound **11**. Protons are assigned where unambiguous.*
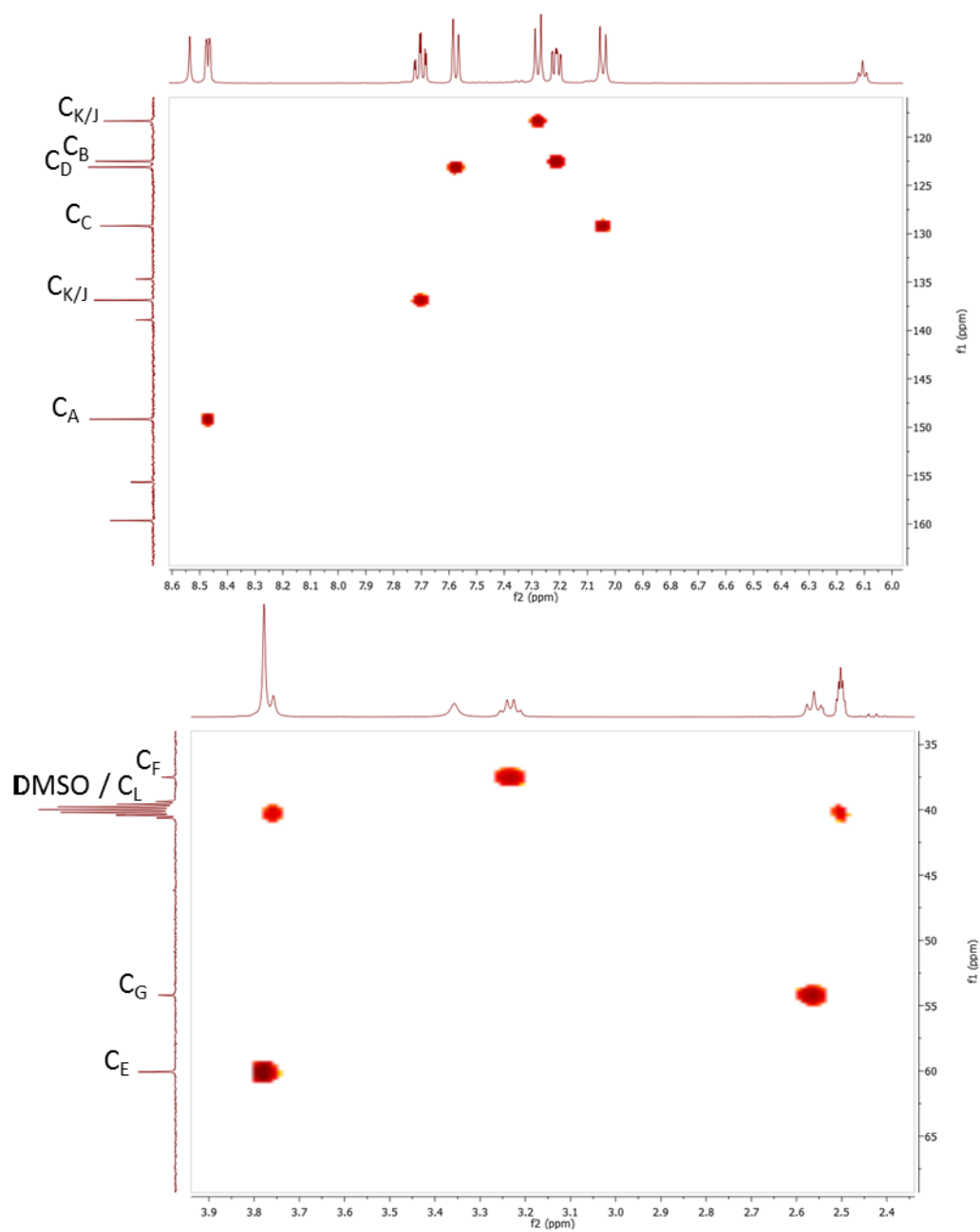
9.1.5 ¹H-¹³C HMQC, Compound 11

*Figure 9.5: Expansions of ¹H-¹³C HMQC crosspeaks for compound **11**. Carbons are assigned to connected protons.*

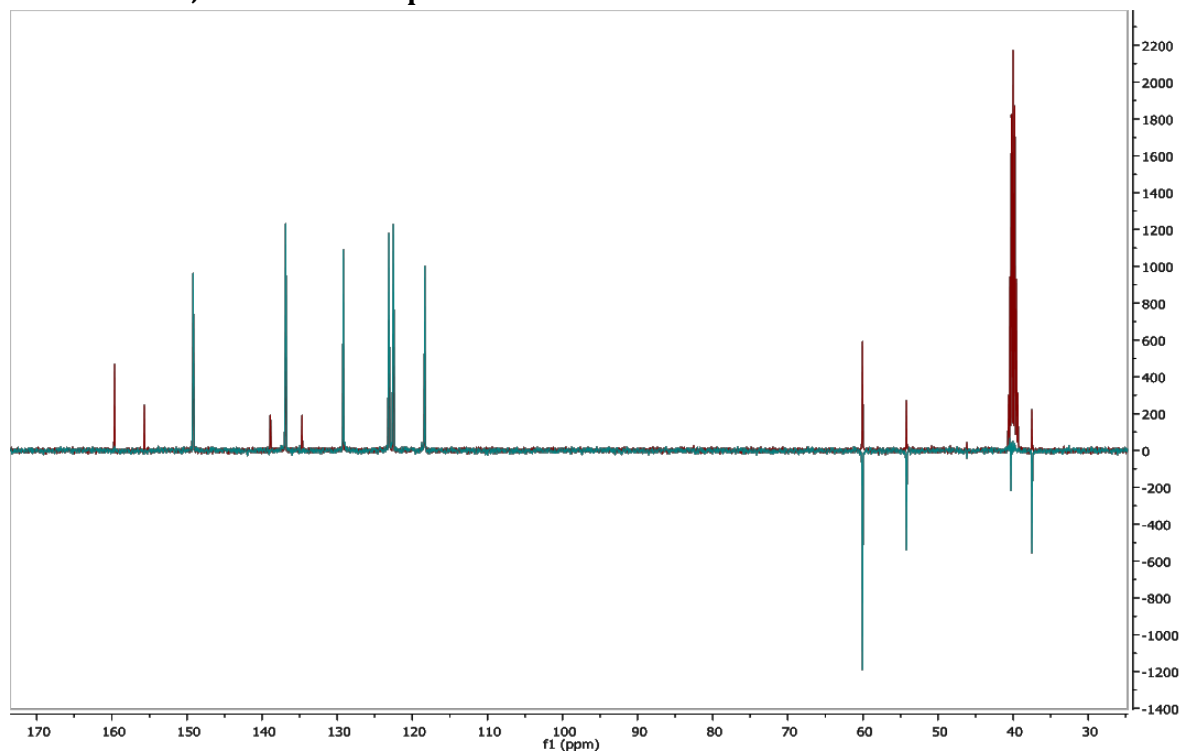## 9.1.6 ^{13}C NMR, 135-DEPT Compound 11

Figure 9.6: ^{13}C NMR (red) overlaid with 135DEPT (blue). Negative peak at 40.4 ppm indicates the presence of a CH$_2$ peak (H$_L$) which overlaps with the solvent, and is therefore obscured in ^{13}C NMR. DMSO possesses two CH$_3$ groups which produce positive peaks in 135DEPT spectroscopy.

9.1.7 Compound 11 and 12: Comparison of ^{1}H NMR
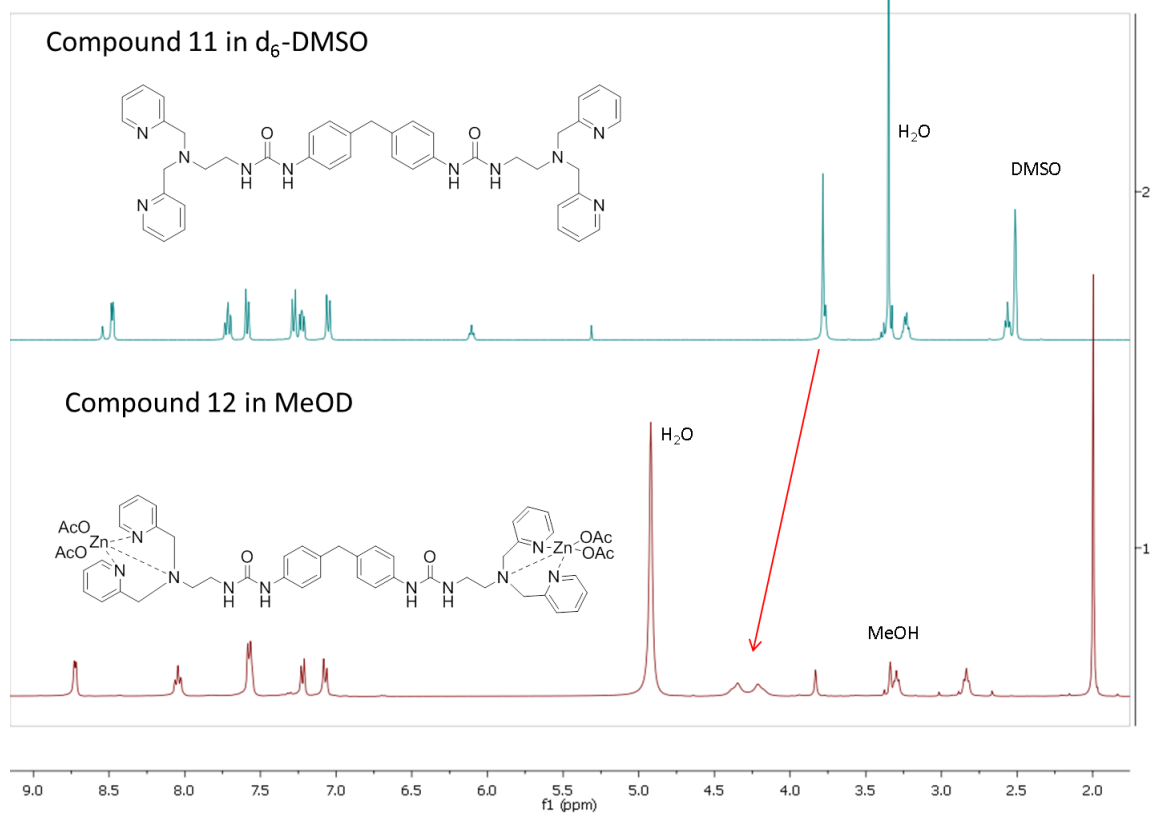

Compound 11 in d_6-DMSO

Compound 12 in MeOD

*Figure 9.7: Benzylic protons of compound **11** are observed as a singlet (blue spectrum). Upon coordination of DPA to zinc the singlet splits and shifts (compound **12**, red spectrum).*
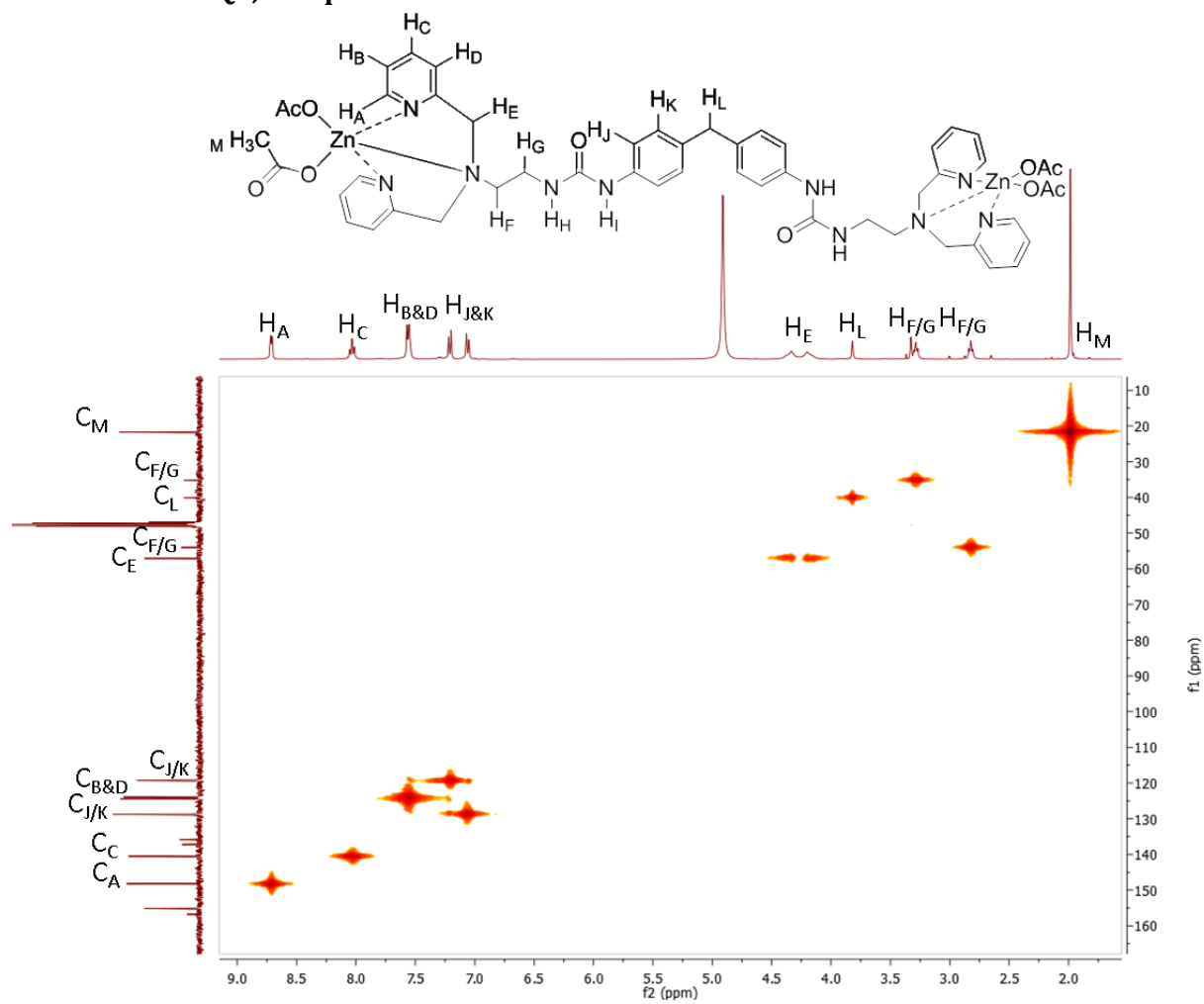
9.1.8 ^{1}H-^{13}C HMQC, Compound 12

Figure 9.8: ^{1}H ^{13}C HMQC of complex **12**.
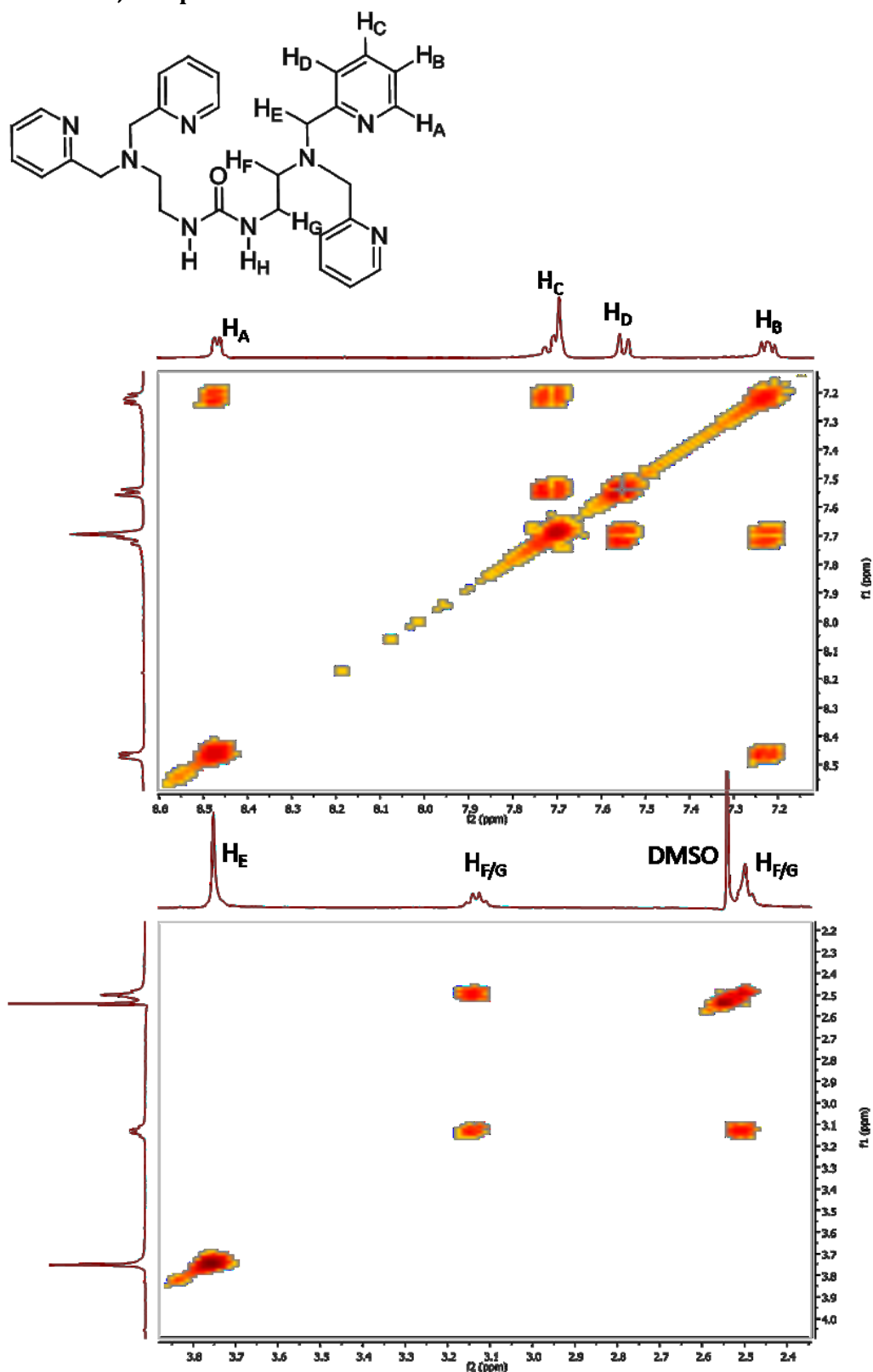
9.1.9 ¹H-¹H COSY, Compound 13

*Figure 9.9: Expansions of ¹H-¹H COSY crosspeaks for compound **13**. Protons are assigned where unambiguous. Urea proton (H_H) not observed.*
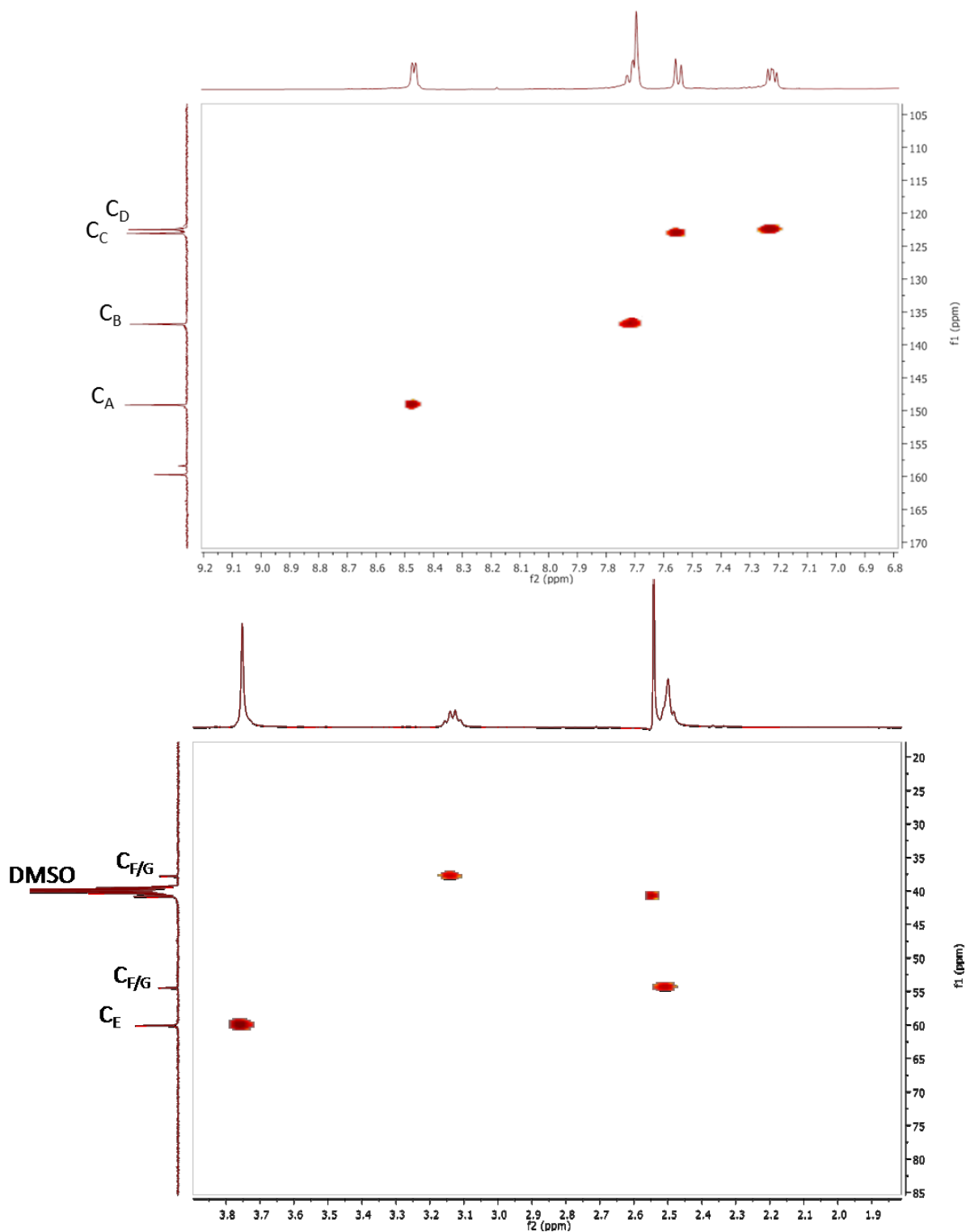
9.1.10 ^{1}H-^{13}C HMQC, Compound 13

Figure 9.10: ^{1}H-^{13}C HMQC expansions for compound **13**. Carbons are assigned to connected protons.

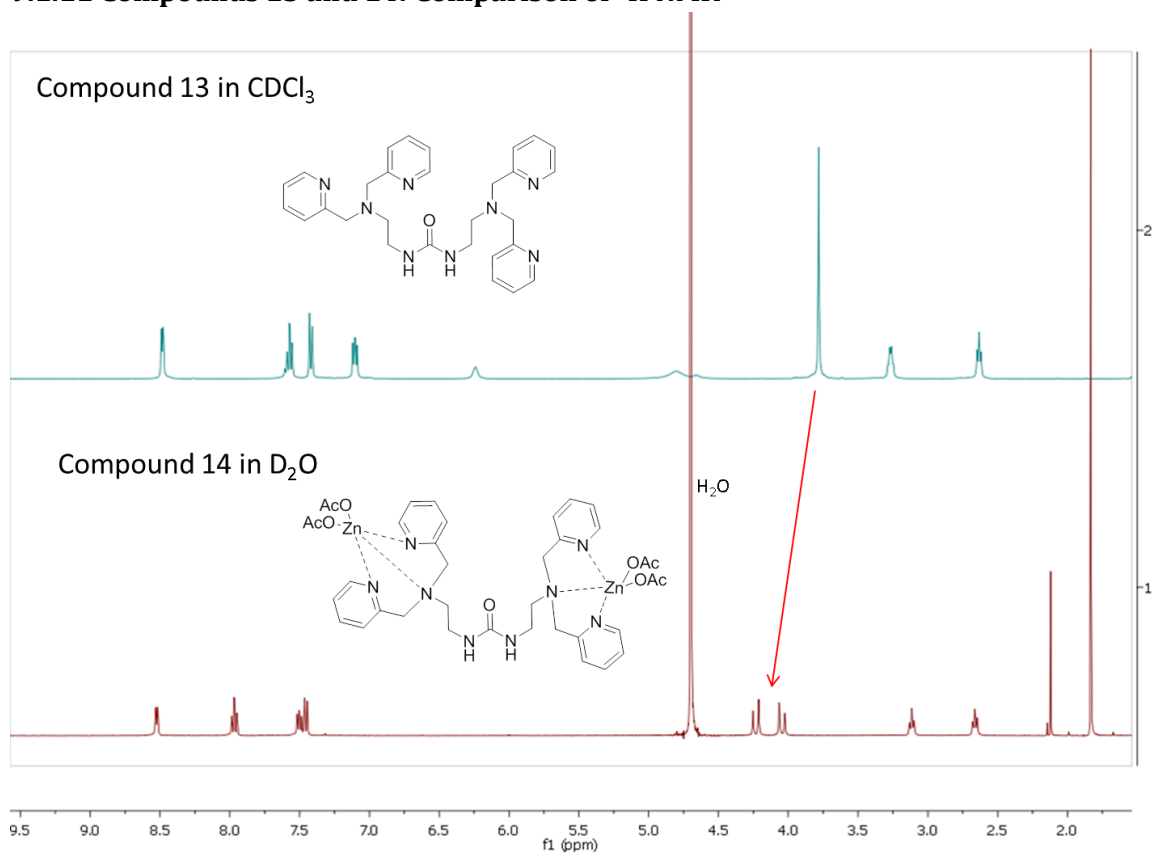### 9.1.11 Compounds 13 and 14: Comparison of ^{1}H NMR

*Figure 9.11: Benzylic protons of compound **13** are observed as a singlet (blue spectrum). Upon coordination of DPA to zinc the singlet splits and shifts (compound **14**, red spectrum).*
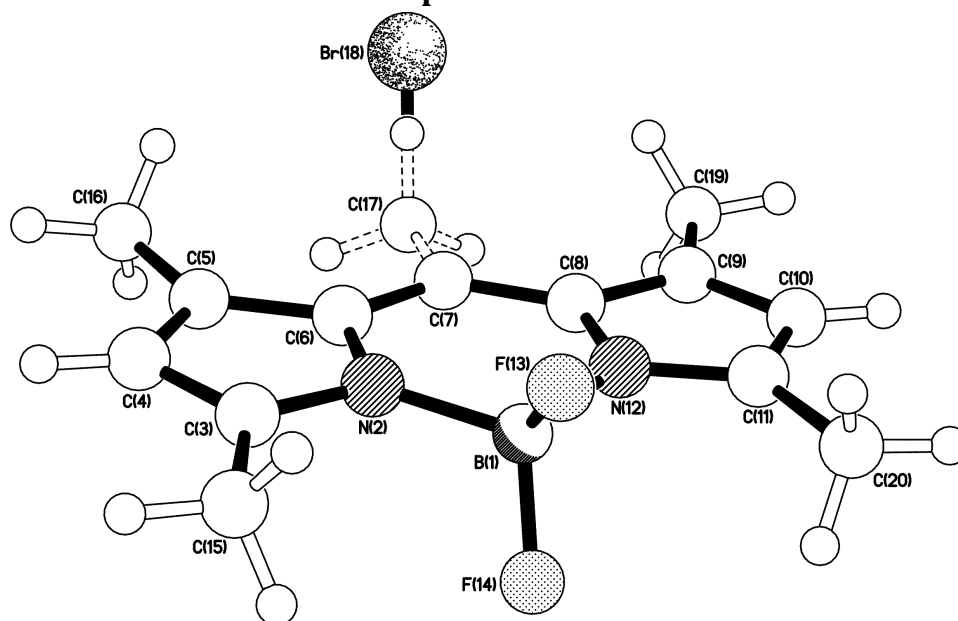
9.2 Crystal structure data for compound 6

*Figure 9.12: Structure of compound **6** as determined by X-ray crystallography.*

Data for **6**:

```
Empirical formula:        (C14 H16 B Br F2 N2)0.53,(C14 H17 B F2 N2)0.47

Formula weight      304.12
```

Temperature	173 K
Diffractometer, wavelength	OD Xcalibur 3, 0.71073 Å
Crystal system, space group	Monoclinic, P2(1)/n
Unit cell dimensions	a = 9.9860(2) Å $\alpha = 90°$
	b = 12.3363(2) Å $\beta = 108.603(3)°$
	c = 11.8813(3) Å $\gamma = 90°$
Volume, Z	1387.19(6) Å^3, 4
Density (calculated)	1.456 Mg/m^3
Absorption coefficient	1.628 mm^{-1}
F(000)	624
Crystal colour / morphology	Red tablets
Crystal size	0.35 x 0.31 x 0.08 mm^3
θ range for data collection	3.22 to 32.70°
Index ranges	-15<=h<=13, -18<=k<=17, -11<=l<=17
Reflns collected / unique	15276 / 4685 [R(int) = 0.0251]
Reflns observed [F>4σ(F)]	3750
Absorption correction	Analytical
Max. and min. transmission	0.880 and 0.648
Refinement method	Full-matrix least-squares on F^2
Data / restraints / parameters	4685 / 6 / 188
Goodness-of-fit on F^2	1.052
Final R indices [F>4σ(F)]	R1 = 0.0402, wR2 = 0.1049
R indices (all data)	R1 = 0.0551, wR2 = 0.1128
Largest diff. peak, hole	0.458, -0.218 eÅ^{-3}
Mean and maximum shift/error	0.000 and 0.000

Bond lengths [Å] and angles [°] for Compound **6**.

B(1)-F(13)	1.3924(15)
B(1)-F(14)	1.3965(16)
B(1)-N(2)	1.5447(17)
B(1)-N(12)	1.5464(18)
N(2)-C(3)	1.3547(16)
N(2)-C(6)	1.4008(15)
C(3)-C(4)	1.401(2)
C(3)-C(15)	1.492(2)
C(4)-C(5)	1.3868(19)
C(5)-C(6)	1.4340(17)
C(5)-C(16)	1.5033(19)
C(6)-C(7)	1.4018(17)
C(7)-C(8)	1.3965(16)
C(7)-C(17')	1.4955(17)
C(7)-C(17)	1.4955(17)
C(8)-N(12)	1.4033(15)
C(8)-C(9)	1.4325(17)
C(9)-C(10)	1.379(2)
C(9)-C(19)	1.5001(19)
C(10)-C(11)	1.406(2)
C(11)-N(12)	1.3520(16)
C(11)-C(20)	1.488(2)
C(17)-Br(18)	1.8551(13)

F(13)-B(1)-F(14)	109.31(10)
F(13)-B(1)-N(2)	110.49(11)
F(14)-B(1)-N(2)	109.94(10)
F(13)-B(1)-N(12)	110.48(10)
F(14)-B(1)-N(12)	109.86(11)
N(2)-B(1)-N(12)	106.73(10)
C(3)-N(2)-C(6)	108.59(10)
C(3)-N(2)-B(1)	125.64(11)
C(6)-N(2)-B(1)	125.67(10)
N(2)-C(3)-C(4)	108.95(12)
N(2)-C(3)-C(15)	123.14(13)
C(4)-C(3)-C(15)	127.90(13)
C(5)-C(4)-C(3)	108.71(12)
C(4)-C(5)-C(6)	106.23(11)
C(4)-C(5)-C(16)	123.46(12)
C(6)-C(5)-C(16)	130.25(12)
N(2)-C(6)-C(7)	119.90(10)
N(2)-C(6)-C(5)	107.50(10)
C(7)-C(6)-C(5)	132.59(11)
C(8)-C(7)-C(6)	121.56(11)
C(8)-C(7)-C(17')	119.17(11)
C(6)-C(7)-C(17')	119.26(11)
C(8)-C(7)-C(17)	119.17(11)
C(6)-C(7)-C(17)	119.26(11)
C(7)-C(8)-N(12)	120.05(11)
C(7)-C(8)-C(9)	132.43(11)
N(12)-C(8)-C(9)	107.52(10)

```
C(10)-C(9)-C(8)        106.35(12)
C(10)-C(9)-C(19)       123.53(13)
C(8)-C(9)-C(19)        130.12(12)
C(9)-C(10)-C(11)       108.80(12)
N(12)-C(11)-C(10)      108.87(12)
N(12)-C(11)-C(20)      123.05(13)
C(10)-C(11)-C(20)      128.08(13)
C(11)-N(12)-C(8)       108.46(11)
C(11)-N(12)-B(1)       125.93(11)
C(8)-N(12)-B(1)        125.38(10)
C(7)-C(17)-Br(18)      110.63(8)
```
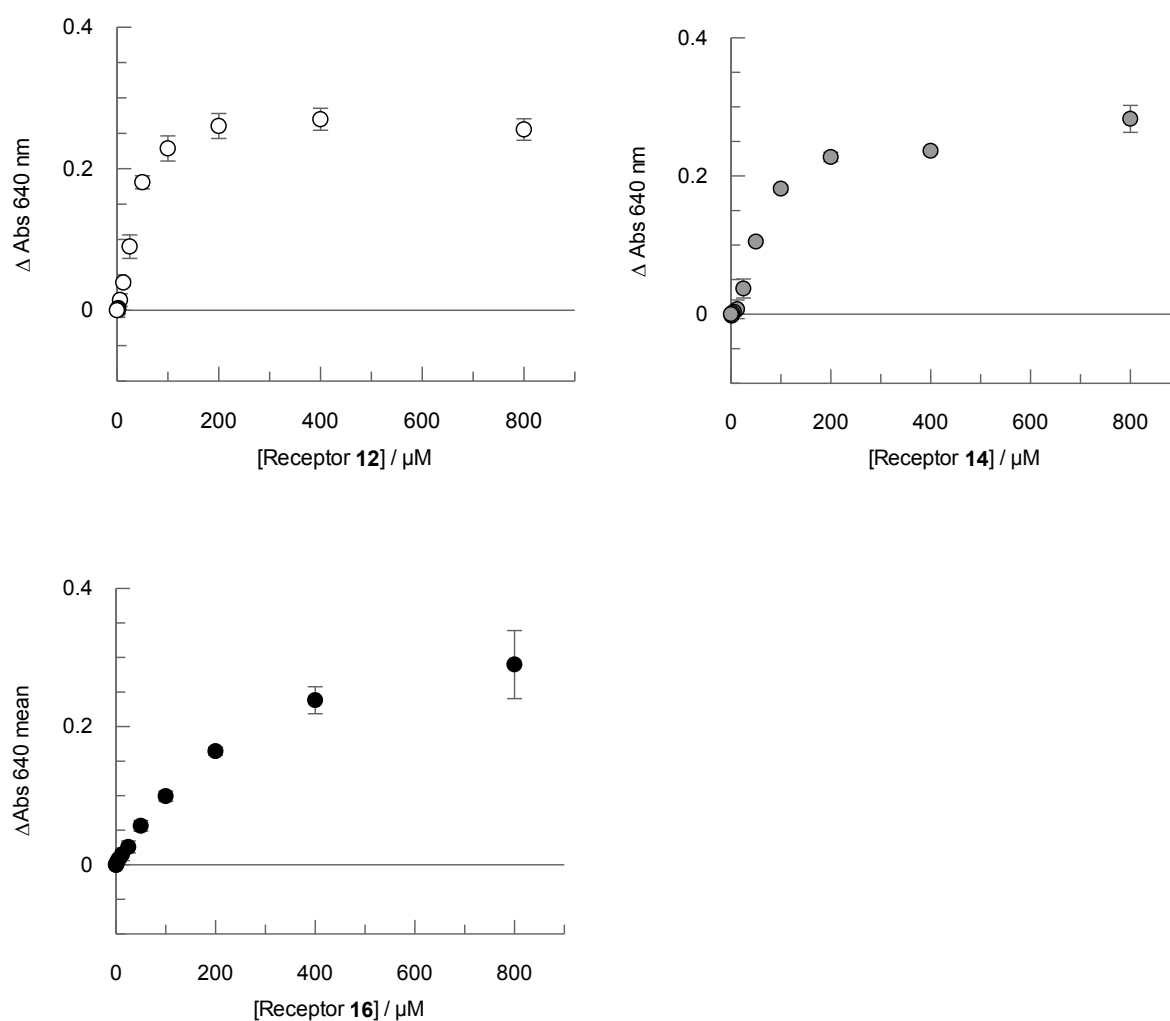
9.3 Binding of receptors 12, 14 and 16 to PV

Figure 9.13: Addition of increasing concentrations of receptors 12, 14 and 16 to pyrocatechol violet (PV, 100 μM in HEPES buffer, 100 mM pH 7.4) induced a colour change which was monitored by UV-Vis spectroscopy. The peak observed at 640 nm corresponded to the receptor-PV complex. Error bars represent standard error of triplicate repeats performed in triplicate (n=3).

9.4 IC_{50} determination of zinc inhibition of PTEN, SopB and ATPase.
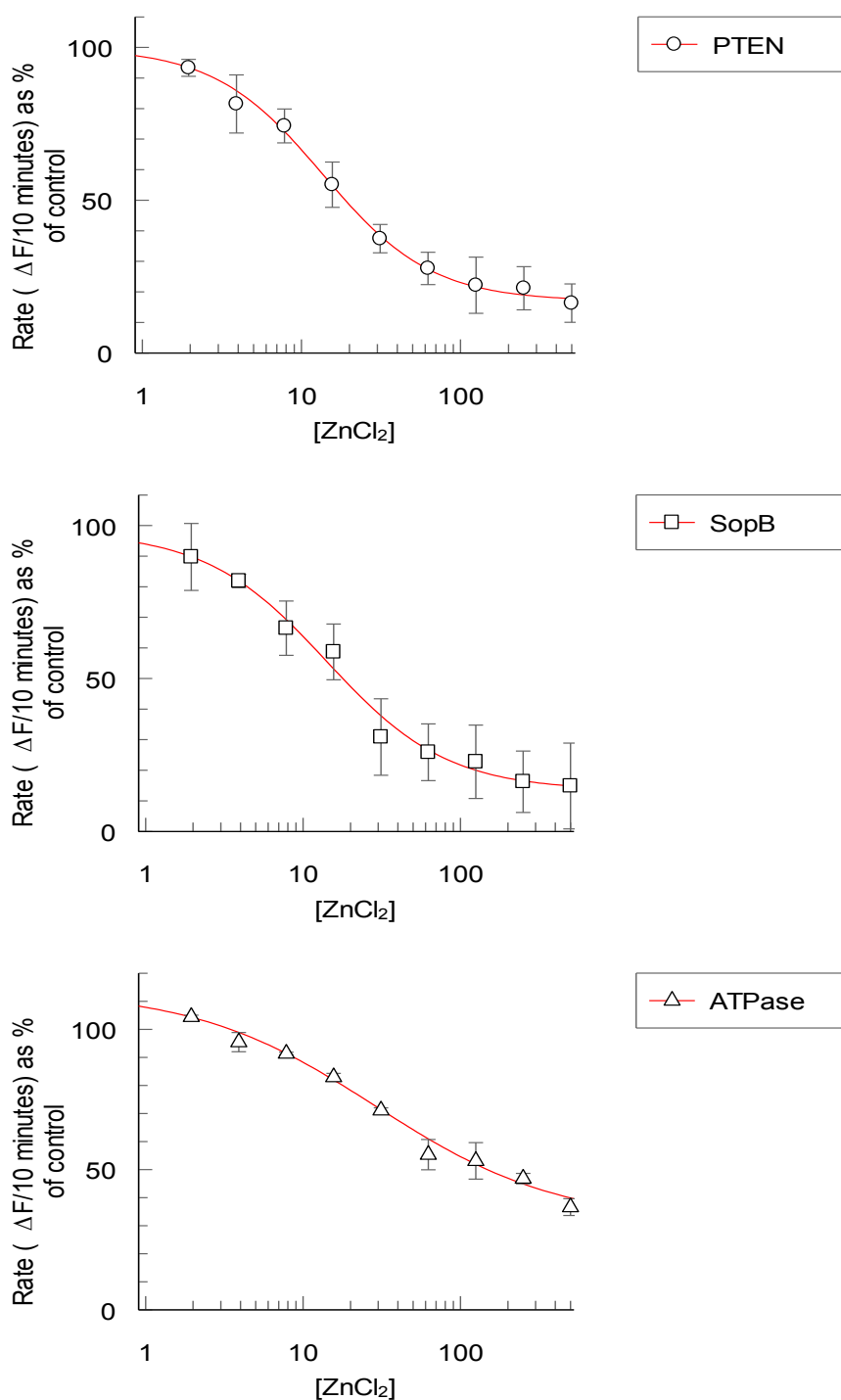

Figure 9.14: Increasing concentrations of zinc inhibit activity of the enzymes PTEN, SopB and ATPase. OMFP (50 μM) added to initiate reactions and fluorescence intensity was monitored over 10 minutes (λex = 485 nm, λem= 525 nm). PTEN 84.6 μg/ml; SopB 2.36 μg/ml; ATPase 0.15 μg/ml. Rate of hydrolysis of OMFP without enzyme has been subtracted for each concentration of $ZnCl_2$. Error bars represent standard deviation of two independent experiments carried out in triplicate. IC_{50} values determined using GraFit version 6.0.12.

PTEN, IC_{50} = 13.6 ± 1.3 μM; SopB, IC_{50} = 14.1 ± 1.1 μM; ATPase IC_{50} = 28.9 ± 4.4 μM [Lit: 22 μM (*155*)].